



UNIVERSITY *of the*  
WESTERN CAPE

## **Heavy and Precious Metal Toxicity Evaluation using a Horseradish Peroxidase Immobilised Biosensor**

By

**Bongiwe Silwana**

B.Tech (Chemistry)

UNIVERSITY *of the*  
WESTERN CAPE

Submitted in fulfillment of the requirements for the degree of

**MAGISTER SCIENTIAE**

in the

Department of Chemistry

Faculty of Science

University of the Western Cape

**November, 2012**

**Supervisors:**

**Dr V.S. Somerset**

**Prof. E.I. Iwuoha**

## **Declaration**

I declare that “**Heavy and precious metal toxicity evaluation using a horseradish peroxidase immobilised biosensor**” is my own work, that it has not been submitted before for any degree or examination in any other university, and that all the sources I have used or quoted have been indicated and acknowledged as complete references.

**Bongiwe Silwana**

**November, 2012**

**Signature:** -----

**Date:** -----



UNIVERSITY *of the*  
WESTERN CAPE

**Supervisors: Dr Vernon S. Somerset**  
**Prof. Emmanuel I. Iwuoha**

## Summary

Environmental pollution is always the hottest topic in public conversation and one of the most concerned aspects of human health. The thin film sputtered microelectrode devices have been developed to improve the quality of human health, by offering better monitoring capabilities. This thesis is divided into three parts and the studies were performed on chemical sensor technology currently available and under development using modified methods. In the first part of this thesis: (i) the studies are related to synthesis, characterisation and polymerisation of polyaniline (PANI) and polyaniline-co-poly(2,2'-dithiodianiline) (PANI-co-PDTDA). Polyaniline (PANI) and the copolymer of aniline with dithiodianiline, an aniline derivative containing S-S-links were of interest in polymer synthesis. Electrochemical synthesis was carried out in 1 M HCl and different concentrations of H<sub>2</sub>SO<sub>4</sub> (1, 2.5, and 5 M) solutions for PANI and PANI-co-PDTDA respectively. The PANI and PANI-co-PDTDA were grown electrochemically on the surface of a glassy carbon electrode (GCE) by repetitive cyclic voltammetric scanning. Cyclic voltammetry (CV) was used to evaluate the differences between the electrochemical characteristics associated with growth of the copolymer and homopolymer, polyaniline (PANI). The surface concentration of PANI was estimated to be  $2.64 \times 10^{-1} \text{ mol.cm}^{-2}$  while the film thickness was estimated to be  $7.09 \times 10^{-10} \text{ cm}$  and  $1.49 \times 10^{-9} \text{ cm}$  for scan rate and square root scan rate. In contrast, PANI-co-PDTDA concentrations (1, 2, 5 and 5 M H<sub>2</sub>SO<sub>4</sub> solutions) gained a surface concentration ( $\Gamma$ ) falling in the range  $6.1 \times 10^{-2} - 7.9 \times 10^2 \text{ mol.cm}^{-2}$  and a film thickness in the range  $8.16 \times 10^{-9} - 2.05 \times 10^{-8} \text{ cm}$ .

The second section of this thesis focused on the development of two sensors, Pt/PANI/HRP and Pt/PANI-co-PDTDA/HRP biosensors. The biosensor described in this chapter focus on the use of horseradish peroxidase (HRP) with hydrogen peroxide as substrate, was constructed with the aim of further investigation of inhibition by heavy metals (Cd<sup>2+</sup>, Pb<sup>2+</sup> and Hg<sup>2+</sup>). To achieve this, the enzyme HRP as the catalytic bio-element, was immobilised on the surface of a platinum electrode with PANI as a mediator. Immobilisation of HRP in conducting polymer matrices of PANI and PANI-co-PDTDA were achieved by electrochemical polymerisation. The use of amperometric detection allowed for the coupling of the biosensor with a portable potentiostat system (PalmSens). Differential pulse voltammetry (DPV) as technique was used as a detection method for inhibition determination. Selection of suitable pH values for biosensor performance was evaluated and the system showed optimal performance at pH 6.8 and 7.2 for Pt/PANI/HRP and Pt/PANI-co-PDTDA/HRP biosensors, respectively. The biosensors developed in this work showed

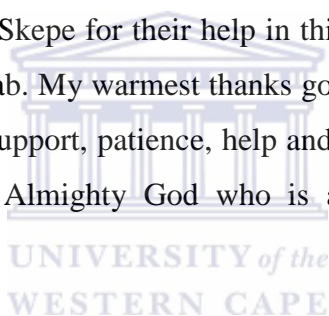
detection limits (LODs) of 0.32 mM and 0.0483 mM for PANI/HRP and PANI-co-PDTDA/HRP, respectively. For the Pt/PANI/HRP biosensor, the apparent Michaelis-Menten constant ( $K_m^{app}$ ) value and maximum current ( $I_{max}$ ) were evaluated from Lineweaver-Burk plots at various  $H_2O_2$  concentrations. The values were found to be 0.6 mM and 1.7  $\mu A$  for the Pt/PANI/HRP biosensor, while for the Pt/PANI-co-PDTDA/HRP biosensor the results were 0.7 mM and 0.27  $\mu A$ , respectively.

The third section investigated the adsorptive cathodic differential pulse stripping voltammetric (AdDPSV) determination of platinum group metals (PGMs), using an *ex situ* bismuth coated screen printed carbon electrode (SPCE/Bi) as the working electrode and ammonium buffer solution (pH = 9.2) as the supporting electrolyte. The cathodic stripping differential pulse method was used for investigating the electrochemical behaviour and the quantitative analysis of platinum group metals (Pt, Pd and Rh) at the SPCE/Bi surface in the presence of dimethylglyoxime (DMG) as a complexing agent. In order to determine the metals at improved detection limits ensuring repeatability and sensitivity, a complete optimisation study of voltammetric parameters was performed. The proposed method was successfully applied to the determination of the real samples (sediments & water) collected in the platinum mining area in the North-West and Limpopo Provinces, South Africa. The results were compared with those obtained by the glassy carbon bismuth film (GC/BiF) voltammetric and ICP-AES spectrometry techniques. Well-shaped voltammograms with clear peak potentials were obtained in the analysis of the real samples, offering excellent perspectives on the use of the constructed modified electrodes. The calibration curves for all PGMs investigated were linear with the limit of detection (LOD) at approximately 0.008, 0.006, and 0.005  $\mu g.L^{-1}$  for Pd, Pt and Rh, respectively.



## Acknowledgement

This study was conducted at the CSIR in the Department of Natural Resources and the Environment, during the years 2011-2012. Chapter 5 of this thesis wasn't too easy, but seems to be much easier than collecting all the people who have contributed somehow to this thesis and saying "Thanks" in a proper way. I wish to express my special thanks to Dr V.S. Somerset for his guidance, support and encouragement during my study. He also taught me to think independently, helped me to overcome difficulties and supported me to develop other skills beyond Chemistry. I am fortunate to have such a great supervisor whose enthusiasm for chemistry and kindness to people set the norm for me in my future career. My deepest gratitude goes also to Prof. E. Iwuoha for allowing me to be part of the SensorLab, Chemistry Department, University of the Western Cape. I express my special thanks to my friends, Charlton van der Horst and Uthi Skepe for their help in this study, not forgetting to mention the friendships from the SensorLab. My warmest thanks go to my late mother and my family for their understanding, endless support, patience, help and encouragement during my whole life. Last but not least, to the Almighty God who is always with me through all my endeavours.



## **Dedication**

This thesis is dedicated to my mother, Nonkosi Constance Silwana (RIP).



## List of Abbreviations and Acronyms

AAS	Atomic absorption spectrometric
ASV	Anodic stripping voltammetry
AuNPs	Gold nanoparticles
$\mu$ A	Micro amperes
BiFE	Bismuth film electrode
CMEs	Chemical modified electrodes
CNTs	Carbon nanotubes
CP	Conducting polymer
CPEs	Carbon paste electrodes
CPs	Conducting polymers
CSV	Cathodic stripping voltammetry
CV	Cyclic voltammetry
DALYS	Disability adjusted life years
DME	Dropping mercury electrode
DMF	Dimethylformamide
DMG	Dimethylglyoxime
AdDPSV	Adsorptive differential pulse stripping voltammetry
DTDA	Dithiodianiline
Eh	Oxidation-reduction potential
FTIR	Fourier transformed infrared
GCE	Glassy carbon electrode
GC-MS	Gas chromatography-Mass spectrometry
HRP	Horseradish peroxidase
ICP-MS	Inductively coupled plasma mass spectrometry
ICP-OES	Inductively coupled plasma optical emission spectrometry
LOD	Limit of detection
LOQ	Limit of Quantification
MWCNT	Multi-walled carbon nanotube
NPs	Nanoparticles
PANI	Polyaniline
PBS	Phosphate buffer solution
PDTDA	Poly (2,2-dithiodianiline)
Pt	Platinum working electrode
PGMs	Platinum group metals
ppb	Parts per billion
ppm	Parts per million
PPy	Polypyrrole
QDs	Quantum dots
Redox	Reduction –Oxidation
rpm	Rotations per minute
RSD	Relative standard deviation
SCE	Saturated calomel electrode
SPCE	Screen printed carbon electrode
SWASV	Square wave anodic stripping voltammetry
SWCNT	Single-walled carbon nanotube

UV-Vis  
WHO  
WRC

Ultra violet-visible  
World Health Organisation  
Water Research Commission



## List of Publications and Presentations

### Publications

C. Van Der Horst, **B. Silwana**, E. Iwuoha and V. Somerset. (2012). Stripping voltammetric determination of palladium, platinum and rhodium in freshwater and sediment samples from South African water resources. *Journal of Environmental Science and Health*, A47: 2084 – 2093.

**B. Silwana**, C. van der Horst, E. Iwuoha and V. Somerset. (2012). Inhibitive determination of metal ions using a horseradish peroxidase amperometric biosensor. In T. Rinken (Ed.), *State of the Art in Biosensors - Book 2*. (pp. xx-yy). INTECH, Croatia. ISBN 980-953-307-691-6. (*Accepted*).

**B. Silwana**, C. van der Horst, E. Iwuoha and V. Somerset. (2012). Amperometric determination of Cd, Pb, Hg, Pt, Pd and Rh metal ions using a SPCE polymer immobilised horseradish peroxidase biosensor system. *Analytical Letters* (*In preparation*).

### Oral and Poster Presentations at Conferences

**13<sup>th</sup> WaterNet WARFSA GWP-SA International Symposium on Intergrated Water Resource Management.** The Birchwood and OR Tambo conference centre, Johannesburg, South Africa. 31 October – 2 November 2012.

Screen-printed carbon electrodes modified with a bismuth film for stripping voltammetric analysis of environmental samples.

**B. Silwana**, C. van der Horst, E. Iwuoha and V. Somerset

**2nd International Symposium on Electrochemistry Electrochemistry for Energy.**

University of the Western Cape, Bellville, South Africa, 19-20 July 2012

Screen-printed carbon electrodes modified with a bismuth film for stripping voltammetric analysis of environmental samples.

**B. Silwana**, C. van der Horst, E. Iwuoha and V. Somerset

**SETAC Europe 21st Annual Meeting**

Milan, Italy, 15 – 19 May 2011

Assessment of bioaccumulation of platinum group metals in a river system in close proximity to mining activities in South Africa.

Vernon Somerset, Charlton van der Horst, **Bongiwe Silwana**, Chavon Williams and Emmanuel Iwuoha.

## Table of Contents

Declaration.....	i
Summary.....	ii
Acknowledgement.....	iv
Dedication.....	v
List of Abbreviations and Acronyms.....	vi
List of Publications and Presentations.....	viii
Table of Contents.....	ix
List of Figures.....	xiii
1.1 Introduction.....	18
1.1.1 General.....	18
1.2 Electrochemical Sensors.....	19
1.3 Pollutants in the Environment.....	20
1.4 Modified Carbon Electrodes.....	21
1.5 Objectives of the Study.....	23
1.5.1 General Objectives.....	23
1.5.2 Specific Objectives.....	23
1.6 Layout of the Thesis.....	24
2.1 Introduction.....	26
2.2 Electrochemical sensors in environmental applications.....	27
2.3 Types of Electrodes for Heavy Metals Analysis Studies.....	29
2.3.1. Glassy Carbon Electrodes.....	29
2.3.2. Carbon Paste Electrodes.....	30
2.3.3. Screen-Printed Carbon Electrodes.....	31
2.4 Techniques for the Detection and Analysis of Metals.....	33
2.4.1 Spectroscopic techniques for metal detection.....	34
2.4.2 Electrochemical Techniques.....	35
2.4.2.1. Cyclic Voltammetry.....	36
2.4.2.2. Stripping Voltammetry.....	39
2.4.2.3. Chronoamperometry.....	41
2.5 Heavy Metals in the Environment.....	42
2.5.1 Impacts on the Aquatic Ecosystem.....	43
2.5.2 Impacts on Human Health.....	44
2.6 Precious metals in the Environment.....	45
2.6.1 Impacts on the Aquatic Ecosystem.....	46
2.6.2 Impacts on Human Health.....	47
2.7 Modified Electrode Surfaces for Stripping Voltammetry.....	48
2.7.1 Polymer Films.....	52
2.7.2 Biosensors.....	54
2.7.3 Carbon Paste Electrodes.....	56
2.7.4 Thin Metal Films.....	57
2.8 Nanomaterials.....	57
2.8.1 Carbon Nanotubes.....	61
2.8.2 The Gold Nanoparticle.....	64
3.1 Introduction.....	66
3.2. Electro-Analytical Techniques.....	66

3.2.1.1	Cyclic voltammetry (CV).....	68
3.2.1.2	Differential Pulse Voltammetry (DPV).....	69
3.2.1.3	Cathodic Stripping Voltammetry (CSV).....	70
3.2.1.4	Anodic Stripping Voltammetry (ASV).....	71
3.3	Solids or Metal Disc Electrodes.....	71
3.3.1	Carbon Paste Electrode (CPE) Construction.....	72
3.3.2	Screen Printed Carbon Electrodes (SPCE).....	73
3.3.3	Glassy Carbon Electrode (GCE) Construction.....	74
3.4	UV-Vis Spectroscopic Characterisation.....	75
3.5	FTIR Spectroscopic Characterisation.....	77
4.1	Introduction.....	79
4.2	Materials and methods.....	81
4.2.1	Chemicals.....	81
4.2.2	Apparatus.....	82
4.2.3	Electropolymerisation of polymer films.....	82
4.3	Results and Discussion.....	83
4.3.1.	Cyclic voltammetric characterisation of polymer composites.....	83
4.3.1.1.	Cyclic Voltammetric analysis of polyaniline.....	84
4.3.1.2	Cyclic Voltammetric analysis of polyaniline-co-2,2'-dithiodianiline.....	85
4.3.2	Effect of electrolyte concentration.....	87
4.3.3.	Scan rate studies (Brown-Anson analysis).....	88
4.3.3.1.	PANI.....	88
4.3.3.2	PANI-co-PDTDA.....	90
4.4	Electrochemical calculations and characterisation of polymer films.....	91
4.4.1	Brown-Anson analysis.....	91
4.4.1.1	Number of electrons in polymer matrices.....	93
4.4.1.2.	PANI:.....	94
4.4.1.3	PANI-co-PDTDA:.....	95
4.4.1.4	Summary of results for all polymer matrices:.....	96
4.4.2	Surface concentration of the polymer matrices.....	96
4.4.2.1	PANI.....	97
4.4.2.2	Summary of results for surface concentration all polymer matrices:.....	98
4.4.3	Electron transport diffusion coefficient in polymer matrices.....	99
4.4.3.1	PANI.....	99
4.4.3.2	Summary of results for the diffusion coefficients all polymer matrices.....	100
4.4.4	Thickness of the polymer films.....	100
4.4.4.1	PANI.....	101
4.4.4.2	Summary of results for film thickness of all polymer matrices.....	102
4.5.	Spectroscopic characterisation of polymers.....	103
4.5.1	UV-Vis spectroscopic characterisation of polymers.....	103
4.5.2	FTIR spectroscopic characterisation of polymers.....	104
4.6	Summary.....	106
5.1	Introduction.....	107
5.2	Materials and Methods.....	111
5.2.1	Chemicals.....	111
5.2.2	Apparatus.....	112
5.2.3	Construction of Pt/PANI/HRP biosensor.....	112
5.2.4	Biosensor response measurements.....	113
5.2.4.2	Differential pulse voltammetric measurements.....	114
5.3.	Results and discussion.....	115

5.3.1	Optimisation of solution pH.....	115
5.3.2	Cyclic voltammetric characterisation of Pt/PANI/HRP biosensor.....	116
5.3.3	Differential pulse voltammetric characterisation of Pt/PANI/HRP biosensor .....	117
5.3.4	Inhibition of Pt/PANI/HRP biosensor by heavy metals .....	119
5.3.4.1	Inhibition results for lowest metal concentration investigated.....	120
5.3.4.2	Inhibition results for intermediary metal concentration investigated.....	121
5.3.4.3	Inhibition results for highest metal concentration investigated .....	122
5.3.5	Inhibition of Pt/PANI-co-PDTDA/HRP biosensor by heavy metals.....	123
5.3.5.1	Inhibition results for lowest metal concentration investigated.....	123
5.3.5.2	Inhibition results for intermediary metal concentration investigated.....	124
5.3.5.3	Inhibition results for highest metal concentration investigated .....	125
5.3.6	Voltammetric results for Pt/PANI/HRP biosensor .....	127
5.3.6.1	Voltammetric results for Cd inhibition .....	127
5.3.6.2.	Voltammetric results for Pb inhibition.....	130
5.3.6.3	Voltammetric results for Hg inhibition .....	135
5.3.7	Voltammetric results for Pt/PANI-co-PDTDA/HRP biosensor .....	138
5.3.7.1	Differential pulse voltammetric characterisation of Pt/PANI-co-PDTDA/HRP biosensor	139
5.3.7.2	Optimisation of solution pH.....	140
5.3.7.3	Voltammetric results for metal ion inhibition.....	141
5.3.7.3.1	<i>Voltammetric results for Cd inhibition</i> .....	142
5.3.7.3.2	<i>Voltammetric results for Pb inhibition</i> .....	143
5.3.7.3.3	<i>Voltammetric results for Hg inhibition</i> .....	144
5.3.8	Evaluation of biosensor inhibition kinetics.....	145
5.3.8.1	<i>Analysis of PANI/HRP biosensor inhibition kinetics</i> .....	145
5.3.8.2	<i>Analysis of PANI-co-PDTDA/HRP biosensor inhibition kinetics</i> .....	149
5.3.9	Comparison between Pt/PANI/HRP and Pt/PANI-co-PDTDA/HRP biosensors	153
5.4	Summary .....	155
6.1	Introduction.....	156
6.2	Materials and Methods.....	157
6.2.1	Chemicals and reagents.....	157
6.2.2	Apparatus .....	157
6.2.3	Preparation of bismuth film electrode (BiFE) .....	159
6.2.4	Analytical procedure for the determination of PGMs.....	159
6.3.	Results and Discussion .....	160
6.3.1	Characterisation of modified screen-printed electrode surface .....	160
6.3.2	Optimisation of complexing reagent concentration.....	161
6.3.3	Deposition potential optimisation studies.....	163
6.3.4	Deposition time optimisation studies.....	166
6.3.5	Stability testing of the SPCE/BiF electrode.....	168
6.3.6	Analytical features of the adsorptive stripping procedure .....	170
6.3.7	Interference studies .....	177
6.4.	Analytical features of adsorptive stripping voltammetry at a SPCE/BiF sensor...	184
6.4.1	PGMs analysis in freshwater samples.....	184
6.4.2	PGMs analysis in sediment samples.....	186
6.5.	Comparison of calculated results for different sensor platforms .....	188
6.6.	Summary .....	189
7.1.	Conclusion .....	190
7.2.	Recommendations for future work .....	192



8.1 References.....193



## List of Figures

Figure 2.1	Important aspect for choosing electrochemical sensors for environmental monitoring.....	28
Figure 2.2	Typical Dropsense screen printed carbon electrode (Dropsens, 2010). .....	33
Figure 2.3	The two common types of connector that links screen printed electrodes to the potentiostat (Dropsens, 2010). .....	33
Figure 2.4	Flow chart representing electrochemical techniques for sample analysis. ....	36
Figure 2.5	Cyclivc voltametric reaction mechanism (Gosser, 1994). .....	37
Figure 2.6	Typical current response for stripping voltammetry (Wang, 1985). .....	41
Figure 2.7	Typical current response for stripping voltammetry (www.serotonin.ucla.edu/electroanalytical). .....	42
Figure 2.8	Electrocatalysis at modified electrodes; electron transfer mediated reaction between the target analyte and surface-bound catalyst (Wang, 2000). .....	49
Figure 2.9	Schematic principle of operation of a biosensor .....	56
Figure 2.10	Illustration of the application of nanotechnology.....	59
Figure 2.11(a)	The unrolled honeycomb lattice of a SWNTs (b) Roll- up molecular models of SWNTs in different chiralities Nanotube (Odom et al 1998).....	63
Figure 2.12	Solutions of gold nanoparticles of various sizes. The size difference causes differences in colour (nanotechnology eLearning centre, 2012). .....	64
Figure 3.1	Typical instrument for voltammetry (Kalinowski, 2005). .....	67
Figure 3.2	Schematic representation of cyclic voltammetry as an electro-analytical technique (en.wikipedia.org/wiki/cyclic_voltammetry).....	68
Figure 3.3	Schematic representation of DPV as an electro-analytical technique (www.basinc.com) .....	69
Figure 3.4	Commonly used solid disc electrodes (BASi Instruments, USA). .....	72
Figure 3.5	Illustration of carbon paste electrode. ....	74
Figure 3.6	Commonly used screen printed electrodes, (A) carbon, (B) platinum and (c) Gold (www.dropsen.com, accessed on 1 August 2012). .....	74
Figure 3.7	Schematic diagram of a single-beam UV-Vis spectrometer (Tissue, 2001). ....	66
Figure 3.8	Schematic diagram showing working of FTIR spectroscopy (www.macmillan.org.uk, 2010). .....	78
Figure 4.1	Molecular designs of the four oxidation states of Polyaniline (Trividi, 1994)..	80
Figure 4.2	Cyclicvoltammogram (CV) displaying the electropolymerisation of PANI in 1 M HCl solution on a GCE surface. The potential was cycled between -0.2 and +1.1 V (vs. Ag/AgCl) at a scan rate of 60 mV s <sup>-1</sup> for 19 cycles. ....	84
Figure 4.3	Cyclic voltammogram (CV) displaying the electropolymerisation of PANI-co-PDTDA in 1 M H <sub>2</sub> SO <sub>4</sub> on a GCE surface. The potential was cycled between -0.2 and +1.1V (vs. Ag/AgCl) at a scan rate of 60mVs-1 for 19 cycles.....	86
Figure 4.4	Cyclic voltamogram for the electropolymerisation of PANI-co-PDTDA on a GCE at a scan rate of 60 mV s <sup>-1</sup> , using different H <sub>2</sub> SO <sub>4</sub> concentrations. The potential was cycled between -0.2 and +1.1V (vs. Ag/AgCl). .....	87
Figure 4.5	Cyclic voltammogram of PANI coated on GC electrode in 0.1M HCl at various scan rates. The potential was cycled from -0.2 to 1.1 V (vs Ag/AgCl) and 1mA .....	89

Figure 4.6	Cyclic voltammograms of PANI-PDTDA coated on GC electrode in 0.1M HCl at various scan rates, The potential was cycled between – 0.2 and + 1.1V and 1 mA.....	90
Figure 4.7	The graphs of peak current vs. scan rate and peak current vs. square root of scan rate for PANI.....	92
Figure 4.8	The graphs of peak current vs. scan rate and peak current vs. square root of scan rate for PANI-co-PDTDA.....	92
Figure 4.9	UV-VIS spectra of PANI and PANI-co-PDTDA collected on a glassy carbon electrode, comparing the absorption maxima of the different polymer films electrosynthesised. ....	103
Figure 4.10	FTIR spectra of PANI prepared in 1 M HCl solution and PANI-co-PDTDA prepared in three different concentrations of sulphuric acid. ....	104
Figure 5.1	Proposed mechanism of the catalytic redox enzymatic cycle for the transformation of H <sub>2</sub> O <sub>2</sub> as substrate by the HRP enzyme with redox mediated electron transfer to the PANI-modified electrode (Adapted from Iwuoha et al., 2004). ....	109
Figure 5.2	X-ray crystal structure of ferric horseradish peroxidase in (A) and the corresponding chemical structure in (B) (RCSB Protein Database, 2011 accessed on 6 January 2011).....	110
Figure 5.3	Graph displaying the effect of pH on the Pt/PANI/HRP biosensor in 0.1 M phosphate buffer (PB) solutions at various pH values, obtained for experiments performed separately.....	115
Figure 5.4	Results for the CV evaluation and responses of the Pt/PANI/HRP biosensor in the presence of different H <sub>2</sub> O <sub>2</sub> concentrations evaluated in 0.1 M PB (pH = 6.8) solution is shown. The potential was scanned between + 0.4 and – 1.2 V (vs. Ag/AgCl) at a scan rate of 10 mV/s.....	116
Figure 5.5	The cathodic differential pulse voltammograms (DPVs) of the Pt/PANI/HRP biosensor in the presence of different H <sub>2</sub> O <sub>2</sub> concentrations evaluated in 0.1 M PB (pH = 6.8) solution is shown. Experimental conditions were: pulse width, amplitude, 20 mV; potential step, 20 mV.....	117
Figure 5.6	Results obtained for inhibition of the Pt/PANI/HRP biosensor in the presence of sequential aliquots of 0.001 ppb of Cd <sup>2+</sup> , Pb <sup>2+</sup> and Hg <sup>2+</sup> , respectively. The individual metal solution was added sequentially to a 0.1 M PB (pH = 6.8) solution.....	120
Figure 5.7	Results obtained for inhibition of the Pt/PANI/HRP biosensor in the presence of sequential aliquots of 0.005 ppb of Cd <sup>2+</sup> , Pb <sup>2+</sup> and Hg <sup>2+</sup> , respectively. The individual metal solution was added sequentially to a 0.1 M PB (pH = 6.8) solution.....	121
Figure 5.8	Results obtained for inhibition of the Pt/PANI/HRP biosensor in the presence of sequential aliquots of 0.01 ppb of Cd <sup>2+</sup> , Pb <sup>2+</sup> and Hg <sup>2+</sup> , respectively. The individual metal solution was added sequentially to a 0.1 M PB (pH = 6.8) solution.....	122
Figure 5.9	Results obtained for inhibition of the Pt/PANI-co-PDTDA/HRP biosensor in the presence of sequential aliquots of 0.001 ppb of Cd <sup>2+</sup> , Pb <sup>2+</sup> and Hg <sup>2+</sup> , respectively. The individual metal solution was added sequentially to a 0.1 M PB (pH = 6.8) solution.....	124
Figure 5.10	Results obtained for inhibition of the Pt/PANI-co-PDTDA/HRP biosensor in the presence of sequential aliquots of 0.005 ppb of Cd <sup>2+</sup> , Pb <sup>2+</sup> and Hg <sup>2+</sup> ,	

	respectively. The individual metal solution was added sequentially to a 0.1 M PB (pH = 6.8) solution. ....	125
Figure 5.11	Results obtained for inhibition of the Pt/PANI-co-PDTDA/HRP biosensor in the presence of sequential aliquots of 0.01 ppb of Cd <sup>2+</sup> , Pb <sup>2+</sup> and Hg <sup>2+</sup> , respectively. The individual metal solution was added sequentially to a 0.1 M PB (pH = 6.8) solution. ....	126
Figure 5.12	Results for the cathodic differential pulse voltammograms (DPVs) of the Pt/PANI/HRP biosensor in the presence of three different Cd concentrations evaluated in 0.1 M PB (pH = 6.8) solution. In (a) the Cd concentration used was 0.001 ppb, followed by 0.005 ppb in (b) and 0.01 ppb in (c). Experimental conditions were: E pulse, 0.02V; scan rate 0.010V/s; potential step, 0.005 V. ....	127
Figure 5.13	Calibration curves obtained for peak current (I <sub>p</sub> ) vs. Cd concentration with 0.001 ppb Cd in (a), 0.005 ppb Cd in (b) and 0.01ppb Cd in (c). Results were obtained using DPV as technique in a 0.1 M PB (6.8) solution. ....	129
Figure 5.14	Results for the cathodic differential pulse voltammograms (DPVs) of the Pt/PANI/HRP biosensor in the presence of three different Pb concentrations evaluated in 0.1 M PB (pH = 6.8) solution. In (a) the Pb concentration used was 0.001 ppb, followed by 0.005 ppb in (b) and 0.01 ppb in (c). Experimental conditions were: E pulse, 0.02V; scan rate 0.010V/s; potential step, 0.005 V. ....	131
Figure 5.15	Calibration curves obtained for peak current (I <sub>p</sub> ) vs. Pb concentration with 0.001 ppb Pb in (a), 0.005 ppb Pb in (b) and 0.01ppb Pb in(c). Results were obtained using DPV as technique in a 0.1 M PB (pH = 6.8) solution. ....	133
Figure 5.16	Results for the cathodic differential pulse voltammograms (DPVs) of the Pt/PANI/HRP biosensor in the presence of three different Hg concentrations evaluated in 0.1 M PB (pH = 6.8) solution. In (a) the Cd concentration used was 0.001 ppb, followed by 0.005 ppb in (b) and 0.01 ppb in (c). Experimental conditions were: E pulse, 0.02V; scan rate 0.010V/s; potential step, 0.005 V. ....	135
Figure 5.17	Calibration curves obtained for peak current (I <sub>p</sub> ) vs. Hg concentration with 0.001 ppb Hg in (a), 0.005 ppb Hg in (b) and 0.01ppb Hg in (c). Results were obtained using DPV as technique in a 0.1 M PB (pH = 6.8) solution. ....	137
Figure 5.18	The cathodic differential pulse voltammograms (DPVs) in (a) of the Pt/PANI-co-PDTDA/HRP biosensor in the presence of different H <sub>2</sub> O <sub>2</sub> concentrations evaluated in 0.1 M PB (pH = 7.2) solution is shown, with the calibration plot in (b). Experimental conditions were: amplitude, 20Mv; potential step, 20Mv. .	139
Figure 5.19	Graph displaying the effect of pH on the Pt/PANI/HRP biosensor in 0.1 M phosphate buffer solutions (PBS) at various pH values. ....	140
Figure 5.20	Results for the cathodic differential pulse voltammograms (DPVs) of the Pt/PANI-co-PDTDA/HRP biosensor in the presence of 0.001ppb Hg concentrations evaluated in 0.1 M PBS (pH = 7,2. Experimental conditions were: E pulse, 0.02V; scan rate 0.010V/s; potential step, 0.005 V. ....	141
Figure 5.21	Calibration curve obtained for peak current (I <sub>p</sub> ) vs. Hg concentration of 0.01 ppb Hg for the use of the Pt/PANI-co-PDTDA/HRP biosensor in 0.1 M PB (pH = 7.2) solution. ....	142
Figure 5.22	The Line weaver-Burk plot results obtained for the Pt/PANI/HRP biosensor response to successive additions of H <sub>2</sub> O <sub>2</sub> substrate in the absence and presence of Cd <sup>2+</sup> metal ions. ....	145

Figure 5.23	The Lineweaver-Burk plot results obtained for the Pt/PANI/HRP biosensor response to successive additions of H <sub>2</sub> O <sub>2</sub> substrate in the absence and presence of Pb <sup>2+</sup> metal ions.....	146
Figure 5.24	The Lineweaver-Burk plot results obtained for the Pt/PANI/HRP biosensor response to successive additions of H <sub>2</sub> O <sub>2</sub> substrate in the absence and presence of Hg <sup>2+</sup> metal ions.....	147
Figure 5.25	The Lineweaver-Burk plot results obtained for the Pt/PANI-co-PDTDA/HRP biosensor response to successive additions of H <sub>2</sub> O <sub>2</sub> substrate in the absence and presence of Cd <sup>2+</sup> metal ions. ....	150
Figure 5.26	The Lineweaver-Burk plot results obtained for the Pt/PANI-co-PDTDA/HRP biosensor response to successive additions of H <sub>2</sub> O <sub>2</sub> substrate in the absence and presence of Pb <sup>2+</sup> metal ions.....	151
Figure 5.27	The Lineweaver-Burk plot results obtained for the Pt/PANI-co-PDTDA/HRP biosensor response to successive additions of H <sub>2</sub> O <sub>2</sub> substrate in the absence and presence of Hg <sup>2+</sup> metal ions.....	152
Figure 6.1	The photograph showing of a portable PalmSens® electrochemical system and set-up used in this study.....	158
Figure 6.2	Cyclic voltammograms for the SPCE/BiF sensor in different buffer solutions at a scan rate of 0.05 V/s in: (I) 0.01M NH <sub>3</sub> buffer (pH = 9); (II) 0.2 M NaOAc buffer (pH = 4.8); (III) 0.1 M HCl (IV); 1 mM K <sub>3</sub> Fe(CN) <sub>6</sub> ; and (V) 4 x 10 <sup>-3</sup> M LiClO <sub>4</sub> solution.....	1600
Figure 6.3	Comparative DPAdSVs of the various electrodes of: (I) SPCE; (II) SPCE/BIF and; (III) SPCE/BiF/DMG in NH <sub>3</sub> buffer (pH = 9) solution. ....	161
Figure 6.4	Results obtained for the effects of various DMG concentration upon the response to 1 ppb of Pd(II) in (A), Pt(II) in (B) and Rh(III) in (C), collected in the presence of 0.01 M ammonium buffer (pH = 9.2) solution. ....	162
Figure 6.5	Results obtained for effects of deposition potential (E <sub>d</sub> ) upon the peak current responses to 1 ppb of Pd(II) in (A), Pt(II) in (B) and Rh(II) in (C), evaluated in the presence of 0.01 M ammonium buffer (pH = 9.2) solution. ....	165
Figure 6.6	Effects of deposition time (t <sub>d</sub> ) upon the response to 1ppb (A) Rh(II), (B) Pd (II) and (C) Pt(II) in the presence of 0.01M ammonia buffer (pH 9.2) solution....	167
Figure 6.7	Results obtained Stability test of the BiSPCE in 0.01M ammonium buffer of pH 9.2 containing 1ppb of selected PGMs with various DMG concentration E <sub>d</sub> = -0.7V, (vs Ag/AgCl) and t <sub>d</sub> = 120s. ....	169
Figure 6.8	Results obtained for the AdDPVs for the increasing concentrations of Pd(HDMG) <sub>2</sub> (0.01 – 0.1 ppb) evaluated using the SPCE/BiF sensor, with E <sub>d</sub> = -0.7 V and t <sub>d</sub> = 150s. In (B) the calibration curve is shown.....	171
Figure 6.9	Results obtained for the AdDPVs for the increasing concentrations of Pt(HDMG) <sub>2</sub> (0.01 – 0.1 ppb) evaluated using the SPCE/BiF sensor, with E <sub>d</sub> = -0.7 V and t <sub>d</sub> = 150s. In (B) the calibration curve is shown.....	173
Figure 6.10	Results obtained for the AdDPVs for the increasing concentrations of Rh(HDMG) <sub>2</sub> (0.01 – 0.1 ppb) evaluated using the SPCE/BiF sensor, with E <sub>d</sub> = -0.7 V and t <sub>d</sub> = 150s. In (B) the calibration curve is shown.....	174
Figure 6.11	Adsorptive differential pulse cathodic stripping voltammetry for the simultaneous increasing concentrations of Pd - Rh -DMG using BiSPCE from 0.01 – 0.1 ppb, E <sub>d</sub> = -0.7 V and t <sub>d</sub> = 150s. (B) Linear regression curves. ....	175
Figure 6.12	Adsorptive differential pulse cathodic stripping voltammetry for the simultaneous increasing concentrations of Pt - Rh -DMG using BiSPCE from 0.01 – 0.1 ppb, E <sub>d</sub> = -0.7 V and t <sub>d</sub> = 150s (B) linear regression curves.....	176

- Figure 6.13 AdDPSVs obtained for the effect of  $\text{Na}^+$  and  $\text{Fe}^{3+}$  as interfering ions on the stripping voltammetric results for Pd(II) in (A), Pt(II) in (B), and Rh(II) in (C) using the SPCE/BiF sensor. The concentrations of Pd(II), Pt(II) and Rh(II) used were 0.3 ppb in (a), 0.6 ppb in (b) and 0.9 ppb in (c) respectively, with 0.01 M ammonia buffer (pH = 9.2) solution containing  $1 \times 10^{-5}$  DMG solution..... 179
- Figure 6.14 AdDPSVs obtained for the effect of  $\text{PO}_4^{3-}$  and  $\text{SO}_4^{2-}$  as interfering ions on the stripping voltammetric results for Pd(II) in (A), Pt(II) in (B), and Rh(II) in (C) using the SPCE/BiF sensor. The concentrations of Pd(II), Pt(II) and Rh(II) used were 0.3 ppb in (a), 0.6 ppb in (b) and 0.9 ppb in (c) respectively, with 0.01 M ammonia buffer (pH = 9.2) solution containing  $1 \times 10^{-5}$  DMG solution..... 181
- Figure 6.15 AdDPSVs obtained for the effect of  $\text{Co}^{2+}$  and  $\text{Ni}^{2+}$  as interfering ions on the stripping voltammetric results for Pd(II) in (A), Pt(II) in (B), and Rh(II) in (C) using the SPCE/BiF sensor. The concentrations of Pd(II), Pt(II) and Rh(II) used were 0.3 ppb in (a), 0.6 ppb in (b) and 0.9 ppb in (c) respectively, with 0.01 M ammonia buffer (pH = 9.2) solution containing  $1 \times 10^{-5}$  DMG solution..... 183





## List of Tables

Table 4.1	Summary of results for the number of electrons for all electrosynthesised polymer matrices.....	96
Table 4.2	Summary of results of slope and R <sup>2</sup> for all polymer matrices investigated.....	97
Table 4.3	Summary of results for the surface concentration of the polymer matrices.....	98
Table 4.4	Summary of results for electron transport diffusion coefficients in polymer matrices.....	100
Table 4.5	Summary of results for the thickness of the polymer films.....	102
Table 5.1	Performance characteristics of the Pt/PANI/HRP biosensor in the presence of Cd <sup>2+</sup> as inhibitor.....	130
Table 5.2	Performance characteristics of the Pt/PANI/HRP biosensor in the presence of Pb <sup>2+</sup> as inhibitor.....	134
Table 5.3	Performance characteristics of the Pt/PANI/HRP biosensor in the presence of Hg <sup>2+</sup> as inhibitor.....	138
Table 5.4	Performance characteristics of the Pt/PANI-co-PDTDA/HRP biosensor in the presence of Cd <sup>2+</sup> as inhibitor.....	143
Table 5.5	Performance characteristics of the Pt/PANI-co-PDTDA/HRP biosensor in the presence of Pb <sup>2+</sup> as inhibitor.....	143
Table 5.6	Performance characteristics of the Pt/PANI-co-PDTDA/HRP biosensor in the presence of Hg <sup>2+</sup> as inhibitor.....	144
Table 5.7	Apparent Michealis- Menten (K <sub>m</sub> <sup>app</sup> ) values and I <sub>max</sub> parameters obtained in the absence of heavy metals and at different concentrations (IC <sub>50</sub> values) of heavy metals (Cd, Pb and Hg). Results evaluated for the Pt/PANI/HRP biosensor in 0.1 M PB (pH = 6.8) solution is shown.....	148
Table 5.8	Apparent Michealis- Menten (K <sub>m</sub> <sup>app</sup> ) values and I <sub>max</sub> parameters obtained in the absence of heavy metals and at different concentrations (IC <sub>50</sub> values) of heavy metals (Cd, Pb and Hg). Results evaluated for the Pt/PANI-co-PDTDA/HRP biosensor in 0.1 M PB (pH = 7.2) solution is shown.....	153
Table 5.9	Kinetic parameters for the Pt/PANI/HRP and Pt/PANI-co-PDTDA/HRP biosensors.....	154
Table 6.1	Results obtained for the effects of various DMG concentration upon the response to 1 ppb of PGMs Pd(II) , Pt(II) and Rh(III), collected in the presence of 0.01 M ammonium buffer (pH =9.2) solution.....	163
Table 6.2	Summary of the optimal conditions for PGMs determination with the SPCE/BiF sensor platform and DMG as complexing agent.....	170
Table 6.3	Calibration data for the determination of PGMs in the presence of [DMG] = 1 x 10 <sup>-5</sup> M as chelating agent, using the SPCE/BiF sensor and a supporting electrolyte of ammonia buffer (pH = 9.2) solution.....	177
Table 6.4	Results for concentrations of PGMs in freshwater samples obtained using AdDPSV analysis with the SPCE/BiF and GCE/BiF sensors, compared with results from ICP-AES spectrophotometric analysis.....	185
Table 6.5	Results for concentrations of PGMs in sediment fractions obtained using AdDPSV analysis with the SPCE/BiF and GCE/BiF sensors, compared with results from ICP-AES spectrophotometric analysis.....	187
Table 6.6	Results obtained for the analytical parameters of applying the SPCE/BiF and GCE/BiF sensors in the AdDPSV analysis of Pd(II), Pt(II) and Rh(III) in ammonia buffer (pH = 9.2) solution as the supporting electrolyte.....	188

# Chapter 1

## Introduction

---

### 1.1 Introduction

#### 1.1.1 General

As the world population grows, so does the ever-increasing demands on the Earth's natural resources. Every day, millions of tons of inadequately treated sewage and industrial and agricultural wastes are poured into the world's waters. The generation of these waste materials continues and affect the environment in numerous ways, most importantly river pollution and disturbance of aquatic ecosystems. This places more pressure on relevant water utility companies to maintain the quality of drinking water from its sources (surface and ground waters) to final distribution, because of waterborne chemicals entering the rivers and streams causing tremendous destruction. There is a constant need for analytical techniques that provide a new breakthrough, allowing better monitoring of environmental pollutants. The rapid development of science and technology has created an overwhelming stream of opportunities for improving and enhancing the quality of human life. A significant amount of development is taking place in the area of electrochemical sensors using various voltammetric electrochemical techniques for the determination of environmental pollutants. These offer advantages over traditional techniques, e.g. spectrometry, for fresh and groundwater monitoring because of their relative cost and are considered to be portable and fast-responding.

The focus of the thesis is on the development and evaluation of sensors based on electrochemical or biological recognition processes. Simple electrochemical techniques fall into three groups: potentiometry, conductivity, voltammetric / amperometric techniques.



This thesis is mostly concerned with the third type of method, the design of this study involves the synthesis and characterisation of new electrochemical sensor material and biosensors with enzyme and controlled surface structure and chemical activity towards metal-contaminated waste-water monitoring. This study also assesses and quantifies other metal ion contamination within the aquatic environment. A quantitative determination of heavy metals associated with platinum group metals (PGMs) is acquired using carbon modified electrodes, while other heavy metals such as lead (Pb), cadmium (Cd) and mercury (Hg) are determined with the use of a horseradish peroxidase (HRP) immobilised on polyaniline.

## 1.2 Electrochemical Sensors

The capability to detect and monitor contaminants in fresh and groundwater using real-time *in situ* measurements promises to be a valuable tool in the environmental industry. Chemical sensors and biosensors are very powerful tools in modern analytical sciences. The new demands of environmental analysis have driven the development of more selective and sensitive sensing systems. An essential component of any detection system is a recognition platform, which is able to bind selectively to a target analyte in the presence of competing analytes. The development of chemical sensors and biosensors to provide *in situ* information on water pollution parameters will eliminate many problems and significantly lower costs associated with conventional sampling and analysis techniques. The main advantages are easy construction, possibility of portability and miniaturisation, high sensitivity and low costs (Dennison and Turner, 1995; Thevenot *et al.*, 1999).

A chemical sensor is defined in Eggins (2002) as a device which responds to a particular biological analyte or chemical species in a selective way through a chemical reaction and can be used for the qualitative and quantitative determination of the analyte. Biosensors can be defined as a device incorporating a biological sensing element connected to a transducer. The history of biosensor began in 1962 with the development of the first device by Clark and Lyons (1967).

Advancement in science and technology has enabled biosensors to be used in a wide variety of disciplines, including medicine, food industry, and environmental science. Nowadays, the main interest of developing chemical and biosensor research field pointed to semiconductors nanomaterials due to their excellent properties (Poltolsky *et al.*, 2006; Cui *et al.*, 2001).

### 1.3 Pollutants in the Environment

In recent years, increased concerns with the toxic effects of chemicals in the environment have led to the necessity of monitoring pollutant levels at various points in industrial processes and recycling processes, in effluents and wastewaters, and at industrial, agricultural, and urban sites. After the industrial revolution and the increase in chemical technologies, concern for minimisation of pollutants and alternative “clean technologies”, have become the common world strategy. The control process started with tighter environmental legislation that was introduced in order to minimise the release of harmful pollutants into the environment. Consequently, the numbers of sites that need to be sampled and monitored for effective environmental monitoring have increased. Additionally, continuous monitoring of environmental pollution in the field requires portable fast-response sensors that are robust and with sufficient sensitivity and long lifetime (Wang *et al.*, 2008).

Agricultural practices affect natural habitats in several ways, such as through land conservation, increased fragmentation and agrochemical contamination (Hayes *et al.*, 2002; Davidson *et al.*, 2002). Since then over 900 pesticides are used throughout the world, screening approaches are being developed to analyse as many pesticides as possible.

Heavy metals are well known to inhibit the activity of enzymes and application of this phenomenon to the determination of these hazardous toxic elements offers several advantages such as simplicity and sensitivity (Rodriguez-Mozaz *et al.*, 2006). Heavy metals such as cadmium (Cd), lead (Pb) and mercury (Hg) present major hazards to ecosystems and are serious danger to humans, because of their ability to accumulate in living organisms (Mehrvar *et al.*, 2000).

The concentration of platinum group metals (PGMs) have been increased in the environment due to the increasing use of autocatalytic converters and in some industrial processes (Locatelli, 2006). In fact use of autocatalytic converters, containing PGMs have been the cause of increasing such amounts of the metals in the environment and resulted to the decrease of pollution like lead, carbon monoxide, nitrogen oxide and unburned hydrocarbons in exhaust gases from motor vehicles.

Due to increasing demand of the toxicity of these metals in soil, environmental companies and pollution monitoring agencies have expressed the need (Farrel-Poe, 2000) for reliable approved procedures for the determination of these elements. However, at this point, its concentration still remains at relatively low level so the methods used for its determination should be highly sensitive. (Bobrowski *et al.*, 2009). The toxicity of platinum group metals has been investigated in various studies: in the metallic states, PGMs are non-toxic and non-allergenic, but some of their compounds, especially the chlorinated ones, are very toxic and allergenic (WHO, 1991; WHO, 2002). Information of the acute toxicity of some Pt-chlorinated salts and evidence of DNA damage due to Pt exposure have been observed both *in vitro* and *in vivo* (Gagnon *et al.*, 2006).

#### **1.4 Modified Carbon Electrodes**

A field of modified solid electrode surface has become very popular with applications in industries, quality control of drug and food, determinations in pharmaceutical dosage forms. The performance of the voltammetric procedure is influenced by the material of working electrode. Carbon-based electrodes usually have wider potential range than the other solid electrodes because their broad potential window, low back ground current, rich surface area, chemically inertness, low cost and suitability for various sensing and detection applications. However electron transfer rates observed at carbon are often slower than those observed on noble metal electrodes (Uslu *et al.*, 2007).

A variety of methods for the modification of electrode surfaces have been developed in the last decades and a number of them possess interesting properties for electrochemical, electronic and electrocatalytic purposes. Electrodes are usually chemically modified using one of four approaches: (i) chemisorption; (ii) covalent bonding; (iii) polymer film coating; and (iv) composite configuration (Wang, 2006). Carbon modified electrodes (CMEs) can also contain multiple chemical modifiers, and sometimes these modifiers and / or the electrode substrate may have a particularly designed spatial configuration. That is, a CME may contain one electrocatalyst that reacts with a substrate or acts as a photon donor or acceptor, and a second one to transport charge between the first catalyst and the electrode.

Alternatively, the carbon modified electrode (CME) may consist of a substrate coated with two different chemical polymers, the second polymer overlaid on the first to form a bilayer of polymer films. Carbonaceous substrates have already been utilised as electrode material, due to their rather attractive electrochemical properties (Vytras *et al.*, 2009; Tang *et al.*, 2009). However, it is well known that variations in the performances of these electrodes are to be expected depending on the source of the material the percentage of graphite in the substrate the type of pasting liquid or impregnating agent used. In comparison to metallic electrodes, carbon material has some extraordinary features relating to their structures and electrochemistry (McCreery, 2008).

Basically, the modification of an electrode surface involves immobilisation of reagents that change the electrochemical characteristics of the bare surface. Inclusion of reagents within the electrode matrix (e.g. carbon paste) is another attractive approach for modifying electrodes. Such manipulation of the molecular composition of the electrode thus allows one to tailor the electrochemical response to meet specific sensing needs. Sensors based on modified electrodes have been the focus of research in the last few decades, such as the preparation of structured interfaces holding great promise for the task of environmental monitoring. There are different directions by which the resulting modified electrodes can benefit environmental analysis, including acceleration of electron-transfer reactions, preferential accumulation or permselective transport (Wang, 2006).

## 1.5 Objectives of the Study

### 1.5.1 General Objectives

This work formed part of a research project conducted for the Water Research Commission (WRC) on the development of an analytical sensor for the assessment of heavy and precious metal pollution in the vicinity of mining sites. Furthermore, it is hoped that it will contribute to the development of the CSIRs and South Africa's capacity as a major role player in trace metal pollution assessment (Somerset, 2009). This research focused on the development of sensors and immobilisation methods that will contribute to the construction of reliable and sensitive electrochemical sensors for the detection of metals associated with mining activities in the environment.

### 1.5.2 Specific Objectives

The objectives of this study can be summarised as:

- To construct and develop various sensors and simple methods for the voltammetric determination of heavy and precious metals voltammetric techniques with special attention to the optimisation of experimental conditions.
- To electropolymerise polymers such as polyaniline (PANI) and poly (2,2'-dithiodianiline) (PANI-co-PDTDA) by employing a dopant during synthesis and characterise the synthesised polymers using cyclic voltammetry (CV), Fourier-transformed infrared spectroscopy (FTIR) and ultra-violet visible (UV-VIS) spectroscopy.
- To design, develop and synthesise modified electrochemical sensors with controlled surface structure and chemical activity towards specific metal ions under investigation in this study.
- To develop and evaluate an enzyme biosensor based on horseradish peroxidase (HRP) immobilisation onto the surface of a platinum electrode modified with either PANI or PANI-co-PDTDA, followed by electrochemical interrogation and application of the Pt/PANI/HRP and Pt/PANI-co-PDTDA/HRP sensors for metal determination.

- To develop and optimise voltammetric methods for the integration, testing and application the new developed sensors formats into a portable potentiostat for possible on-site analysis of identified heavy and precious metals.
- To apply the developed Pt/polymer/HRP biosensor in inhibition studies for the voltammetric determination of selected heavy metals.
- To construct, optimise and apply a bismuth (Bi) thin film screen-printed carbon electrode (SPCE/BiF) and disposable sensor for the analysis of palladium (Pd), platinum (Pt) and rhodium (Rh) in environmental samples.

## 1.6 Layout of the Thesis

The thesis is arranged and presented in such a manner that the reader can understand the scope and goals of the research in a logical approach. Therefore, the structure of this thesis has been divided into eight chapters according to the different areas of investigation that has been conducted.

- Chapter 1 Gives a general introduction, the main objectives of the study as well as an overview of the thesis.
- Chapter 2 Provides a review of available literature regarding the monitoring of metal pollutants using voltammetric methods. This chapter provides a general overview of electrochemical sensors and techniques, electrode modifications, biosensors, analytes to be investigated such as heavy and precious metals.
- Chapter 3 The details of the experimental procedures used to prepare the selected electrochemical sensors and the electrochemical techniques used for characterisation and investigation is discussed.

- Chapter 4 The electrochemical characterisations of the polymer modified electrode surfaces are discussed. The focus of this chapter is on surface modification using electro-polymerisation with polymers in order to functionalise the sensor surface and apply voltammetric determination of metal ions.
- Chapter 5 Focus on the development and characterisation of a horseradish peroxidase (HRP) biosensor in order to conduct inhibition studies for voltammetric determination of selected heavy metals.
- Chapter 6 Modification of screen-printed electrode surfaces and sensor optimisation studies to determine the effect of reagent concentration, supporting electrolyte concentration, chelating reagent concentration for voltammetric determination of PGMs. Application of the constructed screen-printed carbon electrode sensor surface, modified with a bismuth thin film to the determination of PGMs in environmental samples.
- Chapter 7 Conclusions, Recommendations and Future work.
- Chapter 8 References

## Chapter 2

### Literature Review

---

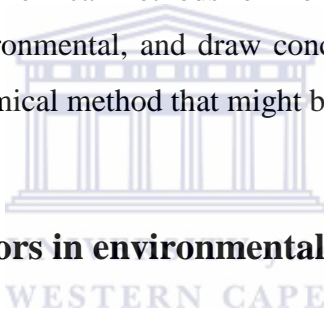
#### 2.1 Introduction

This chapter covers relevant literature in research on the presence and environmental concerns of heavy metals and platinum group metals (PGMs) in the environment. It further covers relevant literature on electro-analytical techniques for the monitoring of these metals in sample matrices. New methods must therefore be developed to detect and quantify these compounds in environmental samples such as water, sediments and biotas. A range of analytical techniques have been applied to the analysis and detection of heavy metals and PGMs in samples and include flame atomic absorption (FLAA), inductive coupled plasma-optical emission spectroscopy (ICP-OES), inductive coupled plasma-mass spectrometry (ICP-MS) and neutron activation analysis (NAA). This chapter also includes a historical overview of previous research, a description of the evaluation of various techniques, and some ways of preventing these pollutants from entering the aquatic environment. The challenges of water in the 21<sup>st</sup> century are one on both quantity and quality, research in this field is concerned with the development of the modified electro-analytical sensors, highlighting the link between clean water and public health and the health of the wider environment. As a result of mismanagement, much of the water available in developed economies is polluted and contaminated to varying levels. It is, of course, also necessary to consider the problem from an economical point of view due to the mass application of instrument techniques. Highly sensitive physical methods are using very expensive instrumentation, which frequently cannot be used as field equipment, from a practical and cost perspective. The instrumentation for environmental monitoring should be easy to operate and not only require personnel with university training to do so. The requirement is met especially well by electrochemical methods because of their sensitivity, simplicity and relatively low investment outlay as well as possible field application.



In view of the fact that electrochemistry combines the extremely high sensitivity, relatively low cost and possibility of construction of the field instrument, it can be concluded that it cannot be surpassed by any other methods, in most cases important in the environmental protection. There are methods the sensitivity of which might equal that of modern electrochemical techniques, they do need, however, extremely expensive equipment mostly in capable of field operation.

In recent years, few environmental issues have aroused the concern of the public in relation to the human health and aquatic organisms. In spite of the many published studies on the subject of heavy metals and human health, there remains deep controversy surrounding this issue. To understand this controversial issue it is helpful to look at the history of heavy metals and PGMs that causes risk to human health and aquatic environment. This research will try to develop simple electrochemical methods for monitoring of heavy metals associated with precious metals in the environmental, and draw conclusions as to the true and simple long- term monitoring electrochemical method that might be used.



## 2.2 Electrochemical sensors in environmental applications

Research has been done on detection of heavy metals associated with PGMs and the researchers have used variety of biosensors and chemical sensors with various modifications of working electrodes. The basic components of an electrochemical sensor are a working (or sensing) electrode, a counter electrode and usually a reference electrode as well. These electrodes are enclosed in the sensor housing in contact with a liquid electrolyte. The working electrode is on the inner face of a Teflon membrane that is porous to gas, but impermeable to the electrolyte. Nowadays many industrial processes produce waste products that contain hazardous chemicals, and these are sometimes discharged directly into sewers, rivers or wetlands. Even those waste products that are disposed of in landfills or slag heaps, for example, may release substances that eventually seep into nearby watercourses (Oberholster *et al.*, 2008). Figure 2.1 shows some important aspect to choose when using electrochemical sensor for environmental monitoring.

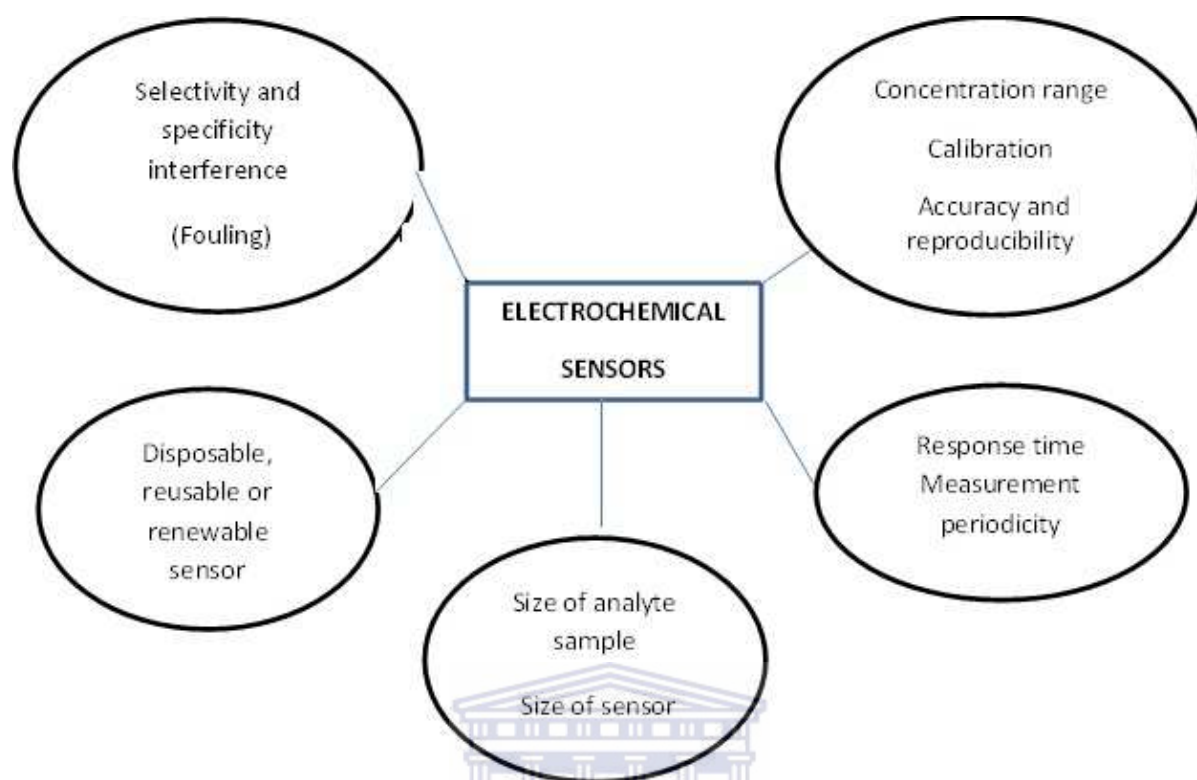


Figure 2.1 Important aspects for choosing electrochemical sensors for environmental monitoring.

Legislation has fostered a huge demand for the sensors necessary in environmental monitoring, e.g. monitoring toxic gases and vapours in the work place or contaminants in natural waters originating from industrial effluents and runoff from agriculture fields, thus, a near revolution is apparent in sensor research giving birth to a large number of sensor devices for medical and environmental technologies. Electrochemical sensors are developed in order to provide information on our physical, chemical and biological environment. It is also known that a chemical sensor furnishes information about its environment and consists of a physical transducer and a chemically selective layer that will interact with the pollutant of choice to provide analytical data on that chosen pollutant (Bonting, 1992). The recent development and application of modified electrodes in sensor construction, in which catalytic species are attached on the electrode surface, has increased the scope of electro catalytic reactions and sensor applications.

This present work attempts to describe the development of both a chemical and biosensor and its application to the determination of heavy metals and PGMs in environmental samples, respectively.

The work described in this thesis is further concerned with methods that can be used for the monitoring of pollutants in different fields of environmental research and protection. Particular emphasis is placed on the electrochemical techniques offering an actual advantage (in comparison with other non-electrochemical methods) if applied to environmental sample analysis. The purpose of a chemical sensor is to transform chemical information ranging from concentration of a specific sample component to total composition of its surrounding environment (Monk, D.J and Walt, D.R., 2004, Janata, 1992).

## **2.3 Types of Electrodes for Heavy Metals Analysis Studies**

Non-traditional electrode materials have played a very useful role in environmental electro-analysis. Portability and non-toxicity have made them useful substitutes of mercury electrodes for electro-analytical monitoring of electrochemically reducible substances and their mechanical properties makes them compatible with measurements in flow system devices. Among the carbon-based electrodes that can be modified not only on the surface but also in bulk during their preparation, carbon paste electrodes (CPE) and screen-printed carbon electrodes (SPCE) belong to the most frequent choice. For modifications, various organic and inorganic compounds can be employed, including metal oxides that are preferably used as bulk modifiers and mediators in the configurations of biosensors. Some of the electrodes that might be used in such applications are discussed in the section below.

### **2.3.1. Glassy Carbon Electrodes**

Carbonaceous electrodes have been used in electro-analytical fields in which they are most often employed for voltammetric measurements and have been very popular because of its excellent electrical and mechanical properties, wide potential range, extremely chemical inertness and relatively reproducible performance the measurement results with the graphite electrode are irreproducible because of its great porosity (Brainina, 1993).

However, much more reproducible results were obtained with the pyrolytic graphite electrode used as an inert redox electrode in redox titration.

Glassy-carbon electrodes are prepared by means of a carefully controlled heating program of pre-modelled polymeric resin body in an inert atmosphere (Wang, 2006). Unlike many non-graphitising carbons, it is impermeable to gases and also highly resistant to acid attack. The structure of glassy carbon consists of graphite planes randomly organised in a complex topology. Glassy carbon possesses isotropic properties and does not require a particular orientation in the electrode device. The performance of the electrode depends on the polishing materials and the procedures. Surface treatment is usually employed to create active and reproducible surface of the glassy carbon electrode and to enhance its analytical performance. Some additional activation steps have also been used to enhance the performance such as electro-chemical, chemical, vacuum heat, or laser treatment (Kessinger *et al.*, 1996; Uslu *et al.*, 2007). The properties of carbonaceous materials depend on the manufacturing process. Carbonaceous electrodes have been used in biomedical fields because of their good conductivity, chemical inertness and mechanical stability.

### 2.3.2. Carbon Paste Electrodes

Carbon paste electrodes (CPEs) represent of more general class of composite electrodes, in which chemically useful functionalities can be introduced during physical mixing of graphite and pasting liquids. Carbon paste electrodes (CPEs) and related sensors underwent an attractive development in the last few decades. CPEs have been employed mainly in studying the mechanisms of electrode reactions of various organic compounds and their utilisation in analytical electrochemistry are well documented in more than 1500 original papers (Wang, 2001).

The carbon paste electrodes are classified as bare or unmodified carbon electrodes. The composite nature of carbon pastes and their easy preparation were undoubtedly stimulating factors for altering the properties of originally binary mixtures and adding another component in the composition. The pasting liquid is chosen for inertness, low solubility in the studied solvent and low volatility (Kalcher *et al.*, 1995).

The first type containing an organic substance dissolved in the binder and was applied to the study the electrode behavior of the substance itself and was considered as a pioneering step in the field of carbon paste electro-active electrodes.

The second electrode was prepared by simply mixing a modifier together with graphite-binder paste and the main reason is for improving the electrode with desired performance (Kalcher *et al.*, 2006; Svancara *et al.*, 2001).

The application of this electrode opened various applications for electrochemistry as a field and its application to numerous sensing applications, was the driving force to minimize the cost of measurements. These electrodes also offer numerous advantages that include: a wide working potential window in both the positive and negative direction; easy working surface renewal; low background currents; and reasonable repeatability (Barek *et al.*, 2001). From 2001 onwards, several new reviews appeared covering the monitoring of environmental carcinogens with the use of CPE (together with other types of electrodes) and amperometric biosensors for environmental samples (Vytras *et al.*, 2009;).

### 2.3.3. Screen-Printed Carbon Electrodes

The attractive mass production of cheap and disposable sensors is the screen-printing technology. Electrode materials other than carbon such have been successfully utilised for the manufacture of screen-printed metals sensors. Principally, these have focused on the application of Au, Ag and Pt. In addition many research laboratories in universities possess screen printing facilities for in-house production of sensors for prototype devices (Honeychurch *et al.*, 2003). The use of screen-printed electrodes (SPEs) in conjunction with portable, electrochemical instrumentation greatly facilitates the feasibility of on-site testing (Honeychurch *et al.*, 2012). Disposable carbon electrodes have a typical complete electrochemical cell configuration, *i.e.* they combine the working, reference and auxiliary electrode together and are highly suitable for working with micro volumes and decentralized assays or to develop specific sensors by modifying their surface with various materials.

The main advantage of screen printed carbon electrode over conventional carbon based electrodes is that the problems of carry over and surface fouling are alleviated, as they are only used once and then discarded. These electrodes clearly have economic benefits when such analytical systems are operated by unskilled people. (Uslu et al., 2007; Eggins, 2002).

The main disadvantage of commercial ink formulations is that their compositions are usually unknown as an intellectual property of the producer and some of the ink components may affect the electrochemical properties of the working electrode (Wang *et al.*, 1998) The typical screen printed carbon electrode by Dropsens® is based on a ceramic substrate with dimensions: (H) 33 x (L) 10 x (W) 0.5 mm; electric contacts: silver. The electrochemical cell consists of a *working electrode* (WE): carbon (4 mm diameter), *counter electrode* (CE): carbon and *reference electrode* (RE). The screen printed electrode is connected to any model of potentiostat by a special type of connector which is manufactured by Dropsens that acts as bridge between the screen-printed electrode and potentiostat ([www.dropsen.com](http://www.dropsen.com)). Figure 2.2 show a typical screen printed electrode and the two kinds of connector used for screen-printed carbon electrodes are shown in Figure 2.3. The sample is usually applied on the working electrode part in the form of small drop on *in-situ* or in the laboratory for stripping analysis of environmental or biological samples. Kadara and Tothill (2005) fabricated single use Bi preplated SPCEs for the voltammetric stripping analysis of Pb (II) and Cd (II), obtaining detection limits of 8 and 10 ng mL<sup>-1</sup> in soil extracts and waste waters for Cd (II) and Pb (II) respectively. Screen-printed carbon working electrodes (SPCEs) have been also explored as supports for Bi modification, including Bi codeposition (so called “in situ” Bi film) and preplated Bi (so called “ex situ” Bi film) approaches. Wang *et al.* (2001) described anodic stripping procedures for lead on home-made Bi preplated disposable SPCEs for the quantification of trace Pb (II) in drinking water by anodic stripping with a detection limit of 0.3 ng mL<sup>-1</sup>.

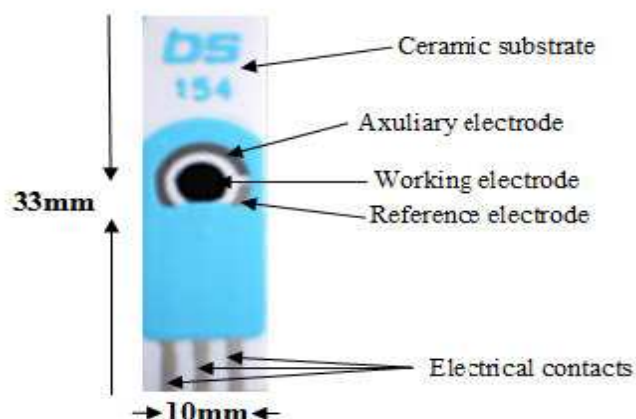


Figure 1.2 Typical Dropsense screen printed carbon electrode (Dropsens, 2010).



Figure 2.2 The two common types of connector that links screen printed electrodes to the potentiostat (Dropsens, 2010).

## 2.4 Techniques for the Detection and Analysis of Metals

Past investigations which are known have been conducted on traditional Analytical methods and electroanalytical method for analysing of metals. This thesis has been focused on the voltammetric measurements that have been sparked by its ability to measure 4 – 6 trace metals simultaneously at concentration level part per billion without chemical separation or prior treatment of sample; carbonaceous and platinum electrodes are employed. The advantage to this method of surface testing over traditional techniques is that the analysis may be performed on site in about 5 minutes without sending a sample to the laboratory.



### 2.4.1 Spectroscopic techniques for metal detection

The monitoring of heavy metals associated with PGMs` s negative effects requires a systematic control of their content remaining in agricultural products, food, soil and water. The content of these metals in various matrices can be determined by a number of methods. Traditional analytical techniques such as atomic absorption spectroscopy (AAS), inductively coupled plasma mass spectrometry (ICP-MS), neutron activation (NAA), etc. can be employed for the bio-monitoring of heavy metals but have expensive running costs with the samples requiring extensive sample digestion / pre-treatments.

However, optical and electrochemical methods of determination have also developed with this purpose (Liorent-Martinez *et al.*, 2010). Among spectroscopic competitors, only flame atomic absorption has nearly the same sensitivity but at much cost and Neutron activation has an overall elemental coverage but also at high costs (Wang, 1985). Multi-residue metal analysis requires a method with the inherent capability of separating analytes from one another to facilitate individual identification and measurement. The advantage of traditional techniques compared to voltammetric technique is that they are applicable to a large number of elements. Their major drawbacks are their much higher cost and, above all, the fact that they allow measurement of total concentration only (Buffle *et al.*, 2005). Consequently, speciation measurements, using these detection techniques, are feasible only by coupling them with separation and extraction procedures. However, such steps significantly increase the risk of contaminations or chemical species modification during sample storage or sample handling, dramatically increase the cost of analysis. This is a major barrier to their application to routine speciation measurements on large sample sets, even though it would be the only means to interpret correctly the environmental impact of metals. The spectroscopic methods generally provide data on the elemental composition of particulate matter. The underlying principle of spectroscopy is the absorption and emission of energy.



## 2.4.2 Electrochemical Techniques

Electroanalytical methods, particularly stripping analysis, are the most widely used competition for atomic spectroscopy, as far as trace metal determination are concerned. The electrode itself can act as a reactant to pump (reduction) /withdraw (oxidation) electron in the reaction, which cannot be expected in spectroscopic characterization methods. Electroanalysis is a methodology which is extremely useful for the portable, sensitive and selective determination of heavy metals. For example, electro-analysis can offer high throughput screening of heavy metals in river water samples at trace levels.

The main trends on modern electroanalysis include development of chemical and biochemical sensors of molecular recognised and development measuring devices of large integration scale, including sensor array nanomaterials and nanostructures development of sufficiently sensitive and selective voltammetric and amperometric methods of electrochemistry (Trajawnowicz, 2009). The voltametric techniques which are referred to voltammetric and chronoamperometric techniques are well suited for automatic in situ speciation measurements, with no or minimum sample change, i.e. under conditions that dramatically minimize contaminations by reagents or losses by adsorption on containers (Buffle *et al.*, 2000). Generally electrochemical methods are based on the transformation of chemical information into an analytically useful signal. Any sensor used in electro-analytical determination contains two basic functional units; one receptor part, which transforms the chemical information into a form of energy and one transducer part which transforms the energy, bearing chemical information, into a useful signal. The flow chart presented in Figure 2.4 illustrates the classes and sub-divisions of electrochemical techniques.

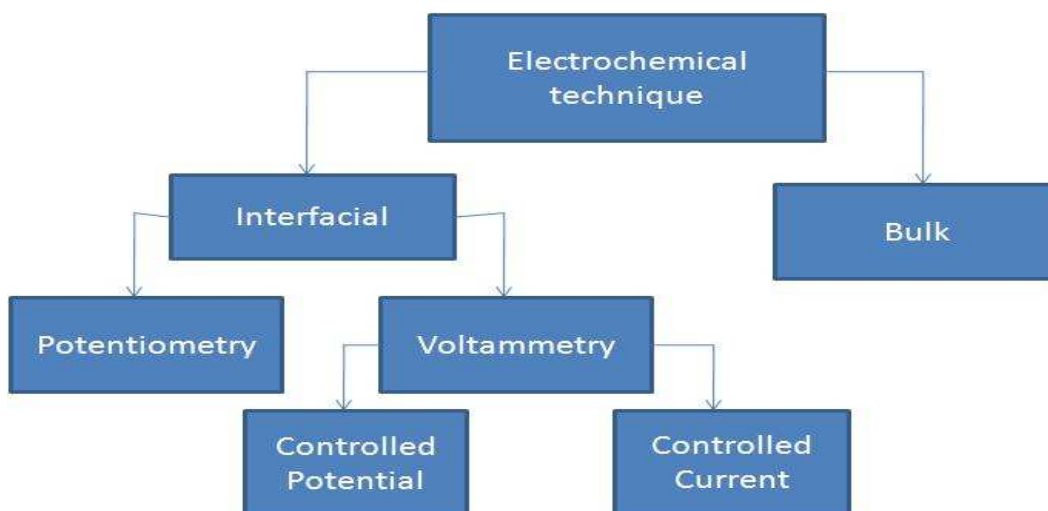


**Figure 2.3** Flow chart representing electrochemical techniques for sample analysis.

This project focused in voltammetric method which is the division of interfacial. Voltammetric techniques may be further divided into controlled potential and controlled current method. Frequently used techniques such as votammetry and chronoamperometry are an example of controlled potential. It involves controlling the potential while measuring the current. The electrode or the faradaic current or both are change with time and there is interrelationship between all three of these variables (Bond *et al.*, 1989). The advantage of this technique includes high sensitivity and selectivity towards electro-active species, portable and low cost instrumentation.

#### 2.4.2.1. Cyclic Voltammetry

Cyclic voltammetry is not sensitive enough for environmental analysis but it is the popular method used in many areas of chemistry and is useful to optimise analytical conditions. It is rarely used for quantitative determinations but widely used for the study of redox processes, electrode mechanism, for the study of intermediate reactions and for obtaining stability of reaction products. It was first practiced at a hanging mercury drop electrode was used and mainly when solid electrodes like platinum (Pt), gold (Au) and carbonaceous were used, particularly to study anodic oxidations (Kemula *et.al.* 1958; Adam, 1968). Several monographs and texts offer excellent information on fundamentals of cyclic voltammetry.

Samples used in this technique should be dissolved in the liquid solvent and capable of being reduced and oxidized within the potential range and should not react with electrode materials. In this technique the working electrode potential is ramped linearly versus time like linear sweep voltammetry. When cyclic voltammetry reaches a set potential, the working electrode's potential ramp is inverted. This inversion can happen multiple times during a single experiment. The potentials at which reversal takes place are called switching potentials. The range of switching potential chosen for a given experiment is one in which a diffusion-controlled oxidation or reduction of one or more analytes occurs. A scan in the direction of more negative potentials is termed a forward scan while one in the opposite direction is called a reverse scan.

The current at the working electrode is plotted versus the applied voltage to give the cyclic voltammogram of results. Cyclic voltammetry is generally used to study the electrochemical properties of an analyte in solution. The response obtained from a CV can be very simple, as shown in Figure 5 for the reversible redox system.

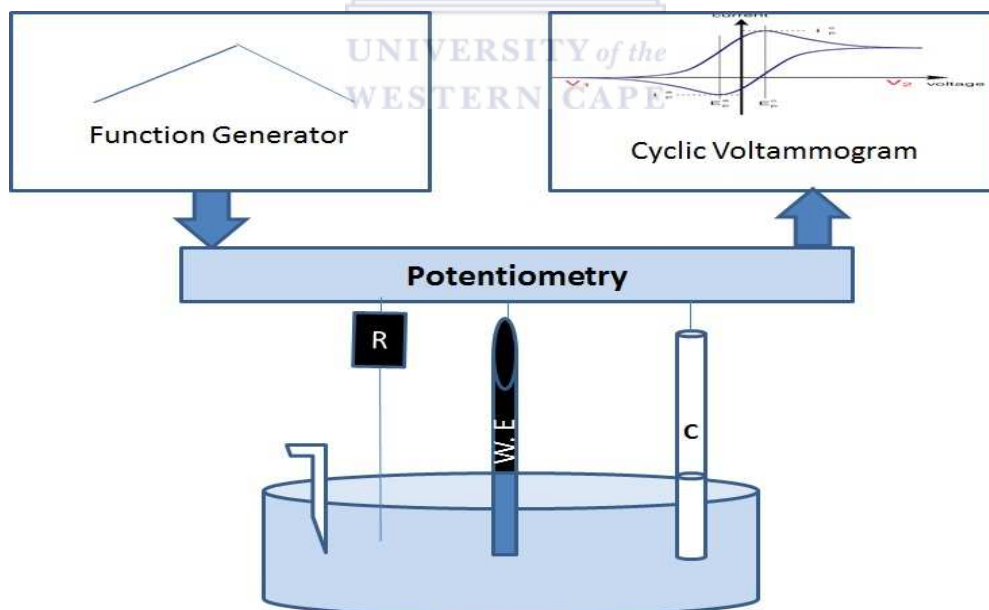


Figure 2.5 Cyclivc voltametric reaction mechanisms (Gosser, 1994).

From the graph in Figure 2.5 the scan shown cyclic voltammogram containing only one species, starting at positive potential, up to some positive switching value, at which the scan is reversed back to the starting potential.

The difference between peak potential ( $E_p$ ) and the point where current is half that at  $E_p$ , halfway potential ( $E_{p/2}$ ), is  $56.5/n$  mV at 25 °C, where  $n$  is the number of electrons transferred. Note that for a Nernstian system,  $E_p$  should be independent of scan rate, but  $I_p$  will depend on the square root of scan rate. Another useful piece of information is that the separation of anodic and cathodic peaks is about  $(59/n)$  mV at 25 °C. It is very difficult to achieve a  $59/n$  mV splitting at most solid electrodes. (If you can achieve 70 mV, you will be doing well. This is a function of electrode preparation as well as scan rate.) If the diffusion constants for the oxidized and reduced species are similar, the value of peak potential ( $E^0$ ) can be estimated from the average of anodic peak potential ( $E_{pa}$ ) and cathodic peak potential ( $E_{pc}$ ). Providing that the charge-transfer reaction is reversible, that there is no surface interaction between the electrode and the reagents, and that the redox products are stable (at least in the time frame of the experiment).

A theoretical description of polarization overpotential is in part described by the Butler-Volmer equation and Cottrell equation. Conveniently in an ideal system the relationship reduces to:

$$E_{pc} - E_{pa} = \frac{57mV}{n} \quad (\text{Eqn. 2.1})$$

For an  $n$  electron process, reversible couples will display a ratio of the peak currents passed at reduction ( $I_{pc}$ ) and oxidation ( $I_{pa}$ ) that is near unity ( $1 = I_{pa}/I_{pc}$ ). When such reversible peaks are observed thermodynamic information in the form of half-cell potential  $E^0_{1/2}$  can be determined. The peak current is given by the equation:

$$I_p = 2.69 \times 10^5 n^{3/2} A C D^{1/2} n^{1/2} \quad (\text{Eqn. 2.2})$$

Where:  $n$  = number of electrons transferred/molecule;  $A$  = electrode surface area ( $\text{cm}^2$ );  $C$  = concentration ( $\text{mol cm}^{-3}$ ) and  $D$  = diffusion coefficient ( $\text{cm}^2 \text{s}^{-1}$ ).

### 2.4.2.2. Stripping Voltammetry

The most sensitive electro-analytical technique, stripping analysis, is highly suitable for the task of field monitoring of toxic metals and is well known for measuring 4-6 trace metals at low concentration levels. In recent years it has become a widely used method for food analysis. This electrochemical method encompasses a variety of electro-analytical procedures having a common characteristic initial step. In all these procedures; the analyte of interest is accumulated on a working electrode by controlled potential electrolysis. After a short rest period, this preconcentration step is followed by the stripping step, which involves the dissolution of the deposit when a linear ramp is applied to the electrode. Thus, a detectable current is produced at the electrode surface following the oxidation or reduction of the analyte at a characteristic potential.

By careful interpretation of the resulted peak shape current–potential voltammogram recorded during the stripping step, important and desired analytical information is readily obtained. The peak potential (position of  $E_p$ ) is characteristic of the given substance and thus it can be used for qualitative identification, whereas the peak current  $I_p$  is proportional to the concentration of the corresponding analyte in the test solution. This analytical quantitative information can be obtained from the height or area of the stripping voltammetric occurs at characteristic potentials, hence several species can often be determined simultaneously.

A comprehensive treatment and discussion of the principles, instrumentation and applications of stripping voltammetry can be found in several monographs (Brainina and Neyman, 1993; Wang, 1994). Among the techniques employing a preconcentration step, the first to be developed has been anodic stripping voltammetry (ASV), which mainly applied to trace analysis of heavy metal ions using a hanging mercury drop electrode. The basis of ASV for metals is the electrolytic dissolution of a metal which previously had been deposited on a mercury electrode. The preconcentration is achieved by cathodic deposition at a controlled time and potential. In the following measurement step, the potential is scanned anodically and linearly.

In general, stripping voltammetric techniques have had enjoyed the reputation of being highly sensitive, selective and in many cases where it has been commercialized, fairly inexpensive as well as fairly easy to run. Additionally, the high accuracy and precision with the possibility of portable analysis with easy to operate and low cost instrumentation have led to the rapid expanding application of stripping voltammetry in food analysis as testified by the numerous publication on this subject in the last few years. Over the years, stripping voltammetric techniques have been shown to possess a great potential for the determination of trace and ultra-trace concentrations of toxic metals such as mercury, arsenic, antimony and uranium. Data on the ultra-trace background levels of lead and cadmium in raw agricultural crops by differential pulse anodic stripping voltammetry was reported by Stazger and his team. Furthermore, stripping voltammetric techniques, especially ASV method, were successfully utilized for the determination of these toxic metals content in various foodstuffs such as leafy vegetables, wheat and rice, common table salt, liver and fish, infant formulas and canned soft drinks.

Additionally electroanalytical data on the stripping voltammetric determination of toxic metals in food commodities, stripping voltammetric technique proved to be highly effective in analyzing various and irrigation water. The adsorptive stripping voltammetric (AdSV) technique has been used to develop a method for the determination of fenthion pesticide in olive oil after the extraction of fenthion by solid-liquid extraction procedure using silica cartridge (Alghamdi, 2010). Similarly adsorptive stripping voltammetric (AdSV) method has also been applied successfully on a mercury free sensor for the determination of the trace concentration of lead ( $Pb^{2+}$ ) assay based on chemical modification of screen-printed carbon electrodes (SPCEs) with acetamide phosphonic acid self-assembled monolayer on mesoporous silica (Ac-Phos SAMMS) (Yantasee *et al.*, 2005.) the anodic stripping voltammetric (ASV) technique has been used for the Mercury-free sensors for lead ( $Pb^{2+}$ ) assay based on chemical modification of screen-printed carbon electrodes (SPCEs) with acetamide phosphonic acid self-assembled monolayer on mesoporous silica (Ac-Phos SAMMS). Recently, Zhuang *et al.* (2011) reported the applicability of gold microelectrode for electrochemical determination of trace copper ions ( $Cu^{2+}$ ) in water samples by anodic stripping voltammetry (ASV). Moreover, there are several published papers dealing with the application of stripping technique in the determination of environmental samples.

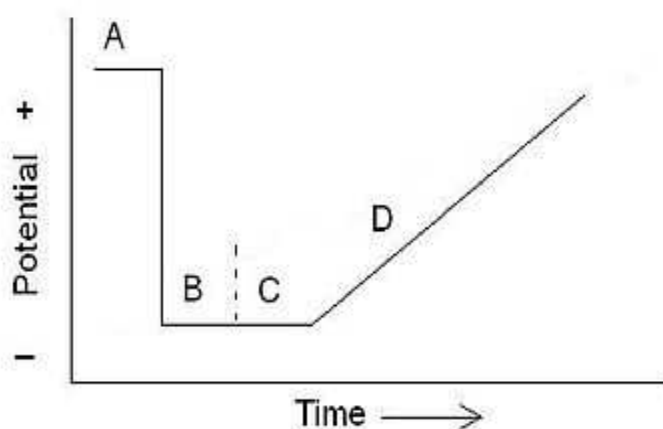
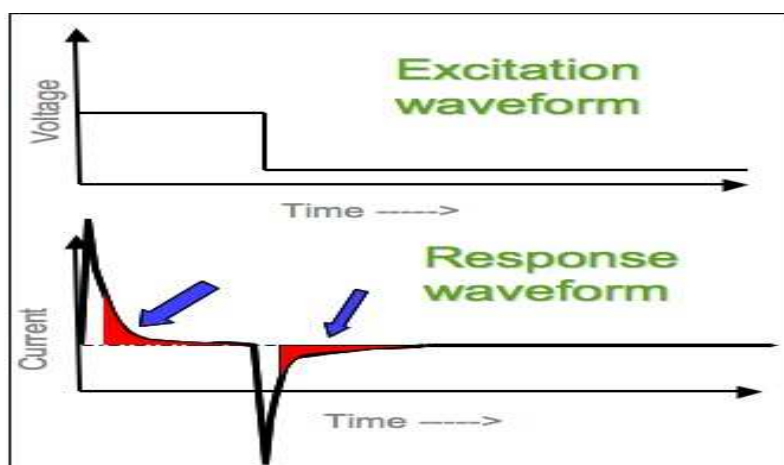


Figure 2.4 Typical current response for stripping voltammetry (Wang, 1985).

#### 2.4.2.3. Chronoamperometry

Chronoamperometry belongs to the family of voltammetric step techniques which is potential-controlled technique. This electrochemical technique involves applying a constant potential and monitoring the change in current,  $I$ , with respect to time,  $t$ . The working electrode potential is suddenly stepped from an initial potential to a final potential, and the step usually crosses the formal potential of the analyte. The solution is not stirred. The initial potential is chosen so that no current flows (*i.e.*, the electrode is held at a potential that neither oxidises nor reduces the predominant form of the analyte). Then, the potential is stepped to a potential that either oxidizes or reduces the analyte, and a current begins to flow at the electrode. The potential can be applied for a fixed period of time or until a desired charge is reached. Chronoamperometry have been commonly employed to determine solution-based physical parameters of electroactive analytes. Such parameters include the analyte diffusion coefficient ( $D$ ), analyte concentration ( $C$ ), and the electron transfer stoichiometry ( $n$ ) of the redox reaction. In matrices such as aqueous solutions, the system is often well characterised and only one of these solution-based parameters is unknown. However, there are a significant number of instances where more than one solution-based parameter is unknown. Such examples include the determination of diffusion coefficients in thermo-sensitive hydrogel media, sol-gels, and polymer films (Petrovic *et al.*, 2000).





**Figure 2.5** Typical current response for chronoamperometry ([www.serotonin.ucla.edu/electroanalytical](http://www.serotonin.ucla.edu/electroanalytical)).

## 2.5 Heavy Metals in the Environment

Metal extraction is an important industry in our modern industrialised society. However, some of these anthropogenic activities such as mining can discharge metals to estuaries, rivers, streams, and lakes. Heavy metals are individual metals and metal compounds that can impact human health although certain are nutritionally essential for health and some are referred to be toxic. These metals become toxic when they are not metabolised by the body and accumulate in soft tissues. Eight common heavy metals are: arsenic (As), barium (Ba), cadmium (Cd), chromium (Cr), lead (Pb), mercury (Hg), selenium (Se), and Aluminium (Al) but among these only four that can be encountered as toxic i.e. Hg, Pb, Cd and Al. Although aluminium is not a heavy metal, it makes up about 8% of the surface of the earth and is the third most abundant and it is toxic. Scientist known Al as a significant neurotoxin and shares many common mechanisms with mercury as a neurotoxin (International Occupational Safety & Health Centre, 1999) These are all naturally occurring substances which are often present in the environment at low levels. In larger amounts, they can be dangerous and detrimental to aquatic and human health. Heavy metals can be determined using sensors based on both potentiometric and amperometric methods. A broad range of electrochemical techniques can be used for this purpose and some of the most commonly used, are described earlier in this chapter.



Heavy metals poisoning may often go unrecognised because of a failure to take a proper exposure history and can have harmful as well as beneficial effects (those naturally found in foodstuff). Contaminated river systems, coastal waters and other ecosystems by metals such as Pb, Cd and Hg do not only pose a health risk, but they also pose a threat to livelihoods and economies (Mehrvar *et al.*, 2000). Both anthropogenic activities and natural phenomena can change the physical, chemical, and biological characteristics of water, and will have specific ramifications for human and ecosystem health in case of negative impacts. Water quality is affected by changes in nutrients, sedimentation, temperature, pH; and the presence of contaminants such as heavy metals, non-metallic toxins, persistent organics and pesticides, and biological factors, among many other factors (Carr and Neary, 2008). Therefore, the monitoring of these contaminants in our water resources and aquatic environment has become important in recent decades with increased industrialisation.

### 2.5.1 Impacts on the Aquatic Ecosystem

Unsafe or inadequate water, sanitation, and hygiene cause approximately 3.1% of all deaths worldwide, and 3.7% of DALYs (disability adjusted life years) worldwide (WHO, 2002). Data on threatened and endangered freshwater species vary by region, and are not encouraging in South Africa, where nearly two-thirds of freshwater species are threatened or endangered (Revenga *et al.*, 2000). Nearly half of all amphibian species have experienced population declines and nearly a third face extinction. Metals dissolve in water and are easily absorbed by fish and other aquatic organisms. At small concentrations (trace levels) some of these metals can be toxic, especially if the metals undergo bioconcentration (or biomagnification), which means that their concentration in an organism is higher than in water or sediment (or their habitual environment). Metal toxicity produces adverse biological effects on an organism's survival, activity, growth, metabolism, or reproduction. Metals can be lethal or harm the organism without killing it directly. Adverse effects on an organism's activity, growth, metabolism, and reproduction are examples of sublethal effects (Wright and Welbourn, 2002).

There are several pathways by which this happens, in addition to diffusion into the bloodstream via the gills and skin; fish can be exposed by drinking water or eating sediments that are contaminated with the metal, or eating other animals or plants that have been exposed to the metal. Fish are more sensitive than algae to lead (Pb). When Pb concentrations exceed 100 ppb, gill function is affected. Embryos and fry are more sensitive to the toxic effects of lead than are adults. Cadmium (Cd) effects on aquatic organisms are analogous to those in humans and include skeletal deformities and impaired functioning of kidneys in fish. Lead is more toxic at lower pH and in soft water (water with few or absolutely no dissolved minerals) (Taub, 2004; Wright and Melbourne, 2002). As is the case with other metals, the toxicity of Pb to fish depends in part on the species. Goldfish are relatively resistant because they can excrete Pb via their gills (Landis and Yu, 2003). Cadmium (Cd) is more toxic in freshwater than in saltwater because Cd combines with chlorides in saltwater to form a molecule that is less available from solution (Bradl, 2005; Wright and Welbourn, 2002). The mercury (Hg) found in fish and shellfish is most often in the more toxic organic form of methylmercury (MeHg), which may bioaccumulate in the food chain.

The reaction takes place at the water-sediment interface and is facilitated by low pH and high dissolved organic carbon. Methylmercury dissolves well in water, crosses biological membranes, and persists in fatty tissues of organisms. In addition to bioconcentration, methylmercury undergoes biomagnification; each level of the food chain has higher tissue concentrations than its prey. Mercury levels at the top of the food chain are thousands or millions of times higher than in water or sediments. Mercury is of particular concern since the harmful effect of this metal to humans is well documented (Wright and Welbourn, 2002).

### **2.5.2 Impacts on Human Health**

Generally humans are exposed to metals via analogous pathways, which include: (i) diffusion into the bloodstream via the lungs and skin; (ii) drinking contaminated water; (iii) eating contaminated food; and (iv) through inhalation (breathing) Working in or living near an industrial site that utilises these metals and their compounds increases ones risk of exposure, as does living near a site where these metals have been improperly disposed.

Subsistence lifestyles can also impose higher risks of exposure and health impacts because of hunting and gathering activities. Cadmium is known as a human carcinogen. Smokers get exposed to significantly higher cadmium levels than non-smokers. Severe damage to the lungs may occur through breathing high levels of cadmium vapours. The International Agency for Research on Cancer has classified cadmium as a category I (human) carcinogen (Bradl, 2005; Landis and Yu, 2003; Wright and Welbourn, 2002). Cadmium is also of concern as long-term, low-level ingestion is associated with kidney damage and can cause bones to become fragile and break easily (ATSDR, 2008). The most bioavailable and therefore most toxic form of mercury is the mercury combines with other elements to form organic and inorganic mercury compounds. Consumption of methylmercury, particularly by small children and pregnant women, can lead to developmental and neurological damage. In adults, it has been linked to coronary heart disease (Mozaffarian and Rimm, 2006). Inorganic mercury also poses a range of acute and chronic health effects, with long-term oral exposure to low amounts potentially leading to renal damage and immunological effects (U.S Environmental Agency, 1997). Other metals present in drinking water also pose serious health risks. Lead can affect every organ and system in the body.

Long-term exposure of adults can result in decreased performance in some tests that measure functions of the nervous system; weakness in fingers, wrists, or ankles; small increases in blood pressure; anaemia and developmental damage to the foetus. Acute exposure can cause vomiting or death. While natural waters contain almost no lead, it can be leached into water supplies from distribution systems and pipes. Copper, while an essential mineral, can cause stomach irritation, nausea, vomiting, and diarrhoea in relatively high concentrations (ATSDR, 2004).

## 2.6 Precious metals in the Environment

Mining, industries, hospitals, and other medical institutions are known to release precious group metals (PGMs) into the environment, especially Pt, because it is used in anti-cancer drugs and dentistry (Rauch *et al.*, 2008; Sures *et al.*, 2005). However, recent studies showed the increasing use of PGMs in vehicle catalytic converters; primarily platinum, palladium and rhodium.

Although the use of catalytic converters has been extremely successful for the improvement of urban air quality, it has been shown that particles of PGMs are being deposited alongside roadways as a result of abrasion and surface deterioration of the catalyst and on adjacent vegetation and soil, and in water bodies either directly, or through run-off (Wei and Morrison, 1994). This deposition is leading to increasing concentrations of PGMs dramatically over the past two decades, raising concerns about the environmental impact and toxicity of these elements in living organisms (Caroli *et al.*, 2000; Palacios *et al.*, 2000; Petrucci *et al.*, 2004; Gomez *et al.*, 2002; Moldovan *et al.*, 2002).

Barbante *et al.* (2001) have roughly estimated that the annual Pt emission only from catalytic converters may be 0.5 - 1.4 ton yr<sup>-1</sup>. These calculations are based on an emission factor of 65 - 180 ng km<sup>-1</sup> from automobile sources and considering that there are about 500 million cars worldwide equipped with catalytic converter and that the averaged mileage is about 15000 km per year. PGMs are becoming an emerging class of contaminants with potential human and environmental health implications, due to their suspected mutagenic and carcinogenic activities (Ravindra *et al.*, 2004).

Contaminants on land can be transported by rivers either in dissolved, colloidal or particulate form to estuaries and finally to coastal oceans, where they enter into the food chain and become concentrated in fish and other edible organisms (known as bioaccumulation), particularly in near-shore areas (Essumang *et al.*, 2008).

### 2.6.1 Impacts on the Aquatic Ecosystem

Marine organisms take up metals from their environment, which then accumulate in their tissues. Analysis of trace metals in tissues of marine organisms is a tool employed in marine pollution studies (Darko, 2004). Measurement of PGMs of ecological, climatic, and anthropogenic changes underpins the formulation of effective management strategies for sustainable use and protection of the marine environment. Studies on PGMs in Ghana may serve as an early warning sign that has a direct bearing on vehicular flow. The levels of PGMs in organisms such as *Sarotherodon melanotheron*, *Chonophorus lateristriga*, *Macrobrachium vollenhovenii*, and *Crassostrea tulipa* have never been evaluated in Ghana, even though most developed countries do have the necessary data (Essumang, 2010).

Interestingly, these species are consumed in Ghana, which implies that the continuous consumption of these species may not exempt the consumers from all the possible negative health effects associated with PGMs. Essumang *et al.* (2010) measured the extent of Pt, Pd and Rh contamination in some aquatic biota species, e.g. blackchin tilapia (*Sarotherodon melanotheron*, Cichlidae), brown goby (*Chonophorus lateristriga*, Gobiidae), shrimp (*Macrobrachium vollehovenii*, Palaemonidae), and mangrove oysters (*Crassostrea tulipa*, Ostreidae). The above biota is commonly found in estuaries and lagoons along the coastal belt of Ghana. Several studies have given an account on the increasing concentration of Pd in aquatic ecosystems. Several Pd compounds have been found to have antiviral, antibacterial and/or fungicidal properties. The Pd compounds that have been tested for effects on aquatic organisms have been found to be significantly toxic and in all cases the toxicity was similar to that of Pt. Platinum is a particular concern as it has known mutagenic and toxic effects, even at very low concentrations, which may be problematic if it's present in urban air and urban water (affecting both ecosystem and human health) (Essumang *et al.*, 2010).

Suspected biomethylation of Pt in the aquatic urban environment gives a similar concern to that attached to mercury. Essumang (2010) conducted a first determination of the levels of platinum group metals in Manta birostris (Manta Ray) caught along the Ghanaian coastline. The analysis showed that Ghana's coastline is fairly polluted with these platinum group metals (PGMs) (Essumang, 2010).

## 2.6.2 Impacts on Human Health

The general belief is that PGMs are harmless that stems from their chemical inertness. Conversely, their role as sensitizers in the evolvement of allergenic conditions such as: asthma, conjunctivitis, dermatitis, rhinitis, and urticaria have been thoroughly ascertained and found to be prevalent in workers exposed to these metals in processing plants (Rosner *et al.*, 1990). Palladium is said to have little environmental impact. It is present at low levels in some soils, and the leaves of trees have been found to contain approximately  $0.4 \text{ mg.L}^{-1}$  of this metal, with the specific source origin unknown but sometimes proposed to come from exhaust emissions (Moldovan *et al.*, 2001; Gomez *et al.*, 2002). Some plants, such as the water hyacinth, are killed by low levels of palladium salts but most plants tolerate it, although tests indicate that their growth is affected at levels above  $3 \text{ mg.L}^{-1}$ .

There is no information on the effects of palladium emitted from automobile catalytic converters on the general population. Effects have been reported due to iatrogenic and other exposures. A few case reports reported skin disorders in patients who had exposure to palladium-containing jewellery or unspecified sources. Palladium compounds are encountered relatively rarely by most people. All palladium compounds should be regarded as highly toxic and as carcinogenic. Palladium chloride is toxic, harmful if swallowed, inhaled or absorbed through the skin. It causes bone marrow, liver and kidney damage in laboratory animals. Irritant, however palladium chloride was formerly prescribed as a treatment for tuberculosis at the rate of 0.065 g per day (approximately 1 mg kg<sup>-1</sup>) without too many bad side effects (Shamspur, 2012).

## 2.7 Modified Electrode Surfaces for Stripping Voltammetry

Sensors based on modified electrodes have been the focus of research in the last two decades, since having desirable properties; they have been designed to interact with specific pollutants (Horáček *et al.*, 2000). Chemically modified electrodes are still in the early stages of their lifetime, such preparation of structured interfaces holds great promise for the task of environmental monitoring. Among the carbon-based electrodes that can be modified not only on the surface but also in bulk during their preparation, carbon paste electrodes (CPE) and screen-printed carbon electrodes (SPCE) belong to the most frequent choice. For modifications, various organic and inorganic compounds can be employed, including metal oxides that are preferably used as bulk modifiers and mediators in the configurations of biosensors (Svobodova *et al.*, 2012). Chemically modified electrodes (CME) are different from classical (bare) electrodes in that the electrode surface is altered by immobilizing molecules in a rational fashion so that the electrode thereafter displays new properties. Drawbacks of bare electrodes, such as adsorption of molecules or ions, unpredictable surface reactivity and sluggish kinetics can be overcome by modifying the electrode surface. Basically, the modification of an electrode involves immobilisation (on its surface) of reagents that change the electrochemical characteristics (and or properties) of the bare electrode surface. Inclusion of reagents within the electrode matrix (e.g. carbon paste) is another attractive approach for modifying electrodes. Such manipulation of the molecular composition of the electrode thus allows one to tailor the sensor response to meet specific sensing needs.

There are different directions by which the resulting modified electrodes can benefit environmental analysis, including acceleration of electron-transfer reactions, preferential accumulation or perm-selective transport (Wang, 2006).

There are numerous techniques that may be used to modify electrode surface. A few are listed and described below:

(i) **Electrocatalysis:** The objective of electrocatalysis is therefore to provide an alternative pathway with lower activation energy and hence to permit such electrode reaction to occur at high current densities close to the equilibrium potential. At a modified electrode is usually an electron transfer reaction between the electrode and some solution substrate which, when mediated by an immobilized redox couple (i.e., the mediator), proceeds at a lower overpotential than would otherwise occur at the bare electrode. This type of mediated electrocatalysis process can be represented by the scheme in figure 2.8: Such catalytic action results in faster electrode reactions at lower operating potentials. Various catalytic surfaces have thus been successfully employed for facilitating the detection of environmentally-relevant analytes (with otherwise slow electron-transfer kinetics). These include the electrocatalytic determination of hydrazines or nitrosamines at electrodes coated with mixed-valent ruthenium films, monitoring of aliphatic aldehydes at palladium-modified carbon paste films, sensing of nitrite at a glassy carbon electrode coated with an osmium-based redox polymer film, or nitrate at a copper modified screen printed carbon electrode for monitoring of organic peroxides at cobalt-phthalocyanine containing carbon pastes, and of hydrogen peroxide at a copper heptacyanonitrosylferrate- coated electrode surface (Wang, 2011).

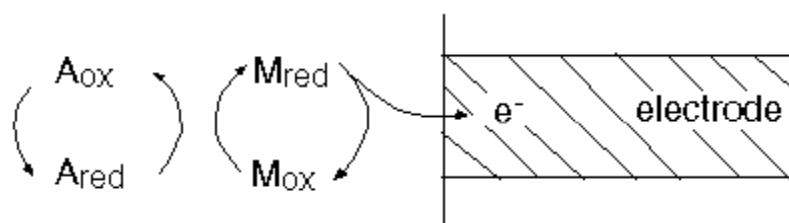


**Figure 2.6.** Electrocatalysis at modified electrodes; electron transfer mediated reaction between the target analyte and surface-bound catalyst (Wang, 2000).



In this scheme, the substrate is irreversibly (or quasi-reversibly) reduced at the bare electrode, which is transported across the film-solution interface (partition coefficient) and diffuses into the film membrane.

The electrocatalyst or mediator undergoes heterogeneous electron transfer at the electrode surface and charge propagation through the film is described by a rate given by the charge-transport diffusion coefficient. The mediator undergoes homogeneous electron transfer with the substrate in the film.

(ii) **Drop-dry Coating:** (solvent evaporation) or a few drops of polymer, modifier or catalyst are dropped onto the electrode surface and left to stand to allow the solvent to dry out, to obtain a modified electrode surface (Diab, 2005).

(iii) **Dip-dry coating:** the electrode is immersed in a solution of the polymer, modifier or catalyst for a period sufficient for spontaneous film formation to occur by adsorption. The electrode is then removed from solution and the solvent is allowed to dry out (Deng et al., 2006).

(iv) **Pre-concentration:** the modified electrodes can also be useful for environmental sensing. In this case an immobilised reagent (e.g. ligand, ion-exchanger) offers preferential uptake of target analytes. This approach enjoys high sensitivity because it is a pre-concentration procedure. A second major advantage lies in the added dimension of selectivity, which is provided by the chemical requirement of the modifier-analyte interactions. Such improvements have been documented for the measurement of nickel, mercury, or aluminium ions at dimethylglyoxime, crown-ether or alizarin containing carbon pastes, respectively, monitoring of nitrite, chromium, or uranyl ions at ion-exchanger modified electrodes, and of copper at an algae-modified electrode (Hanrahan *et al.*, 2004).

(v) **Composite:** the electrode is prepared by simple impregnation of the bulk electrode material with a chemical modifier such as a methylphenylcarbinol (MPC) catalyst a good example is the popular carbon paste electrode (Chen *et al.*, 2006).

(vi) **Spin coating:** (or spin casting), a droplet of a dilute solution of the polymer is applied to the surface of a rotating electrode. Excess solution is spun off the surface and the remaining thin polymer film is allowed to dry. Multiple layers are applied in the same way until the desired thickness is obtained. This procedure typically produces pinhole-free thin films (Pyun et al, 1997).



(vii) **Electrodeposition**: in this method the electrode surface is immersed in a concentrated solution ( $\sim 10^{-3}$  mol L<sup>-1</sup>) of the polymer, modifier or catalyst followed by repetitive voltammetric scans. The first and second scans are similar, subsequent scans decrease with the peak current for example electrochemical deposition of poly (o-toluedine on activated carbon fabric (Sivakumar *et al.*, 2005).

(viii) **Electropolymerisation**: in this technique the electrode is immersed in a monomeric polymer, modifier or catalyst solution and layers of the electropolymerised material builds on the electrode surface, applying repeated cycling in a specific potential window. Generally, the peak current increases with each voltammetric scan such that there is a noticeable difference between the first and final scan indicating the presence of the polymerised material, for example electropolymerisation of aniline (to form polyaniline) on a platinum electrode (Somerset *et al.*, 2006).

(ix) **Langmuir-Blodgett Technique**: this technique involves transferring the monolayer or multilayer film formed at the air-water interface onto the electrode surface. Generally LB film form balancing the interactions at the polymer –water, air-water and polymer air interfaces (Wagner and Remmers, 1995). The resulting film is very well ordered, single layered and the range of molecular thickness.

(x) **Chemisorption**: in this method the chemical film is strongly and ideally irreversible adsorbed (chemisorbed) onto the electrode surface electrode using a self-assembled monolayer, usually a thiol-containing compound on a gold electrode surface (Somerset *et al.*, 2007).

(xi) **Covalent reactions**: can be used for analogous collection or determination of organic analytes, e.g. monitoring of aromatic aldehydes at amine-containing carbon pastes. Routine environmental applications of these pre-concentrated electrodes would require attention to competition for the surface site and the regeneration of an ‘analyte-free’ surface. Another promising avenue is to cover the sensing surface with an appropriate permselective film. Discriminative coatings based on different transport mechanisms (differentiating with analyte size, charge, or polarity) can thus be used for addressing the limited selectivity of controlled-potential probes in complex environmental matrices.

The size-exclusion sieving properties of various polymer-coated electrodes offer highly selective detection of small hydrogen peroxide or hydrazine molecules. In addition, surface passivation (due to adsorption of macromolecules present in natural waters) can be prevented via the protective action of these films (Wang, 2011).

More powerful sensing devices may result from the coupling of several functions (permselectivity, pre-concentration or catalysis) onto the same surface. Additional advantages can be achieved by designing arrays of independent modified electrodes, each coated with a different modifier and hence tuned toward a particular group of analytes. The resulting array response offers a unique fingerprint pattern of the individual analytes, as well as multi-component analysis (in connection with statistical, pattern-recognition procedures). Use of different perm selective coatings or catalytic surfaces thus holds great promise for multi-parameter pollution monitoring. The development and application of electrochemical sensor arrays has been suggested with the use of this technique (Wang, 2011).

Recently related to this process are new molecular devices based on the coverage of interdigitated micro-arrays containing conducting polymers. Eventually we expect to see molecular devices in which the individual components are formed by discrete molecules. Modification of miniaturised screen-printed sensor strips can also be accomplished via the inclusion of the desired reagent (e.g. ligand, catalyst, etc.) in the ink used for the micro fabrication and manufacturing process (Hanrahan *et al.*, 2004).

### **2.7.1 Polymer Films**

Polymer thin films play an important role in the development of electronic devices, passivation coatings, and chemical and biological sensors. However, in order to improve device and system performance and to meet future demands, new approaches are needed to grow thin films on wafer surfaces or small component. Depending on the particular application, one may want to deposit films containing single or multilayer structures of different organic or polymeric materials, homogeneous composite materials, or materials with graded compositions.

In many situations, it will be necessary to deposit these materials discretely, achieve conformal coverage, and provide highly uniform films, especially with regard to surface coverage and thickness control areas with accurate thickness control. Polymers have been very popular modifiers and many papers on polymer modifications are available. The polymer film can be organic, organometallic or inorganic; it can already contain the desired chemical modifier or that chemical can be added to the polymer in a second, functionalizing step; and can contain the equivalent of a few up to many thousands of monomolecular layers of the chemical modifier. Included in this form of modification are the substrate-decoupled surface adsorption monolayer's SAMs in which adsorbate molecules are arranged on the electrode surface independently of any substrate structure. Unfortunately, since polymers have molecular weight distribution and the structures are heterogeneous, it is difficult to control the functions of the modified layer at the molecular level. Furthermore, it is impossible to discuss the mechanism of electron transfer and functions quantitatively. A higher order structure can be controlled better if the electrode surface is modified by sequential deposition of monolayer of functional molecules. In this case, it is much easier to discuss the relation between structure and function of the modified surface at the molecular level. Polymerization reactions can proceed by various mechanisms using various initiators. For addition polymerization of single compounds, initiation of chains may occur via radical, cationic, anionic or coordination-initiators, but some monomers will not polymerize by more than one mechanism. Copolymerisation of several monomers can lead to multifunctional polymers also suitable for the preparation of patternable thin organic films. A work so called "terpolymer" concept was developed, where film forming monomers were combined with monomers which allow for surface anchoring and those which allow surface patterning by lithographic methods. By this method the fabrication of diazosulfonate terpolymers (Braun *et al.*, 2002) was demonstrated which allowed to be covalently attached as thin films to glass and silicon substrate after spin-coating. The Langmuir-Blodgett (LB) method has been the most popular technique to form mono- and multilayers of assembled molecules on solid surfaces (Ngu *et al.*, 1997). The LB method has been applied to form many kinds of devices such as electric insulators and semiconducting thin layers and also has received strong attention as one of the techniques to construct organised molecule structures for molecular and biomolecular devices.

However, a monolayer formed by the LB method adsorbs on solid substrates only physically and therefore, are usually not stable. Recently, a new approach for the formation of oriented stable monolayers, namely the self-assembling method, has been employed by many research groups. In the case of the self-assembling method, molecules that have long hydrocarbon chains chemisorb on a solid surface by making covalent bonds with atoms on the solid surface and self-assembling with high structural order. For example, it was reported that molecules with terminal trichlorosilyl or trimethoxysilyl groups form self-assembled monolayer by reacting with hydroxyl groups on a silicon surface. Similarly, there are many reports of self-assembled monolayer formation of thiols on gold surfaces (Salinguet *et al.*, 2009). Some attempts have also been made to form multilayer films by sequential deposition of self-assembled monolayer. Although many efforts have been made towards the characterisation of self-assembled monolayers of unsubstituted alkanethiols on gold, only a few reports are available on the attempt to make functional monolayers on the surface. Rubinstein and co-workers have constructed the self-assembled monolayer of 2,2'-thiobis(ethyl acetoacetate) on gold and found that the monolayer showed the ionic recognition and ion-selective responses. Recently, Chidsey *and* co-workers have shown that stable monolayers of ferrocene-terminated alkanethiols can be formed by co-adsorption of ferrocenylalkanethiol and an unsubstituted alkanethiol on the electrode surface. They further studied the electrochemical behaviour of the monolayers and proposed a model to explain the adsorption and electrochemical behaviour of the mixed monolayers. In both reports, ester type compounds were mainly used to form the monolayers, although it is also reported that self-assembled monolayers in which alkanethiols are directly linked to the non-polar ferrocene group, can be employed as well (Uosaki *et al.*, 1991).

### 2.7.2 Biosensors

The remarkable specificity of biological recognition processes has led to the development of highly selective biosensing devices. Biosensors and bioanalytical sensors appeared well suited to complement, standard analytical methods for a number of environmental monitoring applications.

The definition for a biosensor is generally accepted in the literature as a self-contained integrated device consisting of a biological recognition element (enzymes, antibody, receptor, DNA or microorganism which is interfaced to a chemical sensor (i.e. analytical device) that together reversible respond in a concentration dependent manner to chemical species. Enzymes are still the most appropriate recognition elements because they combine high chemical specificity and inherent biocatalytic signal amplification.

The use of biosensor for environmental applications has been reviewed in considerable detailed (Thevenot *et al.*, 2000). Many studies are focused on enhancing the electrochemical properties of electrodes through the modification of the working electrode and improving the efficiency of enzyme immobilization (Artyukhin *et al.*, 2004; Katz & Willner, 2004). Different recommendations were postulated for defining and describing the characteristic effect on biosensors performance. Some properties and characteristic behaviours of ideal biosensors were evaluated accordance with the IUPAC protocols or definitions (Andreescu *et al.*, 2004; Daniel *et al.*, 1999), which include selectivity, response time, and linear range, limit of detection, reproducibility, stability and lifetimes. Zhang *et al.* (2008) described a controllable layer-by-layer self-assembly modification technique of multi-walled carbon nanotubes and poly (diallyldimethylammonium chloride) on glassy carbon electrode and introduced a controllable direct immobilization of acetylcholinesterase on the modified electrode. Some authors propose the use of organic conducting polymers as the enzyme-hosting matrix for biomolecules, due to its advantages of permitting a facile electronic charge flow through the polymer matrix, easy preparation, high conductivity and good stability (Njagi & Andreescu, 2007; Vidal *et al.*, 2003). Recently, nanoparticles, specially the gold nanoparticles have been extensively used owing to their extraordinarily catalytic activity, good conductivity and biocompatibility. Also, gold nanoparticles and polymers can be assembled to act as an immobilization matrix of AChE (Willner *et al.*, 2006). Figure 2.9 shows a schematic representation of biosensor setup.

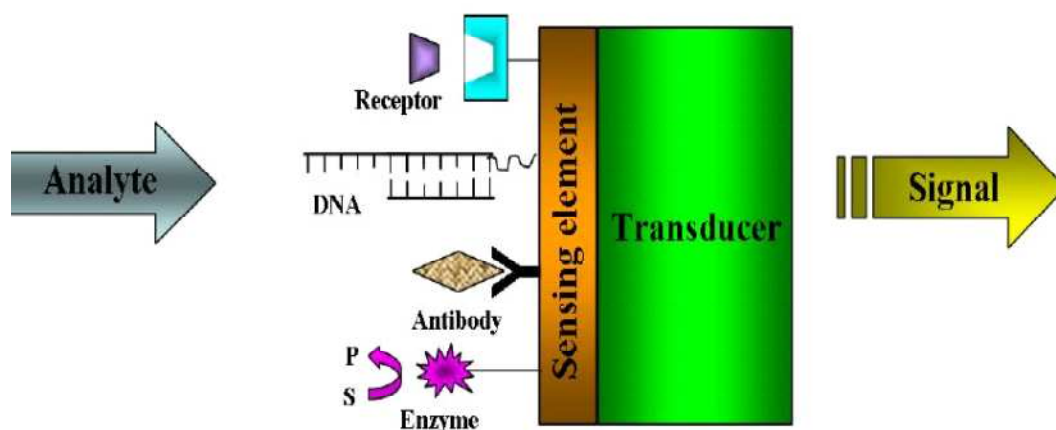


Figure 2.9 Schematic principle of operation of a biosensor (Borgmann et al., 2011)

### 2.7.3 Carbon Paste Electrodes

Its inspiring history, illustrating advantages for electrochemistry as a whole and revealing numerous connections with the current research trends, can be viewed as the driving force for the use of thin metal films. Moreover, their use is driven by low cost of the measurements, wide working potential window in both positive and negative direction, ease of working surface renewal, low background currents and reasonable repeatability. Since 2001, several new reviews appeared covering the monitoring of environmental carcinogens with the use of CPE (together with other types of electrodes) (Barek *et al.*, 2001), and amperometric biosensors for environmental samples (Vytras *et al.*, 2009). In comparison, carbon materials are more significant. Their structures, physicochemical characteristic and some other specific features are decisive factors for the electrochemical properties of the electrode. So they have been paid much attention. From the early era of CPEs up until now, the most often selected carbon material is graphite powder (GP) with particles in the low micrometric scale (Svancara *et al.*, 2009).

#### 2.7.4 Thin Metal Films

Thin metal-film electrodes have become widespread in electrochemical stripping analysis due to their relatively simple fabrication and surface regeneration when combined with advanced electrochemical stripping protocols (Wang, 2006). They also offer almost unsurpassed analytical tools in terms of reliability, simplicity and flexibility. In the last six decades mercury (Hg) electrodes were the most extensively used for electrochemical stripping analysis of several metal ions and some selected organic species. However, due to the toxicity of Hg many other electrode materials have been suggested as substitutes for mercury, e.g. different modifications of carbon, gold, platinum, silver, iridium, several alloys and amalgams etc. (Somerset *et al.*, 2010). Nevertheless, the aforementioned metal substitutes struggle to reach mercury's excellent electro-analytical performance (Wang *et al.*, 2001). A decade ago, the bismuth film electrode was introduced and has proved to be a convenient alternative to its Hg counterpart. However, due to strict regulations and provisions concerning the use of mercury, there are still considerable efforts focused on new mercury-free electrode materials, which can be satisfactorily applied in modern stripping electroanalysis (Wang *et al.*, 2000; Hutton *et al.*, 2005). Recently, the *in situ* prepared antimony film electrode (SbFE) was suggested as another alternative that approaches the electroanalytical performance of mercury- and bismuth-based electrodes featuring some interesting characteristics, such as favourably negative overvoltage of hydrogen evolution, wide operational potential window, convenient operation in relatively strong acidic medium ( $\text{pH} \leq 2$ ), and interestingly low stripping signal for antimony itself (Hocevar *et al.*, 2007; Tesarova *et al.*, 2009).

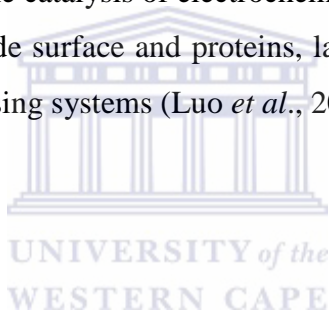
### 2.8 Nanomaterials

Developments in nanotechnology has driven the search for nanoparticles (NPs) in the 1 to 100 nm range that can be synthesized in a variety of shapes of which the most commonly prepared are spheres, rods, cubes, triangles and ellipsoids. Several reviews have addressed the synthesis and properties of different NPs (Niemeyer *et al.*, 2001; Grieve *et al.*, 2000; Gupta *et al.*, 2005).



In this thesis I will use the following definition of nanomaterial, as defined by the Royal Society: “*Nanomaterials are notable for their extremely small feature size in the range of 1-100 nanometers (nm) and have the potential for wide ranging industries*” (The Royal Society & The Royal Academy of Engineering, 2004). Nanomaterials can also be metallic, ceramic, polymeric, or composite materials. The field of nanomaterials has seen a huge increase in funding from private enterprises, government and academic researchers to provide more information on the synthesis, properties, application and environmental behavior of these materials.

An important application of NPs is at the field of electrochemical sensors and biosensors. Other types of NPs, also known as quantum dots (QDs) have been used for constructing electrochemical sensors and biosensors that play different roles in the immobilisation of biomolecule, the catalysis of electrochemical reactions, the enhancement of electron transfer between electrode surface and proteins, labeling of biomolecules, and even acting as reactant in different sensing systems (Luo *et al.*, 2005).



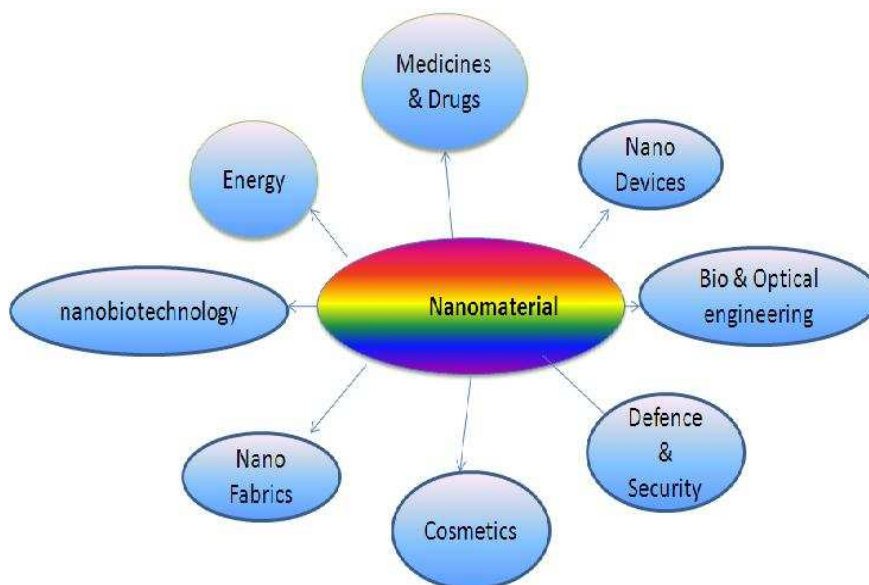


**Figure 2.7** Illustration of the application of nanotechnology (From Nano Science and Technology Consortium).

The above Figure 2.10 shows the applications of nanotechnology to various fields. Nanotechnology often brings together different disciplines and this interdisciplinary approach is expected to contribute to innovations that might solve many of today's challenges in society. A selection of the applications involving nanomaterials (NMs) that exist or show promises are presented here. The cosmetic companies have been active in using nanotechnology to improve their existing products, e.g. L'Oreal holds a very high number of nanotechnology patents (Wood *et al.*, 2003). Recently, nanomaterials evolve as promising alternatives for enzyme modulation. Nanomaterials provide large surface areas for biomolecule adsorption and can be engineered to present multiple surface functional groups for interacting with biomolecules, such as enzymes and/or their substrates. Fluorescent dyes, have been also reported in the use for optical sensors.

Cai *et al.* (2004) reported an electrochemical methodology that enables the rapid identification of different DNA sequences using a microfabric electrode. The use of NPs as fillers has been introduced in the field of composite materials with a current enormous market that is still expanding. Nanoparticles have become known to change a material's properties, e.g. metal gets harder, ceramics get softer and mixtures like alloys may get harder up to a point where they get softer again.

By introducing clay nanoparticles it is possible to make the materials stronger, lighter, more durable and often transparent. These properties of NPs have also increased their potential use in the aerospace industry, packaging and in car manufacturing where they already have been introduced in the General Motor's (GM) Safari and Chevrolet Astro vans (Wood *et al.*, 2003). Other short-term uses include solar energy collection (photovoltaic's), medical diagnostic tools and sensors, flexible display technologies and e-paper, glues, paints and lubricants, various optical components, and new forms of computer memories and electronic circuit boards (Twist, 2004).

There have also been smart textiles developed with the help of nanotechnology and in the long run textiles are expected to be able to change their physical properties according to the surrounding conditions, or even monitor vital signals (Holister, 2002). The introduction of NPs in textiles can make it possible to produce very light and durable textiles with resistance against water, stains and wrinkling.

Medical applications are one of the fields with the biggest expectations regarding human welfare. With the development of new materials and a combination of nanotechnology and biotechnology, it could become possible to make artificial organs and implants through cell growth that could repair damaged nerve cells, replace damaged skin, tissue or bone (Wood *et al.*, 2003). Furthermore, in the synergy of information technology and medicine there are expectations for advancement in the field of diagnostic instruments for personal health monitoring, providing ultra-fine precision and quick response time to diagnostic tests. Another application in the field of medicine is drug-delivery, where research is especially intensive on the possibility of manipulating NPs to assist in drug delivery in order to have a better solubility and absorption potential than in the case of bigger particles. It is hoped that NPs can assist in carrying the drug and perhaps release it in fine-tuned doses over a longer time period to a targeted area, reducing the side-effects of traditional drug applications (Duncan, 2003; Ferari, 2005). Although there is a considerable amount of data on toxicity of NPs, and the assumptions that a lot of effects by Particulate matter are driven by the ultra-fine particle fraction in it (De Jong and Borm, 2008.).

### 2.8.1 Carbon Nanotubes

CNTs are considered as a new form of pure carbon and they can be visualized as rolled hexagonal carbon networks that are capped by pentagonal carbon ring. Carbon nanotubes (CNTs) are divided into two classes, e.g. single walled (SWCNTs) and multi-wall carbon nanotubes (MWCNTs). Multiwalled carbon nanotubes are potentially more attractive electrode materials. Generally, MWCNTs have larger diameters and better electrical conductivity compared to SWNTs. Chen *et al* (2000) indicated that MWNTs films also show large specific capacitance while other studies indicated that MWNTs have a fast electron transfer rate for various redox reactions. In a typical CNT-based device, nanotubes connect two metal electrodes and the conductance between them can be measured as a function of gate bias voltage.

From the chemistry point of view, carbon nanotubes (CNTs) are extremely promising electro-catalysts because of their significant mechanical strength, excellent electrical conductivity, high surface area and good chemical stability (Salimi *et al.*, 2008). Functionalization of carbon nanotubes with various kinds of materials is gaining more attention as the different properties of the attached functionalities are required for specific applications (De la Torre *et al.*, 2003; Rubianes & Rivas, 2003). Electrodes that are CNTs-based have shown selective affinity for phosphate groups (Deo *et al.*, 2005; Li *et al.*, 2005). The images of the nanosized carbon filaments were regarded to be of multi-walled tabular nature but, unfortunately due to the cold war, Russian scientists, publications were not easily accessible. Therefore it is argued that, maybe they should be credited with the discovery of nanotubes. However it is worth mentioning, The first mention of the possibility of forming carbon filaments from the thermal decomposition of gaseous hydrocarbon (methane) was reported in 1889 i.e., more than a century ago in a patent that proposed the use of such filaments in the light bulbs, that had been presented by Edison at the Paris Universal Exposition the same year (Monthieux *et al.*, 2006).

The first group to report the use of CNTs in electro-analysis was Britto and co-workers in 1996. Using a carbon nanotube paste electrode with bromoform as the binder, the electrochemical oxidation of dopamine was explored (Britto, *et al.*, 1996). The concept of a carbon nanotube paste electrode was later adapted by Valentini *et al.* (2003).

However, the explosion of interest in CNTs in the early 21st century for use in electro-analysis can be traced back to the work pioneered by Professor Joe Wang, whilst at New Mexico State University, USA who observed the low-potential stable NADH detection at a CNT-modified glassy carbon electrode (Banks and Compton, 2006). It is interesting to note that observation of hollow fibers with nanometre dimensions were documented by Swedish scientists (Hillert and Lange) as early as 1958. But the renewal of interest in the field has suddenly broken out in 1991 from the famous Japanese microscopic Iijima publication who was studying the material deposited on the cathodic during the arc-evaporation synthesis of fullerenes (Iijima, 1991). In fact, Iijima's "rediscovery" was at the back of a couple of "carbon nanotube" related reports. Wiles and Abrahamson grew fine fibres as small as 4 - 100 nm in diameter (*viz* nanotubes) on graphite and carbon anodes, the discovery of carbon nanotubes was attributed to Iijima (Fernandez-Abedul *et al* 2007). Iijima and Ichihashi (1993) were unquestionable the first to discover single-walled carbon nanotubes. Later that year, Yacaman *et al.* (1993) used a new technique known as chemical vapour decomposition (CVD) to report the catalytic growth of CNT and later Smalley and co-workers (Thess *et al.*, 1996) reported the synthesis of bundles of aligned SWCNT by use of a laser-ablation technique. From these discoveries and other advances made, CNTs are commonly categorised as either SWCNTs or MWCNTs. However, today it is possible to also have double-walled CNTs (Liu *et al.*, 2008). Single-walled nanotubes (SWCNTs) consist of a single sheet of graphene rolled up to form a cylinder with diameter of order of few nanometres and length up to centimetres. Double-wall carbon nanotubes (DWCNTs), formed by two concentric single-wall behave similarly to single-wall carbon nanotubes but they have unique properties suitable for specific applications. Multi-walled nanotubes (MWCNTs) consist of an array of such cylinders formed concentrically and separated by ~0.35 nm, a value similar to the basal plane separation in graphite. Another way to classify carbon nanotubes is how the graphene sheet is rolled up. If you roll-up a graphene sheet you can characterize the NT structure with a pair ( $n,m$ ) of integers. The illustration of the unrolled honeycomb lattice of a nanotube is shown in Figure 2.11a while the molecular models of the rolled up are presented in figure 2.11b. In Figure 2.11b graphene sheet can be rolled more than one way, producing different types of carbon nanotubes. The three main types are armchair, zigzag, and chiral as shown in Figure 2.11 (Osman *et al.*, 2001).

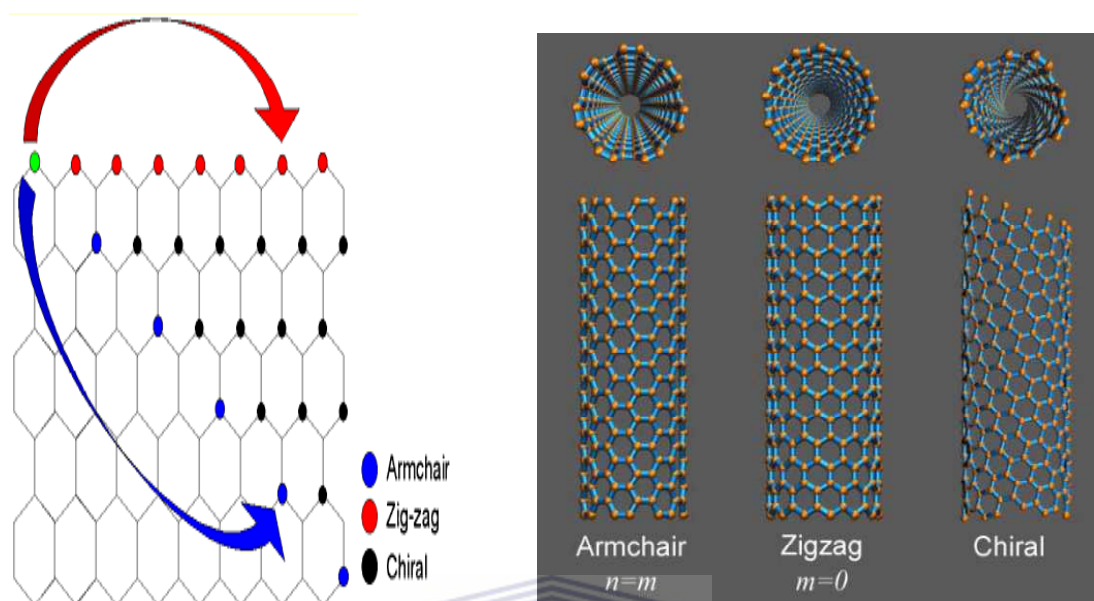


**Figure 2.11(a)** The unrolled honeycomb lattice of a SWNTs (b) Roll- up molecular models of SWNTs in different chiralities Nanotube (Odom *et al* 1998).

A SWNT can be described as a single layer of a graphite crystal rolled up into a seamless cylinder, one atom thick, usually with a small number (perhaps 10–40) of carbon atoms along the circumference and a long length (microns) along the cylinder axis. A nanotube's chiral angle, the angle between the axis of its hexagonal pattern and the axis of the tube determines whether the tube is metallic or semiconducting. Theoretical studies on the electronic properties of carbon tubules indicate that all armchair tubules are metallic, as well as zigzag cylinders exhibiting values of  $n, m$  multiples of three (Yu & Liu, 2007).



## 2.8.2 The Gold Nanoparticle

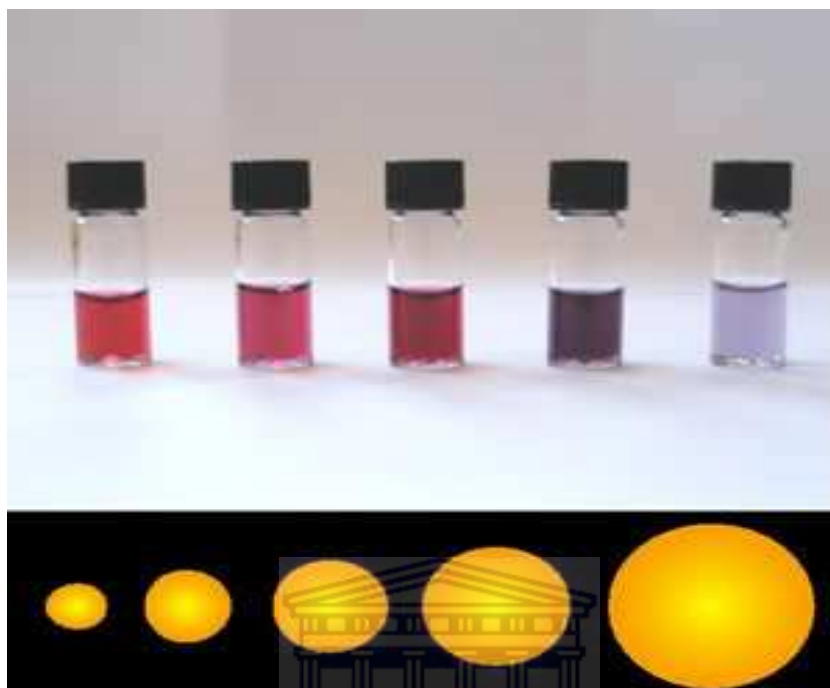


**Figure 2.12** Solutions of gold nanoparticles of various sizes. The size difference causes differences in colour (*nanotechnology eLearning centre, 2012*).

Generally, gold nanoparticles are produced in a liquid (“liquid chemical methods”) by reduction of chloroauric acid ( $\text{HAuCl}_4$ ), although more advanced and precise methods do exist. The solutions of different intensities of colloidal gold nanoparticles can be observed by the change in colour since small nanoparticles of gold are red (Somerset *et al.*, 2011). Gold nanoparticles (AuNPs) have shown great potential for applications in the fields of chemistry, physics, materials, biology, medicine, and related interdisciplinary fields (Yhang *et al.*, 2008). Zhou *et al.* (2008) reported a method to detect copper (II) by azide- and alkyne-functionalized AuNPs based on the fact that the extinction efficient of AuNPs is several orders of magnitude larger than those of traditional organic chromophores. The 50  $\mu\text{M}$  minimum concentration sets the record for detection of  $\text{Cu}^{2+}$  by the naked eye. Sugunan *et al.*, (2005) reported a novel strategy for using gold nanoparticles capped with chitosan for sensing ions of heavy metals.



Another exciting finding is that AuNPs have shown potential in therapies for HIV by attaching multiple copies of a low acting HIV drug onto AuNPs. Bowman *et al.* (2008) have stopped HIV from infecting human white blood cells with the application of their discovery. The results demonstrated that we may find a simple strategy to convert therapeutically poorly active monovalent small organic molecules into highly active drugs by just conjugating them to AuNPs (Bowman *et al.*, 2008). Recently, Lung *et al.*(2007) reported the preparation of AuNPs by arc discharge in water as alternative, cheap effective and environmentally friendly methods. Currently the synthesis of novel AuNPs with unique properties and applications in a wide variety of areas is subjected of substantial research (Panda and Chattopadhyay, 2007; Luo and Sun, 2007 Liang *et al.*, 2007). The catalytic, optical, electrical, magnetic, and electrochemical properties that are exhibited by AuNPs have made them an integral part of research in Nanoscience. The attractive physiochemical properties of AuNPs are highly affected by its shape and size (Burda *et al.*, 2002).

Ouacha *et al.* (2005) reported the laser assisted growth of AuNPs and concluded that this is a powerful method for controlling the shape of the AuNPs irrespective size. On the other hand, size and properties of AuNPs are highly dependent on their preparation conditions (Miscoria *et al.*, 2005; Cuenya *et al.*, 2003). Synthesis of AuNPs of different shapes and sizes has also been reported by Dos Santos *et al.*(2005). Some recent publications reported the use AuNPs based microfluid for a detection of mercury (Lafleur *et al.*, 2012).

In conclusion it can be said that gold nanoparticle have emerged as a new class of inexpensive material which attracted intensive attention in many fields of science. A rapid highly sensitive method uses gold nanoparticles, has been developed by Oak Ridge National Laboratories (ORNL), modified and positively charged by an amine group, to identify hazards such as perchlorates, nitrates, and some radioactive materials as little as one minute of real time in ground water, surface water, soils, and plant (Gu, 2011).

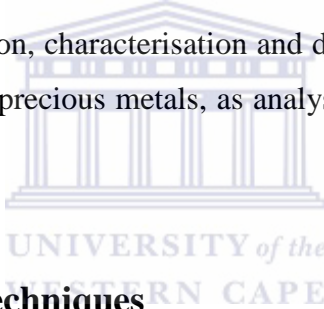
## Chapter 3

### Experimental Methods and Analytical Technique

---

#### 3.1 Introduction

This chapter outlines the experimental techniques and procedures performed during this research project. A brief description of the electrochemical and spectroscopic techniques and some of the voltammetric methods will be presented. The proposed electrochemical sensors described in this work, constructed for the monitoring of heavy metals associated with precious metals would be sputtered thin film devices. These microelectrodes are based on material structures generated by thin metal film or conducting polymer deposition. The study design was based on the fabrication, characterisation and development of the desired sensors for heavy metals associated with precious metals, as analysed in environmental samples (not discussed here).



#### 3.2. Electro-Analytical Techniques

In comparison to other instrumental methods of chemical analysis, electro-analytical instrumentation is relatively easy to miniaturise. Despite the difference in instrumentation, all electrochemical techniques share several common features. The main trends in modern electroanalysis include development of chemical and biochemical sensors based on progress in chemical and biochemical methods of molecular recognition, combined with the development of measuring devices of a large integration scale, including sensor arrays. This is accompanied by the use of new materials, including conducting polymers and nanomaterials. In most electrochemical detectors, such as amperometric and potentiometric detectors, their construction and application are based as surface detectors. They respond to substances that are either oxidisable or reducible and the electrical output results from an electron flow caused by the chemical reaction that takes place at the surface of the electrodes (Vickers, 2000).

### 3.2.1 Voltammetry Instrumentation

In voltammetry there are three important experimental parameters under our control: how we change the potential we apply to the working electrode, when we choose to measure the current, and whether we choose to stir the solution. In this work we applied a time-dependent potential excitation signal to the working electrode (WE), changing its potential relative to the fixed potential of the reference electrode (RE), and measure the current that flows between the working and auxiliary electrodes. The auxiliary electrode (AE) is generally a platinum wire, and the reference electrode used in this study is Ag/AgCl electrode. In this study we have considered cyclic voltammetry, differential pulse voltammert and cathodic differential pulse stripping voltammetry modes. For the working electrode we have chosen platinum and carbon among several different materials. All voltammetric measurements were carried out using a PalmSens® handheld potentiostat / galvanostat, with the PS Trace program and accessories (Palm Instruments BV, 3992 BZ Houten, The Netherlands) interfaced to a microcomputer controlled by PS 2.1 software for data acquisition and experimental control. Alternatively, experiments were performed with an Epsilon electrochemical analyser (BASi Instruments, 2701 Kent Ave., West Lafayette, IN 47906, USA). Figure 3.1 represent basic instrument for voltammetry that have been used when this study was performed.

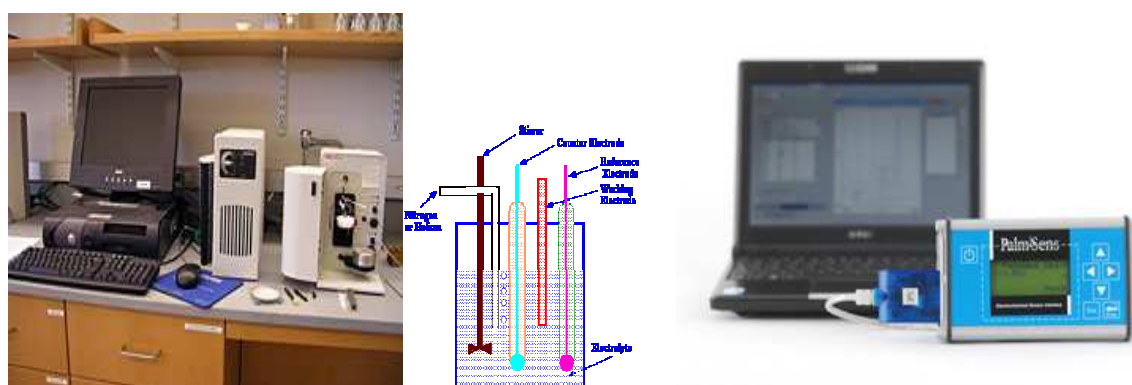


**Figure 3.1** Typical instruments for voltammetry .( accessed on 20 October 2012)

<http://www.bowdoin.edu/chemistry/instrumentation/cyclic-voltammetry/index.shtml>

### 3.2.1.1 Cyclic voltammetry (CV)

Cyclic voltammetry (CV) is the common characterisation technique in voltammetry and is used to search of redox potential(s) which would characterise the electrode (Kissinger and Heineman, 1996). Cyclic voltammetry was employed in the process of characterising the working surface of the electrodes (unmodified and modified). The three-electrode cell consisted of a working electrode (either glassy carbon (GC), platinum (Pt) or a screen-printed carbon electrode (SPCE)), a platinum counter electrode and a silver-silver chloride (Ag/AgCl) reference electrode. Measurements were performed in a batch cell with all electrodes in a vertical position, suspended in a cell with 10 ml of buffer or an appropriate electrolyte solution. For the purpose of this study we complete a scan in both directions. In chapter 4 all the experiments were performed with an Epsilon electrochemical analyser, we first scan the potential from negative to positive values (-0.2 to 1.1 V) vs. Ag/AgCl with sensitivity of 10 mA and a scan rate of  $60 \text{ mVs}^{-1}$  while in chapter 5 and 6 a PalmSens handheld potentiostat was used at a slow scan rate of  $0.01 \text{ V s}^{-1}$  and the scanning potential is from positive to negative (+0.4 to -1.0 V) vs Ag/AgCl in chapter 5 and cathodic for chapter 6 (0.8 to -1.4 V) vs Ag/AgCl.

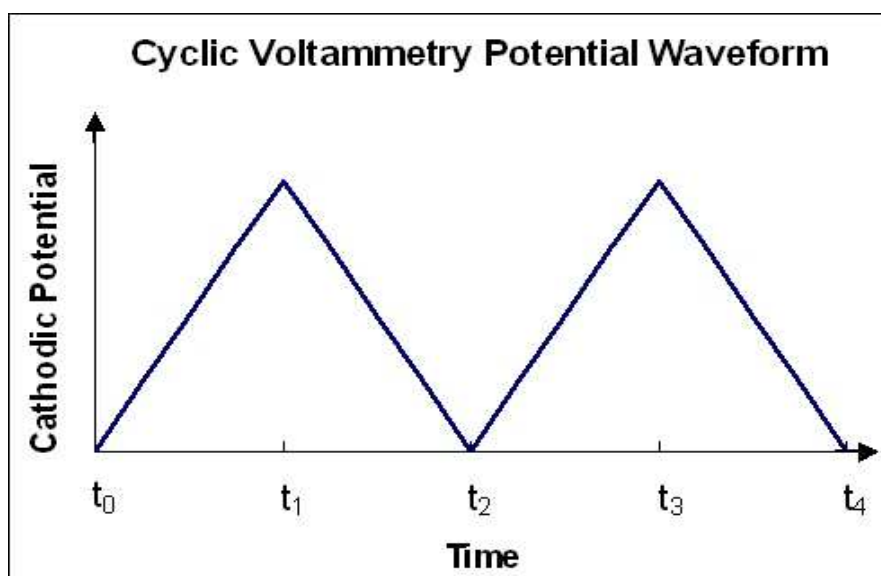


Figure 3.2 Schematic representation of cyclic voltammetry as an electro-analytical technique ([en.wikipedia.org/wiki/cyclic\\_voltammetry](http://en.wikipedia.org/wiki/cyclic_voltammetry)).

### 3.2.1.2 Differential Pulse Voltammetry (DPV)

Differential pulse voltammetry (DPV) is a technique similar to CV. In CV, the potential across the electrodes is varied linearly with time up and down, in cycles. In DPV, the potential across the electrodes is varied in a step pattern. The current is measured before and after each step, and the difference is returned. This allows the charging current to be removed from the output, yielding a more accurate result than CV. Pulse voltammetry was developed to improve the sensitivity of voltammetric measurements. This is achieved by reducing the double layer capacitance to zero so that the current recorded is totally faradaic. There are several types of pulse voltammetry including normal, differential and square wave (Kissinger and Ridgway, 1996).

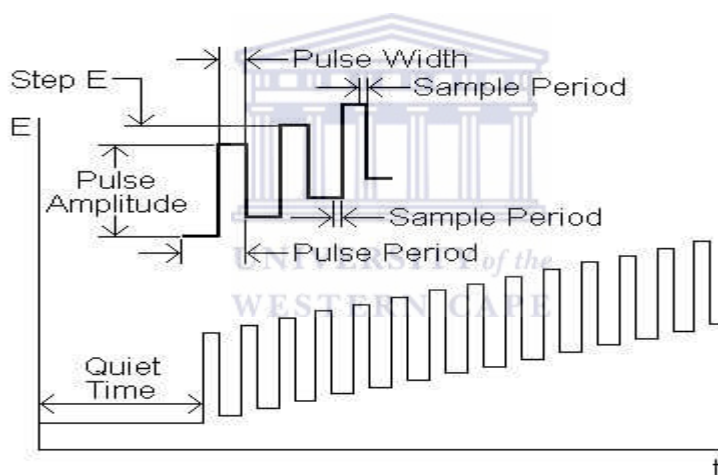
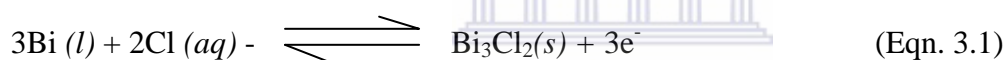


Figure 8 Schematic representation of DPV as an electro-analytical technique ([www.basinc.com](http://www.basinc.com)).

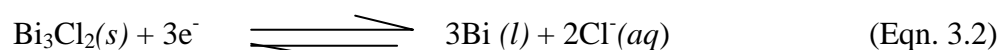
All the DPV experiments were performed in a PalmSens handheld potentiostat using the scanning potential from positive to negative (0.8 to -1.4 V) vs Ag/AgCl with the sensitivity in between the range of 1  $\mu\text{A}$  – 10 mA and a scan rate of 0.05  $\text{mVs}^{-1}$  in chapter 6, while in chapter 5 we also applied the same parameters except the scanning potential was from 0.4 to -1.0 V.

### 3.2.1.3 Cathodic Stripping Voltammetry (CSV)

Cathodic stripping voltammetry is used to determine those materials that form insoluble salts with mercurous ion. In this study, the screen printed carbon working electrode has taken an active part in the formation of the deposit. The experimental design for cathodic stripping voltammetry has involved two steps. First, the deposition step involves the oxidation of the BiF electrode to  $\text{Bi}^{3+}$  which then reacts with the analyte in the presence of the chelating agent to form an insoluble film at the surface of the electrode. Bismuth film was formed by ex situ deposition on SPCE. In detail, the bismuth film was deposited from a separate acetate buffer solution (pH = 4.5) in the presence of dissolved oxygen, containing  $100 \text{ mg}\cdot\text{L}^{-1}$  Bi (III) by electrolysis at  $-1.0 \text{ V}$  vs. vs Ag/AgCl for 300 s while stirring the solution. The electrode was washed with distilled water carefully, and transferred to a 20 mL electrochemical cell containing 0.01 M ammonium buffer solution. For example, when  $\text{Cl}^-$  is the analyte the deposition step is:



Second, stripping is accomplished by scanning cathodically toward a more negative potential, reducing  $\text{Bi}^{3+}$  back to Bi and returning the analyte to solution.



A BiF/SPCE was dipped into a stirring 0.01 M ammonium buffer solution containing 0.01 M DMG chelating agent prepared in ethanol and the desired concentrations of the selected PGMs. DPSV measurements were performed from 0.8 to  $-1.4$  vs Ag/AgCl with a scan rate of  $0.5 \text{ V}$  vs Ag/AgCl, equilibrium time of 15 s, and a deposition time of 150 s. Electrochemical measurements were carried out in deoxygenated solutions, and were performed at room temperature.

#### 3.2.1.4 Anodic Stripping Voltammetry (ASV)

Anodic Stripping Voltammetry (ASV) involves a combination of a concentration step and a stripping step. The most voltammetric techniques employed in ASV are normal pulse (NPASV), differential pulse (DPASV) and square wave (SWASV) modes. Furthermore, ASV is also used to measure concentration in sub-parts per billion (sub-ppb) ranges. This method is normally employed for the detection of species with a positive charge such as positively charge metal ions and has been employed widely in stripping voltammetry of heavy metals in matrices. Anodic stripping voltammetry is very sensitive to experimental conditions, which we must carefully control if our results are to be accurate and precise. Key variables include the area of the mercury film or the size of the hanging Hg drop, the deposition time, the rest time, the rate of stirring, and the scan rate during the stripping step. Anodic stripping voltammetry is particularly useful for metals that form amalgams with mercury. In deposition the working electrode behave as a cathode, allowing the metal ions to be reduced and deposited onto the electrode surface at a suitable fixed negative potential for a specific length of time (also called the deposition time) (Rodriguez *et al.*, 2006).

### 3.3 Solids or Metal Disc Electrodes

Solid electrodes constructed using platinum, gold, silver, or carbon may be used over a range of potentials, including potentials that are negative and positive with respect to the SCE (Figure 3.4). For example, the potential window for a Pt electrode extends from approximately +1.2 V to -0.2 V versus the SCE in acidic solutions, and from +0.7 V to -1 V versus the SCE in basic solutions. A solid electrode can replace a mercury electrode for many voltammetric analyses that require negative potentials, and is the electrode of choice at more positive potentials. Except for the carbon paste electrode, a solid electrode is fashioned into a disk and sealed into the end of an inert support with an electrical lead (Figure 3.4). Solid electrodes are not without problems, the most important of which is the ease with which the electrode's surface is altered by the adsorption of a solution species or by the formation of an oxide layer.



For this reason a solid electrode needs frequent reconditioning, either by applying an appropriate potential or by polishing. Electrodes based on carbon are currently widely used in voltammetric techniques because of their broad potential window, low back ground current, chemically inertness, and suitability for various sensing and detection applications (Wang, 2000). These include the carbon paste electrode (CPE), glassy carbon electrode (GCE) and screen-printed carbon electrode (SPCE) (Figure 15). The working electrodes explored in this study included the platinum (Pt), glassy carbon (GC) and screen-printed carbon electrode (SPCE).



Figure 3.4 Commonly used solid disc electrodes (BASi Instruments, USA).

### 3.3.1 Carbon Paste Electrode (CPE) Construction

The carbon paste electrode is made by filling the cavity at the end of the inert support with a paste consisting of carbon particles and viscous oil. The carbon paste electrode was prepared by thoroughly mixing 0, 6 ml of mineral oil and 2 g of graphite powder in a mortar and pestle to obtain a very fine paste. The resulting paste was squeezed into a polyvinyl chloride (PVC) tube of 3 mm inside diameter (ID), until a paste length of 6 cm was reached. The carbon paste was in turn connected to a copper electric wire (OD = 0.5 mm) to complete the measurement circuit. The carbon paste electrode was renewed by extruding approximately 0.5 mm of paste and cutting the outer paste layer with a sharp knife and polishing the surface on filter paper to produce a smooth shiny surface (Somerset *et al.*, 2007; Somerset *et al.*, 2009). Figure 3.5 shows a diagram of carbon paste electrode.

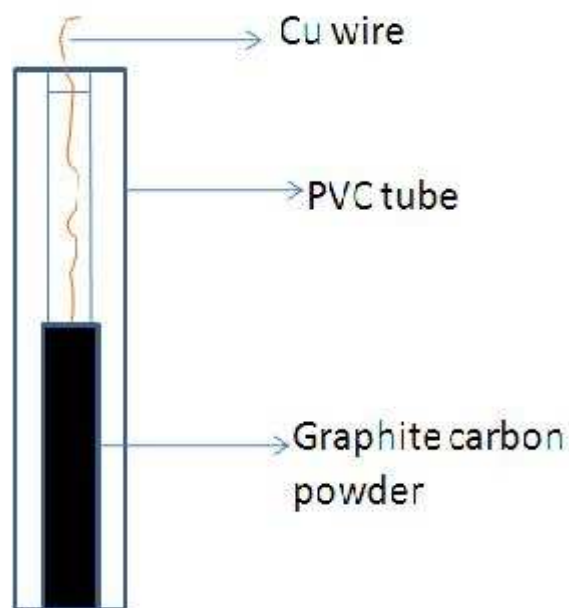
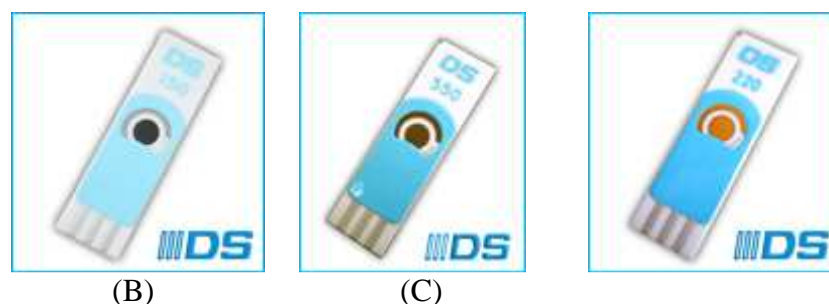


Figure 3.5 Illustration of carbon paste electrode

### 3.3.2 Screen Printed Carbon Electrodes (SPCE)

A typical screen-printed electrode is presented in Figure 3.6. Materials that are very useful for printing electrochemical sensors could be carbon-based inks because they have a very low firing temperature (20 - 120 °C) and can be printed on plastic substrate. Carbon ink can also be directly mixed with different compounds, such as a mediator and enzyme to produce a functionalised chemical or biosensor (Morrin *et al.*, 2008). In this work the SPCEs used were purchased from BVT Technologies, Czech Republic. The sensor has a ceramic base and was produced as follows. In this work the surface of the SPCE was modified with bismuth film (BiF) for a particular application. The sensor is formed on a corundum ceramic base. On to this surface the working, the reference and the auxiliary electrodes are applied. The working and the auxiliary electrodes are made of variety of materials. At the end of the sensor there is a contacting field which is connected with the active part by the carbon conducting paths which are covered by a dielectric protection layer. A biochemically active substance can also be immobilised on the working electrode of the sensor to create a biosensor.



**Figure 3.6** Commonly used screen printed electrodes, (A) carbon, (B) platinum and (c) Gold ([www.dropsen.com](http://www.dropsen.com), accessed on 1 August 2012).

### 3.3.3 Glassy Carbon Electrode (GCE) Construction

The usual electrode construction is as rod of glassy carbon, sealed into an inert electrode body, a disk of electrode material is exposed to the solution. Glassy carbon is produced by slowly baking a suitable resin at elevated temperatures until it is carbonized and then heating it to a very high temperature to cause vitrification. Vitreous carbon is relatively pure, mechanically strong, has good electrical properties and can be readily cleaned mechanically. It also performs particularly well when operated at a negative potential. Glassy carbon electrodes (GCEs) are preferable to carbon paste electrodes due to their inherent resistance to solvents. It is the most commonly used carbon electrode in electro-analytical application (Uslu and Ozkan, 2007). The cleaning of this electrode is important to maintain a reactive and reproducible surface. Pre-treated electrochemically GCE have increased oxygen functionalities that contribute to more rapid electron transfer.

### 3.4 UV-Vis Spectroscopic Characterisation

A Thermo Scientific Helios Omega range UV-VIS spectrometer with vision PC Software was used for spectroscopic characterisation. The schematic diagram of a typical single beam UV-Visible spectrometer is given in Figure 3.7. Ultraviolet-visible (UV-Vis) spectroscopy is a very useful analytical technique as it can be used to determine the amount of substance present in a sample. The absorption of UV-Vis energy gives rise to the electronic transition of occupied energy levels to unoccupied energy levels. More specifically, energy transitions from the highest occupied molecular orbital (HOMO) to the lowest unoccupied molecular orbital (LUMO). The UV-Vis radiation source has wavelengths in the range of 200 to 800 nm, with the UV range going from 200 - 400 nm and the visible range extending from 400 - 800 nm. In general, the radiation from the source was passed through a filter or a suitable monochromator to get a band or a monochromatic radiation. It was then passed through the sample (or the reference) and the transmitted radiation was detected by the photodetector. Typically, two operations were performed, first, the cuvette was filled with the reference solution and the absorbance reading from 200 - 1000 nm range was recorded. Second, the cuvette was taken out and rinsed and filled with sample solution and the process was repeated. The spectrum of the sample was obtained by subtracting the spectrum of the reference from that of the sample solution. The signal so obtained was sent as a read out or was recorded. The wavelength at which the maximum absorption occurs is known as  $\lambda_{max}$ . At this fixed wavelength, the absorbance changes in accordance with concentration, since the absorbance is proportional to the concentration of the absorbing species given by the Beer-Lambert law (Mehta, 2012). For the purposes of this study, UV-Vis spectroscopy was employed to investigate the stoichiometry of PANI and PANI-co-PDTDA as conducting polymers. After electropolymerisation, the samples were dissolved in N,N'-dimethylformamide (DMF) and placed in 1 cm quartz cuvettes and their UV-VIS spectra recorded. The spectra were recorded in the region 200 - 1000 nm. The obtained spectra were then used to characterise the absorption bands and analyse the polymers samples for similarities and differences in structure (Somerset *et al*, 2010).

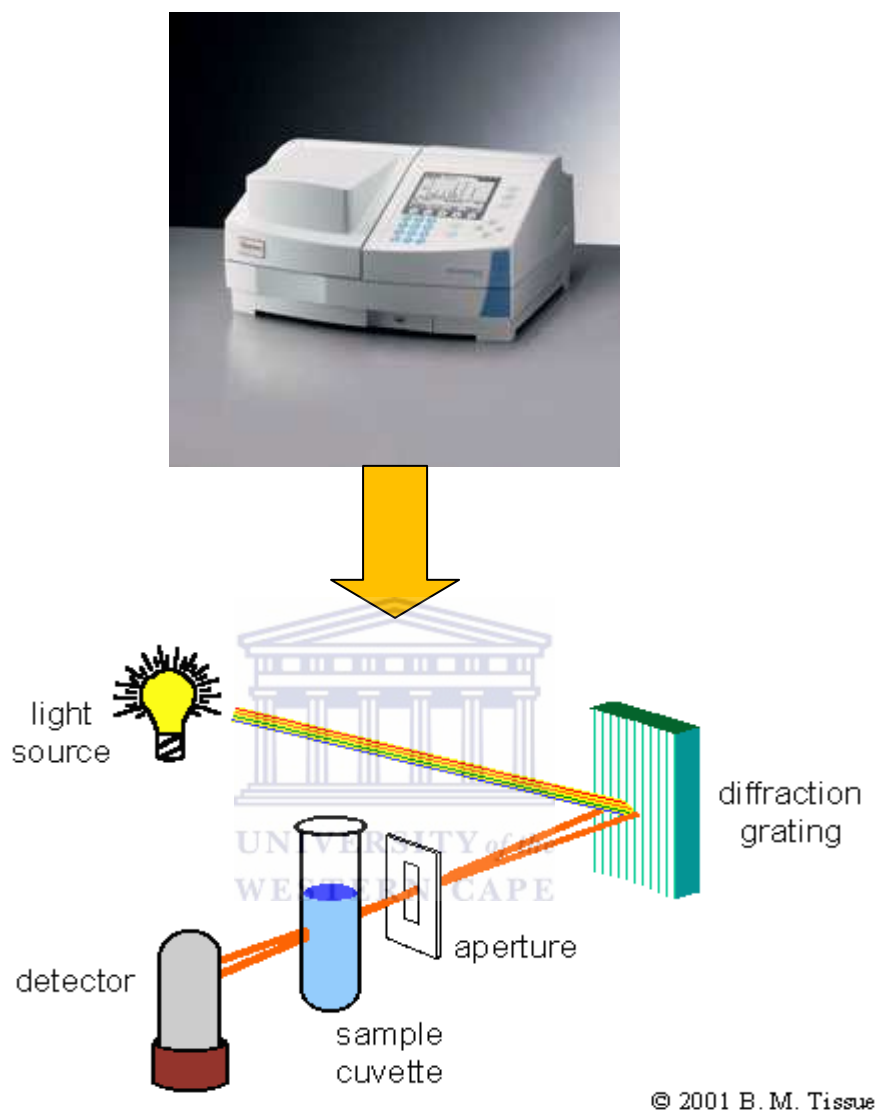


Figure 3.7 Schematic diagram of a single-beam UV-Vis spectrometer.  
<http://www.files.chem.vt.edu/chem-ed/spec/uv-vis/singlebeam.html>

### 3.5 FTIR Spectroscopic Characterisation

Figure 3.8 represent the schematic diagram showing the three basic spectrometer components in FTIR spectroscopy. An interferometer is used to differentiate and measure the absorption component frequencies. It divides radiant beams and generates an optical path difference by detector. An interferometer produces interference signals which contain infrared spectral information generated after passing through a sample when IR beam is directed through the sample, the amplitude of set of waves are reduced by absorption if the frequency of set waves is the same as one of the characteristic frequency of the sample. For the purpose of this study a Bruker® IFS 66/S FTIR spectrometer was used to characterise all the polymer samples synthesised in this study. The polymer samples were prepared by electrodeposition on a Pt disc electrode, followed by dissolution from the surface of the electrode into a 5 ml DMF solution. This process was repeated several times to ensure enough polymer material were dissolved into DMF for characterisation. The FTIR spectra were recorded in the region  $4000 - 100 \text{ cm}^{-1}$ . This method allowed for characterisation of the vibrations in the molecules by measuring the absorption of light of certain energies that correspond to the vibrational excitation of the molecules from lower to higher states (Somerset *et al.*, 2010).

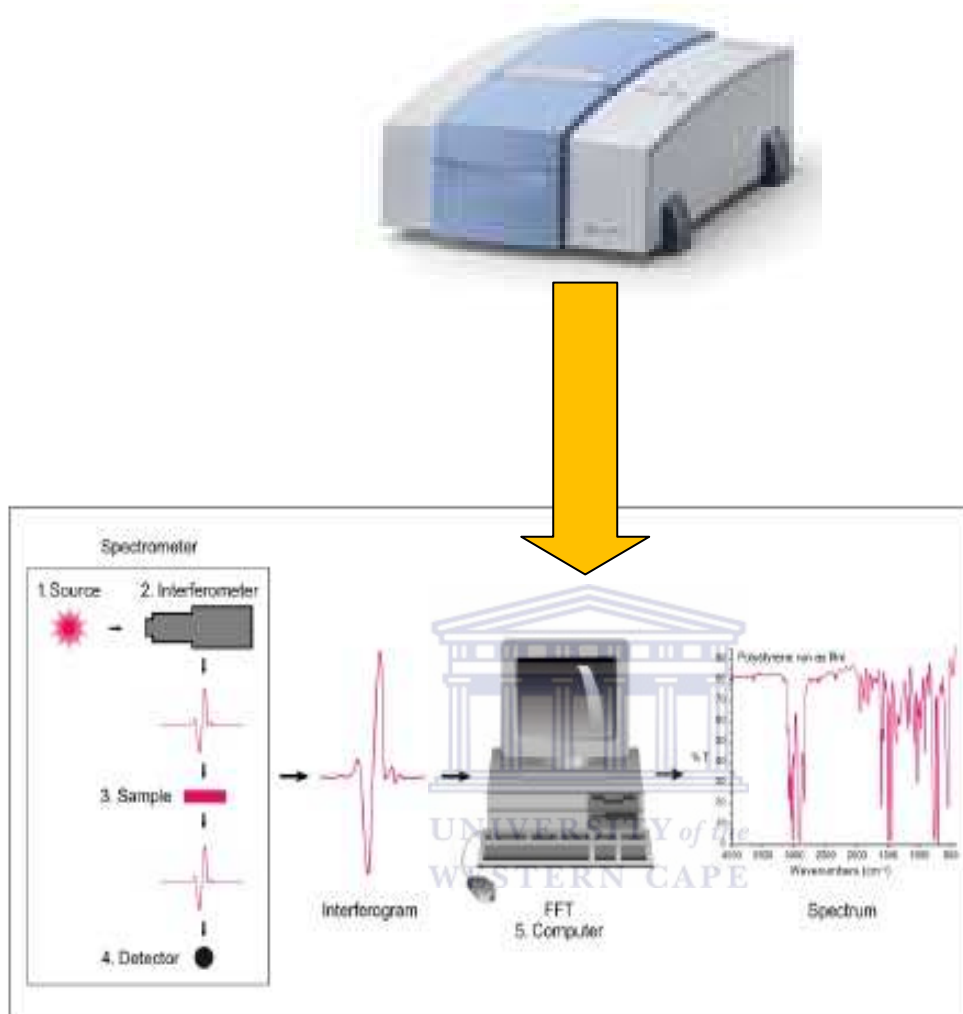


Figure 3.8 Schematic diagram showing working of FTIR spectroscopy ([www.macmillan.org.uk](http://www.macmillan.org.uk), 2010).



## Chapter 4

### Polymer Modified Electrode Surfaces

---

#### 4.1 Introduction

In the year 2000, three scientists, A.J. Heeger, A.G. MacDiarmid and H. Shirakawa, were credited for the discovery and development of electrically conducting polymers and they were awarded the Noble Prize in Chemistry. A bizarre-looking and semi conducting polyacetylene was obtained by accidental addition of 1000 times excess of catalyst. This was a breakthrough in the discovery of the conjugated polymers that created an entirely new field of chemistry. These polymers are comprised of carbon, hydrogen and simple hetero-atoms such as nitrogen and sulphur and contain  $\pi$ -conjugation across the polymer backbone. Typical  $\pi$ -conjugated conducting polymers include polyaniline (PANI), polypyrrole (PPy) and polythiophene (PTh). This chapter presents synthesis, spectroscopic characterisation, and electro-analytical characterisation of conducting polymers. Polyaniline and its derivatives have been studied extensively due to their conductivity (MacDiarmid *et al.*, 1991) and environmental stability in air (Abraham *et al.*, 1996). This electrochemical method is so advantageous compared to the chemical one because the growth rate is easily controlled and also offers a possibility of simultaneous characterisation. Electrochemical polymerisation occurs when a suitable anodic potential or current is applied to a conducting substrate that has been immersed in a monomer electrolyte. A counter (CE) and reference electrode (RE) are also needed in conjunction with the working electrode (WE) for this to take place in a three-electrode electrochemical cell (Somerset *et al.*, 2006). This study has also shown that 2,2'-dithiodianiline (DTDA) can act as a new co-monomer with aniline in the electrochemical copolymerization process to form polyaniline-co-poly (dithiodianiline). Thin films of PANI and PANI-co-PDTDA have been synthesised by using electrochemical polymerisation and copolymerisation respectively (Somerset *et al.*, 2010). This co-polymer has S-S bonds confined among the chains of the polymer.

The resulted polymer was in a form of thin layer on a glassy carbon electrode (GCE) which was characterised by voltammetry, UV-VIS and FTIR spectroscopy techniques. Ultraviolet-visible spectroscopy has been used for determining the polymerisation and band gap of the polymer while a CV has been used for determining the polymerisation and redox behaviour of the polymer, using voltammetry. The functional groups of the polymers were determined using FTIR spectroscopy.

Polyaniline exists in several oxidation states (Figure 4.1) with electrical conductivity varying progressively from  $10^{-8} \text{ S cm}^{-1}$  to more than  $10^2 \text{ S cm}^{-1}$ . These steps has shown that the PANI can be transformed from the leucoemeraldine to the emeraldine state and then from the emeraldine to pernigraniline states and the conducting emeraldine salt is the most important state in these molecular transformations of polyaniline. The existence of different oxidation states for PANI makes it useful as an electrode material in electrochemical capacitors (Iwuoha *et al.*, 1996; Fusalba *et al.*, 2001).

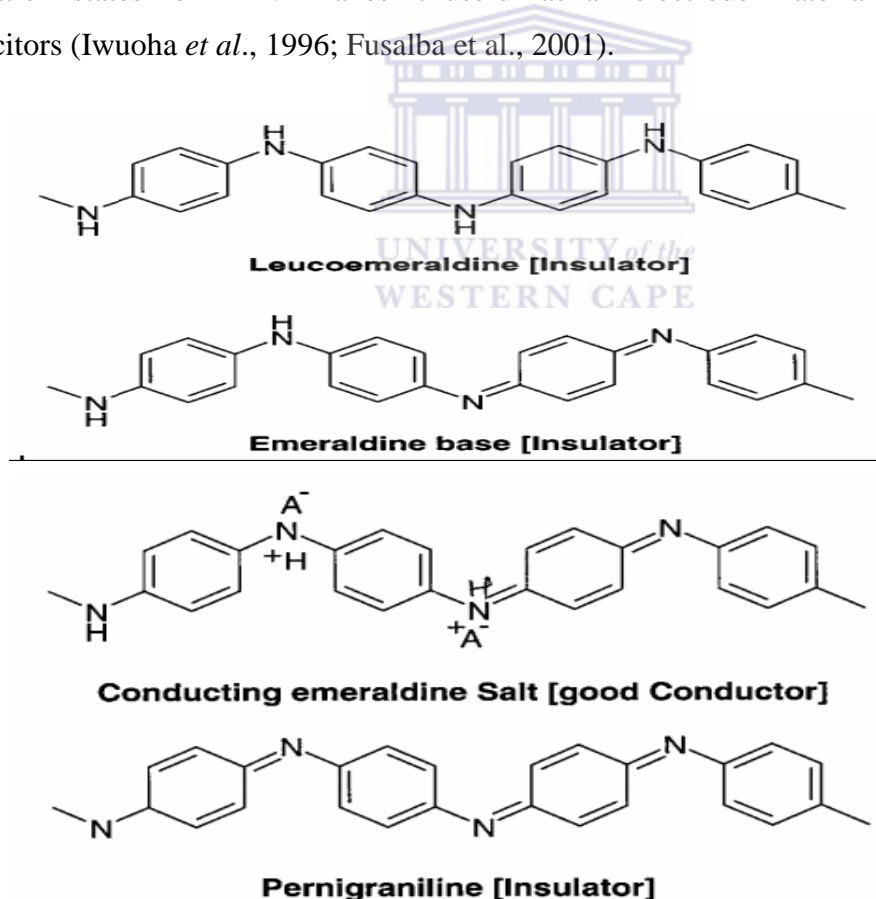


Figure 4.1 Molecular designs of the four oxidation states of Polyaniline (Trividi, 1994).

In this chapter, the objective was to apply a thin polymer film of PANI and PANI-co-PDTDA on the surface of glassy carbon electrode (GCE) for the preparation of a polymer modified electrode surface for biosensor preparation since they are composed of simple repeating units called monomers and are generally known to have good insulating properties. It is this characteristic that has resulted in insulating polymers being used extensively in many studies but conducting polymers differ from everyday polymers in that they are intrinsically conducting. The enzyme called horseradish peroxidase (HRP) was then immobilised onto both sensor platforms during biosensor construction. The final GCE/PANI/HRP and GCE/PANI-co-PDTDA/HRP biosensors were then evaluated and characterised independently, both to evaluate the biosensor characteristics of these sensors, but to also apply and utilise these biosensors in heavy metal inhibition studies. The heavy metal inhibition studies were conducted to evaluate the efficiency of the GCE/PANI/HRP and GCE/PANI-co-PDTDA/HRP biosensors as electrochemical sensors for heavy metal determination.

## 4.2 Materials and methods

### 4.2.1 Chemicals

The reagents aniline (99%) and N, N'-dimethylformamide (98%) were obtained from Aldrich (Germany); all solutions were always prepared using deionised water obtained from a Milli-Q RO Plus (Millipore Water) system. The potassium dihydrogen phosphate (99%) and disodium hydrogen phosphate (98%) were obtained from Aldrich (South Africa), while Merck's (RSA) supplied the sulphuric acid (95%), hydrochloric acid (32%), sodium chloride, ethanol (absolute 99.9%) and these were used as received. All electrochemical measurements were performed in 0.1 M phosphate buffered (PB) solution (1 M Na<sub>2</sub>HPO<sub>4</sub>; 1 M KH<sub>2</sub>PO<sub>4</sub>; pH 7.2).

#### 4.2.2 Apparatus

Electrochemical protocols were performed with two different electrochemical analysers, depending on the objective of the work conducted. Firstly, an Epsilon electrochemical analyser (BASi Instruments, 2701 Kent Ave., West Lafayette, IN 47906, USA), utilising cyclic voltammetry (CV) was used. Alternatively, experiments were performed with the PalmSens® handheld potentiostat / galvanostat, with the PStTrace program and accessories (Palm Instruments BV, 3992 BZ Houten, The Netherlands). A conventional three electrode system was employed, consisting of glassy carbon electrode (GCE; diameter = 1.6 mm diameter) disc working electrode, an Ag/AgCl in 3 M NaCl reference electrode, and a platinum wire auxiliary electrode (Somerset *et al.*, 2006; Somerset *et al.*, 2010). UV-Vis spectroscopic results were recorded between 200 and 1100 nm using a 1-cm path quartz cuvette and N,N'-dimethylformamide (DMF) as the reference solvent, on a Thermo® Fisher Spectronic™ Helios Omega range UV-Vis spectrometer with VISION PC software. Solutions for subsequent spectroscopic studies were by careful dilution or dissolving from the electrode surface in DMF (Somerset *et al.*, 2010). FTIR measurements were carried out using a Bruker® Optics aligned Rock Solid™ interferometer.

#### 4.2.3 Electropolymerisation of polymer films

A three electrode electrochemical cell was used to prepare PANI and PANI-co-PDTDA conducting polymers. A glassy carbon was employed as working electrode, platinum wire was used as the auxiliary electrode, and an Ag/AgCl in 3 M NaCl reference electrode was used as the reference throughout this work. Electropolymerisation was carried out at room temperature. A 10 ml solution consisting of 0.2 M aniline, and 0.02 M of 2,2'-dithiodianiline in aqueous H<sub>2</sub>SO<sub>4</sub> (varying concentrations of 1, 2.5, and 5 M) solution were prepared and placed in a sonicator for a few minutes to dissolve the mixture. The co-polymer film of polyaniline (PANI) and poly (2,2'-dithiodianiline) (called PANI-co-PDTDA) were grown electrochemically on the surface of a GCE by repetitive cyclic voltammetric scanning at 60 mV/s from - 0.2 to + 1.1 V, for 19 cycles at room temperature.

Polyaniline was also electropolymerised as a monopolymer on a GCE surface, using a 10 ml solution of 0.2 M aniline and aqueous 1 M HCl solution, while cycling repetitively at 60 mVs<sup>-1</sup> from - 0.2 to + 1.1 V for 10 cycles at room temperatures. Each GCE was then rinsed with deionised before voltammetric measurements (Somerset *et al.*, 2010).

### 4.3 Results and Discussion

The electrochemical behaviour of PANI and PANI-co-PDTDA were studied in 0.1 M HCl solution as supporting electrolyte using cyclic voltammetry (CV) as method.

#### 4.3.1. Cyclic voltammetric characterisation of polymer composites

Cyclic voltammetry (CV) for the electro-analytical studies of PANI and PANI-co-PDTDA were performed in order to obtain information on its electro-analytical properties. The peak potentials of these compounds were measured throughout this investigation against an Ag/AgCl reference electrode. The potential was scanned for cyclic voltammetric measurement between - 0.2 V and + 1.2 V at scan rate 0.1 Vs<sup>-1</sup> and sensitivity = 1 mAV<sup>-1</sup>. Various concentrations of acidic medium have been used in this experiment for the electropolymerisation and scan rate studies were performed. Analysis of the current response gave considerable information about the thermodynamics of the redox processes involved, the kinetics of heterogeneous electron-transfer reaction and the coupled chemical reactions or adsorption processes for the synthesised polymers. It was noted that during the growth of PANI and PANI-co-PDTDA respectively, the peak current values of the three redox processes increased with an increase in the number of cycles performed, as shown in Figures 20 and 21.

#### 4.3.1.1. Cyclic Voltammetric analysis of polyaniline

The possible redox couples that should be expected during the forward (oxidation) and backward (reduction) scans of potentials are shown in Figure 4.2 below.

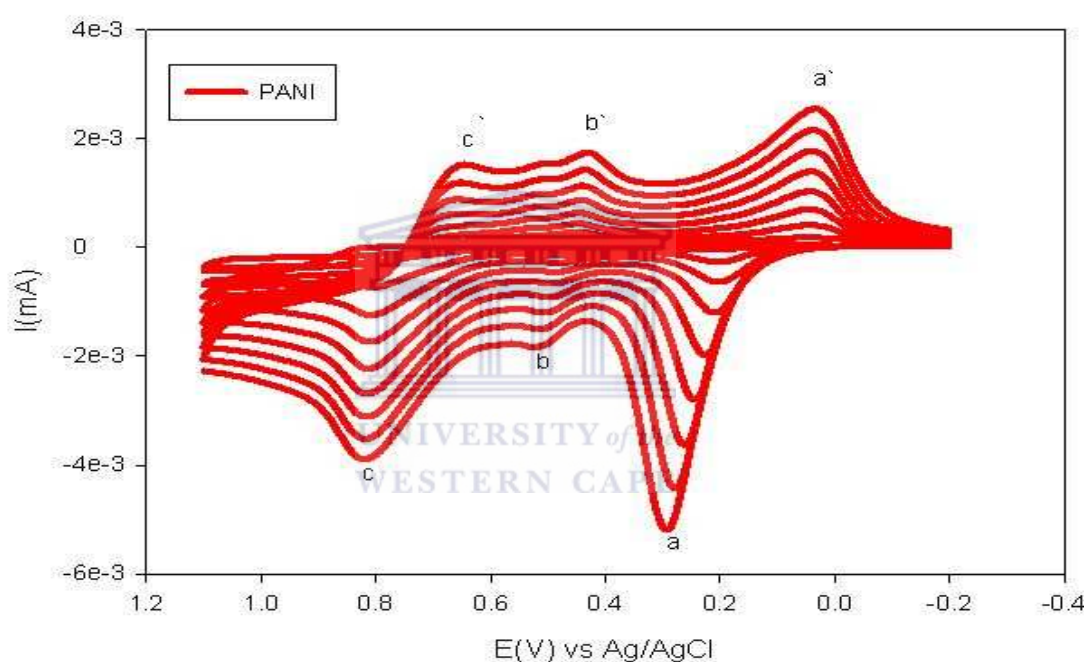


**Figure 4.2** Cyclic voltammogram (CV) displaying the electropolymerisation of PANI in 1 M HCl solution on a GCE surface. The potential was cycled between  $-0.2$  and  $+1.1$  V (vs. Ag/AgCl) at a scan rate of  $60 \text{ mV s}^{-1}$  for 19 cycles.

During the scanning in cyclic voltammetry (Figure 4.2), the repeated cycles for anodic current has been found to increase in subsequent voltammogram, which confirms the (formation of monomer) polymerization of PANI. This voltammogram displays well defined redox couples showing that PANI is electro-active. It can be seen that the anodic and cathodic current increases with the increase in the number of cycles. This may be due to an increase in the mass of PANI film deposited on the surface of the electrode.

The first redox couple ( $a/a'$ ), with a formal potential, around 0.2 V (vs. Ag/AgCl) represents the transformation of the leucoemeraldine form to the emeraldine form of the polymer. The middle redox couple ( $b/b'$ ) was observed at around 0.5 V (vs Ag/AgCl) anodically and around 0.4 V (vs Ag/AgCl) cathodically, due to the redox reaction involving over-oxidized PANI structure indicating degradation products (Wei *et al.*, 2004). Several authors assign this reversible couple to the redox actions of the degradation products hydroquinone to quinone (Huang *et al.*, 2006, Somerset *et al.*, 1996). The degradation can be visualised by the loss of electro-active sites as well as appearance of the peak at around 0.5 V (vs Ag/AgCl). The peaks become more prominent with increase of current. The middle redox couple ( $b/b'$ ) could also be due to defects in the linear structure of the polymer (Castelvetto *et al.*, 2002). The third redox couple ( $c/c'$ ), is attributed to the transition of the emeraldine form to the pernigraniline form of the polymer. The oxidation of this polysemiquinone radical cation (ES) form of PANI (redox couple ( $c/c'$ )) occurred at 0.8 V (vs Ag/AgCl). The formal potentials obtained in this study compare favourably with literature values reported for doped PANI (Somerset *et al.*, 2010).

#### 4.3.1.2 Cyclic Voltammetric analysis of polyaniline-co-2,2'-dithiodianiline

The CV of the co-polymer of PANI-co-PDTDA is shown in Figure 4.3. The results have demonstrated the deposition of the co-polymer when a mixture of aniline and 2,2'-dithiodianiline (DTDA) was polymerised simultaneously. The result in Figure 22 below represents the CV recorded for 19 cycles during copolymerisation. In this case a film of dark green colour was seen on the surface of the working electrode.



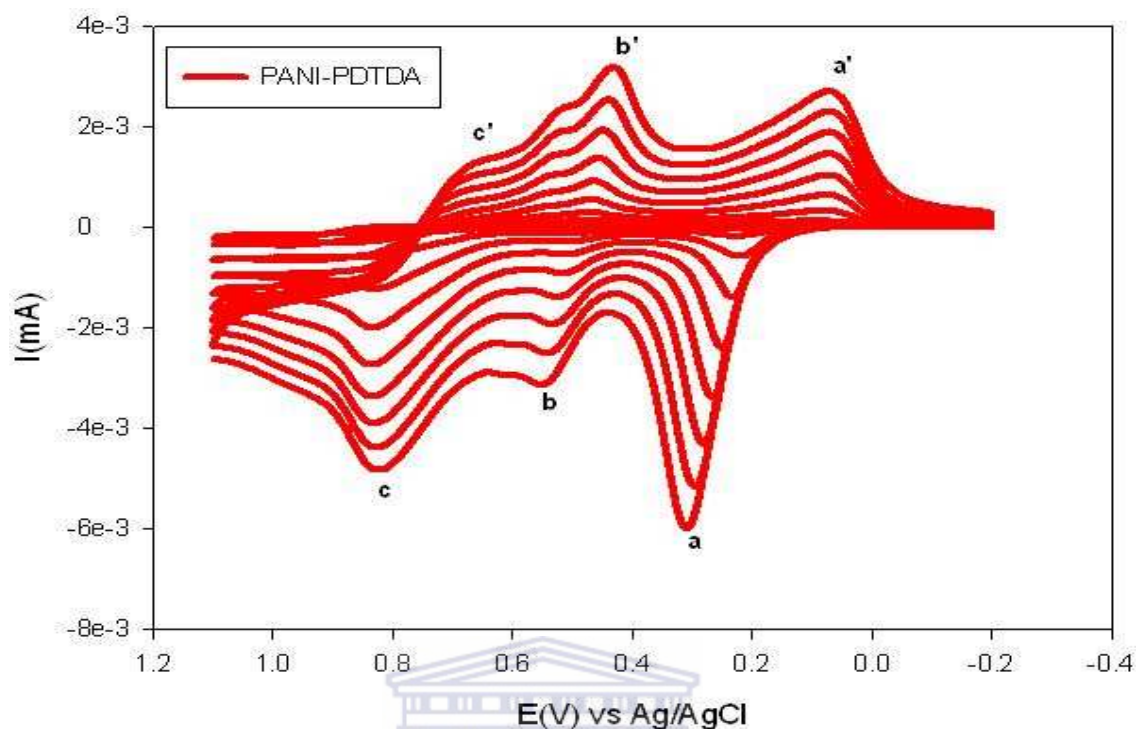


**Figure 4.3** Cyclic voltammogram (CV) displaying the electropolymerisation of PANI-co-PDTDA in 1 M  $\text{H}_2\text{SO}_4$  on a GCE surface. The potential was cycled between  $-0.2$  and  $+1.1$  V (vs. Ag/AgCl) at a scan rate of  $60 \text{ mVs}^{-1}$  for 19 cycles.

UNIVERSITY of the  
WESTERN CAPE

A comparison was made between PANI and PANI-co-PDTDA. Three major redox couples are distinguishable. The cyclic voltammetry (CV) of this copolymer at the same scan rate ( $60 \text{ mVs}^{-1}$ ) shows a shift in all oxidation peaks in comparison to polyaniline (PANI). This suggests that the conjugation length of the copolymer decreases as compared to polyaniline (PANI). Therefore one may also expect that the other physical properties of PANI-co-PDTDA will lie in the polyaniline polymer backbone. The middle peak is found to be different to that of PANI, it might be due to the merging of PANI and PDTDA peaks or the self-doping/undoping of thiolate anions (S) formed by the reductive cleavage of S-S bonds in the PDTDA backbone when the PANI-co-PDTDA co-polymer is formed (Somerset *et al.*, 2007).

The middle anodic current has been found to increase more in PANI-co-PDTDA than in PANI, which confirms the polymerization of PANI-co-PDTDA. The growth of PANI-co-PDTDA films showed three oxidation peaks around 0.32 V, 0.6 V and 0.85 V (vs. Ag/AgCl). Cathodic peaks were observed around 0.5 V, 0.55 V and 0.82 V (vs. Ag/AgCl). The redox couple ( $a/a^+$ ) are assigned for the transformation of leucoemeraldine base to emeraldine salt and the emeraldine salt to pernigraniline salt forms, while the middle oxidation peak indicates the formation of benzoquinone. Analysis of the reduction peaks shows that the first and third peaks correspond to the conversion of pernigraniline salt to emeraldine salt and emeraldine salt to leucoemeraldine base, while the middle peaks can be attributed to the formation of hydroquinone. These assignments have been made based on the earlier reports on PANI-co-PDTDA synthesis and characterisation (Somerset *et al.*, 2007).

#### 4.3.2 Effect of electrolyte concentration

The electrochemical behaviour of the PANI-co-PDTDA polymer film was studied in different concentrations of  $H_2SO_4$  solution at a scan rate of  $60\text{mVs}^{-1}$ .

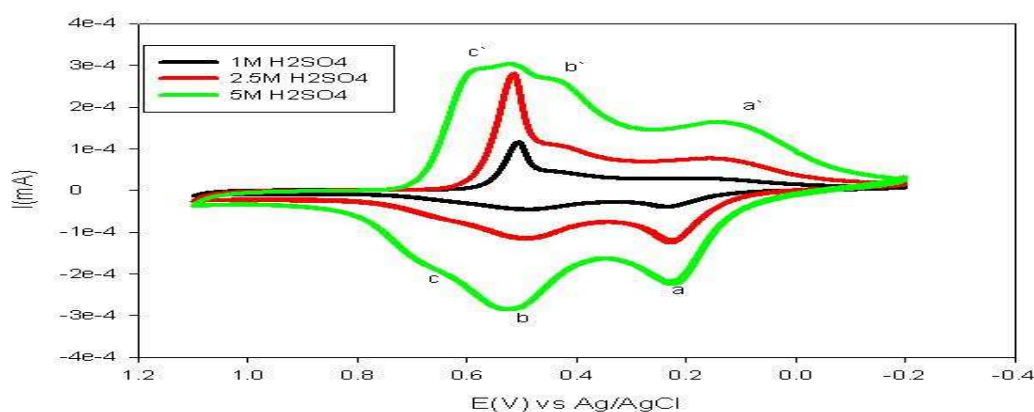
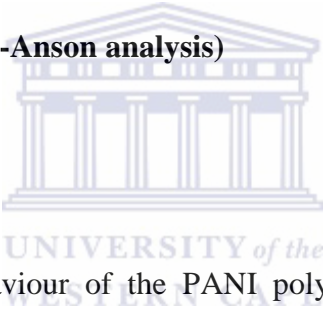


**Figure 4.4** Cyclic voltammogram for the electropolymerisation of PANI-co-PDTDA on a GCE at a scan rate of  $60\text{ mV s}^{-1}$ , using different  $H_2SO_4$  concentrations. The potential was cycled between  $-0.2$  and  $+1.1\text{V}$  (vs. Ag/AgCl).

The CV results in Figure 4.4 shows effects in the presence of supporting electrolytes containing different concentration of H<sub>2</sub>SO<sub>4</sub> solution of 1 M, 2.5 M and 5 M, respectively. Three redox couples were observed at around 0.2 V, 0.55 and 0.74 V (vs. Ag/AgCl) in a 5 M H<sub>2</sub>SO<sub>4</sub> solution. In the case of a 1 M H<sub>2</sub>SO<sub>4</sub> solution, the third redox couple has not been observed. When a 2.5 M H<sub>2</sub>SO<sub>4</sub> solution was used, the third oxidation peak was not clear. We have also noticed an increase in peak current as the concentration of H<sub>2</sub>SO<sub>4</sub> solution increased. This suggested that the film growth was considered greater for the high ionic strength media and the results also showed that 5 M H<sub>2</sub>SO<sub>4</sub> solution as a better supporting electrolyte for the co-polymerisation of aniline with 2,2'-dithioaniline (Haberska *et al.*, 2009).

### 4.3.3. Scan rate studies (Brown-Anson analysis)

#### 4.3.3.1. PANI



The electrochemical behaviour of the PANI polymer film was studied in H<sub>2</sub>SO<sub>4</sub> solution at scan rate 60 mVs<sup>-1</sup>. It was noted that for all concentrations of sulphuric acid, the 5 M one delivered the best results because the anodic and cathodic current was higher. Therefore, with PANI displaying the same behaviour, only the results for PANI in the 1 M H<sub>2</sub>SO<sub>4</sub> solution are displayed in Figure 4.5. This may be due to the increase in proton concentration which favours rapid protonation–deprotonation giving rise to increasing currents. The scan rate studies (Figure 4.5) have also shown that both the cathodic and anodic currents in PANI (similar to PANI-co-PDTDA) increases as the scan rate increases.

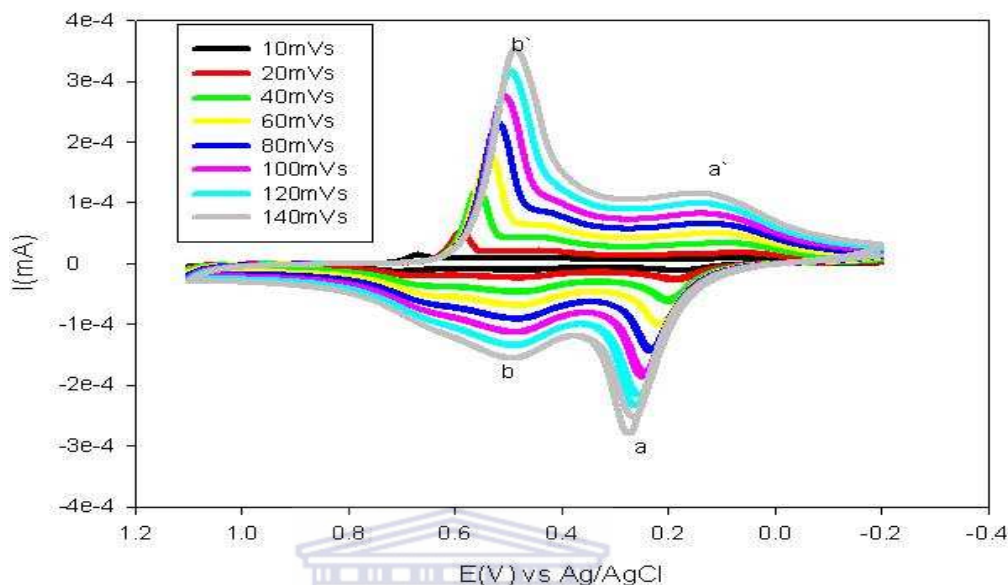


**Figure 4.5** Cyclic voltammogram of PANI coated on GC electrode in 0.1 M HCl at various scan rates. The potential was cycled from - 0.2 to 1.1 V (vs Ag/AgCl) and 1 mA.

For the CV results exhibited in Figure 4.5, two anodic peaks centred approximately at 0.28 V and 0.50 V (vs. Ag/AgCl) were obtained, with the peak heights increasing with the increase in scan rates. The position of the peak moves toward positive potential, for higher scan rates, and the peak height also increases as the scan rate increases. The results further suggest that the film was conductive and also electro-active. The peak currents in the cyclic voltammogram appeared to increase linearly with the increase of scan rate suggesting that an electro-active polymer layer is deposited on the electrode. There is the suggestion of another peak, which starts around 0.8 V (vs. Ag/AgCl) but this peak does not appear at higher scan rates.

#### 4.3.3.2 PANI-co-PDTDA

Cyclic voltammetry (CV) was also used in the scan rate studies of PANI-co-PDTDA, using a 5 M H<sub>2</sub>SO<sub>4</sub> electrolyte solution as shown in Figure 4.6.

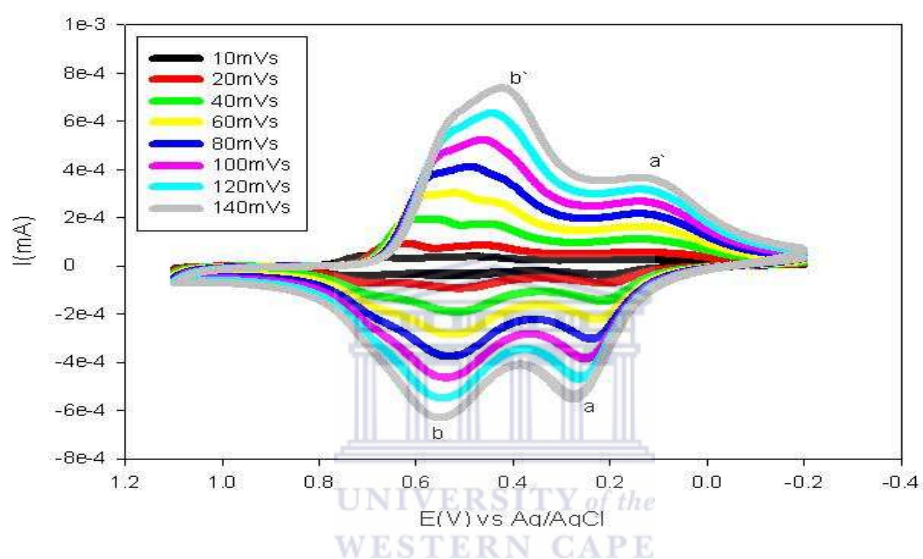


**Figure 4.6** Cyclic voltammograms of PANI-PDTDA coated on GC electrode in 0.1M HCl at various scan rates, The potential was cycled between – 0.2 and + 1.1V and 1 mA.

As shown in Figure 4.6, at a scan rate of 40 mVs<sup>-1</sup> the oxidation peak occurred at approximately 0.20 V (vs Ag/AgCl) and the corresponding reduction peak appeared at approximately 0.10 V (vs Ag/AgCl). A second oxidation peak was observed at approximately 0.55 V (vs Ag/AgCl). At scan rates 60 to 100 mVs<sup>-1</sup> the current peaks shifted outward, which indicated the separation between reaction zone and the surface of the electrode that is due to the thickness of the thin film. It has been noted that a third cathodic peak for PANI-co-PDTDA appeared at slower scan rates while we observed only two peaks at faster scan rates. The third peak might correspond to faster surface coating processes involving aniline.

It is well known that the oxidation of aniline in an acid media involves de-electronation and de-protonation of the monomers whose repetitive occurrence leads to the formation of PANI. The technique of surface polymerization has often been used in the coating of various materials with a conducting polymer overlayer (Trchova *et al.*, 2005). The first two anodic peaks in the cyclic voltammogram may, therefore be associated with this de-electronation and de-protonation steps. The absence of the third peak in this present experiment can be achieved by choosing an appropriate concentration of the solvent, and also by choosing an appropriate scan rate. We experienced well separated peaks at the concentration of 5 M H<sub>2</sub>SO<sub>4</sub> solution. The possibility of using higher concentrations of H<sub>2</sub>SO<sub>4</sub> as a suitable solvent would result in a co-polymer with higher number of S links.

#### 4.4 Electrochemical calculations and characterisation of polymer films

##### 4.4.1 Brown-Anson analysis

Scan rate studies of the PANI and PANI-co-PDTPA polymer films were performed in a 0.1 M HCl solution, in order to calculate the surface concentration of the polymer films on the GCE electrode in accordance with Brown–Anson analysis, using a plot of peak current ( $I_p$ ) against scan rate ( $\nu$ ) with the results calculated using Equation 4.1 (Somerset *et al.*, 2006):

$$I_p = \frac{n^2 \cdot F^2 \cdot A \cdot \Gamma_{PANI}}{4 \cdot R \cdot T} \nu \quad (\text{Eqn. 4.1})$$

where  $n$  represents the number of electrons transferred,  $F$  is the Faraday constant (96,584 Cmol<sup>-1</sup>),  $\Gamma_{PANI}$  is the surface concentration of the PANI film (molcm<sup>-2</sup>),  $A$  is the surface area of the electrode (0.0177 cm<sup>2</sup>),  $\nu$  is the scan rate (Vs<sup>-1</sup>),  $R$  is the gas constant (8.314 J mol<sup>-1</sup> K<sup>-1</sup>), and  $T$  is the temperature of the system (298 K). The  $\Gamma_{PANI}$  value was estimated to be  $1.228 \times 10^{-8}$  mol cm<sup>-2</sup> (Somerset *et al.*, 2006).

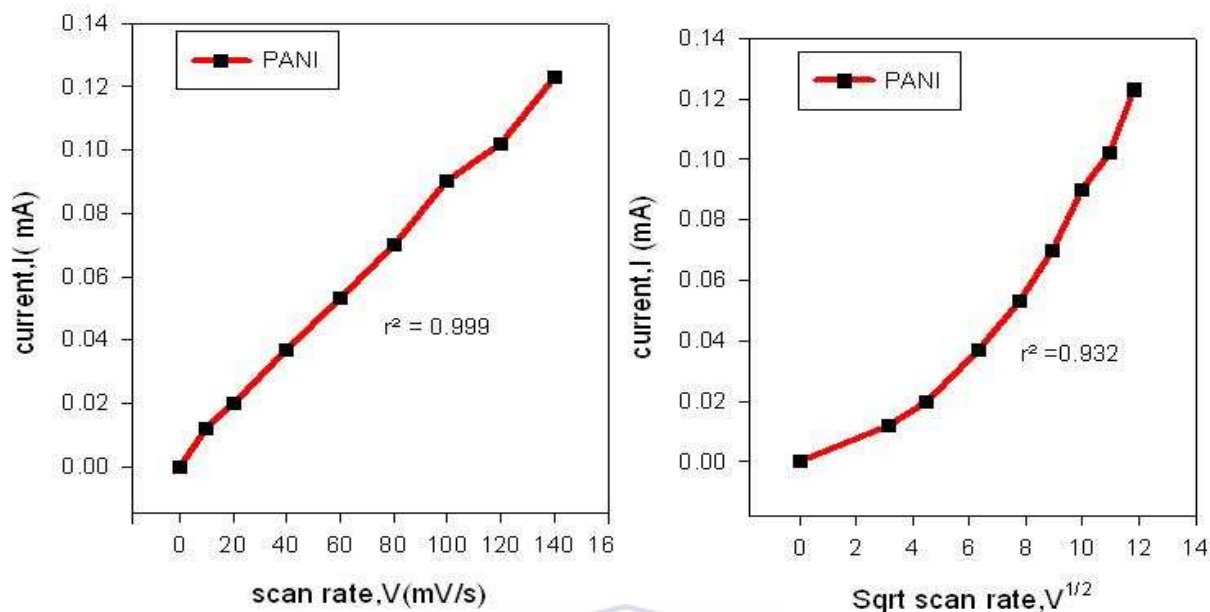


Figure 4.7 The graphs of peak current vs. scan rate and peak current vs. square root of scan rate for PANI.

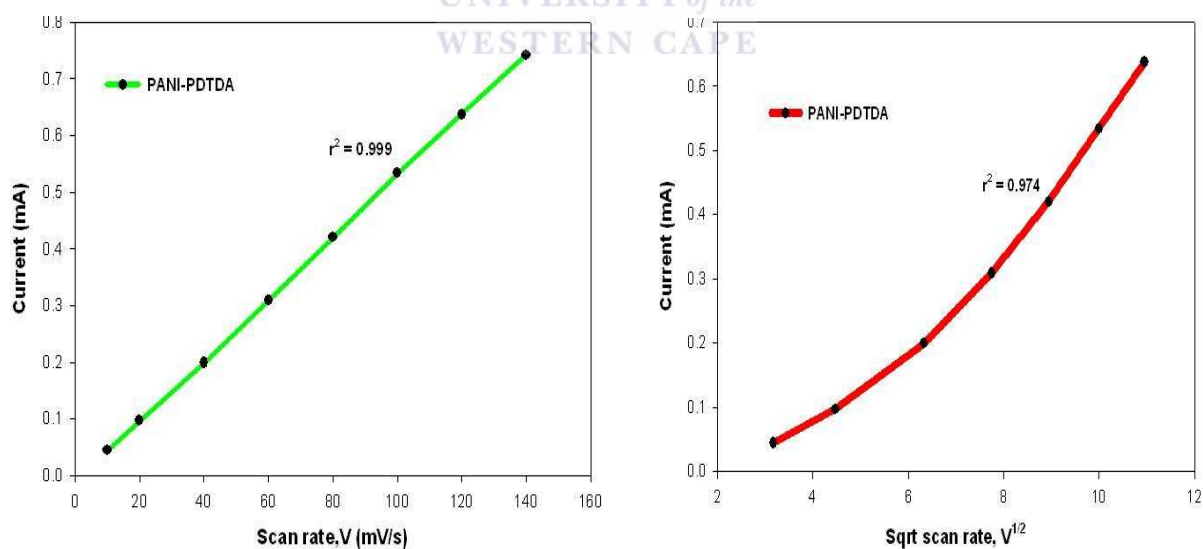


Figure 4.8 The graphs of peak current vs. scan rate and peak current vs. square root of scan rate for PANI-co-PDTDA.



For the reversible reaction of PANI and PANI-co-PDTDA, the dependence of current peak to their scan rate are shown in the plots of current versus scan rate and square root of scan rate are shown in Figures 26 and 27 respectively. The regression of this relationship shows that the peak current of PANI and PANI-co-PDTDA correlates well with the scan rates of the polymers and the list is shown in Table 2. Cyclic voltammograms of PANI and PANI-co-PDTDA for increasing scan rate are shown in Figures 24 and 25. The calculated kinetic parameters, *i.e.* the surface concentration, diffusion current and the thickness of the film for this polymer and copolymer are also listed from Tables 3 – 5.

The electrochemical characteristics of the PANI and PANI-co-PDTDA polymers were calculated using various equations that are shown below, with the results obtained for each of the respective polymers.

#### 4.4.1.1 Number of electrons in polymer matrices

Equation 4.2 was used for calculating the number of electrons in each of the polymer films (Bard and Faulkner, 2001):

$$|E_p - E_{p/2}| = 2.20 \frac{RT}{n.F} \quad (\text{Eqn. 4.2})$$

Where  $F$  is the Faraday constant ( $96,485 \text{ C mol}^{-1} \cdot e^{-}$ ),  $R$  is the universal gas constant ( $8.314 \text{ J.K}^{-1} \cdot \text{mol}^{-1}$ ),  $T$  is the absolute temperature of the system ( $25 \text{ }^{\circ}\text{C} = 298.15 \text{ K}$ ), and  $n$  is the number of electrons.

**4.4.1.2. PANI:**

Calculation of the number of electron for the PANI polymer film.

(i)  $E_p = + 448.7 \text{ mV}; I_p = + 4.61 \times 10^{-2} \text{ mA}$

(ii)  $E_{p/2} = + 523.6 \text{ mV}; I_{p/2} = +2.80 \times 10^{-2} \text{ mA}$

Using Equation 4.3, the following results were obtained:

$$|E_p - E_{p/2}| = 2.20 \frac{RT}{n.F} \quad (\text{Eqn. 4.3})$$

With the calculated parameters for this polymer, the above equation becomes:

$$|448.7 - 523.6| \text{ mV} = (2.20) \cdot \left[ \frac{8.314 \times 294.15}{n \times 96.485} \right] \quad \text{at } 21 \text{ }^\circ\text{C}$$

$n = 0.7546$

$n = 0.76 \text{ e}^-$

**Note:** at 21°C;  $n = 0.76 \approx 1 \text{ e}^-$

#### 4.4.1.3 PANI-co-PDTDA:

Calculation of the number of electrons for the PANI-co-PDTDA copolymer film, delivered the following results:

(i)  $E_p = + 424.8 \text{ mV}; I_p = +3.07 \times 10^{-2} \text{ mA}$

(ii)  $E_{p/2} = + 495.3 \text{ mV}; I_{p/2} = + 2.21 \times 10^{-2} \text{ mA}$

Using Equation 4.4, the following results were obtained:

$$|E_p - E_{p/2}| = 2.20 \frac{RT}{n.F} \quad (\text{Eqn. 4.4})$$

With the calculated parameters for this polymer, the above equation becomes:

$$|424.8 - 495.3| \text{ mV} = (2.20) \cdot \left[ \frac{8.314 \times 294.15}{n \times 96.485} \right] \quad \text{at } 21 \text{ }^\circ\text{C}$$

$$n = 0.8017$$

$$n = 0.80 \text{ e}^-$$

**Note:** at 21 °C;  $n = 0.80 \approx 1 \text{ e}^-$

#### 4.4.1.4 Summary of results for all polymer matrices:

A summary of the results collected for the calculations of the number of electrons involved in the electrosynthesis of the polymer matrices, is shown in Table 4.1.

**Table 4.1** Summary of results for the number of electrons for all electrosynthesised polymer matrices.

Polymer	Media	Current	Number of electrons
PANI	1 M HCl	Cathodic	0.76
PANI-co-PDTDA	1 M H <sub>2</sub> SO <sub>4</sub>	Cathodic	0.8
PANI-co-PDTDA	2.5 M H <sub>2</sub> SO <sub>4</sub>	Cathodic	1.17
PANI-co-PDTDA	5 M H <sub>2</sub> SO <sub>4</sub>	Cathodic	1.81

When comparing the results, it was found that 5 M H<sub>2</sub>SO<sub>4</sub> gave the highest number of electrons involved in the reaction of copolymer PANI-co-PDTDA while in the lowest concentrations we have noticed similar results in both PANI and PANI-co-PDTDA.

#### 4.4.2 Surface concentration of the polymer matrices

In the next step, the surface concentration of the electro-active species or polymer film (e.g. PANI,  $\Gamma_{\text{PANI}}^*$ ) was calculated. Using Randel-Sevcik plots of peak current vs. scan rate (or square root of scan rate); the data needed to perform Brown-Anson analysis were collected. The Brown-Anson equation is given in Equation 4.5 (Zanello, 2003):

$$I_p = \frac{n^2 \cdot F^2 \cdot A \cdot \Gamma_P^*}{4RT} \cdot \nu \quad (\text{Eqn. 4.5})$$

Where the slope is equal to:

$$\text{Slope} = \frac{n^2 \cdot F^2 \cdot A \cdot \Gamma_{PDMA}^*}{4RT} \quad (\text{Eqn. 4.6})$$

Where  $F$  is the Faraday constant ( $96,485 \text{ C} \cdot \text{mol}^{-1} \cdot e^-$ ),  $R$  is the universal gas constant ( $8.314 \text{ J} \cdot \text{K}^{-1} \cdot \text{mol}^{-1}$ ),  $T$  is the absolute temperature of the system ( $25 \text{ }^\circ\text{C} = 298.15 \text{ K}$ ),  $A$  is the surface area of the electrode, and  $n$  is the number of electrons.

**Table 4.1 Summary of results of slope and  $R^2$  for all polymer matrices investigated.**

Polymer	Current	Slope	Slope	$R^2$	$R^2$
		(scan rate)	(sqrt scan rate)	(scan rate)	(sqrt scan rate)
PANI (1 M HCl)	Cathodic	$2.8 \times 10^{-3}$	$4.05 \times 10^{-2}$	0.987	0.997
PANI-co-PDTDA (1 M $\text{H}_2\text{SO}_4$ )	Cathodic	$7.4 \times 10^{-4}$	$1.06 \times 10^{-2}$	0.983	0.93
PANI-co-PDTDA (2.5 M $\text{H}_2\text{SO}_4$ )	Cathodic	$1.9 \times 10^{-3}$	$2.8 \times 10^{-2}$	0.989	0.955
PANI-co-PDTDA (5 M $\text{H}_2\text{SO}_4$ )	Cathodic	$5.5 \times 10^{-3}$	$7.99 \times 10^{-2}$	0.999	0.973

When comparing the results for both PANI and PANI-co-PDTDA, an appropriate linear regression model has been found.

#### 4.2.2.1 PANI

Using the results obtained for the electropolymerisation of PANI, the following results were obtained:

(i) For the final cycle:  $I_p$ , a =  $-5.250 \times 10^{-3} \text{ A}$ ;  $E_p$ , a =  $+290.1 \text{ mV}$

(ii)  $A$  = surface area of the glassy carbon electrode; diameter = 3 mm;  $r = 1.5 \text{ mm} = 0.15 \text{ cm}$

$$A = \pi r^2 = \pi \times (0.15 \text{ cm})^2 = 0.0707 \text{ cm}^2$$

(iii) The following equation was then used to calculate  $\Gamma_{\text{PANI}}^*$

$$I_p = \frac{n^2 \cdot F^2 \cdot A \cdot \Gamma_p^* \cdot \nu}{4RT} \quad (\text{Eqn. 4.7})$$

$$\text{Slope} = \frac{n^2 \cdot F^2 \cdot A \cdot \Gamma_p^*}{4RT} \quad (\text{Eqn. 4.8})$$

$$\text{Thus, for PANI} \quad \Gamma_p^* = \frac{\text{slope} \cdot 4 \cdot R \cdot T}{n^2 \cdot F^2 \cdot A} = \frac{(2.8 \times 10^{-3}) \times 4 \times 8.314 \times 298.15}{(1)^2 \times (96.485)^2 \times 0.0707}$$

$$\Gamma_p^* = 6.19 \times 10^{-1} \text{mol.cm}^{-2}$$

#### 4.4.2.2 Summary of results for surface concentration all polymer matrices:

In a similar method as for PANI, the surface concentration of the PANI-co-PDTDA polymer film was also calculated. A summary of the results are shown in Table 3.

**Table 4.3** Summary of results for the surface concentration of the polymer matrices.

Polymer	Current	$\Gamma_{\text{polymer}}$
PANI (1 M HCl)	Cathodic	$2.64 \times 10^{-1}$
PANI-co-PDTDA (1 M H <sub>2</sub> SO <sub>4</sub> )	Cathodic	$6.13 \times 10^{-02}$
PANI-co-PDTDA (2.5 M H <sub>2</sub> SO <sub>4</sub> )	Cathodic	$7.36 \times 10^{-02}$
PANI-co-PDTDA (5 M H <sub>2</sub> SO <sub>4</sub> )	Cathodic	$7.93 \times 10^{-02}$

Using Brown-Anson equation, the surface coverage,  $\Gamma$ , was calculated and the results are presented in Table 3. When comparing the results, it was found that PANI has the highest surface concentration among the concentrations of the PANI-co-PDTDA polymer.

#### 4.4.3 Electron transport diffusion coefficient in polymer matrices

The electron transport diffusion coefficient,  $D_e$  (in  $\text{cm}^2\text{s}^{-1}$ ), was calculated from the Randle-Sevcik plot of peak current ( $I_p$ ) versus square root of scan rate ( $v^{1/2}$ ). Using the Randle-Sevcik data and Equation 4.3 (Bard and Faulkner, 2001), the following Equation 4.9 was obtained for the determination of  $D_e$ :

$$I_p = 2.69 \times 10^5 \cdot n^{3/2} \cdot A \cdot D_e^{1/2} \cdot C \cdot v^{1/2} \quad (\text{Eqn. 4.9})$$

Where  $F$  is the Faraday constant ( $96,485 \text{ C}\cdot\text{mol}^{-1}\cdot\text{e}^-$ ),  $R$  is the universal gas constant ( $8.314 \text{ J}\cdot\text{K}^{-1}\cdot\text{mol}^{-1}$ ),  $T$  is the absolute temperature of the system ( $25 \text{ }^\circ\text{C} = 298.15 \text{ K}$ ),  $A$  is the surface area of the electrode, and  $n$  is the number of electrons.

The result from a plot of  $I_p$  vs  $v^{1/2}$  is then used and the slope is equal to:

$$\text{Slope} = 2.69 \times 10^5 \cdot n^{3/2} \cdot A \cdot D_e^{1/2} \cdot C \quad (\text{Eqn. 4.10})$$

and using the individual results, the calculation amounts to:

##### 4.4.3.1 PANI

$$\text{Slope} = (2.69 \times 10^5) \times n^{3/2} \times A \times D_e^{1/2} \times C$$

$$2.8 \times 10^{-3} = 2.69 \times 10^5 \times (0.76)^{3/2} \times 0.0707 \times D_e^{1/2} \times 0.1$$

$$(D_e)^{1/2} = 2.22 \times 10^{-6}$$

$$D_e = (2.22 \times 10^{-6})^2$$

$$D_e = 4.94 \times 10^{-12} \text{ cm}^2\cdot\text{s}^{-1}$$



#### 4.4.3.2 Summary of results for the diffusion coefficients all polymer matrices

In a similar method as for PANI, the diffusion coefficient of the PANI-co-PDTDA polymer film was also calculated. A summary of the results are shown in Table 4.

**Table 4.4** Summary of results for electron transport diffusion coefficients in polymer matrices.

Polymer	Current	$D_e$
PANI (1 M HCl)	Cathodic	$1.34 \times 10^{-8}$
PANI-co-PDTDA (1 M H <sub>2</sub> SO <sub>4</sub> )	Cathodic	$7.65 \times 10^{-10}$
PANI-co-PDTDA (2.5 M H <sub>2</sub> SO <sub>4</sub> )	Cathodic	$1.68 \times 10^{-9}$
PANI-co-PDTDA (5 M H <sub>2</sub> SO <sub>4</sub> )	Cathodic	$2.92 \times 10^{-9}$

When comparing the results, it was found that the rate of electron transport along the polymer chain is faster in PANI (0.1 M HCl) solution than the substituted polymer (PANI-co-PDTDA) in various concentrations of H<sub>2</sub>SO<sub>4</sub> solution.

#### 4.4.4 Thickness of the polymer films

The thickness of the polymer film obtained with electrosynthesis on the electrode was also calculated. The following equation from Iwuoha *et al.* (1997) was used in the calculation, where a plot of peak current ( $I_p$ ) versus square root of scan rate ( $v^{1/2}$ ), gives the slope of the curve equal to Equation 4.7.

$$\frac{I_{p,c}}{v^{1/2}} = \frac{0.4463 \cdot (nF)^{3/2} \cdot A \cdot D_e \cdot \Gamma_P^*}{L \cdot (RT)^{1/2}} = \text{slope} \quad (\text{Eqn. 4.11})$$

where  $F$  is the Faraday constant ( $96,485 \text{ C}\cdot\text{mol}^{-1}\cdot\text{e}^{-}$ ),  $R$  is the universal gas constant ( $8.314 \text{ J}\cdot\text{K}\cdot\text{mol}$ ),  $T$  is the absolute temperature of the system ( $25 \text{ }^{\circ}\text{C} = 298.15 \text{ K}$ ),  $A$  is the surface area of the electrode,  $D_e$  is the electron transport diffusion coefficient,  $n$  is the number of electrons,  $\Gamma_P^*$  is the surface concentration of the electro-active species or polymer film, and  $L$  is the thickness of the polymer film (cm).

Thus, when values are substituted into Equation 4.7, the slope is then equal to Equation 4.8:

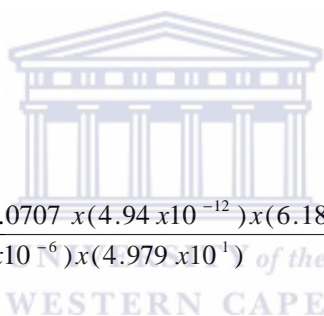
$$\frac{0.4463 \cdot (nF)^{3/2} \cdot A \cdot D_e \cdot \Gamma_P^*}{L \cdot (RT)^{1/2}} = \text{slope} \quad (\text{Eqn. 4.12})$$

And using the individual results, the calculation amounts to:

#### 4.4.4.1 PANI

$$L = \frac{0.4463 \times (6.27 \times 10^2) \times 0.0707 \times (4.94 \times 10^{-12}) \times (6.188 \times 10^{-6})}{(6.039 \times 10^{-6}) \times (4.979 \times 10^1)}$$

$$L = 2.41 \times 10^{-11} \text{ cm}$$



#### 4.4.4.2 Summary of results for film thickness of all polymer matrices

In a similar method as for PANI, the film thickness of the PANI-co-PDTDA polymer film was also calculated. A summary of the results are shown in Table 5.

**Table 4.5 Summary of results for the thickness of the polymer films.**

Polymer	Current	L (CM)scan rate	L (CM) <sub>sqrt scan rate</sub>
PANI (1 M HCl)	Cathodic	$7.09 \times 10^{-10}$	$1.49 \times 10^{-9}$
PANI-co-PDTDA(1 M H <sub>2</sub> SO <sub>4</sub> )	Cathodic	$3.87 \times 10^{-11}$	$8.16 \times 10^{-9}$
PANI-co-PDTDA(2.5 M H <sub>2</sub> SO <sub>4</sub> )	Cathodic	$6.74 \times 10^{-11}$	$1.47 \times 10^{-8}$
PANI-co-PDTDA(5 M H <sub>2</sub> SO <sub>4</sub> )	Cathodic	$9.77 \times 10^{-11}$	$2.05 \times 10^{-8}$

The thickness of the PANI and PANI-co-PDTDA film was calculated and the results in table 5 show the highest film thickness at higher concentrations of the acid media. In summary it was found that the results that are obtained in this study for the kinetic parameters ( $De$ ,  $L$  &  $I$ ) of PANI are in close agreement with results reported by Somerset *et al.* (2010) who studied the electropolymerisation of PANI and PANI-co-PDTDA polymer films.

## 4.5. Spectroscopic characterisation of polymers

### 4.5.1 UV-Vis spectroscopic characterisation of polymers

The UV-Vis spectra obtained of PANI in 1 M HCl solution and PANI-co-PDTDA in three concentrations of H<sub>2</sub>SO<sub>4</sub> solution (e.g. 1, 2.5 and 5 M) are shown in Figure 4.9.

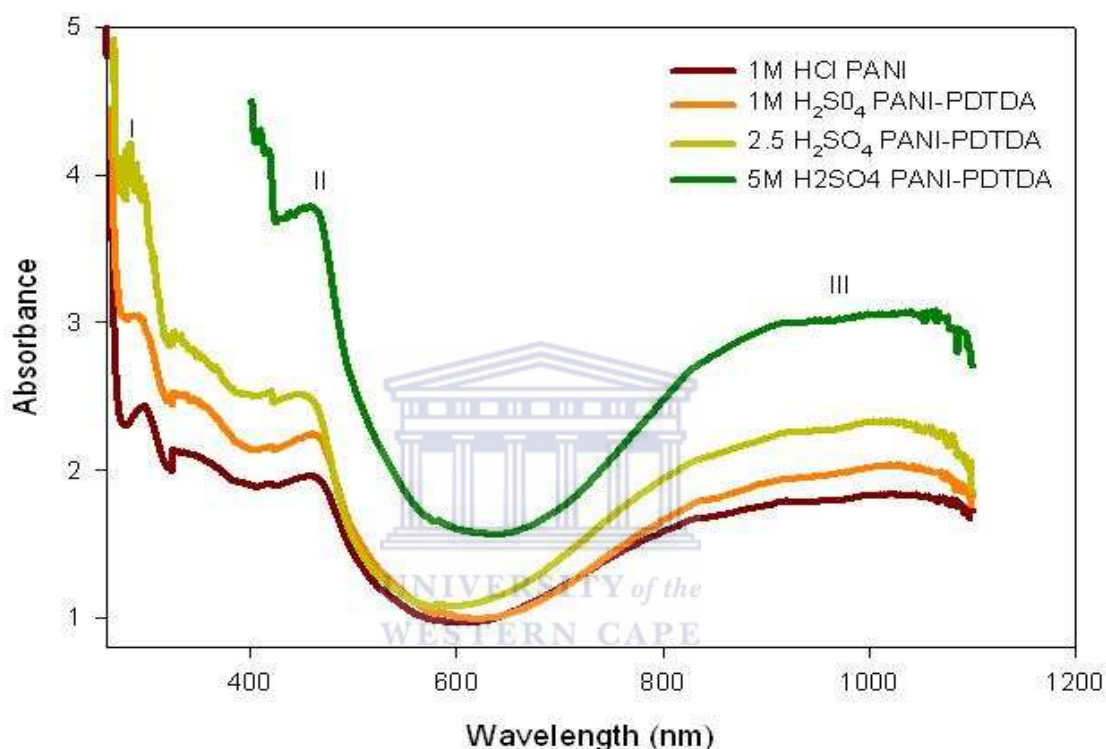


**Figure 4.9** UV-VIS spectra of PANI and PANI-co-PDTDA collected on a glassy carbon electrode, comparing the absorption maxima of the different polymer films electrosynthesised.

The absorption results obtained from electrochemical polymerisation of PANI and PANI-co-PDTDA clearly show the incorporation of PDTDA into the PANI during polymerization. This figure indicates that the spectrum of PANI has shown four bands around 290, 320, 490 and 890 nm. Two peaks that could be seen around 320 nm and 490 nm represent the transition of emeraldine form of the polymer to more oxidised form while the peak at 290 nm corresponds to polaron formation in the emeraldine chain (Huerta-Vic *et al.*, 2003).

These results are in close agreement with the results of doped PANI found in the literature of Michira *et al.* (2007) and Sharma *et al.* (2006). The PANI and PANI-co-PDTDA polymers investigated in this study, have shown that in 1 M H<sub>2</sub>SO<sub>4</sub> solution some similarities exist, although a little difference in the spectroscopic results have been observed for the 5 M H<sub>2</sub>SO<sub>4</sub> solution used.

#### 4.5.2 FTIR spectroscopic characterisation of polymers

The FTIR spectra of PANI and PANI-co-PDTDA are presented in Figure 4.10. The assignment of the spectra bands were made based on the previous literature values for the IR spectra of PANI and PANI-co-PDTDA polymers, which were used for the structural analysis of the synthesised polymers.

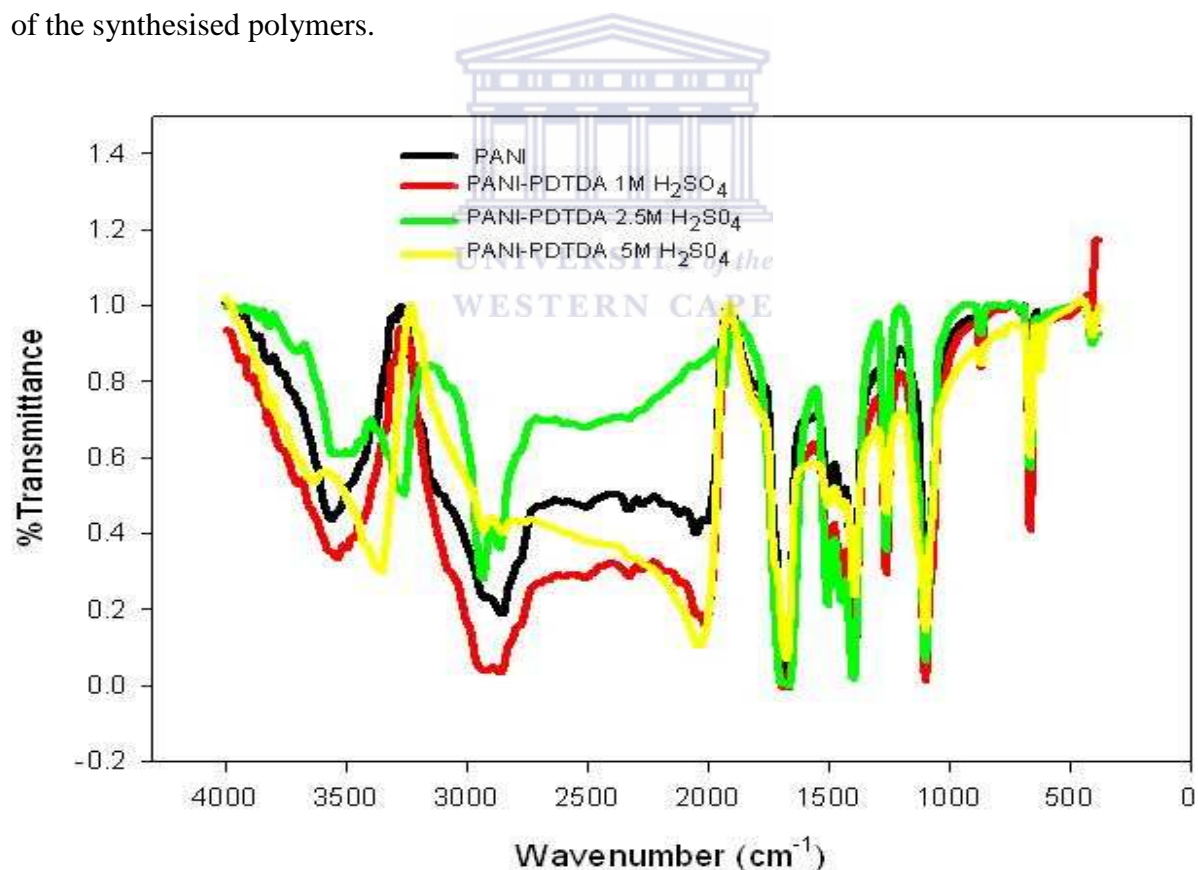


Figure 4.10 FTIR spectra of PANI prepared in 1 M HCl solution and PANI-co-PDTDA prepared in three different concentrations of sulphuric acid.

The peaks for the polymers of PANI doped in HCl and PANI-co-PDTDA in various concentrations of H<sub>2</sub>SO<sub>4</sub> appear at the same region and with similar intensities except for marginal differences. Both PANI and PANI-co-PDTDA (1 M H<sub>2</sub>SO<sub>4</sub>) polymers showed the single peak at approximately 3500 cm<sup>-1</sup> that proves the polymerisation occurs through the –NH<sub>3</sub> group while in 2.5 and 5 M concentrations there appears a doublet peak. The peaks at around 3500 cm<sup>-1</sup> can be assigned as N-H stretching vibrations of secondary amine, while the bands around 2900cm<sup>-1</sup> are ascribed to the aromatic C-H vibrations. The bands in between 1500 – 1600 cm<sup>-1</sup> are assigned as C=C stretching in aromatic nuclei. The bands obtained at 1600-1500 cm<sup>-1</sup> corresponds to C-H stretching in aromatic compounds while the band around 1400cm<sup>-1</sup> are the evidenced to C=N stretching in aromatic compounds. The absorption peaks at 1560 cm<sup>-1</sup> assigned to the quinoid structure does not revealed any significant changes for both polymer and co-polymer at various concentration of sulphuric acid that concludes that the polymers were prepared using di and tri basic acids (Vivekanandan *et al.*, 2011).

The band around 1300 -1200 cm<sup>-1</sup> is due to the C-N stretch of the secondary aromatic amine, while the clear presence of the band around 1100 cm<sup>-1</sup> is characteristic of the conducting polymer due to the delocalisation of electrical charges caused by de-protonation. It can furthermore be attributed to bands characteristics of B-NH-Q or B-NH-B, where B is the benzenic type rings and Q is quinonic- type rings of the polymer backbone. The absorption bands lies below 1000 cm<sup>-1</sup> are the characteristics of mono substituted benzene. The band around 750 cm<sup>-1</sup> is assigned to the C-S stretch of the co-polymer, which obviously suggests the incorporation of DTDA units in co-polymer structure (Widera *et al.*, 1997).

The same finding for PANI has been reported elsewhere. It has been reported that H<sub>2</sub>SO<sub>4</sub> may interact with PANI by donating either hydrogen sulphate, HSO<sub>4</sub> -or sulphate, SO<sub>4</sub><sup>2-</sup> anions as dopant anions. Many authors agreed that HSO<sub>4</sub> - dopant anions are present in PANI/H<sub>2</sub>SO<sub>4</sub> but in this study it interacted with PANI-co-PDTDA (Palaniappan *et al.*, 2004).

## 4.6 Summary

Cyclic voltammetric (CV) experiments are normally performed for the initial electro-analytical studies of any electro-active compound to obtain information on the electrochemical behaviour of the compounds, before it's being investigated in depth using other electro-analytical techniques (Wang, 2000). This chapter focused on the synthesis of PANI and PANI-co-PDTDA as conducting polymers and its electrochemical characterisation to investigate the similarities and differences in structure using various acidic media as dopant. Cyclic voltammetry, UV-Vis spectroscopy and FTIR spectroscopy were used to identify the differences in optical properties and structures between the copolymer and polymer. The voltammetric results for PANI and PANI-co-PDTDA have shown a resemblance although we have noticed a shift in peaks. Clearly, the peaks corresponding to redox processes were shifted to more positive values for the copolymer films in comparison with PANI. This informs that incorporation of PANI in the copolymer resulted difficulty in converting the copolymer into its more oxidized state. This may be attributed to the presence of S-S links in the copolymer which could influence the resonance stabilization of amine cation radical/imine structures.

The ultra-violet visible spectroscopy (UV-VIS) results have shown that PANI in 1 M HCl solution and PANI-co-PDTDA in 1 M H<sub>2</sub>SO<sub>4</sub> solution has shown some similarities although a little different spectroscopic characteristic has been observed at higher concentrations of H<sub>2</sub>SO<sub>4</sub> solution used during polymerisation. The results obtained for the Fourier transformer infrared spectroscopy (FTIR) have shown the appearance at the same region and with similar intensities except for marginal differences. The infrared spectrum of PANI-co-PDTDA in various concentrations of sulphuric acid (Figure 28) were very similar to that of PANI, but with an additional doublet of peaks centred around 3500 cm<sup>-1</sup>. The summary of the results obtained from this chapter will be further combined with the overall results of Chapter 5.



## Chapter 5

# Inhibition Analysis of Selected Heavy Metals Using Amperometric HRP Biosensor

---

### 5.1 Introduction

The development of biosensors began with the advancement of biomolecules immobilisation and stabilisation on the one hand, and miniaturisation and fictionalisation of more sophisticated transducers on the other hand. As enzymes are known to be inhibitors by trace quantities of metals and to exploit this, several enzymatic methods have been developed for the determination of these species. The number of recently reported biosensors for environmental applications and the innovations demonstrated for detection of significant pollutants indicate that biosensors may become devices that fill existing technology gaps in the area of environmental monitoring. These devices combine the selectivity and specificity of the biological component with a suitable transducer (Malhotra *et al.*, 2003, Freire *et al.*, 2003, Calvo *et al.*, 1997). A large number of reports have been made, utilising enzymatic electrodes. The area of biosensors is driven towards the development of small, hand-held and battery-operated instruments suited for on-site decentralised environmental technology for monitoring pollutants, heavy metals and pesticides. It can also offer many advantages over conventional analytical techniques in terms of simplicity, detection limit, specificity and sensitivity. Heavy metals are well known to inhibit the activity of enzymes and the application of this phenomenon to the determination of these hazardous toxic elements offers several advantages, such as simplicity and sensitivity (Rodriguez-Mozaz *et al.*, 2006). Polyaniline (PANI)-based biosensors have attracted a great deal of interest in recent years due to its capability as a biomolecule entrapment matrix and its ability to couple electrons directly from enzyme active site(s) to the electrode (Li *et al.*, 2009). Biosensors can be classified into five main groups, which are piezoelectric, calorimetric, photometric, optical and amperometric sensors.

According to Turner (2005), biosensors are currently defined as analytical devices incorporating either a biological material (e.g. a tissue, microorganism, organelle, cell receptor, enzyme, antibody or nucleic acid; (ii) a biologically derived material (e.g. recombinant antibody, engineered protein or aptamer; (iii) a biomimic (e.g. a synthetic catalyst, combinatorial ligand or imprinted polymer (Turner, 2005). Furthermore, the recognition element should be intimately associated with, or integrated within, a physico-chemical transducer or transducing microsystem, which may be optical, electrochemical, thermometric, piezoelectric, magnetic or micro-mechanic (Calvo *et al.*, 1997).

Biosensors have been developed for use in a wide variety of sectors including medicine, drug discovery, environment, food, process industries, security and defense where analyses represent natural substrates of used enzymes. The main aim of this chapter was to develop an enzymatic electrode of horseradish peroxidase that can be used for indirect monitoring of heavy metals. The design of the sensor employed involved immobilising horseradish peroxidase (HRP) onto PANI and PANI-co-PDTDA films (conducting polymers) as mediators on a platinum electrode surface (see Figure 29). These sensors were applied for the detection of hydrogen peroxide ( $H_2O_2$ ) and for further investigation of the inhibition by heavy metals. Although a direct electron transfer is possible between an electrode and an enzyme catalysing the reduction of hydrogen peroxide, mediators are generally used to accelerate the reaction rates. Enzymes are the most frequently used biological components in biosensors, because a wide range of enzymes are suitable for acting as recognition elements and very often their catalytic properties and substrate specificity can be modified by means of genetic engineering (Rodriguez-Mozaz *et al.*, 2006). The biosensor concept was initiated by Clark and Lyons (1962) and subsequent technology was transferred to Yellow Spring Company for launching dedicated glucose analyser (YSI analyser, model 23) in 1975 (Pandey *et al.*, 2003). The hydrogen peroxide ( $H_2O_2$ ) is one of the most important products or substrate of enzyme catalysed oxidation reactions (Tang *et al.*, 2003). The mechanism of electron transfer in the Pt/PANI/HRP biosensor system is as follows:

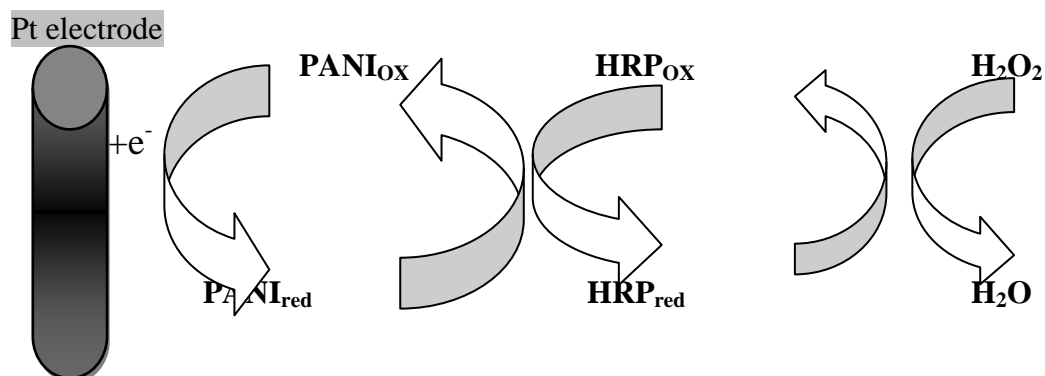
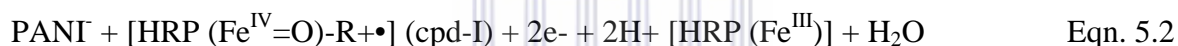
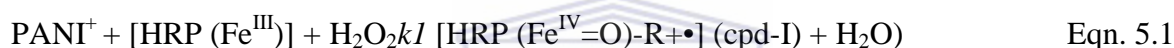


**Figure 5.1** Proposed mechanism of the catalytic redox enzymatic cycle for the transformation of H<sub>2</sub>O<sub>2</sub> as substrate by the HRP enzyme with redox mediated electron transfer to the PANI-modified electrode (Adapted from Iwuoha *et al.*, 2004).



As a mediator, polyaniline (PANI) is able to accelerate the redox reaction and the ping-pong mechanism of the electron transfer taking place in the Pt/PANI/HRP biosensor system is shown in Figure 5.1. In the presence of H<sub>2</sub>O<sub>2</sub>, immobilised peroxidase (HRP-Fe<sup>3+</sup>) is oxidised to compound I (oxyferryl iron) and the porphyrincation radical during the redox reaction. The hydrogen peroxide bonds to the vacant octahedral position on the iron atom that initiates the reaction. There are three different intermediate horseradish peroxidase compounds that form during the reaction. The reduction of compound I to compound II and compound II back to the rest state is carried out by reduction substrates. The natural reaction (also known as the peroxidative reaction) involves the oxidation of aromatic amines and phenols with hydrogen peroxide, thereby producing aromatic radicals which can then undergo non-enzymatic polymerisation reaction in aqueous solutions (Veitch *et al.*, 2004). Upon oxidation with hydrogen peroxide, the horseradish peroxidase is converted into compound I. This oxidation state complex of peroxidase exists in a formal Fe<sup>5+</sup> oxidation state. Once electron reduction of compound I (via oxidation of phenols) an aromatic amine yields compound II (formally at the Fe<sup>4+</sup> state).

It has been proposed that compound II also has single oxidation equivalent residing on the porphyrin similar to that in compound I. A final reduction brings compound II back to the native ( $\text{Fe}^{3+}$ ) state again with concomitant oxidation of a molecule of phenol or aromatic amines (Dunford, 1999).

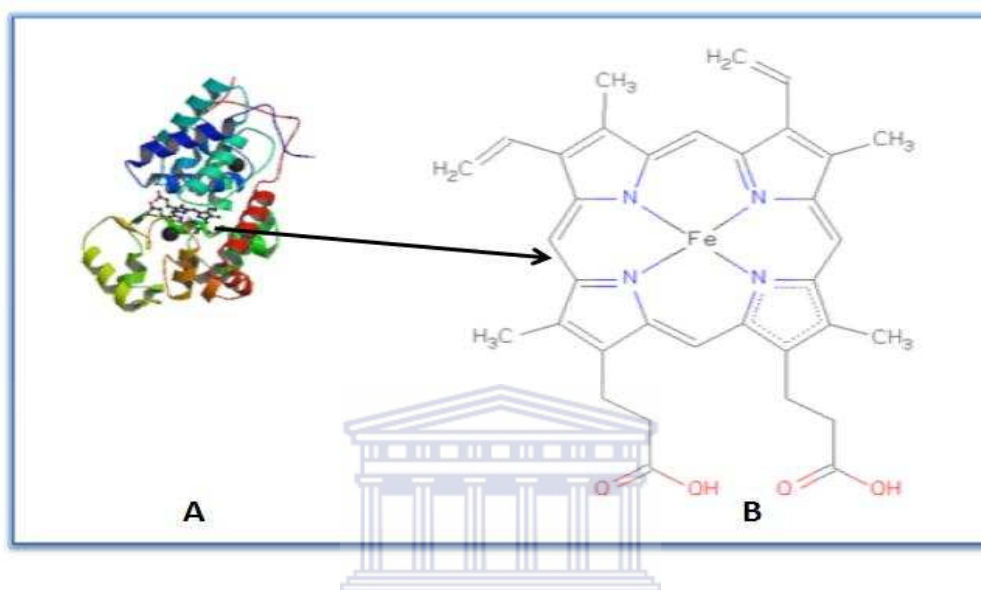
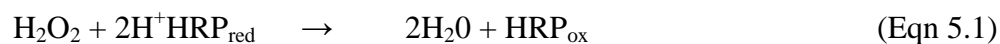


**Figure 5.2** X-ray crystal structure of ferric horseradish peroxidase in (A) and the corresponding chemical structure in (B) (RCSB Protein Database, 2011 accessed on 6 January 2011).

Figure 5.2 shows the three-dimensional structure of horseradish peroxidase. The iron heme is in the centre of the enzyme shown in black with the iron atom as the red sphere. The two calcium atoms are black spheres and lie within the helical regions of the enzyme, with one in the distal region and one in the proximal region. The  $\alpha$ -Helical and  $\beta$ -sheet regions of the enzyme are shown as the multi-coloured helical structures. According to Veitch (2004), it is known that each calcium site is seven-coordinated with oxygen-donor ligands provided by a combination of amino acid side-chain carboxylates (Asp), hydroxyl groups (Ser, Thr), backbone carbonyls and a structural water molecule (distal site only). Both the heme group and the calcium atoms are crucial to the enzyme working properly and the loss of one would result in instability. In the case of a horseradish peroxidase (HRP)-based electrode, the catalytic reaction that produces the mediator is described below:



HRP<sub>red</sub>, HRP<sub>ox</sub>, and MED<sub>red</sub>, MED<sub>ox</sub> are the reduced and oxidised forms of the enzyme and the mediator respectively.

## 5.2 Materials and Methods

In this section horseradish peroxidase (HRP) has been immobilised onto the sensor surface using PANI Polymer and PANI-co-PDTDA co-polymer, respectively. The two respective biosensors evaluated were Pt/PANI/HRP and Pt/PANI-co-PDTDA/HRP. A three-electrode arrangement and set-up was employed with the Pt electrode as the working electrode, platinum wire as counter electrode and silver/silver-chloride (Ag/AgCl) as the reference electrode. The surface of the working electrodes (Pt) was prepared for the deposition of polyaniline and polyaniline-co-polydithiodianiline films using a thorough cleaning process. The counter electrode was cleaned by first flaming in a Bunsen burner until white hot, followed by deionised water rinsing.

### 5.2.1 Chemicals

The reagents aniline (99%), 2,2'-dithiodianiline (98%), potassium dihydrogen phosphate (99%), disodium hydrogen phosphate (98%) and diethyl ether (99.9%) were obtained from Sigma-Aldrich, Germany. The enzyme peroxidase (EC 1.11.1.7 type IV from horseradish) was also purchased from Sigma-Aldrich, Germany. All reagents were of analytical grade and used without further purification. Hydrogen peroxide (30% v/v) was obtained from Merck (South Africa). Phosphate buffer solutions (PBS, 0.1 M) with various pH values were prepared by mixing stock standard solutions of KH<sub>2</sub>PO<sub>4</sub> and Na<sub>2</sub>HPO<sub>4</sub>.

The enzyme peroxidase (EC 1.11.1.7 type IV from horseradish, 250-330 units/ mg<sup>-1</sup>) was used for biosensor preparation. A 0.2 M aniline in 1M HCl and a 0.2 M aniline plus 0.02 M 2,2'-dithiodianiline solution prepared in 5 M H<sub>2</sub>SO<sub>4</sub> were used for the PANI-co-PDTDA co-polymer electrosynthesis. All other solutions were made up with Millipore water. The potassium chloride, sulphuric acid (95%), ethanol (98%) and hydrochloric acid (32%) were obtained from Merck, South Africa. The standards for cadmium (Cd), lead (Pb) and mercury (Hg) were purchased as atomic adsorption standard solutions (1000 mg.L<sup>-1</sup>, AAS) from Sigma-Aldrich, Germany.

### 5.2.2 Apparatus

All electrochemical measurements were performed with a PalmSens® portable electrochemical potentiostat / galvanostat, with the PS Trace program and accessories (PalmSens® Instruments BV, 3992 BZ Houten, and Netherlands). Cyclic voltammetry (CV), differential pulse voltammetry (DPV) and all amperometric measurements were carried out in 20 ml electrochemical cells. The electrode set-up consisted of a conventional three electrode configuration, which comprised a platinum (Pt) working electrode, a Pt wire as counter electrode and silver/silver chloride (Ag/AgCl) as a reference electrode. Alumina micro polish and polishing pads (Buehler, IL, USA) were used for electrode polishing.

### 5.2.3 Construction of Pt/PANI/HRP biosensor

The polymerisation was done by a reported procedure for the electropolymerisation of PANI on a Pt electrode (Mathebe *et al.*, 2004; Somerset *et al.*, 2006). In particular, the Pt electrode surface was first cleaned by polishing with 1.0, 0.3, 0.05 μm alumina slurry, respectively and then washing the electrode thoroughly with double distilled water after each polishing. Polymerisation was achieved in 0.2M aniline per 1M HCl solution for polyaniline (PANI) and a mixture of 0.2 M aniline with 0.02 M 2,2'-dithiodianiline per 5M H<sub>2</sub>SO<sub>4</sub> solution for polyaniline-co-poly(2,2'-dithiodianiline) synthesis. The potential was cycled repetitively between - 200 and + 1100 mV at a scan rate of 60 mVs<sup>-1</sup> for 10 cycles.

The enzyme HRP was immobilised by covalent binding onto the PANI film and PANI-co-PDTDA film, respectively. The stock solution of HRP ( $2 \text{ mg ml}^{-1}$ ) prepared in 1 ml of 0.1 M phosphate buffer (PB) ( $\text{pH} = 6.8$ ) solution was adsorbed onto the surface of the polymer film. The enzymatic incorporation was done using the methodology outlined in Mathebe *et al.* (2004).

#### 5.2.4 Biosensor response measurements

Cyclic voltammetry (CV) and differential pulse voltammetric (DPV) experiments were performed with the portable PalmSens instrument. The PANI and PANI-co-PDTDA polymer films were used in the following experiments as mediators in HRP immobilised electrodes, having  $\text{H}_2\text{O}_2$  as the substrate. A reduction potential of  $-0.5 \text{ V}$  (vs. Ag /AgCl) was used to monitor the electrocatalytic reduction of  $\text{H}_2\text{O}_2$ , as substrate. The solution was degassed with nitrogen before any substrate was added. The Pt/PANI/HRP sensor was immersed in the 0.1 M PB (2 ml) under stirring conditions with direct additions of standard substrate solutions using a micropipette. The signal for the sequential additions was recorded until the current response had reached a steady state. The response of the biosensor towards  $\text{H}_2\text{O}_2$  was investigated by successively adding aliquots of  $\text{H}_2\text{O}_2$  to a continuously stirred 0.1 M PB ( $\text{pH} = 6.8$ ) solution under the optimised conditions. In all experiments hydrogen peroxide was added until a final concentration of 0.86 mM was reached.

##### 5.2.4.1 Cyclic voltammetric measurements

Cyclic voltammetry (CV) measurements allow the rapid location of the potential at which the analyte undergoes reduction and oxidation, allowing an understanding of the redox activity of the analyte. Cyclic voltammetry (CV) was performed at a slow scan rate of  $10 \text{ mVs}^{-1}$  to study the catalytic oxidation of hydrogen peroxide by applying a potential scan between  $+0.4 \text{ V}$  and  $+1.0 \text{ V}$  (vs. Ag/AgCl).



The cyclic voltammogram was first obtained in the absence of the substrate  $\text{H}_2\text{O}_2$ , followed by analysis in the presence of  $\text{H}_2\text{O}_2$  as substrate. Sequential addition of 1 ml aliquots of 1 mM  $\text{H}_2\text{O}_2$  to the 1 ml of 0.1 M phosphate buffer (pH = 6.8) solution, degassed with nitrogen were performed to record the biosensor responses. The phosphate buffer solution was stirred after each addition of peroxide and the biosensor signal was recorded in the absence of stirring. This was done to ensure homogeneity of the solution before measurements were taken (Mathebe *et al.*, 2004; Iwuoha *et al.*, 1997b).

#### 5.2.4.2 Differential pulse voltammetric measurements

Differential pulse voltammetric (DPV) analysis of the Pt/PANI/HRP biosensor in 1 ml of 0.1 M phosphate buffer (pH = 6.8) solution was also performed to compliment the CV measurements. The differential pulse voltammogram (DPV) was collected in the cathodic direction only by applying a linear potential scan between + 0.4 V and - 1.0 V (vs. Ag/AgCl) at a scan rate of  $10 \text{ mVs}^{-1}$  and pulse amplitude of 20 mV. The pulse width of 100 ms was used. The DPV was first obtained in the absence of the substrate  $\text{H}_2\text{O}_2$ , followed by analysis in the presence of  $\text{H}_2\text{O}_2$  as substrate (Morrin *et al.*, 2004; Iwuoha and Smyth 2003).

### 5.3. Results and discussion

#### 5.3.1 Optimisation of solution pH

In Figure 5.3 the results for the optimisation of the working pH of the Pt/PANI/HRP biosensor is shown

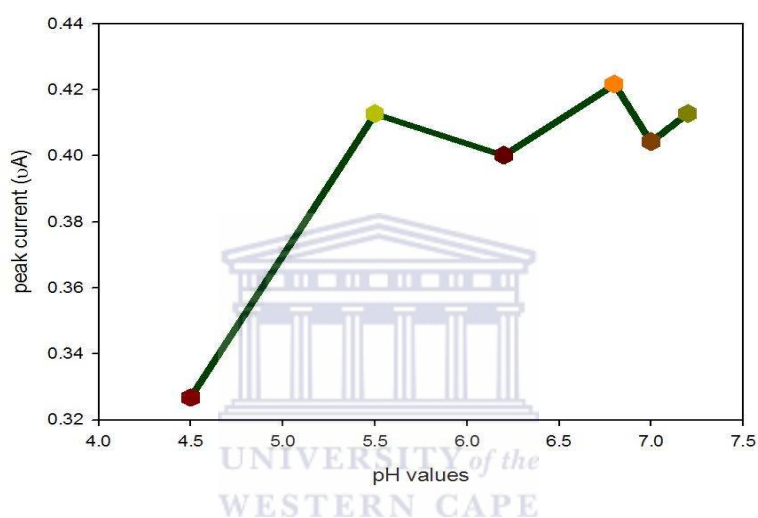


**Figure 5.3** Graph displaying the effect of pH on the Pt/PANI/HRP biosensor in 0.1 M phosphate buffer (PB) solutions at various pH values, obtained for experiments performed separately.

In Figure 5.3 it can be seen that the Pt/PANI/HRP biosensor was evaluated at pH values of 4.5, 5.5, 6.2, 6.8, 7.0 and 7.2. The amperometric responses of the biosensor was collected independently by evaluating the biosensor in a 0.1 M phosphate buffer solution, to which sequential addition of 1 mM of  $\text{H}_2\text{O}_2$  substrate solution was added. After steady-state was reached, the current response data was measured (Somerset *et al.*, 2006). The results further indicate that the maximum current response was obtained at pH = 6.8 in accordance with the results obtained by Mathebe *et al.*, (2004). It was then decided to collect all the Pt/PANI/HRP biosensor data at a pH = 6.8. In a similar manner the optimum pH for the Pt/PANI-co-PDTDA/HRP biosensor was determined (graph not shown here). The results obtained for this biosensor have shown that the optimum pH value of 7.2 was obtained.

### 5.3.2 Cyclic voltammetric characterisation of Pt/PANI/HRP biosensor

In Figure 5.4 below the results for the cyclic voltammetric (CV) evaluation of the Pt/PANI/HRP biosensor in 0.1 M phosphate buffer solution (pH = 6.8) is shown.

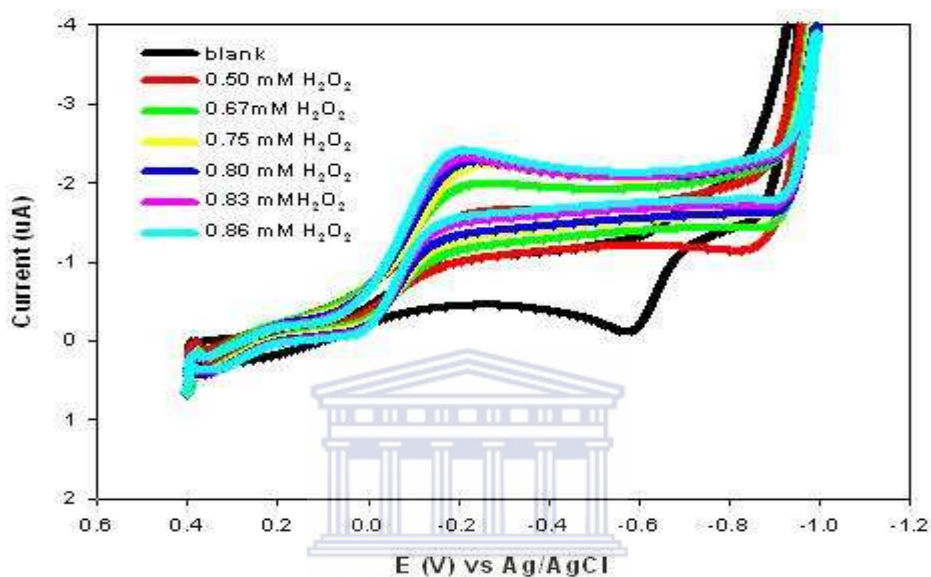


**Figure 5.4** Results for the CV evaluation and responses of the Pt/PANI/HRP biosensor in the presence of different  $\text{H}_2\text{O}_2$  concentrations evaluated in 0.1 M PB (pH = 6.8) solution is shown. The potential was scanned between + 0.4 and - 1.2 V (vs. Ag/AgCl) at a scan rate of 10 mV/s.

For the results in Figure 5.4, the catalytic reduction of  $\text{H}_2\text{O}_2$  at the Pt/PANI/HRP biosensor is shown. With each addition of 1 mM  $\text{H}_2\text{O}_2$  to the 0.1 M PB (pH = 6.8) solution, it was observed that the cathodic peak current of the voltammogram increased. It was further observed that the cathodic peak current ( $I_{p,c}$ ) showed relatively small increases as the  $\text{H}_2\text{O}_2$  concentrations were varied between 0.8 – 0.86 mM. From these results it was deduced that the maximum  $I_{p,c}$  value is obtained at a concentration of 0.86 mM, which was used in the inhibition experiments.

### 5.3.3 Differential pulse voltammetric characterisation of Pt/PANI/HRP biosensor

Figure 5.5 shows the results for the cathodic differential pulse voltammograms (DPVs) of the Pt/PANI/HRP biosensor in the presence of different  $\text{H}_2\text{O}_2$  concentrations evaluated in 0.1 M PB (pH = 6.8) solution, plus the calibration lot obtained for the peak current vs. increasing  $\text{H}_2\text{O}_2$  concentrations.

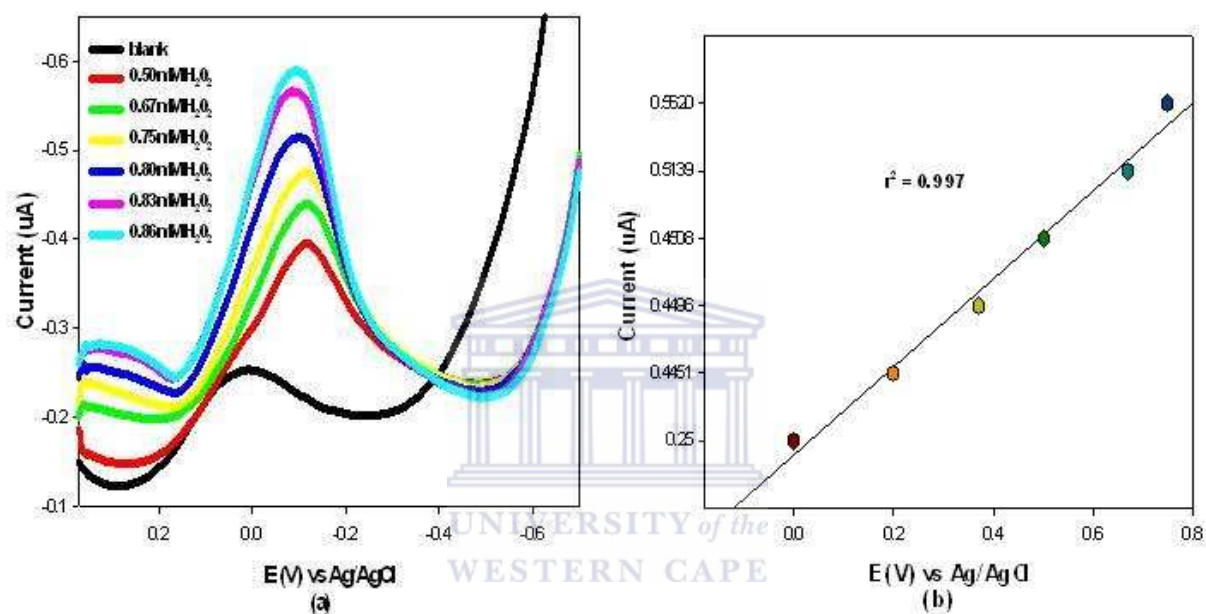


**Figure 5.5** The cathodic differential pulse voltammograms (DPVs) of the Pt/PANI/HRP biosensor in the presence of different  $\text{H}_2\text{O}_2$  concentrations evaluated in 0.1 M PB (pH = 6.8) solution is shown. Experimental conditions were: pulse width, amplitude, 20 mV; potential step, 20 mV.

The results for the DPVs shown in Figure 5.5 (a) clearly indicate that the electrocatalytic reduction of  $\text{H}_2\text{O}_2$  at the Pt/PANI/HRP biosensor can be observed around potential of  $-0.1$  V (vs. Ag/AgCl). These results show a clear increasing trend in the cathodic peak current ( $I_{p,c}$ ) values, compared to the results obtained for the CVs shown in Figure 5.4.

In Figure 5.5 (b) the calibration curve generated from the peak current responses versus increasing H<sub>2</sub>O<sub>2</sub> substrate concentration is shown. For the six concentrations of H<sub>2</sub>O<sub>2</sub> investigated with the Pt/PANI/HRP biosensor, a linear calibration curve was obtained for the concentrations ranging between 0 and 0.75 mM, with good correlation of 0.997 ( $n = 6$ ). In a higher concentration range of 0.8-0.86 mM, the calibration already exhibited a typical curvature due to saturation of the electrode surface with the analyte at high concentration.

The slope of the above plot represent the sensitivity, which was found to be 0.403  $\mu\text{A}\text{mM}^{-1}$  with a detection limit of 0.32 mM using equation,  $LOD = \frac{3 \times SD}{m}$ , where s is the standard deviation and m is the slope of the calibration plot. The repeatability in the measurement, expressed as relative standard deviation (R.S.D), was 14%, obtained by recording 1 mM H<sub>2</sub>O<sub>2</sub> through 10 successive experiments.

The obtained biosensor data was further used for kinetic modelling of the Pt/PANI/HRP biosensor to determine some of its kinetic parameters Michaelis-Menten kinetics describes the kinetic properties of many enzymes (Runge *et al.*, 2006). It involves the enzyme (E) binding to a substrate (S) to form an enzyme-substrate complex (E-S). The Michaelis constant ( $K_m$ ) can be used to describe the kinetics of the reaction, if the data fit the hyperbolic curve. A low  $K_m$  value indicates tight binding, whereas a high  $K_m$  value suggests weak binding. Typical  $K_m$  values for enzyme systems range from micromolar to millimolar concentration range (Liu and Ju, 2002; Nomngongo *et al.*, 2011). The Michaelis-Menton kinetics at low substrate concentration is calculated with the following equation:

$$I = \frac{I_{m \max}[H_2O_2]}{[H_2O_2] + K'_m} \quad \text{Eqn. 5.3}$$

(Which simplifies to):

$$I = \left( \frac{I_{m \max}}{K'_m} \right) [H_2O_2] \quad \text{Eqn. 5.4}$$

And when used for the Pt/PANI/HRP biosensor, the value was found to be:

$$\text{Sensitivity} = \left( \frac{I_{m \max}}{K'_m} \right) = 4.10 \times 10^{-1} \mu\text{AmM}^{-1}$$

The  $K_m^{app}$  in this work was evaluated at 0.6 mM with  $I_{max}$  of 1.7 which revealed that that the whole system was controlled by catalytic kinetic process of the enzyme. These results are in good agreement with  $K_m^{app}$  of 0.9 mM obtained by Yao *et al* (2005).

The second biosensor constructed in this work is the Pt/PANI-co-PDTDA/HRP biosensor. Similarly, the kinetic parameters were also analysed and calculated for this biosensor. The results obtained have shown that the  $K_m^{app}$  and  $I_{max}$  value are 0.7 mM and 0.27  $\mu\text{A}$ , respectively.

In comparing the kinetic results obtained for the Pt/PANI/HRP biosensor to that of the Pt/PANI-co-PDTDA/HRP biosensor, it was observed that Pt/PANI/HRP biosensor obtained a higher  $I_{max}$  value and low  $K_m^{app}$  value, which is what is desirable in the construction of a biosensor.

#### 5.3.4 Inhibition of Pt/PANI/HRP biosensor by heavy metals

Inhibition plots for each of the heavy metals studied (e.g.  $\text{Cd}^{2+}$ ,  $\text{Pb}^{2+}$ , and  $\text{Hg}^{2+}$ ) were obtained using the percentage inhibition method. This procedure involved the study of the Pt/PANI/HRP biosensor in the presence of  $\text{H}_2\text{O}_2$  solution first, followed by exposure to sequential additions of the heavy metal solutions. This method is also referred to as the direct method, since no incubation is involved. The direct method was further employed to establish the metal ion concentration that causes 50% inhibition ( $IC_{50}$ ) (Nomngongo *et al.*, 2011). The heavy metal concentrations evaluated during sequential addition were 0.001 ppb, 0.005 ppb and 0.01 ppb for each of  $\text{Cd}^{2+}$ ,  $\text{Pb}^{2+}$ , and  $\text{Hg}^{2+}$  ions.

The percentage inhibition was then calculated using the formula (Somerset *et al.*, 2007; Guascito *et al.*, 2008; Nomngongo *et al.*, 2011):

$$I\% = \frac{I_1 - I_2}{I_1} \times 100\% \quad \text{Eqn. 5.5}$$

where  $I\%$  is the degree of inhibition,  $I_1$  is the steady-state current obtained in buffer solution with no heavy metal ion present, while  $I_2$  is the steady-state current obtained after the biosensor was exposed to sequential additions of the separate heavy metal ions of  $\text{Cd}^{2+}$ ,  $\text{Pb}^{2+}$ , and  $\text{Hg}^{2+}$  respectively.

#### 5.3.4.1 Inhibition results for lowest metal concentration investigated

The percentage inhibition plots obtained for the inhibition of HRP when aliquots of 0.001 ppb of  $\text{Cd}^{2+}$ ,  $\text{Pb}^{2+}$  and  $\text{Hg}^{2+}$  was sequentially added to the 0.1 M PB (pH = 6.8) solution, are shown in Figure 5.6.

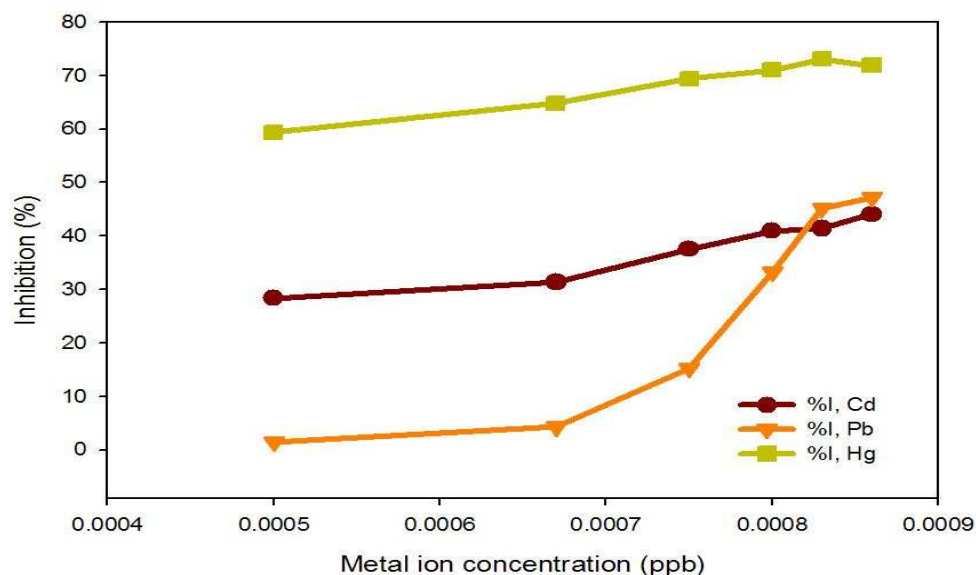


Figure 5.6 Results obtained for inhibition of the Pt/PANI/HRP biosensor in the presence of sequential aliquots of  $0.001 \mu\text{g. L}^{-1}$  of  $\text{Cd}^{2+}$ ,  $\text{Pb}^{2+}$  and  $\text{Hg}^{2+}$ , respectively. The individual metal solution was added sequentially to a 0.1 M PB (pH = 6.8) solution.



For the results shown in Figure 5.7, it was observed that the inhibition results obtained for the respective  $\text{Cd}^{2+}$ ,  $\text{Pb}^{2+}$  and  $\text{Hg}^{2+}$  metal ions, had distinctive patterns. In the concentration range between 0.0005 and 0.0008  $\mu\text{g.L}^{-1}$ , the decreasing inhibition trend observed was  $\text{Hg}^{2+} > \text{Cd}^{2+} > \text{Pb}^{2+}$ . For the concentrations higher than 0.0008  $\mu\text{g.L}^{-1}$ , the inhibition trend observed was  $\text{Hg}^{2+} > \text{Pb}^{2+} > \text{Cd}^{2+}$ . For the three metal ions investigated, it was further observed that  $\text{Hg}^{2+}$  had the highest initial inhibition of 59%, while  $\text{Pb}^{2+}$  had the lowest value of 1.5%. The highest inhibition percentages obtained for the individual metal ions were 44% for  $\text{Cd}^{2+}$ , 47% for  $\text{Pb}^{2+}$  and 73% for  $\text{Hg}^{2+}$ . These results have clearly indicated the toxicity of the investigated metal ions to HRP as enzyme.

#### 5.3.4.2 Inhibition results for intermediary metal concentration investigated

Figure 5.7 displays the results obtained for the percentage inhibition plots of HRP when aliquots of 0.005  $\mu\text{g.L}^{-1}$  of  $\text{Cd}^{2+}$ ,  $\text{Pb}^{2+}$  and  $\text{Hg}^{2+}$  was sequentially added to the 0.1 M PB (pH = 6.8) solution.

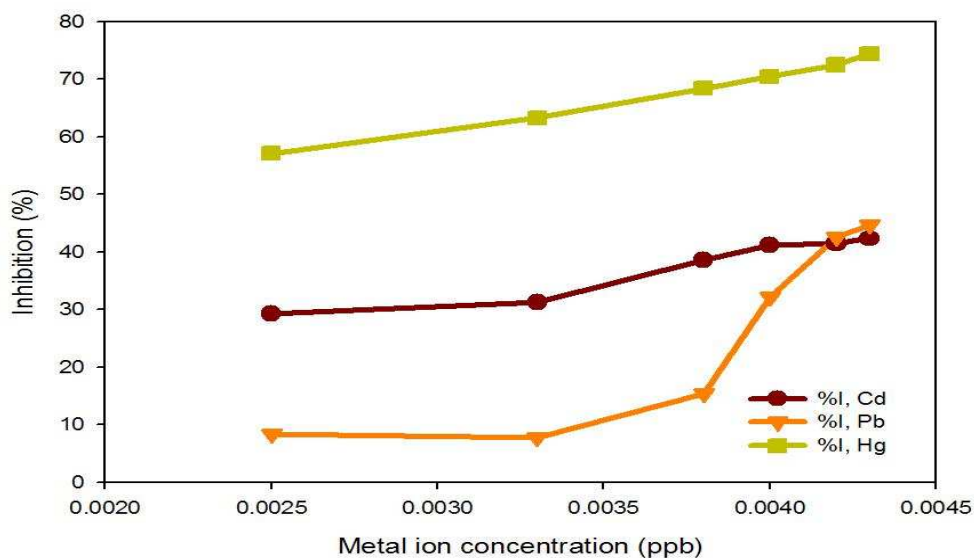


**Figure 5.7** Results obtained for inhibition of the Pt/PANI/HRP biosensor in the presence of sequential aliquots of 0.005  $\mu\text{g.L}^{-1}$  of  $\text{Cd}^{2+}$ ,  $\text{Pb}^{2+}$  and  $\text{Hg}^{2+}$ , respectively. The individual metal solution was added sequentially to a 0.1 M PB (pH = 6.8) solution.

Analysis of the results in Figure 5.7 has shown that  $\text{Cd}^{2+}$ ,  $\text{Pb}^{2+}$  and  $\text{Hg}^{2+}$  inhibited HRP at the same pattern and at the same order of magnitude when  $0.005 \mu\text{g.L}^{-1}$  of the inhibitors were sequential added. In the concentration range between  $0.0025$  and  $0.004 \mu\text{g.L}^{-1}$ , the decreasing inhibition trend observed was  $\text{Hg}^{2+} > \text{Cd}^{2+} > \text{Pb}^{2+}$ . For the concentrations higher than  $0.0008 \mu\text{g.L}^{-1}$ , the inhibition trend observed was  $\text{Hg}^{2+} > \text{Pb}^{2+} > \text{Cd}^{2+}$ . For the three metal ions investigated, it was further observed that  $\text{Hg}^{2+}$  had the highest initial inhibition of 57%, while  $\text{Pb}^{2+}$  had the lowest value of 8%. The highest inhibition percentages obtained for the individual metal ions were 42% for  $\text{Cd}^{2+}$ , 45% for  $\text{Pb}^{2+}$  and 74% for  $\text{Hg}^{2+}$ . These results have clearly indicated the toxicity of the investigated metal ions to HRP as enzyme with  $\text{Hg}^{2+}$  being the highest inhibitor of these metals tested.

#### 5.3.4.3 Inhibition results for highest metal concentration investigated

The percentage inhibition plots obtained for the inhibition of HRP when aliquots of  $0.01 \mu\text{g.L}^{-1}$  of  $\text{Cd}^{2+}$ ,  $\text{Pb}^{2+}$  and  $\text{Hg}^{2+}$  was sequentially added to the  $0.1 \text{ M PB}$  ( $\text{pH} = 6.8$ ) solution, are shown in Figure 5.8.

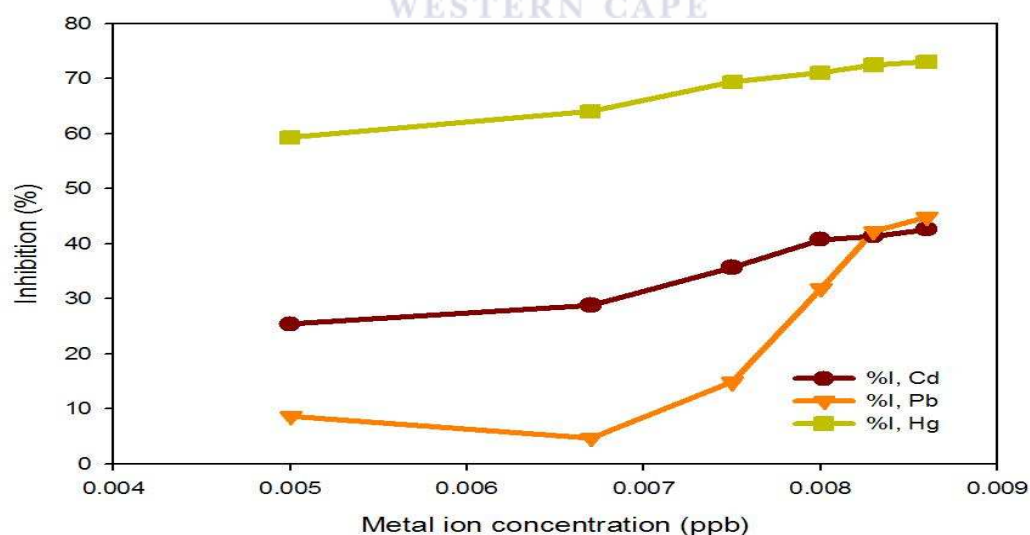


**Figure 5.8** Results obtained for inhibition of the Pt/PANI/HRP biosensor in the presence of sequential aliquots of  $0.01 \mu\text{g.L}^{-1}$  of  $\text{Cd}^{2+}$ ,  $\text{Pb}^{2+}$  and  $\text{Hg}^{2+}$ , respectively. The individual metal solution was added sequentially to a  $0.1 \text{ M PB}$  ( $\text{pH} = 6.8$ ) solution.

For the results shown in Figure 5.8, it was found that the effects of these metal ions were also in the same pattern with Figures 5.6 and 5.7. In the concentration range between 0.005 and 0.008  $\mu\text{g.L}^{-1}$ , the decreasing inhibition trend observed was  $\text{Hg}^{2+} > \text{Cd}^{2+} > \text{Pb}^{2+}$ . For the concentrations higher than 0.0008  $\mu\text{g.L}^{-1}$ , the inhibition trend observed was  $\text{Hg}^{2+} > \text{Pb}^{2+} > \text{Cd}^{2+}$ . For the three metal ions investigated, it was further observed that  $\text{Hg}^{2+}$  had the highest initial inhibition of 59%, while  $\text{Pb}^{2+}$  had the lowest value of 9%. The highest inhibition percentages obtained for the individual metal ions were 42% for  $\text{Cd}^{2+}$ , 43% for  $\text{Pb}^{2+}$  and 73% for  $\text{Hg}^{2+}$ . These results have clearly indicated the toxicity of the investigated metal ions to HRP as enzyme with  $\text{Hg}^{2+}$  being the highest inhibitor of these metals tested.

### 5.3.5 Inhibition of Pt/PANI-co-PDTDA/HRP biosensor by heavy metals

The second sensor evaluated in the inhibition studies of heavy metals was the Pt/PANI-co-PDTDA biosensor. This sensor contained the co-polymer of PANI-co-PDTDA and this was a novel application of this biosensor for inhibition studies towards heavy metal determination. As in section 5.3.4, inhibition plots for each of the heavy metals studied (e.g.  $\text{Cd}^{2+}$ ,  $\text{Pb}^{2+}$ , and  $\text{Hg}^{2+}$ ) were obtained using the percentage inhibition method. This procedure involved the study of the Pt/PANI-co-PDTDA/HRP biosensor in the presence of  $\text{H}_2\text{O}_2$  solution first, followed by exposure to sequential additions of the heavy metal solutions. The direct method was again applied in the inhibition studies performed. The purpose was to use PANI-co-PDTDA as a mediator in order to get better quality of biosensor.

#### 5.3.5.1 Inhibition results for lowest metal concentration investigated

Figure 5.9 displays the results obtained for the inhibition of HRP when aliquots of 0.001  $\mu\text{g. L}^{-1}$  of  $\text{Cd}^{2+}$ ,  $\text{Pb}^{2+}$  and  $\text{Hg}^{2+}$  was sequentially added to the 0.1 M PB (pH = 6.8) solution.

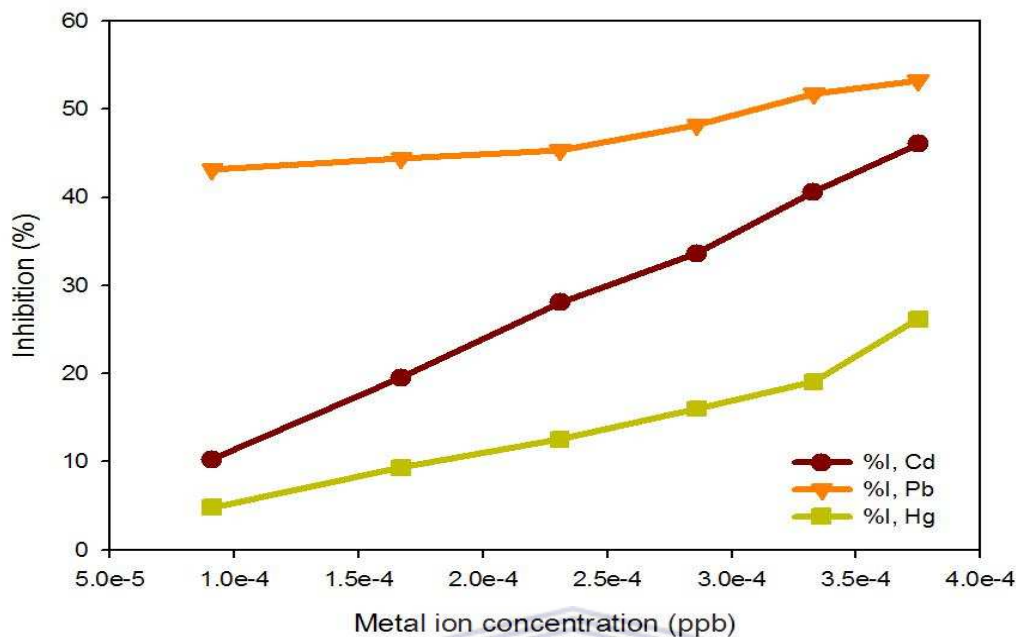


**Figure 5.9** Results obtained for inhibition of the Pt/PANI-co-PDTDA/HRP biosensor in the presence of sequential aliquots of  $0.001 \mu\text{g. L}^{-1}$  of  $\text{Cd}^{2+}$ ,  $\text{Pb}^{2+}$  and  $\text{Hg}^{2+}$ , respectively. The individual metal solution was added sequentially to a  $0.1 \text{ M PB}$  ( $\text{pH} = 6.8$ ) solution.

Analysis of the results in Figure 5.9 has shown that the inhibition trend observed was on order  $\text{Pb}^{2+} > \text{Cd}^{2+} > \text{Hg}^{2+}$  which is the vice versa for the results we have obtained for Pt/PANI/HRP biosensor in higher concentrations of these metals. For the three metal ions investigated, it was further observed that  $\text{Pb}^{2+}$  had the highest initial inhibition of 50%, while  $\text{Hg}^{2+}$  had the lowest value of 5%. The highest inhibition percentages obtained for the individual metal ions were 48% for  $\text{Cd}^{2+}$ , 50% for  $\text{Pb}^{2+}$  and 24% for  $\text{Hg}^{2+}$ . These results have clearly indicated that only  $\text{Pb}^{2+}$  inhibited 50% of the HRP activity.

### 5.3.5.2 Inhibition results for intermediary metal concentration investigated

Figure 5.10 displays the results obtained for the inhibition of HRP when aliquots of  $0.005 \mu\text{g. L}^{-1}$  of  $\text{Cd}^{2+}$ ,  $\text{Pb}^{2+}$  and  $\text{Hg}^{2+}$  was sequentially added to the  $0.1 \text{ M PB}$  ( $\text{pH} = 6.8$ ) solution.

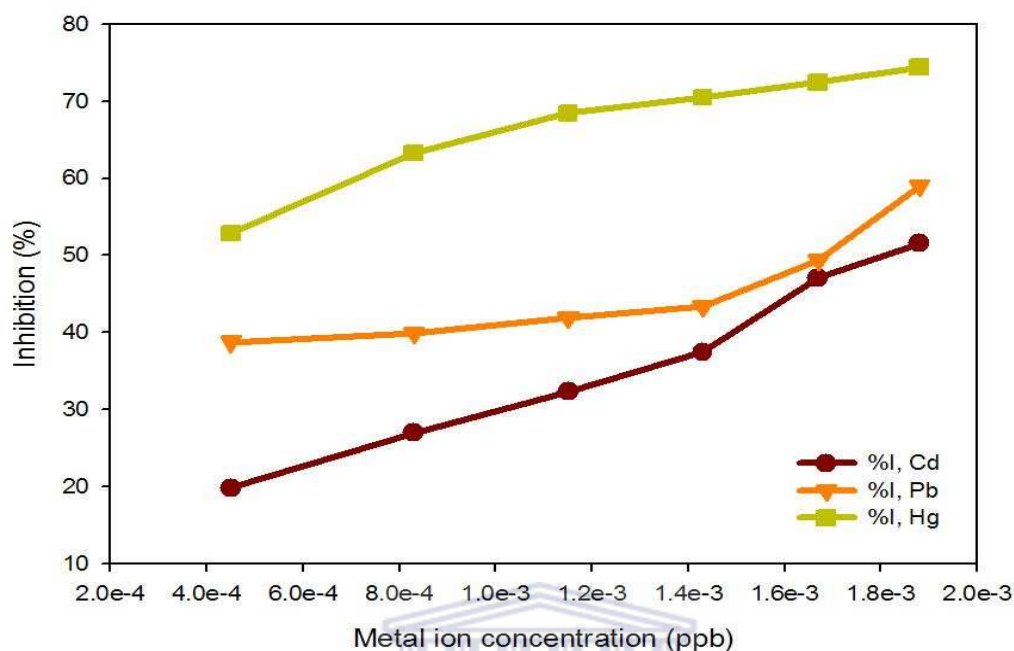


Figure 5.10 Results obtained for inhibition of the Pt/PANI-co-PDTDA/HRP biosensor in the presence of sequential aliquots of  $0.005 \mu\text{g}\cdot\text{L}^{-1}$  of  $\text{Cd}^{2+}$ ,  $\text{Pb}^{2+}$  and  $\text{Hg}^{2+}$ , respectively. The individual metal solution was added sequentially to a  $0.1 \text{ M PB}$  ( $\text{pH} = 6.8$ ) solution.

Analysis of the results in Figure 5.10 has shown that metals were inhibitory to HRP at metal concentration of  $0.005 \mu\text{g}\cdot\text{L}^{-1}$  in order of increasing toxicity  $\text{Hg}^{2+} > \text{Pb}^{2+} > \text{Cd}^{2+}$ . It was further observed that  $\text{Hg}^{2+}$  had the highest initial inhibition of 52%, while  $\text{Pb}^{2+}$  had the lowest value of 19%. The highest inhibition percentages obtained for the individual metal ions were 49% for  $\text{Cd}^{2+}$ , 59% for  $\text{Pb}^{2+}$  and 78% for  $\text{Hg}^{2+}$ . These results have clearly indicated the toxicity of the investigated metal ions to HRP as enzyme with  $\text{Hg}^{2+}$  being the highest inhibitor of these metals tested.

### 5.3.5.3 Inhibition results for highest metal concentration investigated

Figure 5.11 displays the results obtained for the inhibition of HRP when aliquots of  $0.01 \mu\text{g}\cdot\text{L}^{-1}$  of  $\text{Cd}^{2+}$ ,  $\text{Pb}^{2+}$  and  $\text{Hg}^{2+}$  was sequentially added to the  $0.1 \text{ M PB}$  ( $\text{pH} = 6.8$ ) solution.

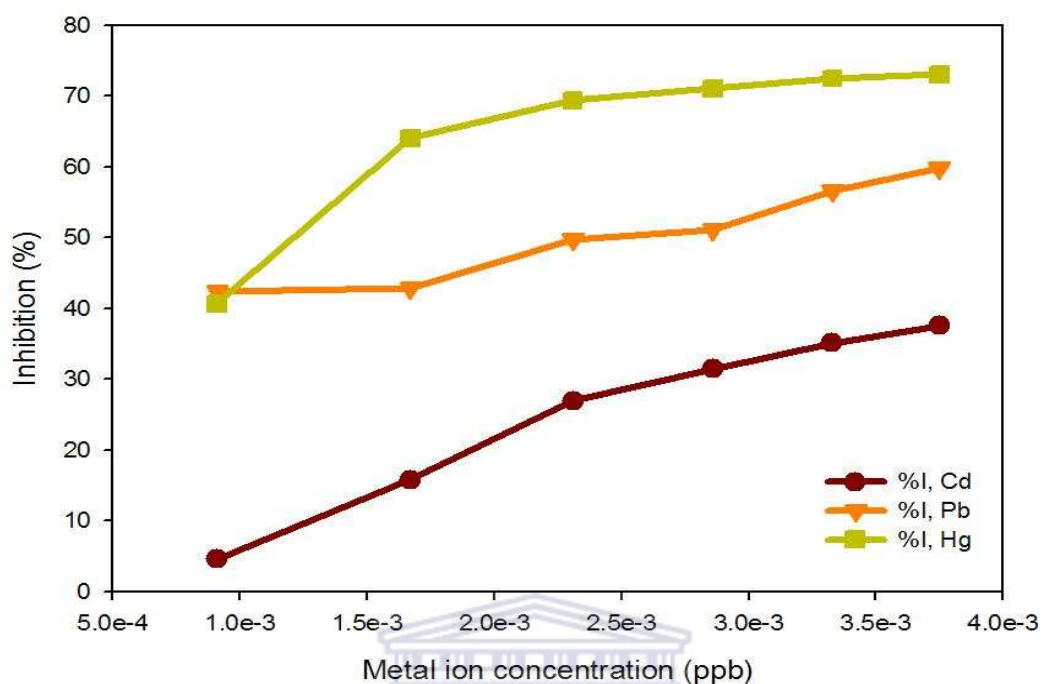


Figure 5.11 Results obtained for inhibition of the Pt/PANI-co-PDTDA/HRP biosensor in the presence of sequential aliquots of  $0.01 \mu\text{g}\cdot\text{L}^{-1}$  of  $\text{Cd}^{2+}$ ,  $\text{Pb}^{2+}$  and  $\text{Hg}^{2+}$ , respectively. The individual metal solution was added sequentially to a  $0.1 \text{ M PB}$  ( $\text{pH} = 6.8$ ) solution.

Analysis of the results in Figure 5.11 has shown that metals were inhibitory to HRP at metal concentration of  $0.01 \mu\text{g}\cdot\text{L}^{-1}$  in order of increasing toxicity  $\text{Hg}^{2+} > \text{Pb}^{2+} > \text{Cd}^{2+}$ . It was further observed that  $\text{Pb}^{2+}$  and  $\text{Hg}^{2+}$  interacted initial inhibition of around 40%, while  $\text{Cd}^{2+}$  had the lowest value of 2.5%. The highest inhibition percentages obtained for the individual metal ions were 38% for  $\text{Cd}^{2+}$ , 59% for  $\text{Pb}^{2+}$  and 75% for  $\text{Hg}^{2+}$ . These results have clearly indicated the toxicity of the investigated metal ions to HRP as enzyme with  $\text{Hg}^{2+}$  being the highest inhibitor of these metals tested.

### 5.3.6 Voltammetric results for Pt/PANI/HRP biosensor

#### 5.3.6.1 Voltammetric results for Cd inhibition

Figure 5.12 shows the DPVs obtained for the Pt/PANI/HRP biosensor for the successive increments of aqueous cadmium ions ( $\text{Cd}^{2+}$ ) with starting concentrations of 0.001, 0.005 and 0.01  $\mu\text{g}\cdot\text{L}^{-1}$ , respectively.

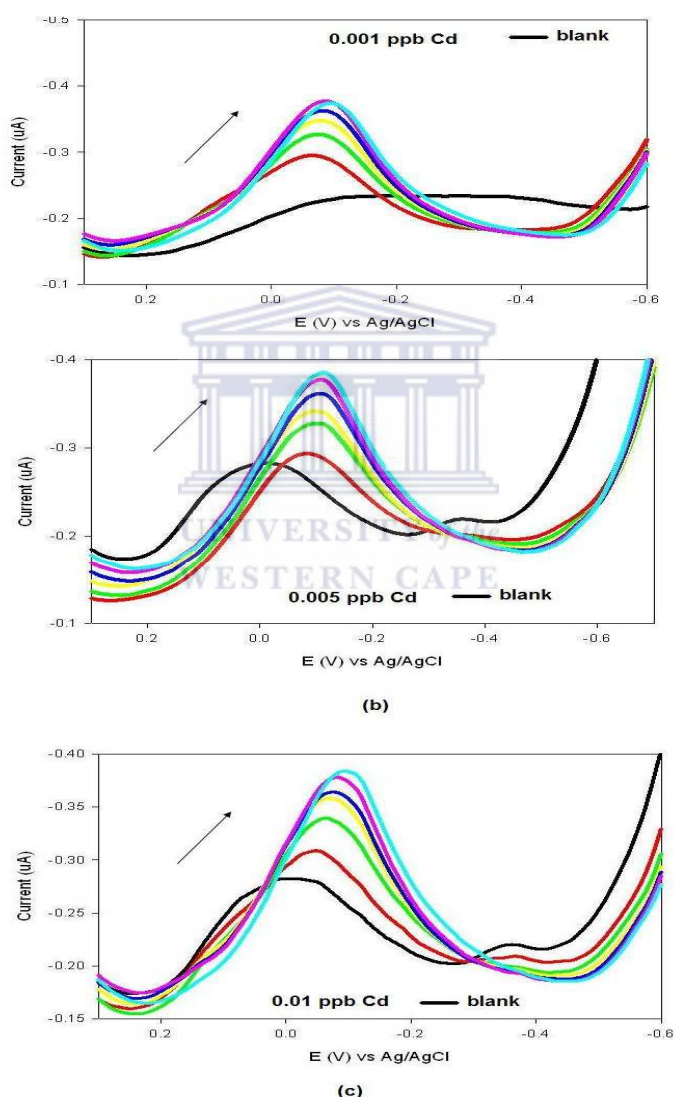


**Figure 5.12** Results for the cathodic differential pulse voltammograms (DPVs) of the Pt/PANI/HRP biosensor in the presence of three different Cd concentrations evaluated in 0.1 M PB (pH = 6.8) solution. In (a) the Cd concentration used was 0.001  $\mu\text{g}\cdot\text{L}^{-1}$ , followed by 0.005  $\mu\text{g}\cdot\text{L}^{-1}$  in (b) and 0.01  $\mu\text{g}\cdot\text{L}^{-1}$  in (c). Experimental conditions were: E pulse, 0.02V; scan rate 0.010V/s; potential step, 0.005 V.



Analysis of the results in Figure 5.12 indicates that an amperometric response was still obtained for the Pt/PANI/HRP biosensor when exposed to  $\text{Cd}^{2+}$  ions in the voltammetric evaluation of the biosensor. When the  $[\text{Cd}^{2+}] = 0.001 \mu\text{g.L}^{-1}$ , comparison of the DPV results in Figure 5.12 (a) to that of the biosensor response in Figure 5.5, it was clearly observed that a diminished peak current response was obtained. Comparison of the results in Figure 5.12 (a) and (b) also shows that relatively small differences in the peak current responses for these concentrations were observed. However, when the  $[\text{Cd}^{2+}] = 0.01 \mu\text{g.L}^{-1}$ , the difference in peak current response to that of the 2 smaller concentrations were more apparent. These results further indicate that the concentration of the metal ions, determine the extent of the inhibition of HRP enzyme observed.

Figure 5.13 shows the calibration curves for the DPV responses evaluated for peak current versus increasing concentrations of cadmium (Cd). The three plots in Figure 5.12 were obtained for each of the 0.001, 0.005 and 0.01  $\mu\text{g.L}^{-1}$  Cd concentrations evaluated. This information was further used to determine the sensitivity for each of the concentrations evaluated and were found to be  $3.04 \times 10^{-2} \text{ uA ppb}^{-1}$  for  $[\text{Cd}^{2+}] = 0.001 \mu\text{g.L}^{-1}$ ,  $5.52 \times 10^{-2} \text{ uA ppb}^{-1}$  for  $[\text{Cd}^{2+}] = 0.005 \mu\text{g.L}^{-1}$  and  $2.41 \times 10^{-2} \text{ uA ppb}^{-1}$  for  $[\text{Cd}^{2+}] = 0.01 \mu\text{g.L}^{-1}$ . The apparent Michaelis–Menten constant ( $K_m^{\text{app}}$ ) and  $I_{\text{max}}$  were also calculated and their values are presented in Table 6.

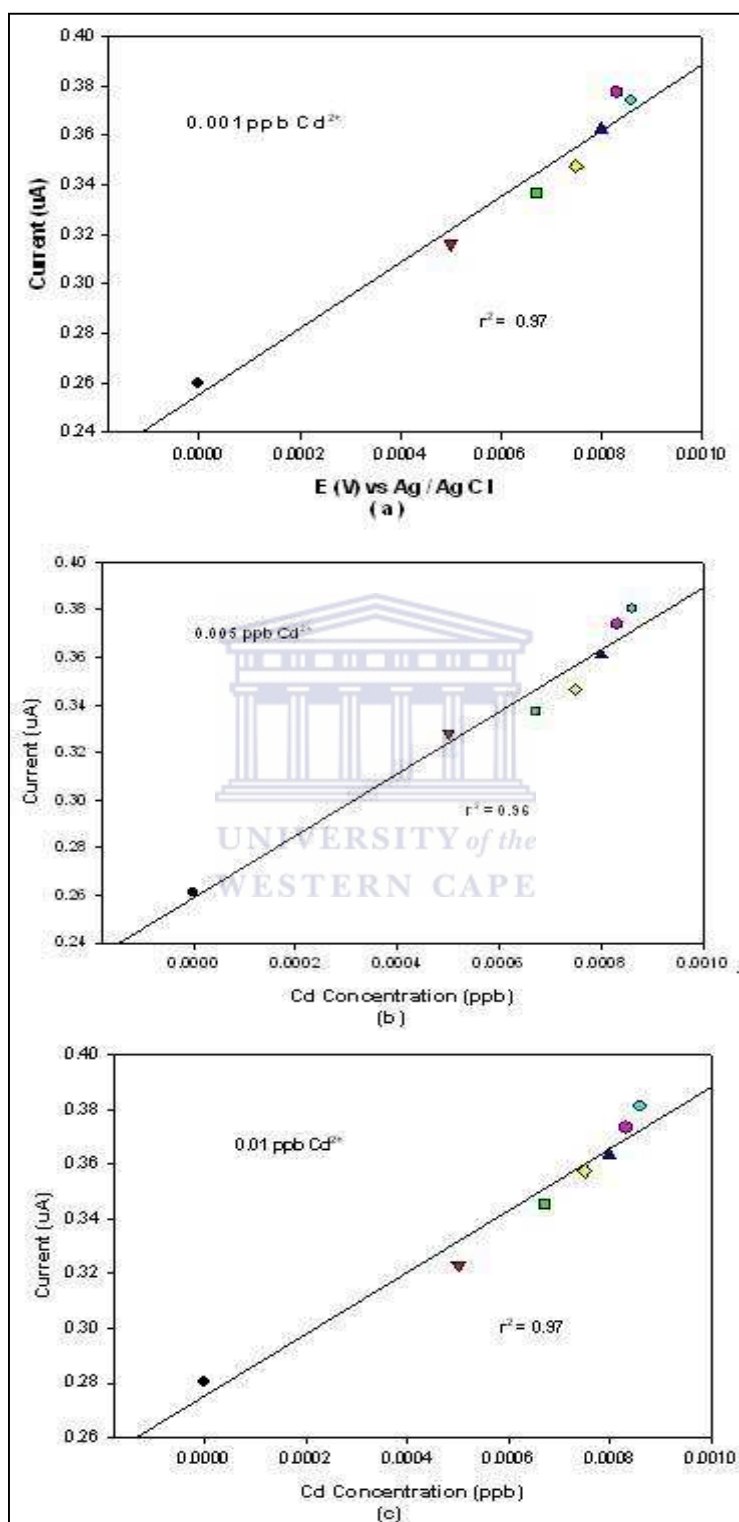


Figure 5.13 Calibration curves obtained for peak current ( $I_p$ ) vs. Cd concentration with  $0.001 \mu\text{g.L}^{-1}$  Cd in (a),  $0.005 \mu\text{g.L}^{-1}$  Cd in (b) and  $0.01 \mu\text{g.L}^{-1}$  Cd in (c). Results were obtained using DPV as technique in a 0.1 M PB (6.8) solution.

The results obtained for the characteristics of the performance of the Pt/PANI/HRP biosensor for  $\text{Cd}^{2+}$  evaluation are shown in Table 5.1. The parameters for the analytical characteristics of the sensor evaluated are presented.

**Table 5.1** Performance characteristics of the Pt/PANI/HRP biosensor in the presence of  $\text{Cd}^{2+}$  as inhibitor.

Metal ion [ $\text{Cd}^{2+}$ ], $\mu\text{g.L}^{-1}$	$\text{Cd}^{2+}$		
	0.001	0.005	0.01
Linear range ( $\mu\text{g.L}^{-1}$ )	0-3 ( $n = 4$ )	0-5 ( $n = 5$ )	0-3 ( $n = 4$ )
Sensitivity ( $\mu\text{A ppb}^{-1}$ )	$3.04 \times 10^{-2}$	$5.52 \times 10^{-2}$	$2.41 \times 10^{-2}$
Correlation coefficient ( $R^2$ )	0.962	0.964	0.961
LOD (ppb)	$6.64 \times 10^{-4}$		
LOQ (ppb)	$2.21 \times 10^{-3}$		

Analysis of the results in Table 5.1 indicates that the Pt/PANI/HRP biosensor had a linear range that ranged between 0 – 5  $\mu\text{g.L}^{-1}$  for the three concentrations evaluated. It was also found that the sensitivity was uniform at the same order, although some variations in the magnitude were obtained. The LOD value obtained for the biosensor in the presence of  $\text{Cd}^{2+}$  was  $6.64 \times 10^{-4}$  ppb, with the LOQ  $2.21 \times 10^{-3}$  ppb.

### 5.3.6.2. Voltammetric results for Pb inhibition

Figure 5.14 shows the DPV recordings obtained at the Pt/PANI/HRP biosensor for the successive increments of aqueous lead ions with starting concentrations of 0.001, 0.005 and 0.01  $\mu\text{g.L}^{-1}$ , respectively.

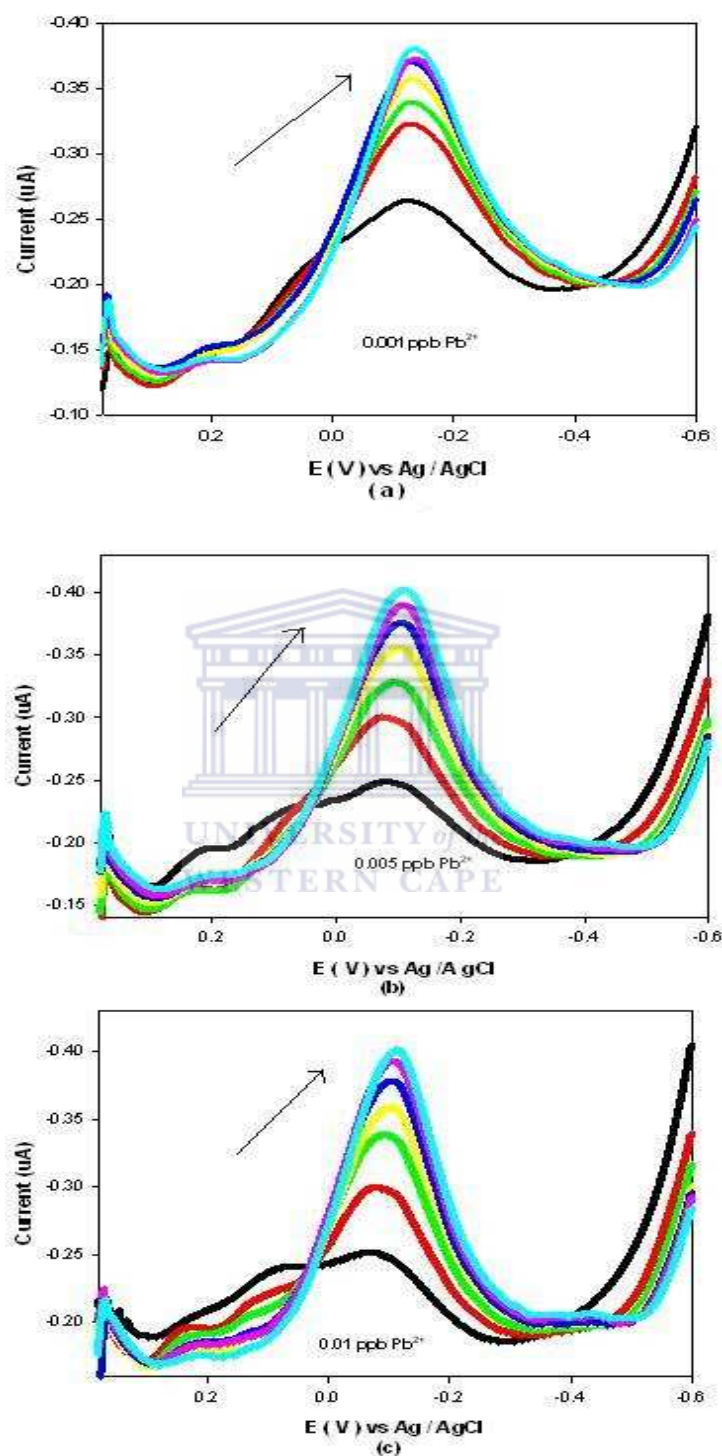


Figure 5.14 Results for the cathodic differential pulse voltammograms (DPVs) of the Pt/PANI/HRP biosensor in the presence of three different Pb concentrations evaluated in 0.1 M PB (pH = 6.8) solution. In (a) the Pb concentration used was  $0.001 \mu\text{g.L}^{-1}$ , followed by  $0.005 \mu\text{g.L}^{-1}$  in (b) and  $0.01 \mu\text{g.L}^{-1}$  in (c). Experimental conditions were: E pulse, 0.02V; scan rate 0.010V/s; potential step, 0.005 V.

Analysis of the results in Figure 5.14 indicates that the Pt/PANI/HRP biosensor when exposed to  $\text{Pb}^{2+}$  ions in the voltammetric evaluation of the biosensor. When the  $[\text{Pb}^{2+}] = 0.001 \mu\text{g.L}^{-1}$ , comparison of the DPV results in Figure 5.14 (a) to that of the biosensor response in Figure 5.5, it was clearly observed that a diminished peak current response was obtained. Comparison of the results in Figure 5.14 (a) also shows that relatively small differences in the peak current responses for these concentrations were observed. However, when the  $[\text{Pb}^{2+}] = 0.005$  and  $0.01 \mu\text{g.L}^{-1}$ , the difference in peak current response to that of the smaller concentrations (a) were more apparent. These results further indicate that the concentration of the metal ions, determine the extent of the inhibition of HRP enzyme observed.

Figure 5.15 shows the linearity between the lead (II) concentrations for the DPV responses evaluated. The three plots in Figure 5.14 were obtained for each of the 0.001, 0.005 and  $0.01 \mu\text{g.L}^{-1}$  Pb concentrations evaluated. This information was further used to determine the sensitivity for each of the concentrations evaluated and were found to be  $1.32 \times 10^{-2} \text{ uAppb}^{-1}$  for  $[\text{Cd}^{2+}] = 0.001 \mu\text{g.L}^{-1}$ ,  $1.71 \times 10^{-2} \text{ uAppb}^{-1}$  for  $[\text{Cd}^{2+}] = 0.005 \mu\text{g.L}^{-1}$  and  $1.70 \times 10^{-2} \text{ uAppb}^{-1}$  for  $[\text{Cd}^{2+}] = 0.01 \mu\text{g.L}^{-1}$ . The apparent Michaelis–Menten constant ( $K_m^{app}$ ) and  $I_{\text{max}}$  were also calculated and their values are presented in Table 7.

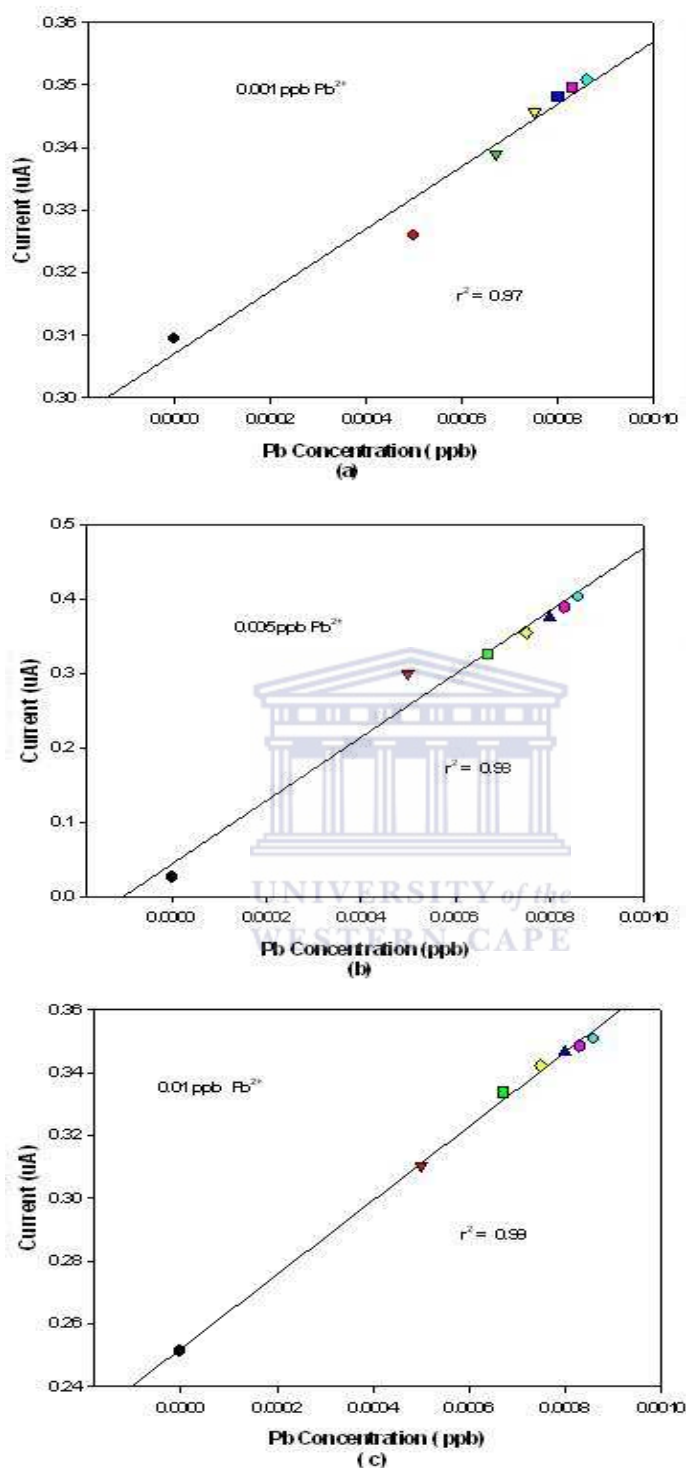


Figure 5.15 Calibration curves obtained for peak current ( $I_p$ ) vs. Pb concentration with 0.001 ppb Pb in (a), 0.005  $\mu\text{g}\cdot\text{L}^{-1}$  Pb in (b) and 0.01  $\mu\text{g}\cdot\text{L}^{-1}$  Pb in (c). Results were obtained using DPV as technique in a 0.1 M PB (pH = 6.8) solution.

The results obtained for the characteristics of the performance of the Pt/PANI/HRP biosensor for  $\text{Pb}^{2+}$  evaluation are shown in Table 5.2. The parameters for the analytical characteristics of the sensor evaluated are presented.

**Table 5.2** Performance characteristics of the Pt/PANI/HRP biosensor in the presence of  $\text{Pb}^{2+}$  as inhibitor.

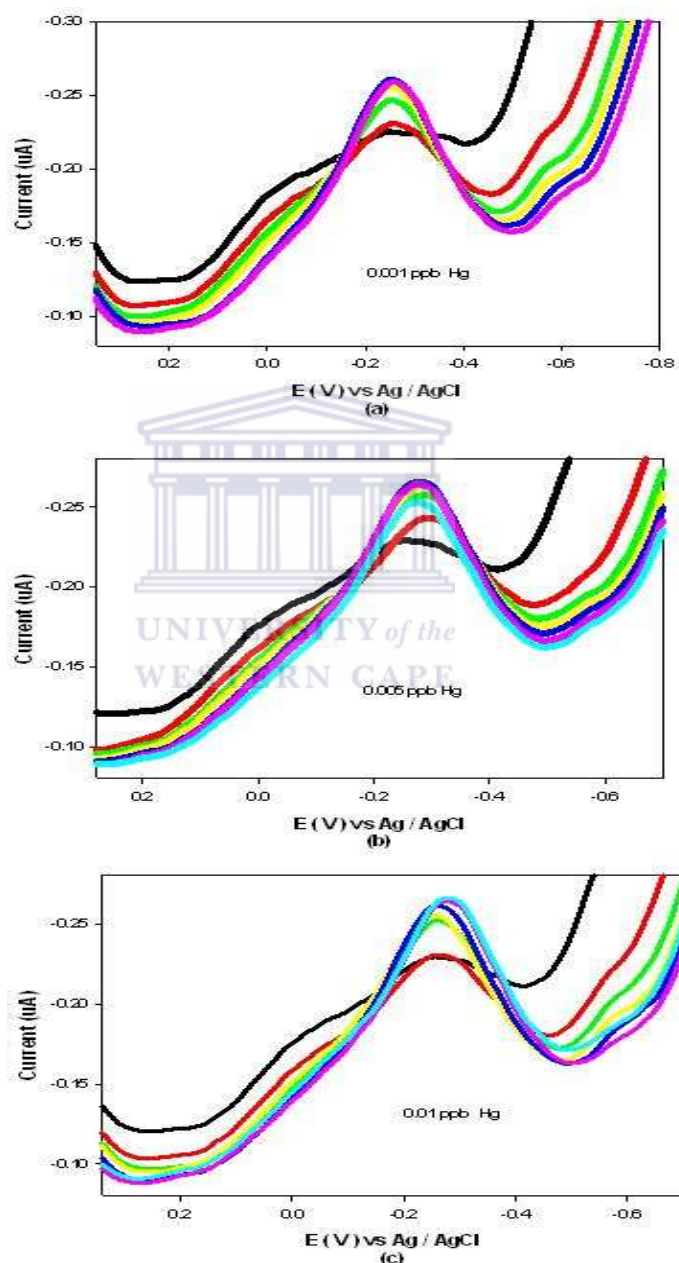
Metal ion	$\text{Pb}^{2+}$		
	0.001	0.005	0.01
$[\text{Pb}^{2+}]$ , $\mu\text{g. L}^{-1}$	0.001	0.005	0.01
Linear range ( $\mu\text{g.L}^{-1}$ )	1-4 ( $n = 4$ )	1-4 ( $n = 4$ )	2-4 ( $n = 3$ )
Sensitivity ( $\mu\text{A/ppb}$ )	$1.32 \times 10^{-2}$	$1.71 \times 10^{-2}$	$1.70 \times 10^{-2}$
Correlation coefficient ( $R^2$ )	0.986	0.992	0.996
LOD(ppb)	$1.23 \times 10^{-3}$		
LOQ (ppb)	$4.09 \times 10^{-3}$		

Analysis of the results in Table 5.2 has shown that the Pt/PANI/HRP biosensor had a linear range that ranged between 0 – 0.86  $\mu\text{g.L}^{-1}$  for the three concentrations evaluated. It was also found that the sensitivity was uniform at the same order, although some variations in the magnitude were obtained. The LOD value obtained for the biosensor in the presence of  $\text{Pb}^{2+}$  was  $1.23 \times 10^{-3} \mu\text{g.L}^{-1}$ , with the LOQ  $4.09 \times 10^{-3} \mu\text{g.L}^{-1}$ .



### 5.3.6.3 Voltammetric results for Hg inhibition

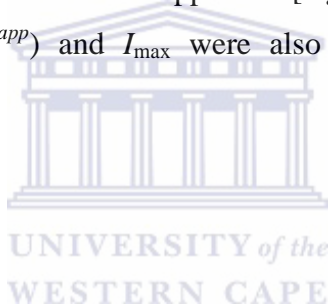
Figure 5.16 shows the DPV recordings obtained at the Pt/PANI/HRP biosensor for the successive increments of aqueous mercury ions with starting concentrations of 0.001, 0.005 and 0.01  $\mu\text{g}\cdot\text{L}^{-1}$ , respectively.



**Figure 5.16** Results for the cathodic differential pulse voltammograms (DPVs) of the Pt/PANI/HRP biosensor in the presence of three different Hg concentrations evaluated in 0.1 M PB (pH = 6.8) solution. In (a) the Cd concentration used was 0.001  $\mu\text{g}\cdot\text{L}^{-1}$ , followed by 0.005  $\mu\text{g}\cdot\text{L}^{-1}$  in (b) and 0.01  $\mu\text{g}\cdot\text{L}^{-1}$  in (c). Experimental conditions were: E pulse, 0.02V; scan rate 0.010V/s; potential step, 0.005 V.

Analysis of the results in Figure 5.16 indicates that an amperometric response was still obtained for the Pt/PANI/HRP biosensor when exposed to  $\text{Hg}^{2+}$  ions in the voltammetric evaluation of the biosensor. When the  $[\text{Hg}^{2+}] = 0.001 \mu\text{g.L}^{-1}$ , comparison of the DPV results in Figure 5.16(a) to that of the biosensor response in Figure 5.5, it was clearly observed that a diminished peak current response was obtained. Comparison of the results in Figure 5.16 (a) (b) and (c) also shows no significant different in the peak current responses.

Figure 5.17 shows the calibration curves for the DPV responses evaluated for peak current versus increasing concentrations of mercury (Hg). The three plots in Figure 5.16 were obtained for each of the 0.001, 0.005 and 0.01  $\mu\text{g.L}^{-1}$  Hg concentrations evaluated. This information was further used to determine the sensitivity for each of the concentrations evaluated and were found to be  $1.54 \times 10^{-2} \text{ uAppb}^{-1}$  for  $[\text{Hg}^{2+}] = 0.001 \mu\text{g.L}^{-1}$ ,  $1.47 \times 10^{-2} \text{ uAppb}^{-1}$  for  $[\text{Hg}^{2+}] = 0.005 \mu\text{g.L}^{-1}$  and  $7.69 \times 10^{-2} \text{ uAppb}^{-1}$  for  $[\text{Hg}^{2+}] = 0.01 \mu\text{g.L}^{-1}$ . The apparent Michaelis–Menten constant ( $K_m^{app}$ ) and  $I_{max}$  were also calculated and their values are presented in Table 8.



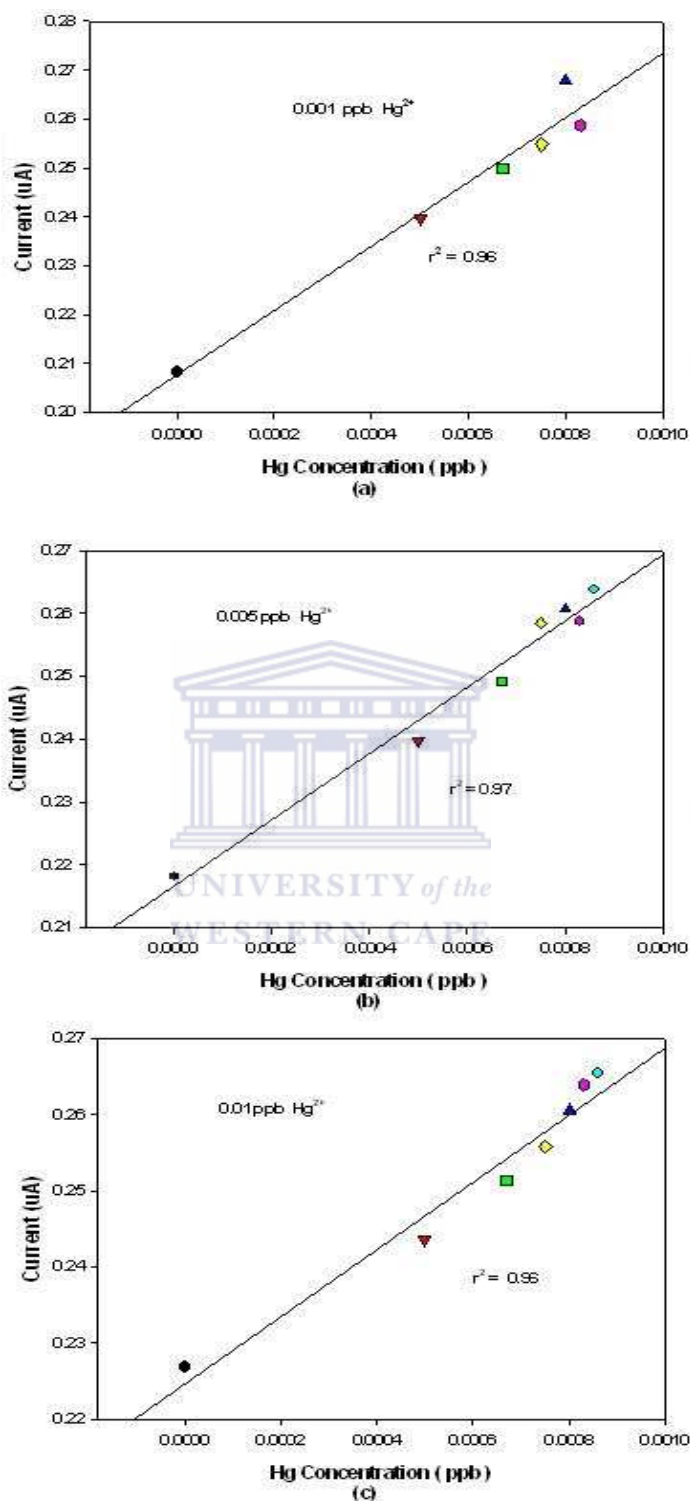


Figure 5.17 Calibration curves obtained for peak current ( $I_p$ ) vs. Hg concentration with  $0.001 \mu\text{g.L}^{-1}$  Hg in (a),  $0.005 \mu\text{g.L}^{-1}$  Hg in (b) and  $0.01 \mu\text{g.L}^{-1}$  Hg in (c). Results were obtained using DPV as technique in a 0.1 M PB (pH = 6.8) solution.

The results obtained for the characteristics of the performance of the Pt/PANI/HRP biosensor are shown in Table 5.3. The parameters for the analytical characteristics of the sensor evaluated are presented.

**Table 5.3** Performance characteristics of the Pt/PANI/HRP biosensor in the presence of Hg<sup>2+</sup> as inhibitor.

Metal ion	Hg <sup>2+</sup>		
	0.001	0.005	0.01
[Hg <sup>2+</sup> ], µg. L <sup>-1</sup>			
Linear range (µg.L <sup>-1</sup> )	0-4 (n = 4)	0-2 (n = 3)	0-2 (n = 3)
Sensitivity (µAppb <sup>-1</sup> )	1.56×10 <sup>-2</sup>	1.47×10 <sup>-2</sup>	7.69×10 <sup>-2</sup>
Correlation coefficient (R <sup>2</sup> )	0.964	0.968	0.962
LOD(ppb)	1.59 × 10 <sup>-3</sup>		
LOQ (ppb)	5.29 × 10 <sup>-3</sup>		

Analysis of the results in Table 5.3 has shown that the Pt/PANI/HRP biosensor had a linear range that ranged between 0 – 4 µg.L<sup>-1</sup> for the three concentrations evaluated. It was also found that the sensitivity was uniform at the same order, although some variations in the magnitude were obtained. The LOD value obtained for the biosensor in the presence of Pb<sup>2+</sup> was 1.59 × 10<sup>-3</sup> µg.L<sup>-1</sup>, with the LOQ 5.29 × 10<sup>-3</sup> µg.L<sup>-1</sup>.

In summary, when the results shown in Tables 5.1, 5.2 and 5.3 are compared it was observed that the best linear range was obtained for Cd<sup>2+</sup>, ensuring that a wider range of concentrations are covered. The best sensitivity was obtained for Hg<sup>2+</sup> with a value of 7.69 × 10<sup>-2</sup>(µAppb<sup>-1</sup>). Furthermore, the lowest LOD value was 6.64 × 10<sup>-4</sup> µg.L<sup>-1</sup>, which was obtained for Cd<sup>2+</sup>.

### 5.3.7 Voltammetric results for Pt/PANI-co-PDTDA/HRP biosensor

The voltammetric results for the Pt/PANI-co-PDTDA/HRP biosensor was also evaluated and obtained for the successive addition of H<sub>2</sub>O<sub>2</sub> concentrations in 0.1 M PB (pH = 7.2) solution. These results are discussed in this section.

### 5.3.7.1 Differential pulse voltammetric characterisation of Pt/PANI-co-PDTDA/HRP biosensor

In Figure 5.18 the results obtained for the cathodic differential pulse voltammograms (CDPVs) of the Pt/PANI-co-PDTDA/HRP biosensor in the presence of increasing  $\text{H}_2\text{O}_2$  concentrations in 0.1 M PB (pH = 7.2) solution is shown, including the calibration plot obtained for the peak current vs. increasing  $\text{H}_2\text{O}_2$  concentrations.

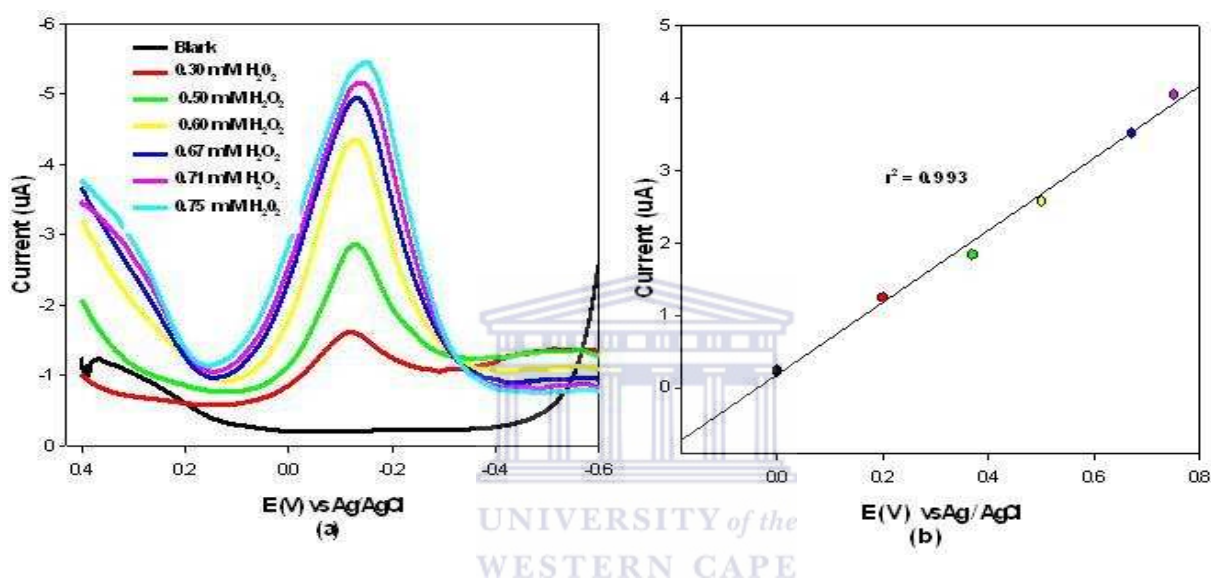


Figure 5.18 The cathodic differential pulse voltammograms (DPVs) in (a) of the Pt/PANI-co-PDTDA/HRP biosensor in the presence of different  $\text{H}_2\text{O}_2$  concentrations evaluated in 0.1 M PB (pH = 7.2) solution is shown, with the calibration plot in (b). Experimental conditions were: amplitude, 20 mV; potential step, 20 mV.

Figure 5.18 shows an increase in  $\text{H}_2\text{O}_2$  concentration is accompanied by an increase in reduction currents obtained at a constant applied potential of - 0.25 V. As can be seen in Figure 5.18, the gaps in between at higher concentrations become to close compared to lower concentrations. The current is close to its maximum, suggesting saturation with  $\text{H}_2\text{O}_2$ . Therefore, the concentration of  $\text{H}_2\text{O}_2$  was set at 0.67 for all the subsequent experiments. A detection limit of  $4.83 \times 10^{-2}$  mM was achieved with a relative standard deviation of 4.3% under DPV conditions. Figure 5.18 (b) shows the dependencies of the signal and background current the calibration curve was linear in concentration between 0 – 0.67 mM of hydrogen peroxide correlation with coefficient  $R^2 = 0.993$ .

The sensitivity was  $5.0 \mu\text{A}/\text{mM}$  compared to lower value of  $0.40 \mu\text{A}/\text{mM}$  obtained for the Pt/PANI/HRP biosensor. Furthermore, for the Pt/PANI-co-PDTDA/HRP biosensor, a smaller  $K_m^{app}$  value of  $0.7 \text{mM}$  with  $I_{max}$  of  $0.27 \mu\text{A}$  was obtained.

### 5.3.7.2 Optimisation of solution pH

This study has broadened the biosensor investigation by using the co-polymer of PANI-co-PDTDA as a second mediator for enzyme immobilisation, in order to compare the biosensor results to that of the homopolymer of PANI. As a first step the pH optimisation of the Pt/PANI-co-PDTDA/HRP biosensor was performed with the results shown in Figure 5.19. The purpose of this experiment was to determine which pH would allow for the optimum value in both sensors and also which sensor would allow a greater current signal.

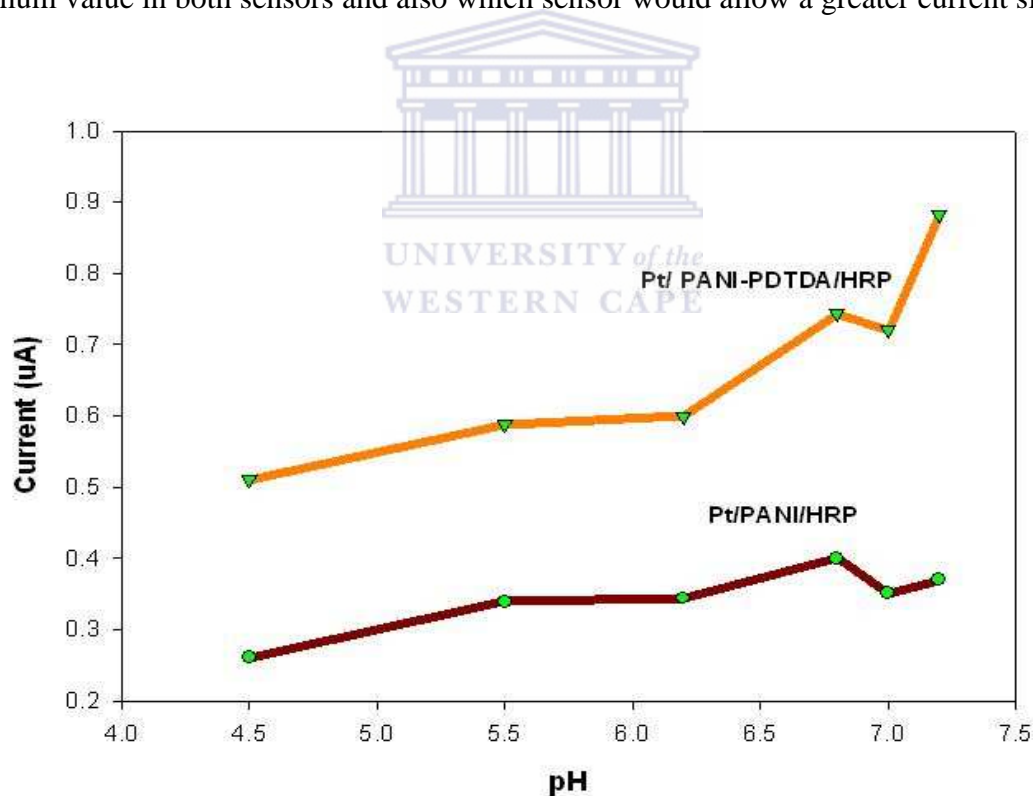


Figure 5.19 Graph displaying the effect of pH on the Pt/PANI/HRP biosensor in  $0.1 \text{M}$  phosphate buffer solutions (PBS) at various pH values.

Analysis of the results in Figure 5.19 has shown that the Pt/PANI-co-PDTDA/HRP biosensor gave the greatest current signal and the optimum value pH = 7.2, compared to most reported PANI values, which gave pH = 6.8 (Mathebe et al., 2004). The effect of pH was studied in 3 mM H<sub>2</sub>O<sub>2</sub> in 0.2 M phosphate buffer (pH = 7.2) solution. Both these values are close to the optimum pH observed for soluble peroxidase (Mello *et al.*, 2003). In an optimised polymerisation the pH of the reaction medium, allow an efficient covalently bonding of the enzyme. It also prevents the loss of the enzyme activity under polymerisation conditions (Gaikwad *et al.*, 2006).

### 5.3.7.3 Voltammetric results for metal ion inhibition

In Figure 5.20 the results obtained for the sequential addition of aliquots of 0.01 μg. L<sup>-1</sup> of Hg<sup>2+</sup> solution is shown. Comparison of the results shown in Figure 5.20 to that in Figure 5.18, it was observed that a diminished current response was obtained. Although there was an increase in the current response for successive addition of the Hg<sup>2+</sup> concentrations, the peak current values are smaller, indicating that inhibition of the HRP enzyme is occurring.

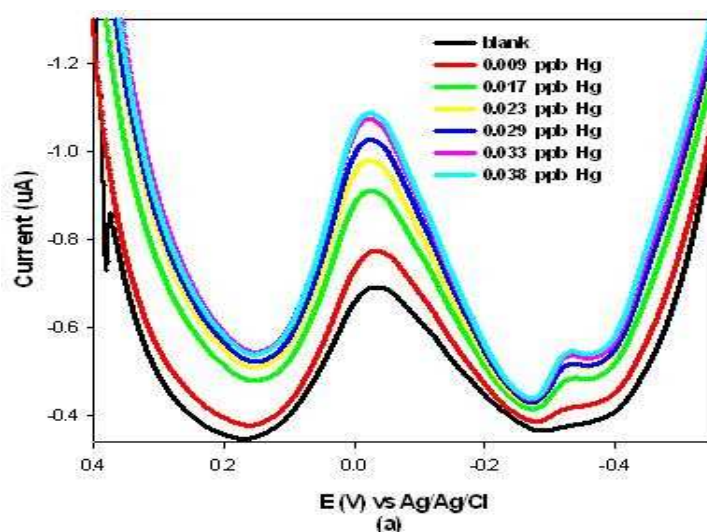


Figure 5.20 Results for the cathodic differential pulse voltammograms (DPVs) of the Pt/PANI-co-PDTDA/HRP biosensor in the presence of 0.001 μg.L<sup>-1</sup> Hg concentrations evaluated in 0.1 M PBS (pH = 7.2). Experimental conditions were: E pulse, 0.02V; scan rate 0.010V/s; potential step, 0.005 V.



In Figure 5.21 the calibration plot for the DPV results obtained in Figure 5.19 is shown. These results were used to determine the inhibition parameters for the Pt/PANI-co-PDTDA/HRP biosensor that are discussed further below.

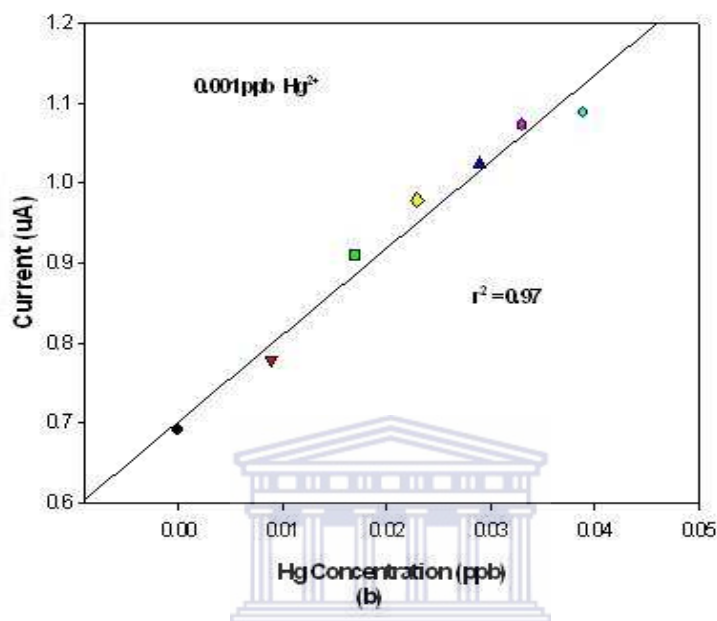


Figure 5.21 Calibration curve obtained for peak current ( $I_p$ ) vs. Hg concentration of  $0.01 \mu\text{g.L}^{-1}$  Hg for the use of the Pt/PANI-co-PDTDA/HRP biosensor in  $0.1 \text{ M PB}$  ( $\text{pH} = 7.2$ ) solution.

The above results will be discussed in the next section where the voltammetric results for Hg inhibition are shown.

#### 5.3.7.3.1 Voltammetric results for Cd inhibition

As for the Pt/PANI/HRP biosensor, differential pulse voltammetric (DPV) evaluation of the Pt/PANI-co-PDTDA/HRP biosensor in the presence of  $\text{Cd}^{2+}$ ,  $\text{Pb}^{2+}$  and  $\text{Hg}^{2+}$  metal ions were performed. The results obtained for the characteristics of the performance of the Pt/PANI-co-PDTDA/HRP biosensor for  $\text{Cd}^{2+}$  analysis are shown in Table 9. The parameters for the analytical characteristics of the sensors evaluated are presented.

**Table 5.4** Performance characteristics of the Pt/PANI-co-PDTDA/HRP biosensor in the presence of Cd<sup>2+</sup> as inhibitor.

Metal ion	Cd <sup>2+</sup>		
[Cd <sup>2+</sup> ], µg. L <sup>-1</sup>	0.001	0.005	0.01
Linear range (µg.L <sup>-1</sup> )	0-1 × 10 <sup>-2</sup> (n = 3)	0-1 × 10 <sup>-2</sup> (n = 3)	0-1 × 10 <sup>-2</sup> (n = 3)
Sensitivity (µAppb <sup>-1</sup> )	1.07 × 10 <sup>-2</sup>	1.93 × 10 <sup>-2</sup>	1.59 × 10 <sup>-2</sup>
Correlation coefficient (R <sup>2</sup> )	0.993	0.996	0.998
LOD(ppb)	8.01 × 10 <sup>-4</sup>		
LOQ (ppb)	2.67 × 10 <sup>-3</sup>		

Analysis of the results in Table 5.4 has shown that indicates that the Pt/PANI/HRP biosensor had a linear range that ranged between 0 – 0.01 µg.L<sup>-1</sup> for the three concentrations evaluated. It was also found that the sensitivity was uniform at the same order, although some variations in the magnitude were obtained. The LOD value obtained for the biosensor in the presence of Cd<sup>2+</sup> was 8.01 × 10<sup>-4</sup> µg.L<sup>-1</sup>, with the LOQ 2.67 × 10<sup>-3</sup> µg.L<sup>-1</sup>.

#### 5.3.7.3.2 Voltammetric results for Pb inhibition

The results obtained for the characteristics of the performance of the Pt/PANI-co-PDTDA/HRP biosensor for Pb<sup>2+</sup> analysis are shown in Table 5.5. The parameters for the analytical characteristics of the sensors evaluated are presented.

**Table 5.5** Performance characteristics of the Pt/PANI-co-PDTDA/HRP biosensor in the presence of Pb<sup>2+</sup> as inhibitor.

Metal ion	Pb <sup>2+</sup>		
[Pb <sup>2+</sup> ], µg. L <sup>-1</sup>	0.001	0.005	0.01
Linear range (µg.L <sup>-1</sup> )	0-1 (n = 3)	0-1 (n = 3)	0-1 (n = 3)
Sensitivity (µAppb <sup>-1</sup> )	5.37 × 10 <sup>-2</sup>	2.36 × 10 <sup>-2</sup>	1.22 × 10 <sup>-2</sup>
Correlation coefficient (R <sup>2</sup> )	0.949	0.983	0.958
LOD(ppb)	9.38 × 10 <sup>-4</sup>		
LOQ (ppb)	3.13 × 10 <sup>-3</sup>		

Analysis of the results in Table 5.5 indicates that the Pt/PANI/HRP biosensor had a linear range that ranged between 0 – 1 $\mu\text{g.L}^{-1}$  for the three concentrations evaluated. It was also found that the sensitivity was uniform at the same order, although some variations in the magnitude were obtained. The LOD value obtained for the biosensor in the presence of  $\text{Pb}^{2+}$  was  $9.38 \times 10^{-4} \mu\text{g.L}^{-1}$ , with the LOQ  $3.13 \times 10^{-3} \mu\text{g.L}^{-1}$ .

### 5.3.7.3.3 Voltammetric results for Hg inhibition

The results obtained for the characteristics of the performance of the Pt/PANI-co-PDTDA/HRP biosensor for  $\text{Hg}^{2+}$  analysis are shown in Table 5.6. The parameters for the analytical characteristics of the sensors evaluated are presented.

**Table 5.6 Performance characteristics of the Pt/PANI-co-PDTDA/HRP biosensor in the presence of  $\text{Hg}^{2+}$  as inhibitor.**

Metal ion	$\text{Hg}^{2+}$			
	$[\text{Hg}^{2+}], \mu\text{g. L}^{-1}$	<b>0.001</b>	<b>0.005</b>	<b>0.01</b>
<b>Linear range</b> ( $\mu\text{g.L}^{-1}$ )	0-1 ( $n = 3$ )	0-1 ( $n = 3$ )	0-1 ( $n = 3$ )	
<b>Sensitivity</b> ( $\mu\text{Appb}^{-1}$ )	$1.02 \times 10^{-2}$	$2.56 \times 10^{-2}$	$2.14 \times 10^{-2}$	
<b>Correlation coefficient (<math>R^2</math>)</b>	0.987	0.993	0.983	
<b>LOD(ppb)</b>	$7.89 \times 10^{-4}$			
<b>LOQ (ppb)</b>	$2.63 \times 10^{-3}$			

Analysis of the results in Table 5.6 has shown that the Pt/PANI/HRP biosensor had a linear range that ranged between 0 – 1 $\mu\text{g.L}^{-1}$  for the three concentrations evaluated. It was also found that the sensitivity was uniform at the same order, although some variations in the magnitude were obtained. The LOD value obtained for the biosensor in the presence of  $\text{Hg}^{2+}$  was  $7.89 \times 10^{-4} \mu\text{g.L}^{-1}$ , with the LOQ  $2.63 \times 10^{-3} \mu\text{g.L}^{-1}$ .

### 5.3.8 Evaluation of biosensor inhibition kinetics

#### 5.3.8.1 Analysis of PANI/HRP biosensor inhibition kinetics

In this section the inhibition kinetics and parameters of the Pt/PANI/HRP biosensor was evaluated by collecting the amperometric responses of the biosensor to increasing  $\text{H}_2\text{O}_2$  concentrations in 0.1 M PB (pH = 6.8) solution. This was evaluated in the absence and presence of metal ion ( $\text{Cd}^{2+}$ ;  $\text{Pb}^{2+}$ ;  $\text{Hg}^{2+}$ ) inhibitors. The results obtained for each of the metal inhibitors are discussed below.

In Figure 5.22 the results obtained for the response of the Pt/PANI/HRP biosensor to various  $\text{H}_2\text{O}_2$  concentrations in the presence and absence of  $\text{Cd}^{2+}$  as inhibitor is shown.

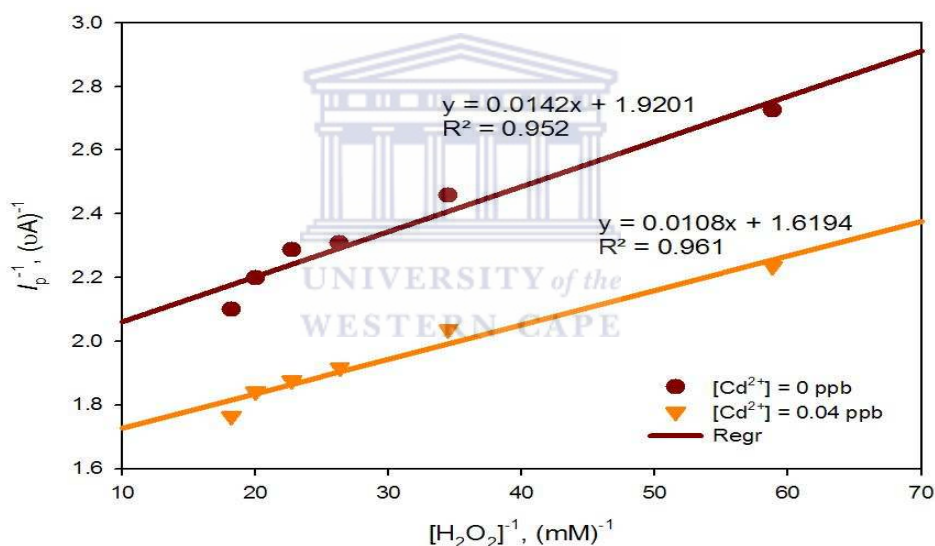


**Figure 5.22** The Line weaver-Burk plot results obtained for the Pt/PANI/HRP biosensor response to successive additions of  $\text{H}_2\text{O}_2$  substrate in the absence and presence of  $\text{Cd}^{2+}$  metal ions.

The results for the response of the biosensor to increasing  $\text{H}_2\text{O}_2$  concentrations were first collected in the absence of the metal ion inhibitor in 0.1 M PB (pH = 6.8) solution. The Pt/PANI/HRP biosensor was then exposed to  $0.04 \mu\text{g}\cdot\text{L}^{-1}$   $\text{Cd}^{2+}$  ( $IC_{50}$  value determined) in 0.1 M PB (pH = 6.8) solution.

In Figure 5.22 the Lineweaver-Burk plots for the HRP biosensor performance is shown and the results obtained for the slope and y-intercept values were calculated. These values were further used to calculate the apparent Michaelis-Menten constants ( $K_M^{app}$ ) in the absence and presence of  $Cd^{2+}$  (Table 9). Analysis of these results indicates that the HRP enzyme undergoes **non-competitive inhibition** in the presence of  $Cd^{2+}$  metal ions, for two reasons. Firstly, the line plots have different y-intercept values that is an indication of the  $V_{max}$  values ( $y\text{-intercept} = \frac{1}{V_{max}}$ ), with  $V_{max}$  being the reaction velocity. Secondly, in the case of  $Cd^{2+}$  ions it was observed that the  $\frac{1}{V_{max}}$  value is bigger compared to the results in the absence of the inhibitor (Figure 5.22), therefore resulting in a smaller  $V_{max}$  value for Cd as inhibitor.

In Figure 5.23 the results obtained for the response of the Pt/PANI/HRP biosensor to various  $H_2O_2$  concentrations in the presence and absence of  $Pb^{2+}$  as inhibitor is shown. The Pt/PANI/HRP biosensor was exposed to  $0.008 \mu\text{g}\cdot\text{L}^{-1} Pb^{2+}$  ( $IC_{50}$  value determined) in 0.1 M PB (pH = 6.8) solution.

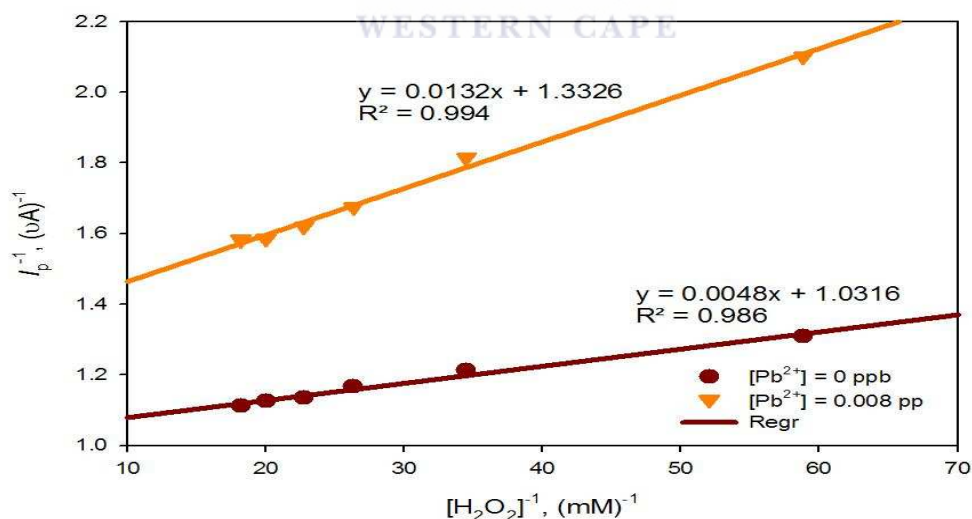


**Figure 5.23** The Lineweaver-Burk plot results obtained for the Pt/PANI/HRP biosensor response to successive additions of  $H_2O_2$  substrate in the absence and presence of  $Pb^{2+}$  metal ions.

Analysis of the shapes of the Lineweaver-Burk plots in Figure 5.23, also gave interesting results on the enzyme inhibition behaviour. It can be assumed that the HRP enzyme undergoes **non-competitive inhibition** metal ions  $\text{Pb}^{2+}$ . Firstly, the line plots have different y-intercept values that is an indication of the  $V_{\max}$  values ( $y\text{-intercept} = \frac{1}{V_{\max}}$ ), with  $V_{\max}$  being the reaction velocity. Secondly, in the case of  $\text{Pb}^{2+}$  ions it was observed that the  $\frac{1}{V_{\max}}$  value in the presence of inhibitor is bigger compared to the results in the absence of the inhibitor (Figure 5.23), therefore resulting in a bigger  $V_{\max}$  value in the absence of inhibitor.

Figure 5.24 displays the results obtained for the response of the Pt/PANI/HRP biosensor to various  $\text{H}_2\text{O}_2$  concentrations in the presence and absence of  $\text{Hg}^{2+}$  as inhibitor. The Pt/PANI/HRP biosensor was then exposed to  $0.005 \mu\text{g}\cdot\text{L}^{-1} \text{Hg}^{2+}$  ( $IC_{50}$  value determined) in 0.1 M PB (pH = 6.8) solution.

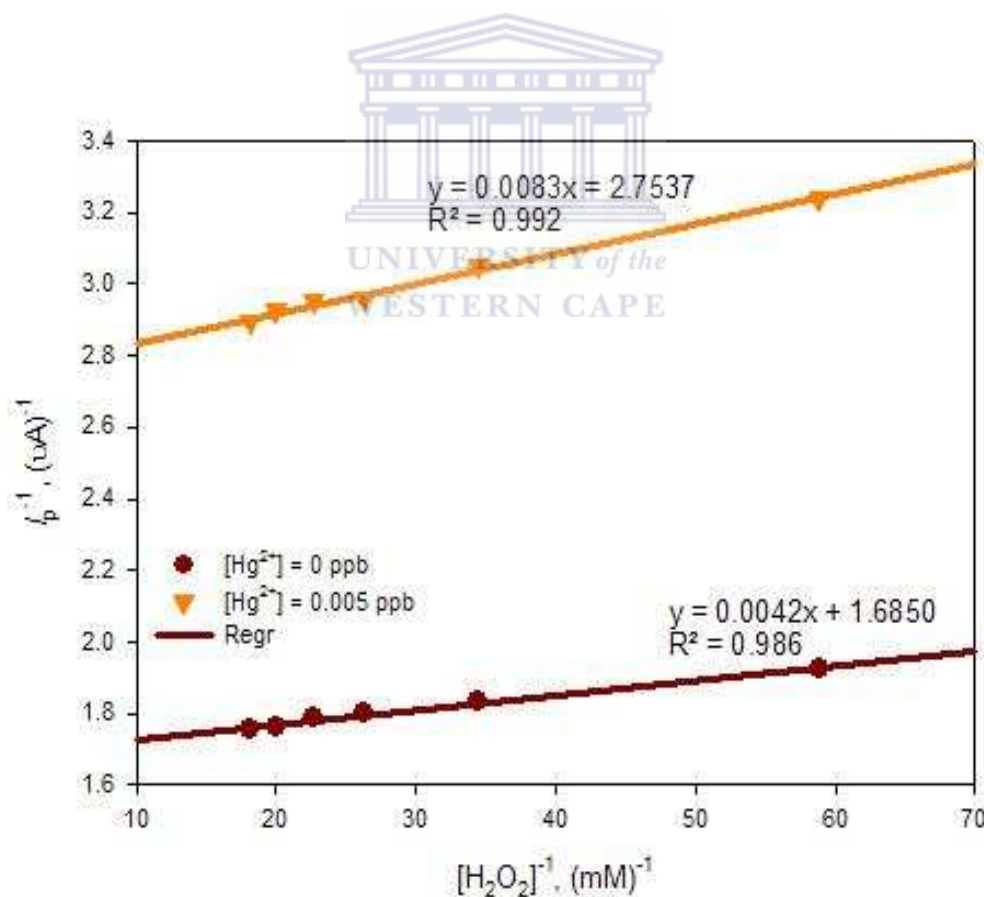


**Figure 5.24** The Lineweaver-Burk plot results obtained for the Pt/PANI/HRP biosensor response to successive additions of  $\text{H}_2\text{O}_2$  substrate in the absence and presence of  $\text{Hg}^{2+}$  metal ions.

Analysis of the results for the Lineweaver-Burk plot in Figure 5.24, indicate that the HRP enzyme undergoes **non-competitive inhibition** in the presence of  $\text{Hg}^{2+}$  metal ions, for two reasons. Firstly, the line plots have different y-intercept values that is an indication of the  $V_{\max}$  values (y-intercept  $=\frac{1}{V_{\max}}$ ), with  $V_{\max}$  being the reaction velocity. Secondly, in the case of  $\text{Hg}^{2+}$  ions it was observed that the  $\frac{1}{V_{\max}}$  value is bigger compared to the results in the absence of the inhibitor (Figure 5.21), therefore resulting in a bigger  $V_{\max}$  value in the absence of inhibitor.

In Table 5.7 a summary of the results obtained for the inhibition kinetics of the Pt/PANI/HRP biosensor in the absence and presence of Cd, Pb and Hg as metal ion inhibitors are shown.

**Table 5.7** Apparent Michealis- Menten ( $K_m^{\text{app}}$ ) values and  $I_{\max}$  parameters obtained in the absence of heavy metals and at different concentrations ( $IC_{50}$  values) of heavy metals (Cd, Pb and Hg). Results evaluated for the Pt/PANI/HRP biosensor in 0.1 M PB (pH = 6.8) solution is shown.

Kinetic parameters	Metal ion inhibitor					
	0 $\mu\text{g.L}^{-1}$ $\text{Cd}^{2+}$	0.04 $\mu\text{g.L}^{-1}$ $\text{Cd}^{2+}$	0 $\mu\text{g.L}^{-1}$ $\text{Pb}^{2+}$	0.008 $\mu\text{g.L}^{-1}$ $\text{Pb}^{2+}$	0 $\mu\text{g.L}^{-1}$ $\text{Hg}^{2+}$	0.005 $\mu\text{g.L}^{-1}$ $\text{Hg}^{2+}$
Slope (uA/mM)	$2.25 \times 10^{-3}$	$1.72 \times 10^{-3}$	$4.33 \times 10^{-4}$	$1.46 \times 10^{-3}$	$3.87 \times 10^{-4}$	$8.42 \times 10^{-4}$
y-intercept (1/uA)	2.049	1.718	1.076	1.453	1.723	2.829
$K_m^{\text{app}}$ (mM)	2.41	2.94	2.05	4.32	1.47	4.11
$I_{\max}$ (uA)	0.54	0.51	0.89	0.63	0.57	0.35

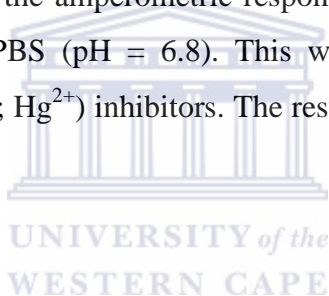
Comparison and analysis of the results shown in Table 5.7 indicate that the best sensitivity has been obtained in  $\text{Cd}^{2+}$  for all the three metals analysed. It was also found that the  $K_m^{\text{app}}$  value was affected by the presence of  $\text{Cd}^{2+}$  ions and absence slightly increased whereas there is no significant difference in  $I_{\max}$  value. This is the indication of the competitive inhibition.



A competitive inhibitor decreases the apparent affinity of the substrate for the enzyme thus increasing  $K_m^{app}$  but does not alter the reactivity of the enzyme hence  $I_{max}$  remain unchanged. This observation explain that the  $Cd^{2+}$  compete with  $H_2O_2$  to bind to the active site of HRP. The presence of  $Pb^{2+}$  and  $Hg^{2+}$  ions affected the  $K_m^{app}$  value in the presence of inhibitor which leads to decrease  $I_{max}$  values. The decrease in  $I_{max}$  values suggest that the inhibition mechanism is mixed inhibitor. As a non-competitive, this inhibitor at a site other than the active site and causes changes in the overall 3d shape of the enzyme that lead to a decrease in in activity.

#### 5.3.8.2 Analysis of PANI-co-PDTDA/HRP biosensor inhibition kinetics

The inhibition kinetics and parameters of the Pt/PANI-co-PDTDA/HRP biosensor was also evaluated by collecting the amperometric responses of the biosensor to increasing  $H_2O_2$  concentrations in 0.1 M PBS (pH = 6.8). This was evaluated in the absence and presence of metal ion ( $Cd^{2+}$ ;  $Pb^{2+}$ ;  $Hg^{2+}$ ) inhibitors. The results obtained for each of the metal inhibitors are discussed below.



In Figure 5.25 the results obtained for the response of the Pt/PANI-co-PDTDA/HRP biosensor to various  $\text{H}_2\text{O}_2$  concentrations in the presence and absence of  $\text{Cd}^{2+}$  as inhibitor is shown.

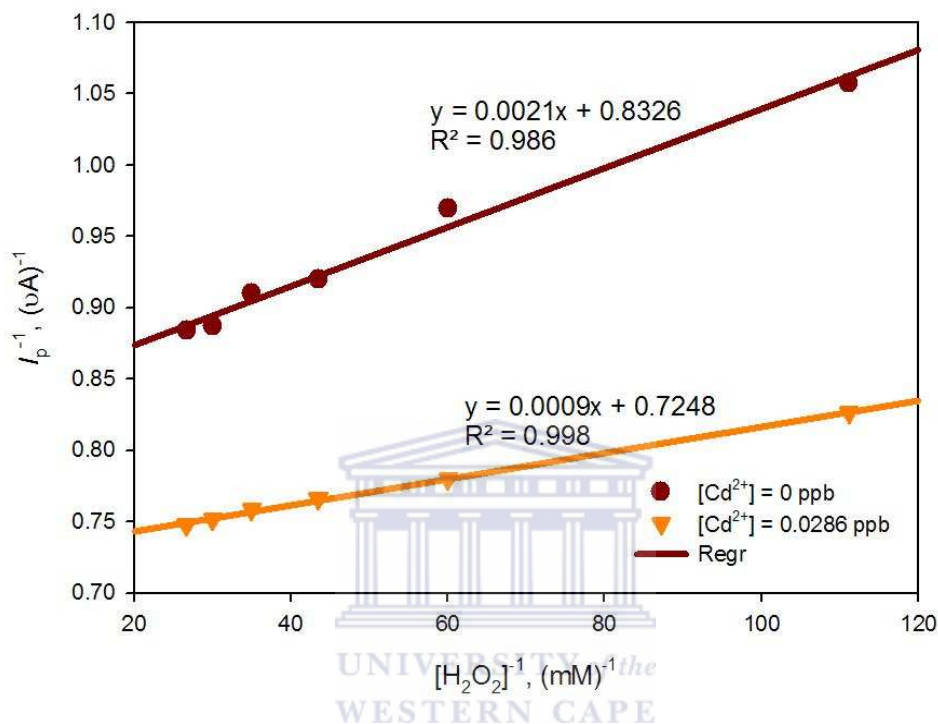
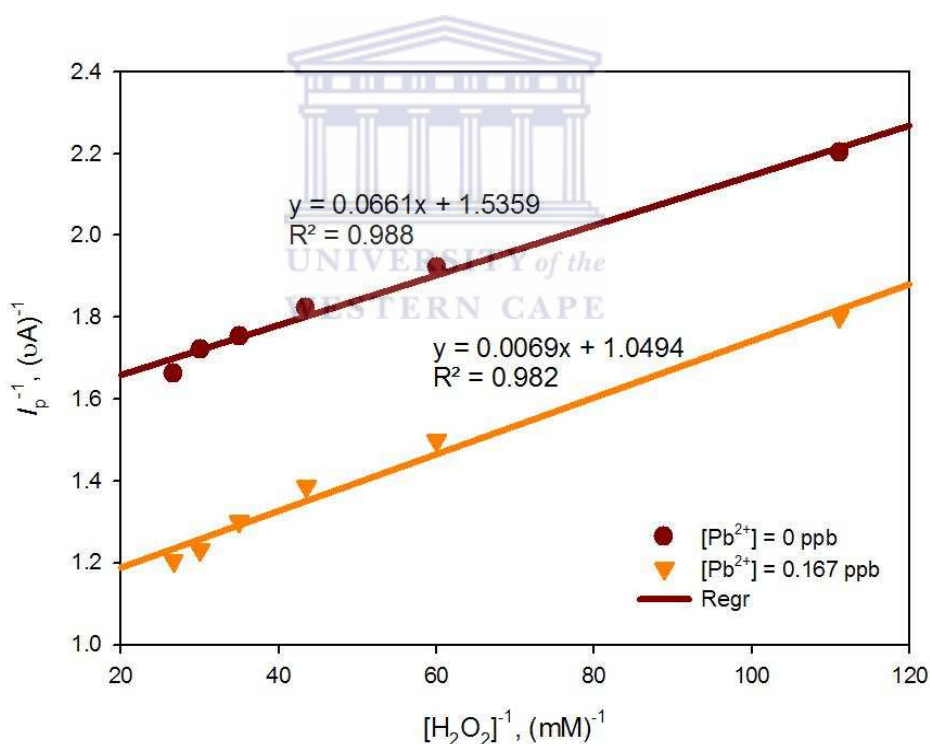


**Figure 5.25** The Lineweaver-Burk plot results obtained for the Pt/PANI-co-PDTDA/HRP biosensor response to successive additions of  $\text{H}_2\text{O}_2$  substrate in the absence and presence of  $\text{Cd}^{2+}$  metal ions.

Analysis of the results in Figure 5.25 the Lineweaver-Burk plots for the HRP biosensor performance is shown and the results obtained for the slope and y-intercept values were calculated. These values were further used to calculate the apparent Michaelis-Menten constants ( $K_M^{\text{app}}$ ) in the absence and presence of  $\text{Cd}^{2+}$  (Table 10).

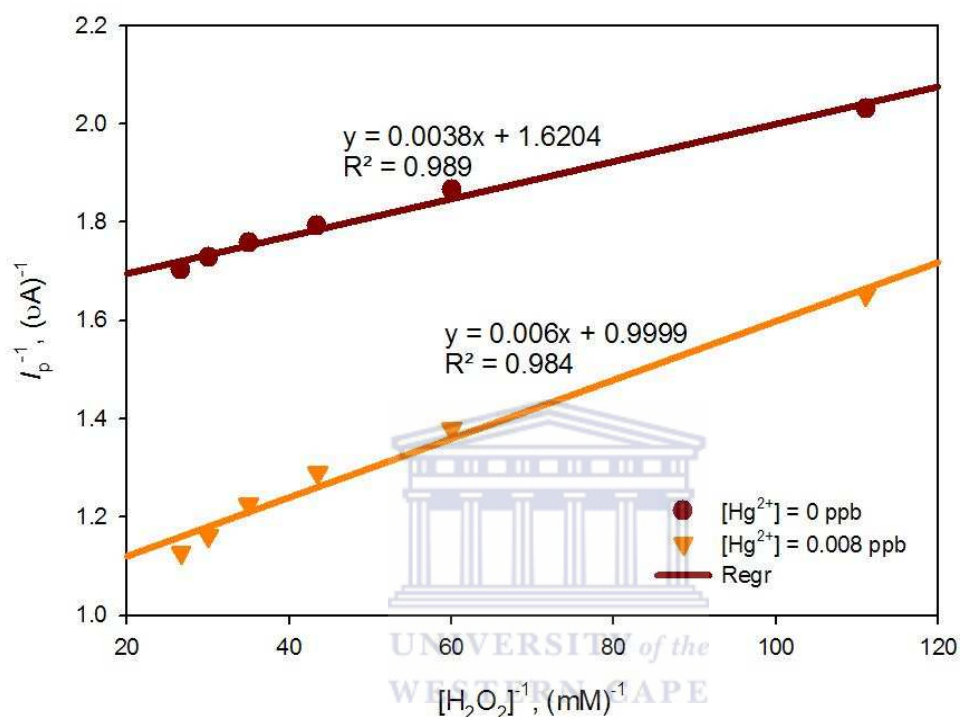
Analysis of these results indicates that the HRP enzyme undergoes **non-competitive inhibition** in the presence of  $\text{Cd}^{2+}$  metal ions, for two reasons. Firstly, the line plots have different y-intercept values that is an indication of the  $V_{\max}$  values ( $y\text{-intercept} = \frac{1}{V_{\max}}$ ), with  $V_{\max}$  being the reaction velocity. Secondly, in the case of  $\text{Cd}^{2+}$  ions it was observed that the  $\frac{1}{V_{\max}}$  value is bigger compared to the results in the absence of the inhibitor (Figure 50), therefore resulting in a smaller  $V_{\max}$  value for Cd as inhibitor.

Figure 5.26 displays the results obtained for the response of the Pt/PANI-co-PDTDA/HRP biosensor to various  $\text{H}_2\text{O}_2$  concentrations in the presence and absence of  $\text{Pb}^{2+}$  as inhibitor.



**Figure 5.26** The Lineweaver-Burk plot results obtained for the Pt/PANI-co-PDTDA/HRP biosensor response to successive additions of  $\text{H}_2\text{O}_2$  substrate in the absence and presence of  $\text{Pb}^{2+}$  metal ions.

In Figure 5.27 the results obtained for the response of the Pt/PANI-co-PDTDA/HRP biosensor to various  $\text{H}_2\text{O}_2$  concentrations in the presence and absence of  $\text{Hg}^{2+}$  as inhibitor were first collected in in 0.1 M PB (pH = 7.2) solution. The Pt/PANI/HRP biosensor was then exposed to  $0.167 \mu\text{g. L}^{-1} \text{Hg}^{2+}$  ( $IC_{50}$  value determined) in 0.1 M PB (pH = 6.8) solution.



**Figure 5.27** The Lineweaver-Burk plot results obtained for the Pt/PANI-co-PDTDA/HRP biosensor response to successive additions of  $\text{H}_2\text{O}_2$  substrate in the absence and presence of  $\text{Hg}^{2+}$  metal ions.

In Figure 5.27 the Lineweaver-Burk plots for the HRP biosensor performance is shown and the results obtained for the slope and y-intercept values were calculated. These values were further used to calculate the apparent Michaelis-Menten constants ( $K_M^{\text{app}}$ ) in the absence and presence of  $\text{Hg}^{2+}$  (Table 9). Analysis of these results indicates that the HRP enzyme undergoes **non-competitive inhibition** in the presence of  $\text{Hg}^{2+}$  metal ions, for two reasons. Firstly, the line plots have different y-intercept values that is an indication of the  $V_{\text{max}}$  values ( $y\text{-intercept} = \frac{1}{V_{\text{max}}}$ ), with  $V_{\text{max}}$  being the reaction velocity. Secondly, in the case of  $\text{Hg}^{2+}$  ions it was observed that the  $\frac{1}{V_{\text{max}}}$  value is bigger compared to the results in the absence of the inhibitor (Figure 56), therefore resulting in a smaller  $V_{\text{max}}$  value for Hg as inhibitor.

In Table 5.8 a summary of the results obtained for the inhibition kinetics of the Pt/PANI-co-PDTDA/HRP biosensor in the absence and presence of Cd, Pb and Hg as metal ion inhibitors are shown.

**Table 5.8** Apparent Michealis- Menten ( $K_m^{app}$ ) values and  $I_{max}$  parameters obtained in the absence of heavy metals and at different concentrations ( $IC_{50}$  values) of heavy metals (Cd, Pb and Hg). Results evaluated for the Pt/PANI-co-PDTDA/HRP biosensor in 0.1 M PB (pH = 7.2) solution is shown.

Kinetic parameters	Metal ion inhibitor					
	0 $\mu\text{g.L}^{-1}$ Cd <sup>2+</sup>	0.028 $\mu\text{g.L}^{-1}$ Cd <sup>2+</sup>	0 $\mu\text{g.L}^{-1}$ Pb <sup>2+</sup>	0.167 $\mu\text{g.L}^{-1}$ Pb <sup>2+</sup>	0 $\mu\text{g.L}^{-1}$ Hg <sup>2+</sup>	0.008 $\mu\text{g.L}^{-1}$ Hg <sup>2+</sup>
Slope (uA/mM)	$2.10 \times 10^{-3}$	$8.97 \times 10^{-4}$	$5.90 \times 10^{-3}$	$6.57 \times 10^{-3}$	$3.60 \times 10^{-3}$	$5.59 \times 10^{-3}$
y-intercept (1/uA)	0.833	0.725	1.536	1.049	1.620	1.685
$K_m^{app}$ (mM)	5.37	7.45	1.08	1.39	1.68	1.67
$I_{max}$ (uA)	1.127	1.337	0.637	0.919	0.607	0.937

Comparison and analysis of the results shown in Table 5.8 indicate the best sensitivity has been obtained in Cd<sup>2+</sup> for all the three metals analysed. It was also found that the presence of Cd<sup>2+</sup> ions affected the  $K_m^{app}$  value although there is no apparent change in  $I_{max}$  value for Cd<sup>2+</sup> in the presence and absence of the inhibitor. This is the indication of the competitive inhibition and this process is reversible as increasing concentration of substrate act to wash out the inhibitor from the active site. The  $K_m^{app}$  value in the presence of Pb<sup>2+</sup> and Hg<sup>2+</sup> ions were not significantly different whereas the  $I_{max}$  value became affected. The increase in  $I_{max}$  values suggests that the inhibition mechanism is reversible and non-competitive.

### 5.3.9 Comparison between Pt/PANI/HRP and Pt/PANI-co-PDTDA/HRP biosensors

The important parameters obtained for the enzyme electrodes are summarized in Table 14. The lowest  $K_m^{app}$  and  $I_{max}$  values were calculated for the Pt/PANI/HRP., the best detection limit was observed in Pt/PANI-co-PDTDA/HRP with a smaller relative standard deviation (%RSD) of 4.3% to that of 14% for Pt/PANI/HRP.

Sensitivities were calculated as  $0.410 \mu\text{AmM}^{-1}$  and  $5.00 \mu\text{AmM}^{-1}$  for PANI and PANI-PDTDA enzyme electrodes, respectively by dividing  $I_{\text{max}}$  to  $K_m^{\text{app}}$ . The Pt/PANI-co-PDTDA/HRP biosensor was also found to be more sensitive than Pt/PANI/HRP for detecting these metal ions; unfortunately, there are no other reports of the values for LOD and kinetic parameters for Pt/PANI-co-PDTDA/HRP biosensor. The Pt/PANI/HRP biosensor has obtained the highest  $I_{\text{max}}$  than  $K_m^{\text{app}}$  of which this is what is desirable in the construction of biosensor. The Pt/PANI-co-PDTDA/HRP biosensor has obtained lower  $I_{\text{max}}$  than  $K_m^{\text{app}}$ , however the  $I_{\text{max}}$  value is smaller. It is likely that the lower  $I_{\text{max}}$  arises due to complex formation between  $\text{H}_2\text{O}_2$  and the polymer, which effectively decreases the binding. A comprehensive literature survey reveals that many assays for developing the enzymatic activity of HRP from  $\text{H}_2\text{O}_2$  have been previously reported and the previously reported literatures are based on different electrodes, mediators and different enzymes. This comparison is only specific to electrodes that were immobilised with conducting polymers and other films. This comparison shows that the  $K_m$  and  $I_{\text{max}}$  value obtained from the Pt/PANI/HRP biosensor is in close agreement with values obtained using other assays; (Michira *et al.*, 2007, Yang *et al.*, 1997) and the value of  $K_m^{\text{app}}$  was lower compared to the studies of (Nomngongo *et al.*, 2011, Wang *et al.* 2005, Wang *et al.*, 2009a). The  $K_m^{\text{app}}$  value for  $\text{Cd}^{2+}$  is higher than the one reported by Nomngongo *et al.* (2007).

**Table 5.9 Kinetic parameters for the Pt/PANI/HRP and Pt/PANI-co-PDTDA/HRP biosensors.**

Immob. Matrices	$K_m(mM)$	$I_{\text{max}} (\mu\text{Acm}^{-2})$	$LOD (mM)$	Sensitivity ( $\mu\text{AmM}^{-1}$ )
PANI	0.6	1.7	0.32	0.410
PANI-PDTDA	0.7	0.27	0.00483	5.00

## 5.4 Summary

An amperometric biosensor based on the inhibitory effects on horseradish peroxidases (HRP) activity towards the reduction of hydrogen peroxide ( $\text{H}_2\text{O}_2$  substrate) by selected heavy metals (Hg, Cd, and Pb) has been investigated. The polymer (PANI) and PANI-co-PDTDA were used as mediators since they provide a suitable platform for the immobilisation of HRP on the platinum electrode surface and it also mediate in electron transfer between HRP and the electrode (Gerard *et al.*, 2002).

The results obtained by both of these methods were compared. A 0.1 M buffer solution (pH = 6.8) was used throughout the study for Pt/PANI/HRP biosensor, while a pH = 7.2 solution was used for the Pt/PANI-co-PDTDA/HRP biosensor. These were optimum pH values obtained for maximal current output, which correspond to the one that was reported by Mathebe *et al.* (2004) for Pt/PANI/HRP. The kinetic studies were also investigated using the Lineweaver-Burk method. The important part of the curve is usually the linear range where variation in substrate concentration gives a variation in the current. The slope of the curve in the linear zone corresponds to the sensitivity of the biosensor because it expresses a variation in the signal obtained as a function of the analyte concentration. Through this information it was able to find the Michaelis-Menten parameters. The apparent Michaelis – Menten parameters ( $K_m^{\text{app}}$ ) and  $I_{\text{max}}$  values, which provide an indication of catalytic activity of an enzyme were calculated to be 0.6 mM and 1.7  $\mu\text{A}$  for the Pt/PANI/HRP biosensor, and 0.7 mM and 0.27  $\mu\text{A}$  for the Pt/PANI-co-PDTDA/HRP biosensor in 1 mM  $\text{H}_2\text{O}_2$  substrate solution. The smaller value of  $K_m^{\text{app}}$  indicates that the complex formed in both biosensors with  $\text{H}_2\text{O}_2$  is strong. The evidence of high  $I_{\text{max}}$  and low  $K_m^{\text{app}}$  value in the case of Pt/PANI/HRP is what is actually desired in the construction of a biosensor. The heavy metals detection limit has also shown close agreement with previous reported literature values of Pt/PANI/HRP biosensors. For repeatability, 10 successive measurements were done of 1 mM  $\text{H}_2\text{O}_2$  in order to see the current response of Pt/PANI/HRP biosensor. The %RSD values for the Pt/PANI/HRP and Pt/PANI-PDTDA/HRP biosensors were calculated to be 14% and 4.3% respectively. The Hg(II) ions were noted to have higher degree of enzyme inhibition with a value of 73% and 84% for Pt/PANI/HRP and Pt/PANI-PDTDA/HRP biosensors, respectively. Although additional development is required before this technique is ready for widespread use, it shows great promise as a means of rapidly screening numerous aqueous samples for metal contamination.



## Chapter 6

### Voltammetric Stripping Analysis of PGMs

---

#### 6.1 Introduction

The year 2012 represent the twentieth anniversary of the first reported application of screen-printed electrodes (SPCEs) for the determination of metal ions(Honeychurch, 2012). By Combining these electrode with stripping voltammetry, the mass transport which occurs as the result of this type of diffusion can increase and also enhanced the signal to noise ratio. The acceptance of stripping methods has however suffered from the use of mercury working electrodes, with lack of market penetration compared to other techniques. The beauty of electrochemical techniques is the construction of a chemically modified electrode (CME), tailor made for sensitive and selective analytical applications, avoiding application of the toxic mercury film (Kalcher *et al.*, 2006 ; Svancara *et al.*, 2009;Khaled *et al.*, 2012).

The rough surface of SPCEs has shown itself to be an excellent approach to pre-concentrate a substrate on the electrode surface, providing more sensitive methods using lab-constructed hand-held instruments. Voltammetric stripping methods involve a pre-concentration step that is generally very sensitive when used for metal-ion determination. The combination of chemically modified electrodes with stripping methods can offer an excellent alternative for electrochemical analysis of metals at trace levels, increasing not only the sensitivity but also selectivity of the analysis. A common approach to increasing selectivity is to attach host molecules, which selectively interact with specific guest molecules. The coupling of disposable SPCEs with stripping techniques is more favourable in comparison with conventional stripping analysis, as the design and operation are greatly simplified, in accordance with the requirements of a decentralized assay (Khaled *et al.*, 2010).

The biosensor that was developed in chapter 5 was not suitable for the determination of PGMs because of this; our research was diverted to develop a sensor that is suitable for these metals since they were part of our project. In this study the construction and evaluation of SPCEs chemically modified with a bismuth film (BiF) were used as a working electrode for the determination of PGMs (Pd, Pt, and Rh) in alkaline medium, in the presence of a chelating agent of dimethylglyoxime (DMG).

## 6.2 Materials and Methods

### 6.2.1 Chemicals and reagents

The standards for platinum (Pt), palladium (Pd) and rhodium (Rh) (1000 mg/L atomic absorption standard solution) and a standard Bi (III) solution (999 mg/L, AAS) and DMG were provided by Fluka (Germany). All other reagents used were provided by Merck (South Africa) and included sodium acetate, ammonia with a purity of ca 25% ammonium chloride, hydrochloric acid with purity 32% and nitric acid with purity 55%. Glacial acetic acid and ethanol (95%) were purchased from Kimix (South Africa).

Precious group metal (PGM) stock solutions were prepared from 1000 mg/L AAS standards solutions and standardised Bi (III) ( $100 \text{ mg.L}^{-1}$ ) was used for the formation of the film on a SPCE. A stock solution of 0.01 M DMG was prepared by dissolution of the pure substance in absolute ethanol. Ammonium buffer solution was prepared from ammonium chloride and the pH was adjusted to the value of 9.2 with the addition of ultra-pure ammonia ( $\text{NH}_3$ ; 25%) and employed as supporting electrolyte solution. Acetic acid was used for pH control for the preparation of a sodium acetate buffer (pH = 4.8) solution. Ultrapure water (Milli-Q plus; 18.2 M $\Omega$ ; Millipore systems) was used in all experiments.

### 6.2.2 Apparatus

Voltammetric measurements were performed using a PalmSens portable potentiostat / galvanostat, with the PS Trace program and accessories (PalmSens® Instruments BV, 3992 BZ Houten, The Netherlands), interfaced to a microcomputer controlled by PS 2.1 software for data acquisition and experimental control.

The measurements were performed in a conventional electrochemical cell of 20.0 mL, employing the bismuth modified carbon screen-printed electrode (SCPE/Bi) with 4 mm diameter provided by Dropsens (Oviedo, Spain) as working electrodes. The electrochemical system set-up is shown in Figure 6.1

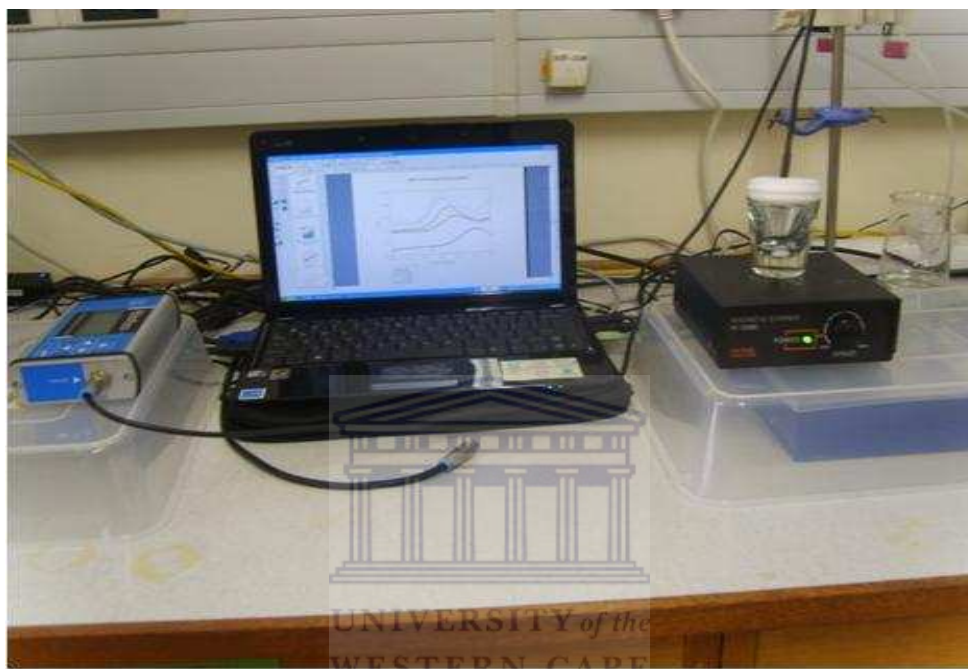


**Figure 6.1** The photograph showing of a portable Palmsens® electrochemical system and set-up used in this study.

The measurement of pH values during the experiments was carried out by means of a microprocessor pH meter with custom buffers (the model HI 221 series, Hanna, instruments). All experiments were performed at a controlled room temperature of  $20 \pm 1$  °C.

### 6.2.3 Preparation of bismuth film electrode (BiFE)

The screen-printed carbon electrode (SPCE) was connected to the potentiostat as working electrode using a 1 meter length cable provided by the electrode manufacturer (PalmSens®). The three electrode system was placed into cell containing a 10 mL solution of 100 mg.L<sup>-1</sup> Bi (III) in 0.2 M acetate buffer (pH = 4.8) solution. The solution was deoxygenated with pure nitrogen for 5 min followed by deposition of bismuth onto the screen-printed electrode at a deposition potential of - 1.0. V (vs. Ag/AgCl) for 300 seconds with solution stirred (by means of a mechanical stirrer bar), and then the solution was left for 15 s without stirring to equilibrate.

Next, the whole electrode system was rinsed with ultrapure water several times without scratching or disturbing the bismuth film on the SPCE. Finally, this was followed using voltammetric stripping measurements of the analyte solution and employing adsorptive differential pulse stripping voltammetry (AdDPSV) in the cathodic scanning direction.

### 6.2.4 Analytical procedure for the determination of PGMs

Before each voltammetric titration process, the presence of PGMs was checked by recording the DPAdSV of the blank buffer solution. The electrode surface was activated by 10 replicate direct current sweeps from + 0.8 to - 1.4 V with scan rate 50 mVs<sup>-1</sup> in 0.01 M ammonium buffer (pH = 9.2) solution. The solution was then exchanged by a sample solution containing the same supporting electrolyte purged by pure nitrogen gas for 5 min. The procedure used to obtain the differential pulse adsorptive stripping voltammograms (DPAdSVs) was as follows. A 10 mL of 0.01 M ammonium buffer (pH = 9.2) solution containing 5 × 10<sup>-5</sup> M DMG was transferred into the voltammetric cell. The stirrer was switched on and the solution was purged with nitrogen gas for 5 min. Then the analyte was pre-concentrated for 150 s at - 0.7 V (vs. Ag/AgCl) whilst stirring the solution at 2000 rpm. At the end of the accumulation time the stirrer was switched off. After resting for 10 s, the AdDPSV was performed, with the potential scanned from + 0.8 to - 1.4 V at a scan rate 50 mVs<sup>-1</sup>.

When further metal solution was added to the cell, the solution was deoxygenated with nitrogen before performing further voltammetric analysis. The peak current was used for the construction of calibration curves for each metal investigated.

### 6.3. Results and Discussion

#### 6.3.1 Characterisation of modified screen-printed electrode surface

Initial studies of the SPCE/BiF were carried out using cyclic voltammetry (CV) in different types of supporting electrolytes. The supporting electrolytes examined included 0.01 M  $\text{NH}_3$  buffer (pH = 9.2), 0.2 M NaOAc buffer (pH = 4.8), 0.1 M HCl, 1 mM  $\text{K}_3\text{Fe}(\text{CN})_6$ , and  $4 \times 10^{-3}$  M  $\text{LiClO}_4$  solutions. It was found that the SPCE/BiF gave the highest reduction peak current response in the 0.2 M NaOAc buffer (pH = 4.8) solution. In this study ammonia buffer (pH = 9.2) was selected for further studies because it was pointed out that basic pH conditions give the widest potential range with minimum solvent reduction signal. This voltammetric behaviour of ammonium buffer (pH = 9.2) solution is seen in Figure 6.2 and was in close agreement with the one reported in literatures (Hutton *et al.*, 2001).

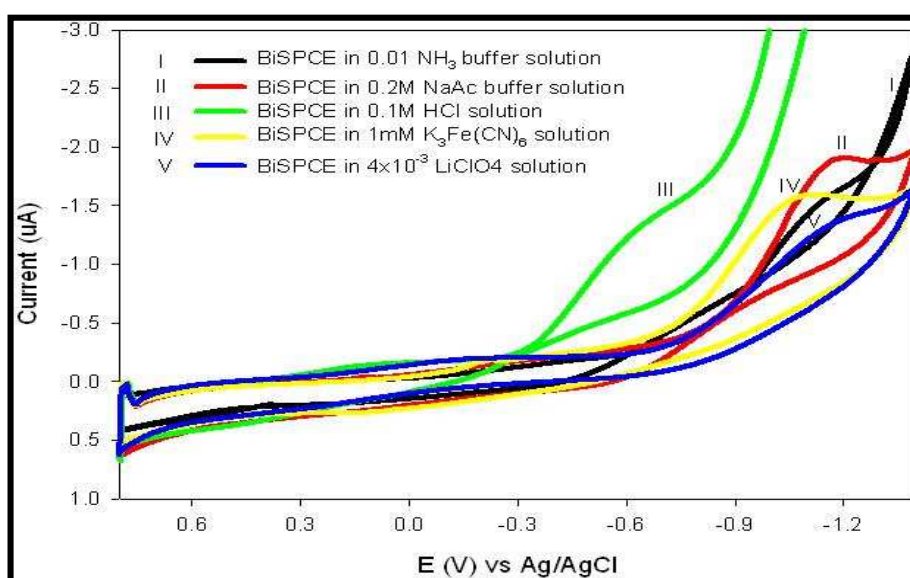


**Figure 6.2** Cyclic voltammograms for the SPCE/BiF sensor in different buffer solutions at a scan rate of  $0.05 \text{ V s}^{-1}$  in: (I) 0.01M  $\text{NH}_3$  buffer (pH = 9); (II) 0.2 M NaOAc buffer (pH = 4.8); (III) 0.1 M HCl (IV); 1 mM  $\text{K}_3\text{Fe}(\text{CN})_6$ ; and (V)  $4 \times 10^{-3}$ M  $\text{LiClO}_4$  solution.

Moreover, the SPCE was compared with SPCE/BiF in ammonium and SPCE/BiF in ammonium buffer with 0.01 M DMG solution using AdDPSV. When the SPCE/BiF was immersed in buffer solution with the DMG complex agent, the signal was more enhanced. Furthermore, when comparing the signal from the SPCE/BiF electrode in ammonium buffer (pH = 9.2) solution with that of the SPCE/BiF in ammonium buffer (pH = 9.2) solution containing DMG, the results show the characteristics are different and a well-behaved reduction response at a peak potential of  $-0.35$  V (vs. Ag/AgCl) was obtained

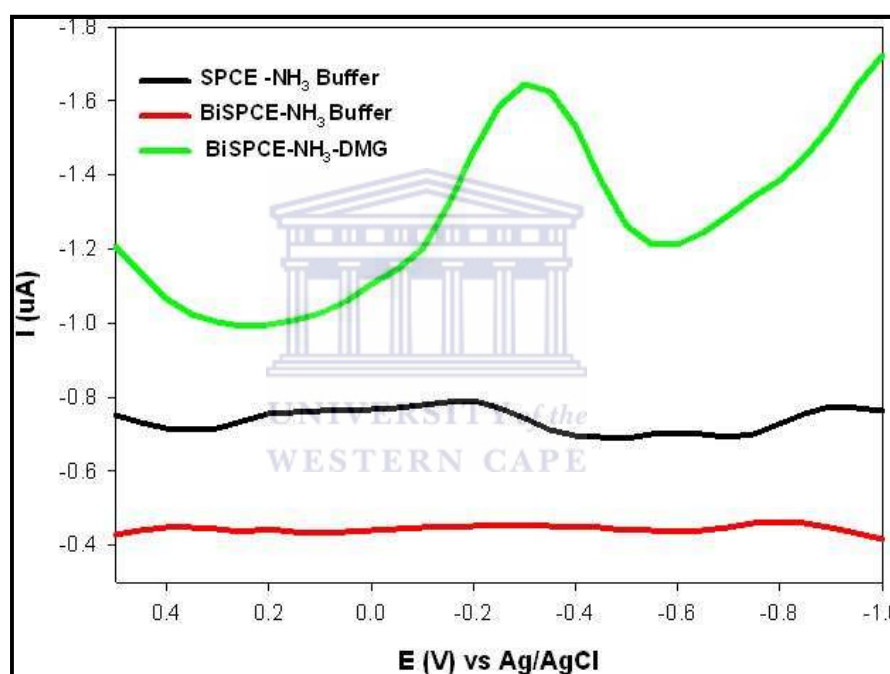


Figure 6.3 Comparative DPAdSVs of the various electrodes of: (I) SPCE; (II) SPCE/BiF and; (III) SPCE/BiF/DMG in  $\text{NH}_3$  buffer (pH = 9) solution.

### 6.3.2 Optimisation of complexing reagent concentration

The concentration of dimethylglyoxime (DMG) were varied using three different concentrations to establish the optimal analytical condition for the determination of PGMs (e.g. Pt, Pd & Rh), using bismuth modified SPCE. These DMG concentrations were chosen after consideration of the recent work done by Van der Horst (2012).



During the experimental phase the reagent concentration of DMG were varied between the three concentrations of  $1 \times 10^{-4}$  M,  $5 \times 10^{-5}$  M and  $1 \times 10^{-5}$  M. With the results obtained for this work, the best results were obtained when a DMG concentration of  $1 \times 10^{-5}$  M was used. The voltammetric results obtained are presented in Figure 6.4. The Pt(HDMG)<sub>2</sub> complex showed a maximum current response at a peak potential of -0.45 V (vs. Ag/AgCl) as shown in Figure 6.4 (B). One cathodic peak with a maximum current response was observed at -0.60 V (vs. Ag/AgCl) in the presence of Rh(HDMG)<sub>3</sub> complex (see Figure 6.4 (C)). The Pd(HDMG)<sub>2</sub> complex was reduced yielding a well-defined peaks at 0.40 V (Figure 44 (A)). The concentration of chelating complex can affect the electrochemical response of the complexes and these parameters were optimised as the results showed in Figure 6.4.

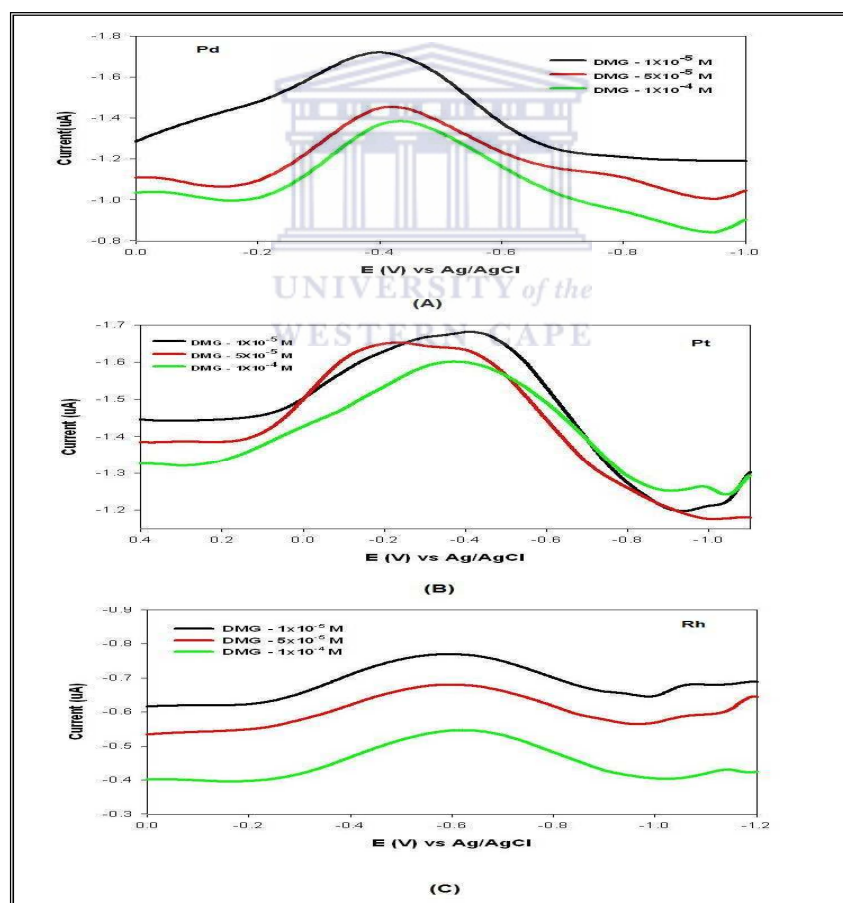


**Figure 6.4** Results obtained for the effects of various DMG concentration upon the response to 1 ppb of Pd(II) in (A), Pt(II) in (B) and Rh(III) in (C), collected in the presence of 0.01 M ammonium buffer (pH =9.2) solution.



Table 6.1 presents the current response of PGMs complexes (Pd(HDMG)<sub>2</sub>, Pt(HDMG)<sub>2</sub>, Rh (HDMG)<sub>3</sub> and the potentials in different concentrations of DMG.

**Table 2** Results obtained for the effects of various DMG concentration upon the response to 1 ppb of PGMs Pd(II) , Pt(II) and Rh(III), collected in the presence of 0.01 M ammonium buffer (pH =9.2) solution.

Metal complex	DMG Concentration (M)			Potential (V)
	$1 \times 10^{-5}$	$5 \times 10^{-5}$	$1 \times 10^{-4}$	
	Current ( $\mu\text{A}$ )			
Pd(HDMG) <sub>2</sub>	- 1.721	- 1.448	- 1.381	- 0.40
Pt(HDMG) <sub>2</sub>	- 1.675	- 1.633	- 1.588	- 0.45
Rh(HDMG) <sub>3</sub>	- 0.7693	- 0.6797	- 0.5451	- 0.60

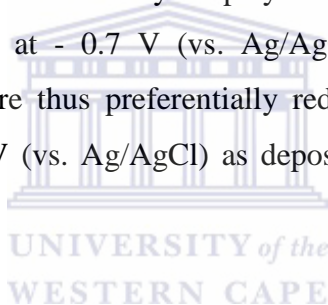
In summary, the results obtained for the optimisation of the DMG concentration have showed that among all the concentrations of DMG evaluated, the best results were obtained in  $1 \times 10^{-5}$  M. Certainly  $1 \times 10^{-5}$  M. concentration and was used in further work.

### 6.3.3 Deposition potential optimisation studies

As discussed by other authors (Gonzalez *et al.*, 2004), the deposition potential ( $E_d$ ) at which the metal ion is able to deposit on the electrode surface is critical. Thus, the effect of deposition potential was optimised in order to obtain maximum sensitivity and optimum results. The voltammetric analysis of Pd(II), Pt(II) and Rh(III) as dimethylglyoxime (DMG) complexes on the SPCE/BiF sensor was determined as a function of deposition potential ( $E_d$ ) in ammonium buffer (pH = 9.2) solution and plotted against the peak current ( $I_p$ ) values to make it easy to select the optimal deposition potential.

The deposition potential was varied in the + 0.3 to - 0.8V potential range but only negative deposition potential has been considered in this study (as determined by Van der Horst, (2011)) and the solution was stirred during the deposition time of 120 s. Figure 6.5 represent the results obtained for the optimisation of the deposition potential for all three PGMs investigated.

In Figure 6.5 (A), the results obtained for the Pd(II) peak current is displayed, indicating that the  $I_p$  values increased as the deposition potential became more negative. The results obtained for the Pt(II) peak current is shown in Figure 6.5 (B) For Pt(II) it was observed that the peak current decreased over most of the potentials investigated and increased minimally only at - 0.7 V (vs. Ag/AgCl), before it started decreasing again. The results for Rh(III) in displayed in Figure 61 (C). The peak current for Rh(III) remained a maximum and the deposition potential only displayed a minimum value at 0.0 V (vs. Ag/AgCl), and slightly increase at - 0.7 V (vs. Ag/AgCl) Pd(II), Pt(II) and Rh(II) are positively charged ions which are thus preferentially reduced at more negative potential, Hence, for all the metals - 0.7 V (vs. Ag/AgCl) as deposition potential was applied in all subsequent experiments.



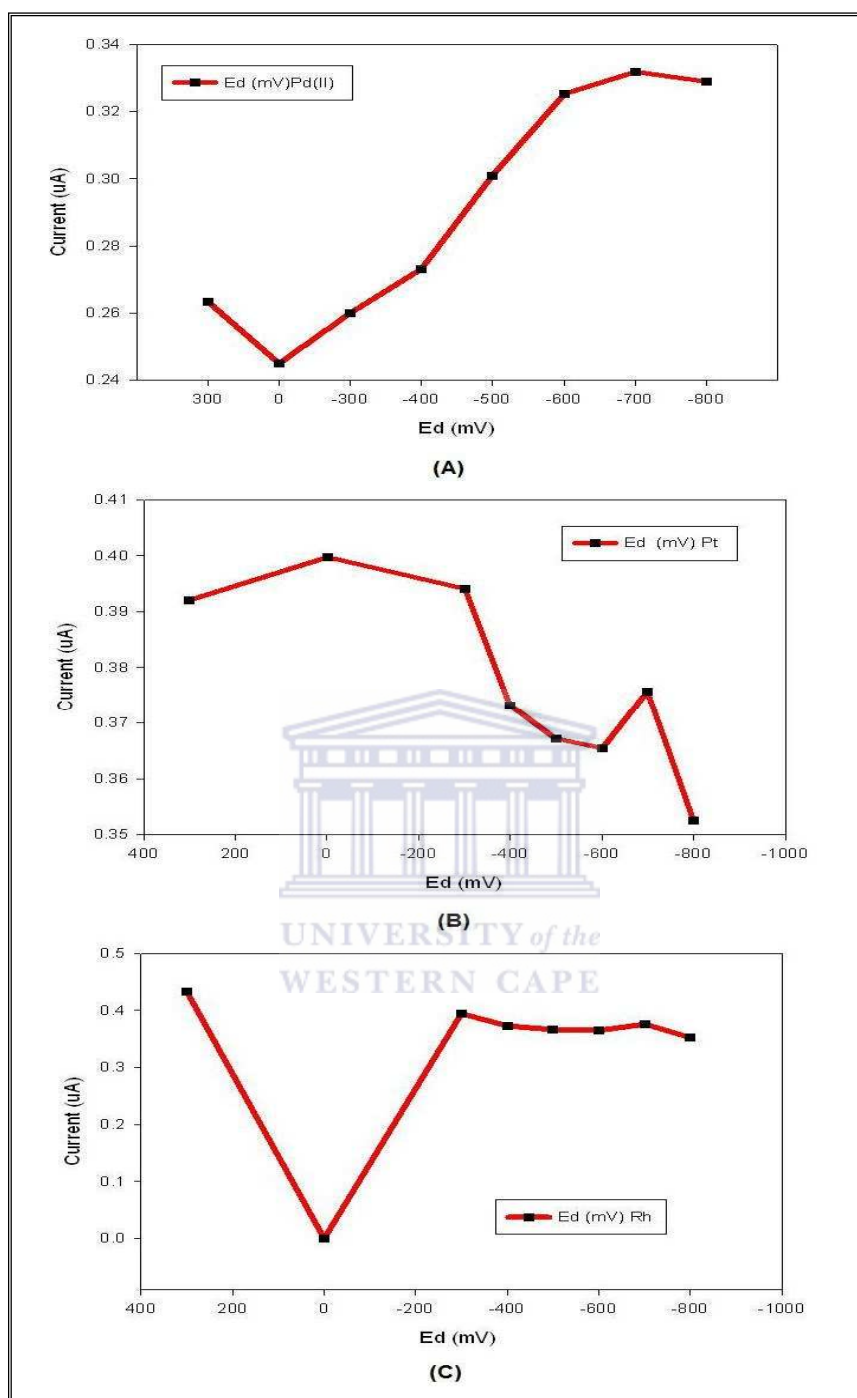


**Figure 6.5** Results obtained for effects of deposition potential ( $Ed$ ) upon the peak current responses to  $1 \mu\text{g. L}^{-1}$  of Pd(II) in (A), Pt(II) in (B) and Rh(II) in (C), evaluated in the presence of 0.01 M ammonium buffer (pH = 9.2) solution.

After analysis of the results shown in Figure 6.5, it was decided that a deposition potential of -0.7 V (vs. Ag/AgCl) was used as an optimum value through the rest of the experiment.

#### 6.3.4 Deposition time optimisation studies

Deposition time ( $t_d$ ) is another important stripping voltammetric parameter, which should be precisely controlled during the stripping experiment. The effect of the deposition time on the cathodic stripping peak of platinum group metals (PGMs = Pd, Pt and Rh) was studied in ammonia buffer (pH = 9.2) solution, containing 1 ppb of the selected PGMs in the time range from 0 – 300 s. The results obtained are illustrated in Figure 6.6 showing that the current intensity increased slowly to reach a maximum value between 150 and 180 s for all three PGMs. After 180 s of deposition, a sharp increase was observed for all the selected metals as seen in Figure 6.6. For both Pd(II) and Pt(II) the increase was linear after 180 s to 300 s, whereas there was a sharp fall at 240 s for Rh(III), followed by another increase.

In summary, it was decided in order to prevent a long deposition time of 300 s as the increasing peak current values suggest in Figure 6.6, to rather use a deposition time of 150 s as the optimum value. For all stripping experiments, I have chosen the optimum values of -0.7 V (vs. Ag/AgCl) for deposition potential and 150 s as the deposition time to proceed with in the experiments.

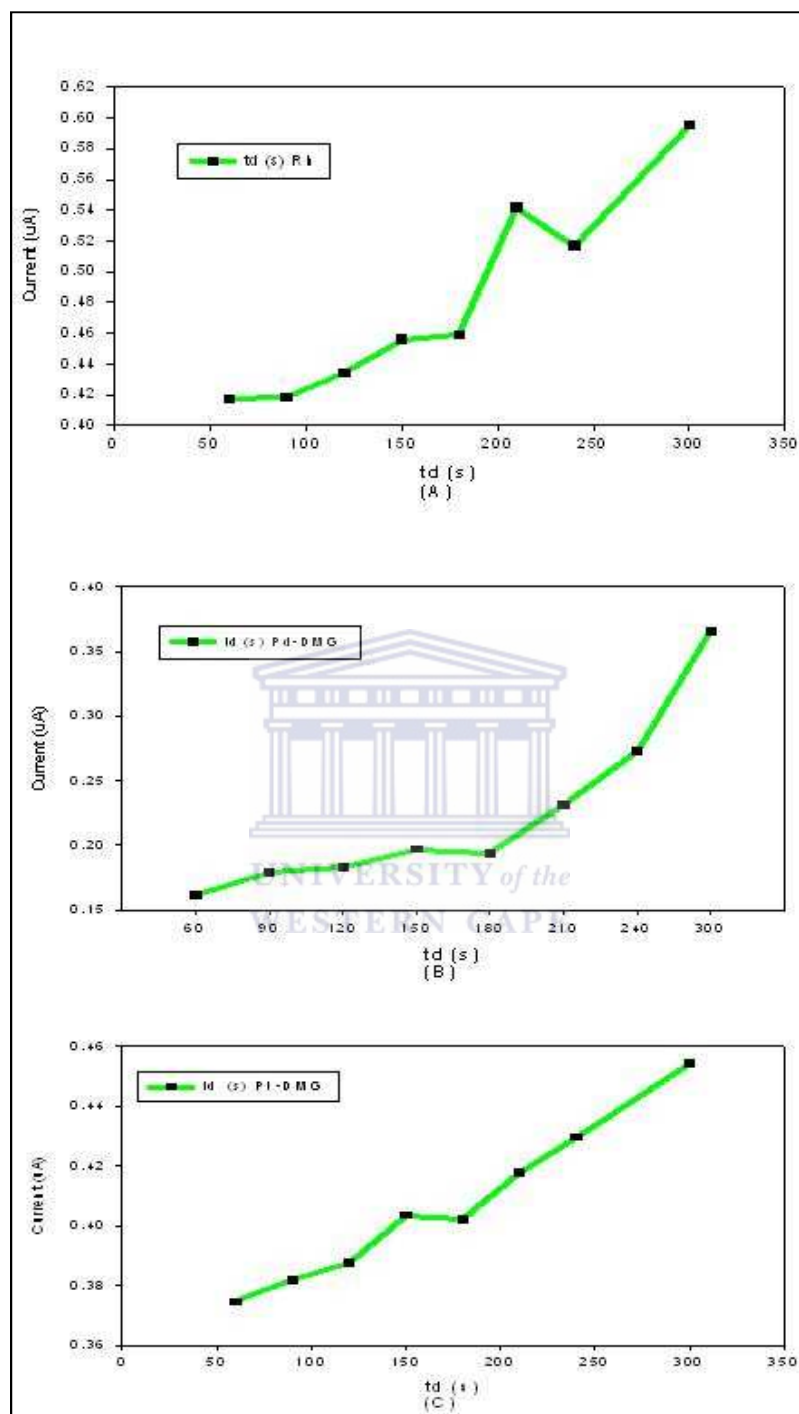


Figure 6.6 Effects of deposition time ( $t_d$ ) upon the response to  $1 \mu\text{g} \cdot \text{L}^{-1}$  (A) Rh(III), (B) Pd (II) and (C) Pt(II) in the presence of 0.01M ammonia buffer (pH = 9.2) solution.

### 6.3.5 Stability testing of the SPCE/BiF electrode

The operational stability of a bismuth-modified screen-printed carbon electrode was investigated in 0.01 M ammonia buffer (pH = 9.2) solution, containing various concentrations of the PGM-(HDMG)<sub>x</sub> complexes and using cathodic adsorptive stripping voltammetry in the potential range from + 0.8 to - 1.4 V at a scan rate of 50 mVs<sup>-1</sup>. The SPCE/BiF electrode was stored in ammonium buffer (pH = 9.2) solution at 4° C. The peak current results obtained for the selected PGMs was plotted against time for each of the DMG concentration investigated, as shown in Figure 6.3. The prepared sensors were stored for up to 28 hours when the results reported in this section were collected. The results obtained for the evaluation of the Pd(HDMG)<sub>2</sub> complex as shown in Figure 6.7 (A), indicate that for the [DMG] = 1 × 10<sup>-5</sup> M, it was observed that the peak current results was the lowest over the time period investigated. For the [DMG] = 5 × 10<sup>-5</sup> M and 1 × 10<sup>-4</sup> M, the results have shown close similarities in the peak current for the entire duration of the experiment, with the only difference obtained at the end of the experiment.

The results for the Pt(HDMG)<sub>2</sub> complex shown in Figure 6.7 (B) indicate that for the [DMG] = 1 × 10<sup>-5</sup> M, it was observed that the peak current results was the highest with the lowest current obtained over the time period of 15 hours. For the [DMG] = 5 × 10<sup>-5</sup> M and 1 × 10<sup>-4</sup> M, the results have shown close similarities in the peak current for the entire duration of the experiment, with the only little difference obtained in at the end of the experiment.

In the case of the Rh(HDMG)<sub>3</sub> complex, the results in Figure 6.7 (C) indicated that indicate that for all DMG concentration, the results have shown close similarities in the peak current for the entire duration of the experiment especially for [DMG] = 5 × 10<sup>-5</sup> M and 1 × 10<sup>-4</sup> M. For the [DMG] = 1 × 10<sup>-5</sup> M stability was observed between 7 and 28 hours and between 14 and 28 hours a higher signal was observed while we observed the stability between 14 and 28 hours for [DMG] = 5 × 10<sup>-5</sup> M and 1 × 10<sup>-4</sup> M., with the a slightly current enhancement obtained at the end of the experiment for [DMG] = 5 × 10<sup>-5</sup> M.

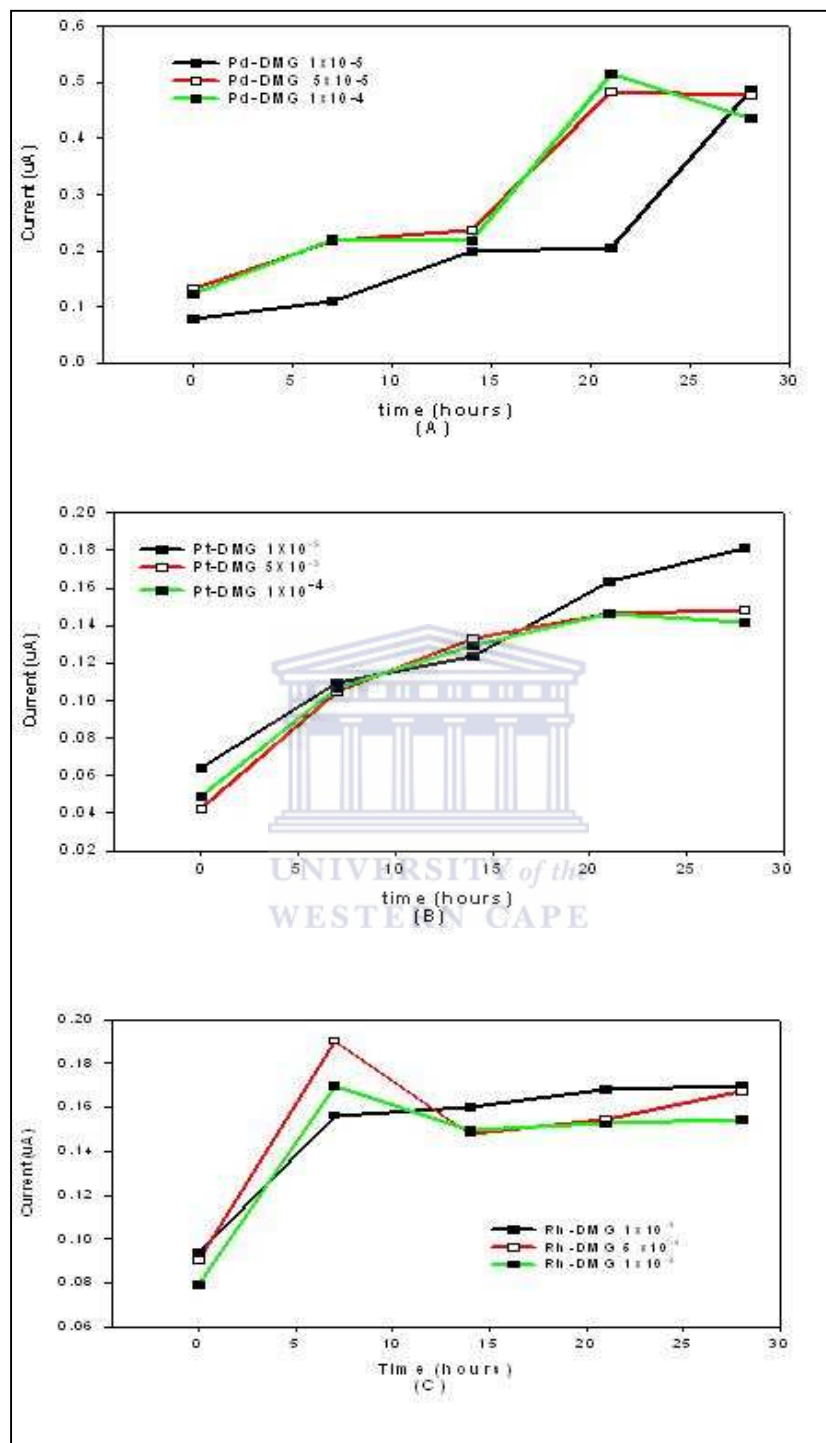


Figure 6.7 Results obtained Stability test of the BiSPCE in 0.01 M ammonium buffer of pH 9.2 containing  $1 \mu\text{g} \cdot \text{L}^{-1}$  of selected PGMs with various DMG concentration  $E_d = -0.7\text{V}$ , (vs Ag/AgCl) and  $t_d = 120 \text{ s}$ .



In summary, after evaluation of the results for each of the PGM-(HDMG)<sub>x</sub> complexes [DMG] = 5 × 10<sup>-5</sup> M and 1 × 10<sup>-4</sup> M has shown similar behaviour throughout of the experiment. [DMG] = 1 × 10<sup>-5</sup> M, in Figure 6.7 (C) has shown stability over a period of 7 to 28 hours.

### 6.3.6 Analytical features of the adsorptive stripping procedure

The sensitivity of the SPCE/BiF sensor was tested using various standard solutions of the selected PGMs and a [DMG] = 1 × 10<sup>-5</sup> M. The calibration curve for each PGM determination was established by applying the developed stripping voltammetric procedure as outlined in Table 16.

**Table 6.2** Summary of the optimal conditions for PGMs determination with the SPCE/BiF sensor platform and DMG as complexing agent.

Step	Condition / Analysis		
	Pd(II)	Pt(II)	Rh(III)
<i>Reduction step</i>			
pH	9.2	9.2	9.2
Reduction potential	- 700 mV	- 700 mV	- 700 mV
Reduction time	150 s	150 s	150 s
Complexing agent	Dimethylglyoxime (DMG)		
Supporting electrolyte	0.01 M ammonia buffer solution		
<i>Measurement step</i>			
Supporting electrolyte	0.01 M ammonia buffer solution		
Measurement technique	Adsorptive differential pulse voltammetry		
Potential window	Sweep potential from + 0.8 to - 1.4 V		

Table 6.2 provides a summary of the optimal conditions for the adsorptive differential pulse stripping voltammetric (AdDPSV) evaluation of Pd(II), Pt(II) and Rh(III). These parameters were applied in the next stage of the investigation for the analysis of the PGMs.

The results obtained showed that a deposition time of 150 s and deposition potential of -0.7 V (vs. Ag/AgCl) gave well defined peaks for the SPCE/BiF electrode and PGM-(HDMG)<sub>x</sub> complexes. Calibration curves were obtained from the results obtained from standard addition of PGMs and the corresponding equation for this dependence is shown on each graph. The results obtained for the peak current of the Pd(HDMG)<sub>2</sub> complex with increasing concentration is shown in Figure 6.8. The voltammograms shown in Figure 64 (A) has a stripping potential at approximately -0.7 V (vs. Ag/AgCl), which shifted in the more positive potential direction as the concentration increased. The peak potential is also absent in the results obtained for the blank, while after a potential of -1.0 V (vs. Ag/AgCl) the peaks obtained for hydrogen generation is observed. A good linear increase in the peak current was observed that is reflected in the calibration curve shown in Figure 6.8 (B).

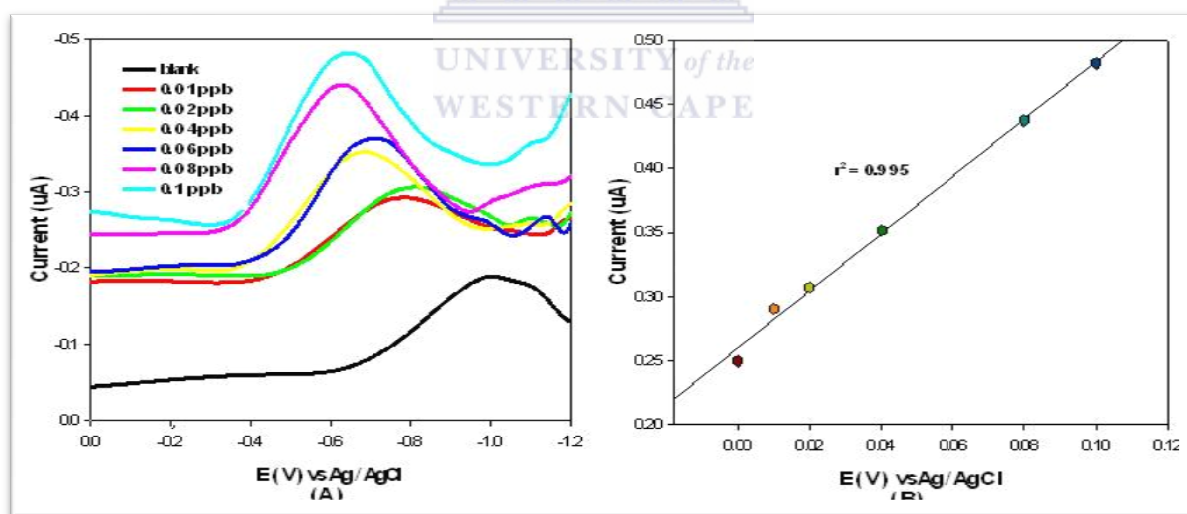
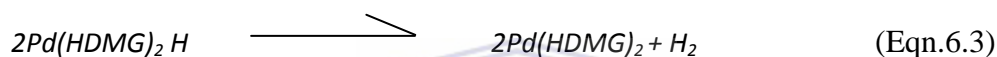
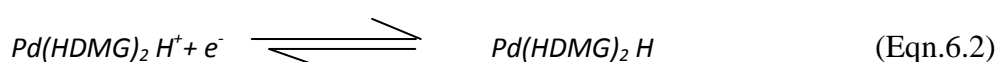
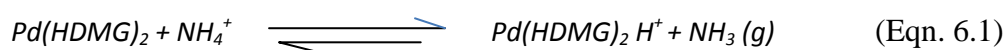
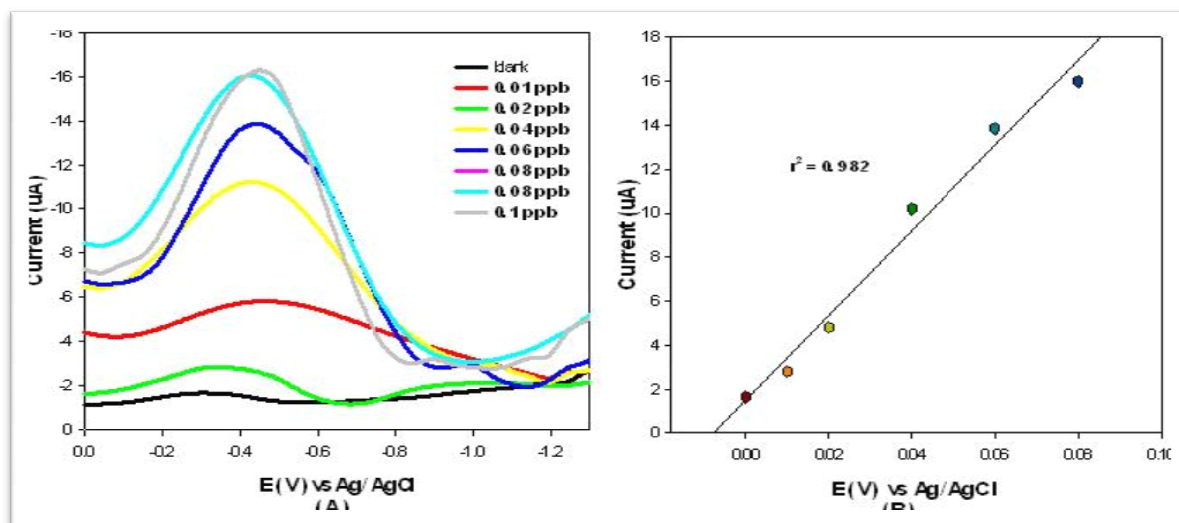


Figure 6.8 Results obtained for the AdDPVs for the increasing concentrations of Pd(HDMG)<sub>2</sub> (0.01 – 0.1  $\mu\text{g. L}^{-1}$ ) evaluated using the SPCE/BiF sensor, with  $E_d = -0.7$  V and  $t_d = 150$ s. In (B) the calibration curve is shown.

The evolution of hydrogen gas ( $H_2$  (g)) was observed during each of the PGMs investigated. This observation is in accordance with recent studies that have shown that the use of ammonia buffer solution (pH = 9) can be attributed to  $H_2$  (g) formation (Cordon *et al.*, 2002; Hutton *et al.*, 2003). When ammonia buffer solution is used, a catalytic hydrogen wave is also absorbed, which can be explained by the following reactions taking place:



The gas formation deliver a characteristic peak at approximately  $-1.4$  V (vs. Ag/AgCl), which are not shown in the AdDPSVs. Figure 6.9 displays the results obtained for the  $Pt(HDMG)_2$  complex with increasing concentration. The voltammograms shown in Figure 6.9 (A) has a stripping potential at approximately  $-0.7$  V (vs. Ag/AgCl), with increase in peak current as the concentration increased.



**Figure 6.9** Results obtained for the AdDPVs for the increasing concentrations of  $\text{Pt}(\text{HDMG})_2$  (0.01 – 0.1  $\mu\text{g. L}^{-1}$ ) evaluated using the SPCE/BiF sensor, with  $E_d = -0.7$  V and  $t_d = 150$  s. In (B) the calibration curve is shown.

In this voltammogram the hydrogen evolution peak is absent in the results obtained for the blank compared to  $\text{Pd}(\text{HDMG})_2$  complex. A good linear increase in the peak current was observed that is reflected in the calibration curve shown in Figure 6.5 (B).

Figure 6.10 displays the results obtained for the  $\text{Rh}(\text{HDMG})_3$  complex with increasing in peak current as concentration increases. The voltammograms shown in Figure 6.10 (A) has a stripping potential at approximately  $-0.85$  V (vs. Ag/AgCl). A good linear increase in the peak current was observed that is reflected in the calibration curve shown in Figure 6.10 (B).

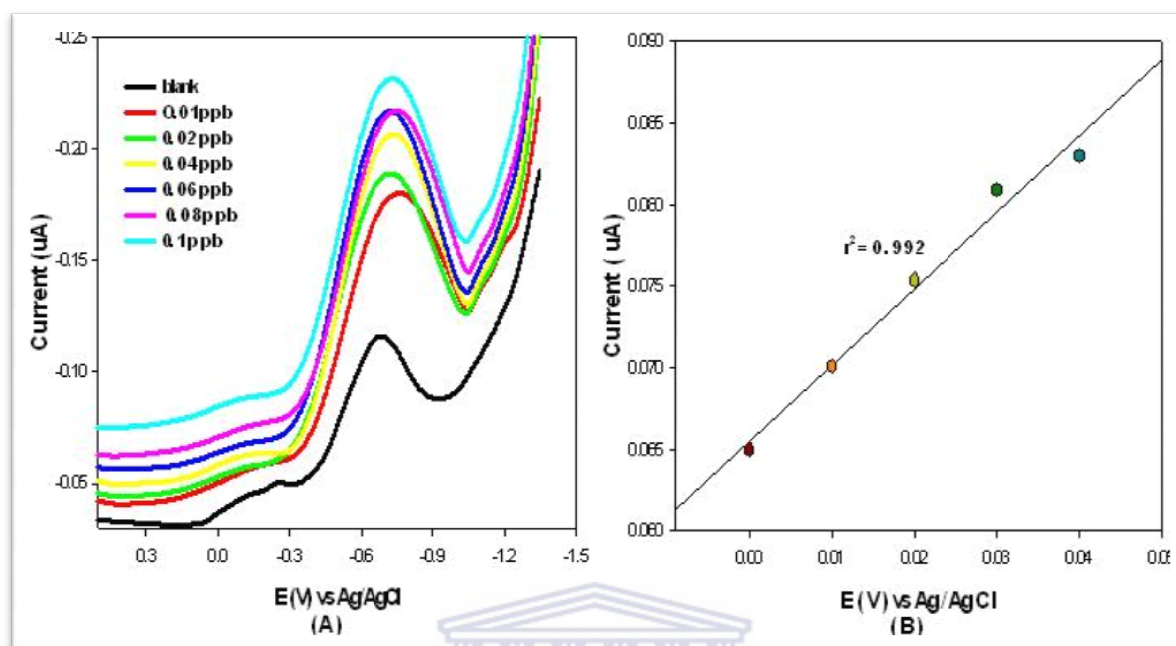
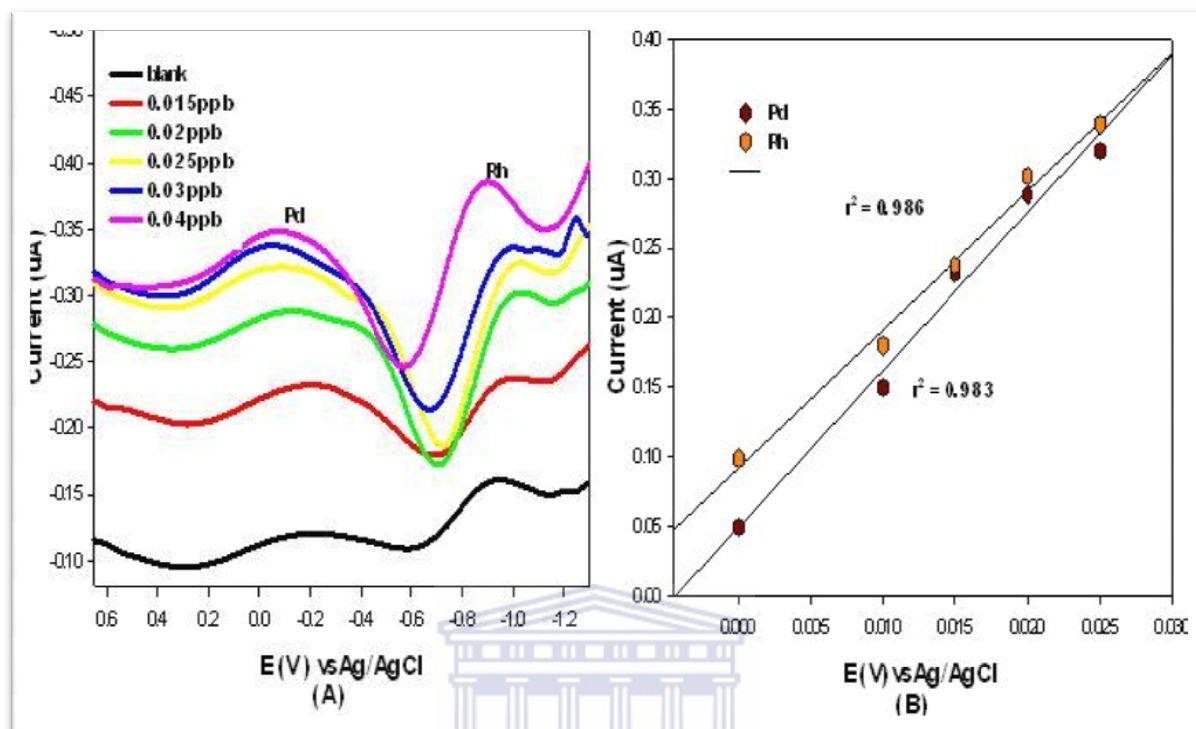


Figure 6.10 Results obtained for the AdDPVs for the increasing concentrations of Rh(HDMG)<sub>3</sub> (0.01 – 0.1  $\mu\text{g. L}^{-1}$ ) evaluated using the SPCE/BiF sensor, with  $E_d = -0.7$  V and  $t_d = 150$ s. In (B) the calibration curve is shown.

Figure 6.11 displays the results obtained for the simultaneous determination of Pd(HDMG)<sub>2</sub> and Rh(HDMG)<sub>3</sub> complexes. This simultaneous determination of these two noble elements was done successfully, although we have noticed a broad peak for Pd(II) around  $-0.1$  V (vs. Ag/AgCl) and  $-0.95$  V (vs. Ag/AgCl) for Rh(III). The broad peak might be due to interferences in the solution. The stripping peaks obtained are almost the same height displayed an increase in concentrations as the current.



**Figure 6.11** Adsorptive differential pulse cathodic stripping voltammetry for the simultaneous determination of Pd-Rh-(HDMG)<sub>x</sub> complexes ( $0.01 - 0.1 \mu\text{g. L}^{-1}$ ) using a SPCE/BiF sensor,  $E_d = -0.7 \text{ V}$  and  $t_d = 150\text{s}$ . In (B) the linear regression curve is shown.

A good linear increase in the peak current was observed that is reflected in the calibration curve shown in Figure 6.11 (B).

Figure 6.12 displays the results obtained for the simultaneous determination of Pt(HDMG)<sub>2</sub> and Rh(HDMG)<sub>3</sub> complexes. The simultaneous determination of Rh(III) and Pt(II) is possible but the current for Rh(III) peak is smaller than that of Pt(II) for the same concentration. This simultaneous determination of this two noble elements was done successfully and Pd(II) stripping peak has been observed at  $-0.25 \text{ V}$  (vs. Ag/AgCl) followed by the stripping peaks obtained at potential  $-0.7 \text{ V}$  (vs. Ag/AgCl) for Rh(III).

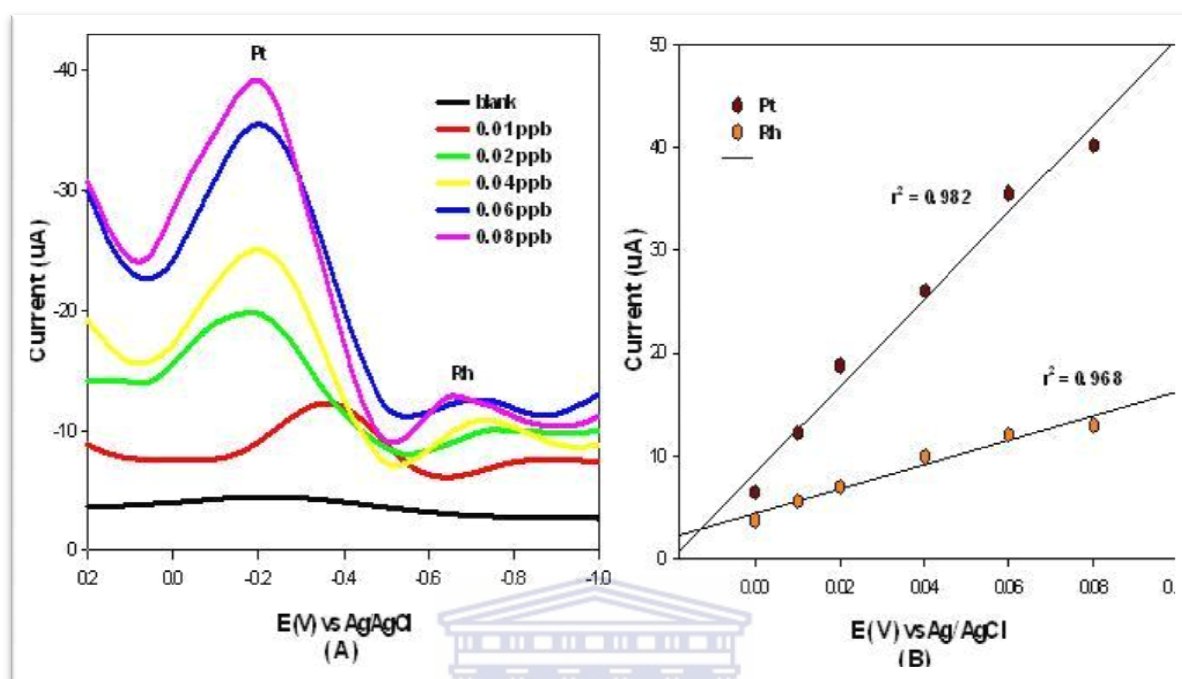


Figure 6.12 Adsorptive differential pulse cathodic stripping voltammetry for the simultaneous determination of Pt-Rh-(HDMG)<sub>x</sub> complexes (0.01 – 0.1  $\mu\text{g. L}^{-1}$ ) using a SPCE/BiF sensor,  $E_d = -0.7$  V and  $t_d = 150$  s. In (B) the linear regression curve is shown.

A good linear increase in the peak current was observed that is reflected in the calibration curve shown in Figure 6.12 (B).

In Table 17 the results obtained from the calibration plots for the PGM-(HDMG)<sub>x</sub> complexes analysed with the SPCE/BiF sensor is displayed. The stripping voltammograms were obtained with the experimental conditions outlined in Table 16.



**Table 6.3** Calibration data for the determination of PGMs in the presence of [DMG] =  $1 \times 10^{-5}$  M as chelating agent, using the SPCE/BiF sensor and a supporting electrolyte of ammonia buffer (pH = 9.2) solution.

PGM	Regression	R <sup>2</sup>
Pd	$y = 2.234x + 0.259$	0.995
Pt	$y = 193.3x + 1.456$	0.982
Rh	$y = 0.49x + 0.064$	0.977
Pd – Rh	$y = 10.05x + 0.088$ (Pd)	0.983 (Pd)
Pd – Rh	$y = 11.43x + 0.045$ (Rh)	0.986 (Rh)
Pt – Rh	$y = 423.9x + 8.364$ (Pt)	0.982 (Pt)
Pt – Rh	$y = 118.1x + 4.391$ (Rh)	0.968 (Rh)

From all the results for the AdDPSV studies, it was evident that all PGMs are reduced and adsorbed onto the SPCE/BiF sensor and gave cathodic peaks for the stripping voltammetric analysis. In both case (single and simultaneous determination), the slope of the linear regression equation of the calibration plot was the highest for platinum, a factor which is favourable for the use in potentiometric determination. Even though the plot of the calibration for Pd was relatively linear compared to other metals, the slope was lower than that for platinum. Due to these properties, an adsorptive cathodic stripping voltammetric technique was developed to obtain more sensitive method for the determination of trace levels of PGMs. Standard additions of each PGM analysed showed that the peak current increases with increasing concentrations. The results of the calibration plots are proof of this and the summary of the corresponding regression equations for this dependence are given in Table 6.3.

### 6.3.7 Interference studies

The effect of interferences between metals is potentially important because the metals compete for complexation with the same ligands and for adsorption on electrode. It is, therefore, necessary to check if the standard addition of one of the metals affects the peak height and therefore the sensitivity of the others. In this work, interferences were investigated under the optimum conditions described and they were considered to be common cations and anions present in PGM side-stream solutions or effluent.

Specifically Fe(II), Ni(II), Co(II), sodium ( $\text{Na}^+$ ), sulphate ( $\text{SO}_4^{2-}$ ) and phosphate ( $\text{PO}_4^{3-}$ ) ions were investigated. The interfering effect of these cations and anions on the determination of PGMs with the SPCE/BiF sensor was studied by addition the interfering ions in standard solutions containing the supporting electrolyte solution plus 1 ppb of interfering ions and the PGM-(HDMG)<sub>x</sub> complex solutions (in the concentration range of 0.3, 0.6, and 0.9 ppb). Figure 6.13 illustrate the behaviour of the SPCE/BiF sensor in the presence of sodium and iron cations. The peaks of PGMs were monitored and compared to those without any impurities added.

The detection of the Pd(HDMG)<sub>2</sub> complex with the SPCE/BiF sensor has been seriously affected by the addition of sodium and iron ions to the standard solution, as shown in Figure 6.13. The presence of the interfering ions caused broadening and diminishing of the stripping peaks for the Pd(HDMG)<sub>2</sub> complex as observed in Figure 6.13 (A). As a result, a poorly defined peak at a stripping potential of approximately  $-0.3$  V (vs. Ag/AgCl) has been obtained. An adjacent shoulder peak at a stripping potential of approximately  $-0.6$  V (vs. Ag/AgCl) is also visible in the voltammograms for concentrations of 0.3 and 0.9 ppb of Pd(II). The presence of this peak may be attributed to  $\text{Fe}^{3+}$  ions present in the solution.

In the case of the Pt(HDMG)<sub>2</sub> complex, the results displayed in Figure 6.13 (B) has shown that the sodium and iron ions did not actually interfere with the complex as we seen well-defined stripping peaks at potential of approximately  $-0.4$  V (vs. Ag/AgCl). The presence of the interfering ions only have an impact on the stripping peaks height for the Pt(HDMG)<sub>2</sub> complex as observed in Figure 6.13 (B). An additional peak around  $-0.9$  V (vs. Ag/AgCl) at a low concentration of Pt(II) of 0.3 ppb, also be attributed to the presence of  $\text{Fe}^{3+}$  in the solution as observed for Pd(II) in Figure 6.13 (A).

The Rh(HDMG)<sub>3</sub> complex was not affected by the addition of sodium and iron interfering ions, as the well-defined stripping peaks shown in Figure 6.13 (C). The stripping peaks were obtained at a stripping potential of approximately  $-0.9$  V (vs. Ag/AgCl), and a slight shift in potential to a less negative value for higher concentrations.

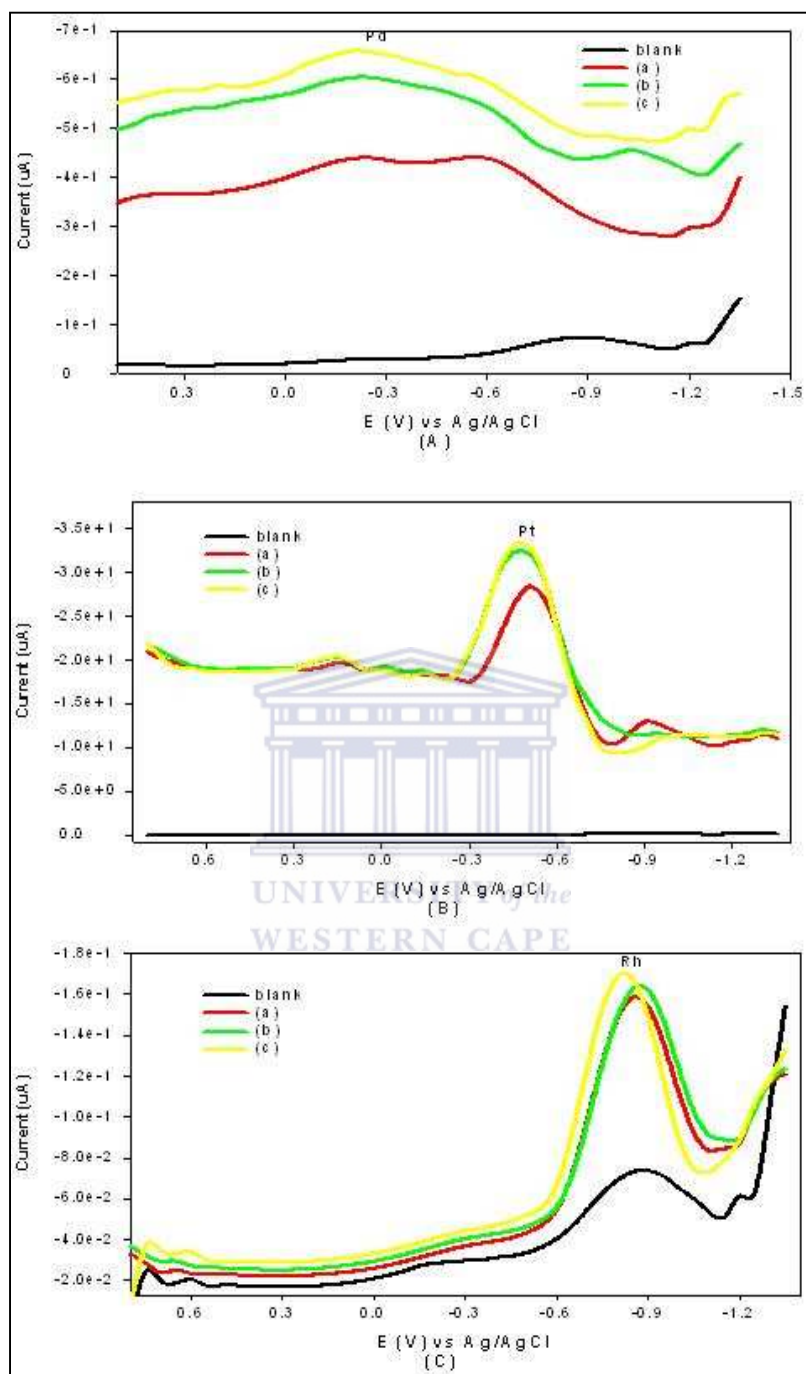


**Figure 6.13** AddPSVs obtained for the effect of  $\text{Na}^+$  and  $\text{Fe}^{3+}$  as interfering ions on the stripping voltammetric results for Pd(II) in (A), Pt(II) in (B), and Rh(III) in (C) using the SPCE/BiF sensor. The concentrations of Pd(II), Pt(II) and Rh(III) used were  $0.3 \mu\text{g} \cdot \text{L}^{-1}$  in (a),  $0.6 \mu\text{g} \cdot \text{L}^{-1}$  in (b) and  $0.9 \mu\text{g} \cdot \text{L}^{-1}$  in (c) respectively, with  $0.01 \text{ M}$  ammonia buffer ( $\text{pH} = 9.2$ ) solution containing  $1 \times 10^{-5} \text{ DMG}$  solution.

Interferences arising from oxygen containing inorganic ions, phosphate and sulphate ( $\text{PO}_4^{3-}$  and  $\text{SO}_4^{2-}$ ) that are expected to co-exist in PGM sidestream solutions, were also evaluated. The AdDPSVs for the PGM-DMG complexes are shown in Figure 6.14.

In Figure 6.14 (A) the results obtained for the  $\text{Pd}(\text{HDMG})_2$  complex in the presence of phosphate and sulphate interfering ions are shown. The AdDPVs shows that for the lower concentration of Pd(II), broad stripping peaks at approximately - 0.40 V (vs. Ag/AgCl) were obtained, which are well defined at higher concentration and shifted to more negative potential. These broad peaks are indicating that phosphate and sulphate ions interfere with the measurement of Pd at higher concentrations. Another observation when this high concentration (0.9 ppb) of Pd(II) was analysed, two smaller shoulder peaks at approximately - 0.45 V (vs. Ag/AgCl) and - 0.95 V (vs. Ag/AgCl) were observed.

In Figure 6.14 (B) the results obtained for the  $\text{Pt}(\text{HDMG})_2$  complex in the presence of phosphate and sulphate interfering ions are shown. Analysis of the AdDPSVs has shown that a single stripping peak at approximately + 0.1 V (vs. Ag/AgCl) for all the three concentrations of Pt, which followed by Pt peak at approximately - 0.50 V (vs. Ag/AgCl). In these voltammograms we have seen an increase in current.

Figure 6.14 (C) displays the results obtained for the  $\text{Rh}(\text{HDMG})_3$  complex in the presence of phosphate and sulphate interfering ions. Analysis of the results has shown that the AdDPVs for the lower concentration of Rh(III), a stripping peak at approximately - 0.80 V (vs. Ag/AgCl) was obtained, which shifted to more negative potential at higher concentrations of Rh (III). This peak was found at approximately - 0.95 V (vs. Ag/AgCl).

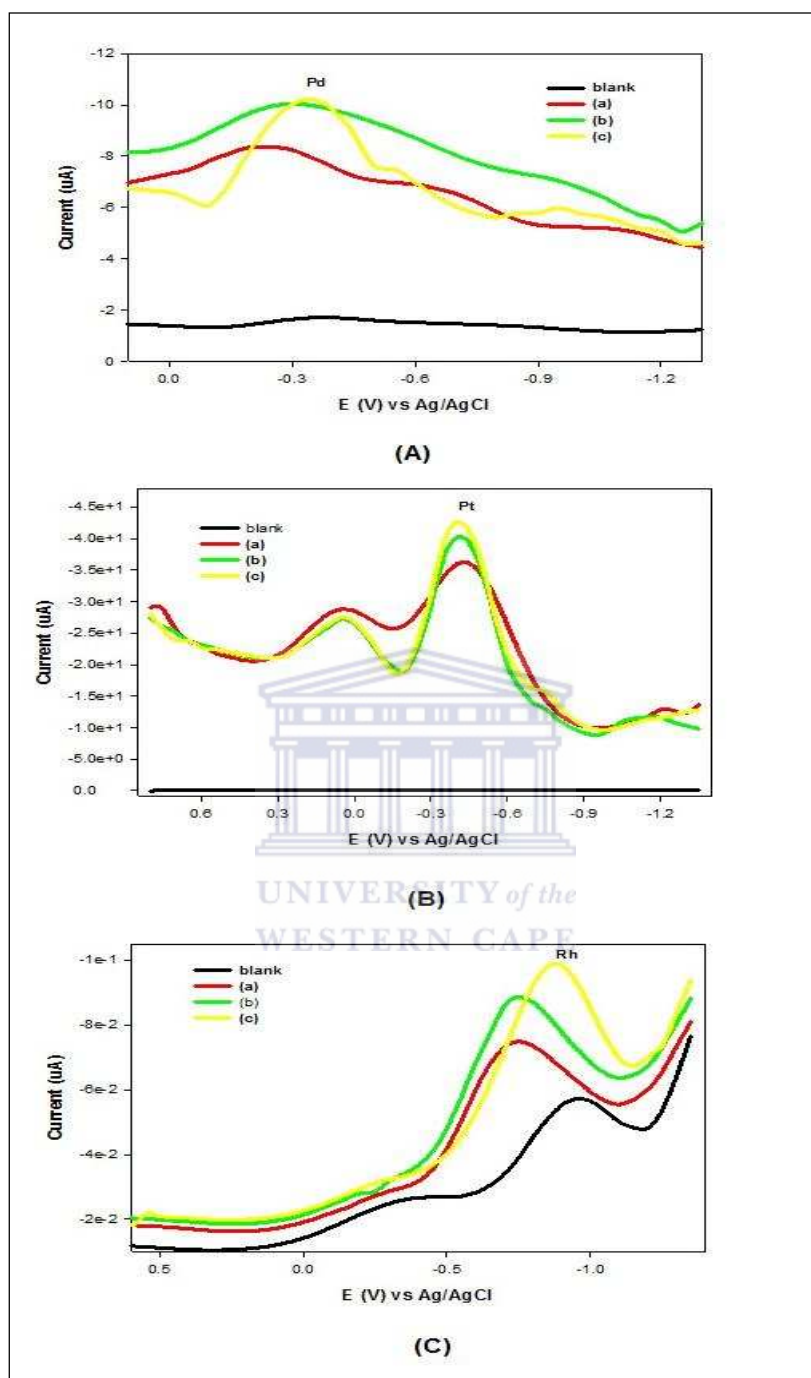


Figure 6.14 AddPSVs obtained for the effect of  $\text{PO}_4^{3-}$  and  $\text{SO}_4^{2-}$  as interfering ions on the stripping voltammetric results for Pd(II) in (A), Pt(II) in (B), and Rh(III) in (C) using the SPCE/BiF sensor. The concentrations of Pd(II), Pt(II) and Rh(III) used were  $0.3 \mu\text{g. L}^{-1}$  in (a),  $0.6 \mu\text{g. L}^{-1}$  (b) and  $0.9 \mu\text{g. L}^{-1}$  in (c) respectively, with 0.01 M ammonia buffer (pH = 9.2) solution containing  $1 \times 10^{-5}$  DMG solution.

The presence of cobalt and nickel ( $\text{Co}^{2+}$  and  $\text{Ni}^{2+}$ ) as interfering ions was next investigated in the voltammetric determination of all studied PGMs. The results obtained are displayed in Figure 6.15.

In Figure 6.15 (A) the results obtained for the  $\text{Pd}(\text{HDMG})_2$  complex in the presence of cobalt and nickel ( $\text{Co}^{2+}$  and  $\text{Ni}^{2+}$ ) as interfering ions are shown. Analysis of the AdDPSVs has shown that this metal has not been affected by the presence of these interfering ions as we seen the extra peaks are in the vicinity of - 0.6 and - 1.2V (vs. Ag/AgCl). We have also experienced a good signal compared to other interferences that have been diminished the signal of the stripping peaks.

In Figure 6.15 (B) the results obtained for the  $\text{Pt}(\text{HDMG})_2$  complex in the presence of cobalt and nickel as interfering ions are shown. Analysis of the AdDPSVs has shown that it was possible to determine Pt(II) in the presence of cobalt and nickel. None of them were found to affect the Pt(II) peaks when present in solution. As observed from the stripping peaks the signal has not been affected by these interfering ions.

Figure 6.15 (C) displays the results obtained for the  $\text{Rh}(\text{HDMG})_3$  complex in the presence of cobalt and nickel as interfering ions. Analysis of the AdDPSVs has shown that it was also possible to determine Rh(III) in the presence of cobalt and nickel although we have experienced a diminished in signal. This diminished in current must be the results of close proximity of the reduction potential of these metals. As shown in the voltammograms, one cathodic peak at - 0.3 V (vs. Ag/AgCl) was observed. Therefore it can be related with reduction of cobalt (II). These findings of the cobalt peak agreed with Mohadesil *et al* (2011). The stripping peak followed at potential - 0.95V (vs. Ag/AgCl) is proportional to Rh(III) concentrations in solution. We have noticed an extra peak at potential - 1.2V (vs. Ag/AgCl) and this peak is referred to Ni(II). These peaks affected the Rh(III) signal, probably due to the close proximity of the reduction potential of these metals.

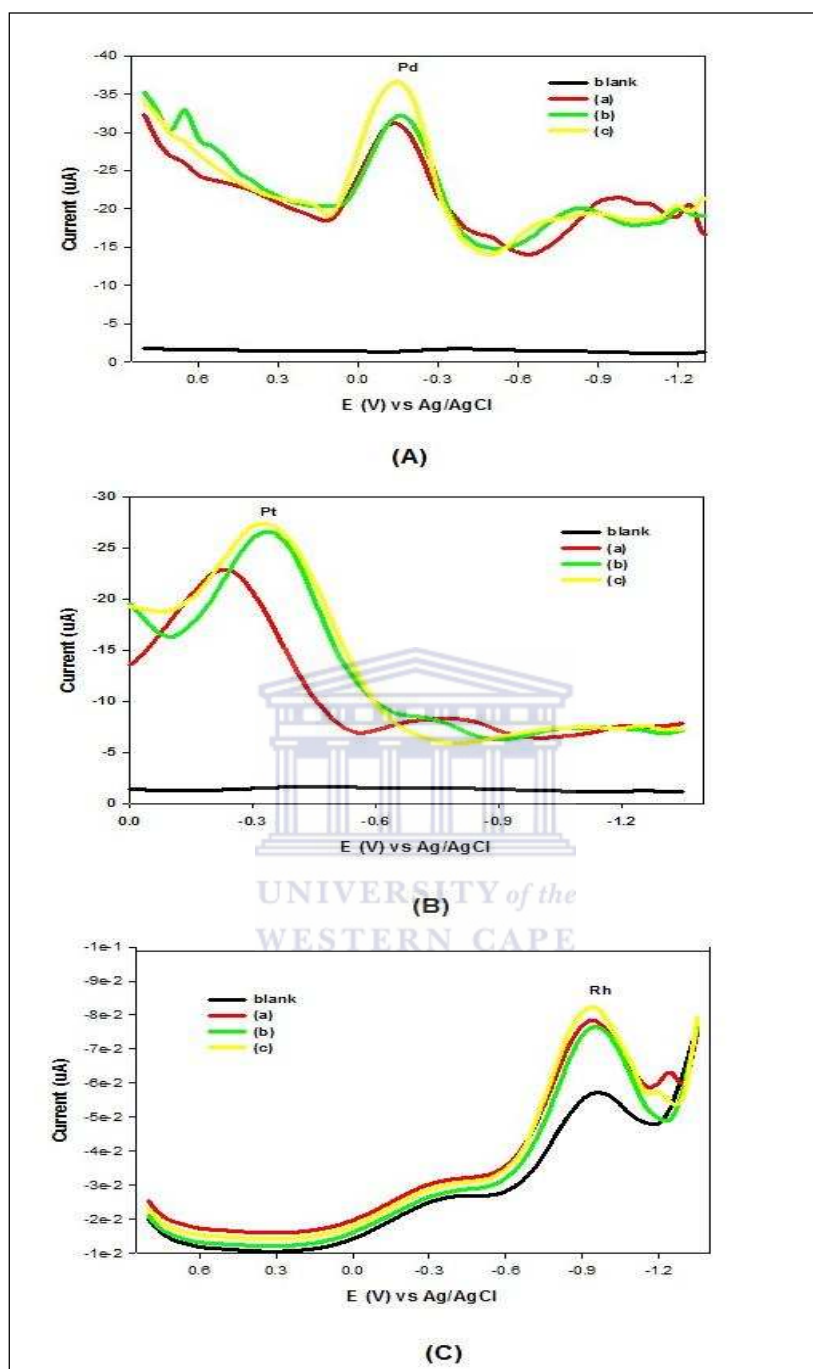


Figure 6.15 AdDPSVs obtained for the effect of  $\text{Co}^{2+}$  and  $\text{Ni}^{2+}$  as interfering ions on the stripping voltammetric results for Pd(II) in (A), Pt(II) in (B), and Rh(III) in (C) using the SPCE/BiF sensor. The concentrations of Pd(II), Pt(II) and Rh(III) used were  $0.3 \mu\text{g. L}^{-1}$  in (a),  $0.6 \mu\text{g. L}^{-1}$  in (b) and  $0.9 \mu\text{g. L}^{-1}$  in (c) respectively, with  $0.01 \text{ M}$  ammonia buffer ( $\text{pH} = 9.2$ ) solution containing  $1 \times 10^{-5}$  DMG solution.



In summary, the determination of interfering ions was made by forming the selected PGM-(HDMG)<sub>x</sub> complexes that are adsorbed on the BiF/SPCE. The results obtained for the effect of interfering ions on the stripping analysis of PGM-(HDMG)<sub>x</sub> complexes were monitored and compared to those without any interference. The difference between the PGM-(HDMG) complex peaks with interferences and without interferences indicate that the metal that has been affected showed slight variations in the magnitude of the signal responses.

#### **6.4. Analytical features of adsorptive stripping voltammetry at a SPCE/BiF sensor**

The behaviour of the selected PGMs was studied by adsorptive cathodic differential pulse stripping voltammetry between + 0.8 to - 1.4 V (vs. Ag/AgCl) in water and sediments samples collected in the Limpopo and North-West Provinces, South Africa. For each PGM investigated, the calibration curve was prepared by a series of standard addition of PGMs to a 0.01 M ammonia buffer (pH = 9.2) solution. Statistical parameters such as linearity range for concentrations evaluated, R<sup>2</sup> value (regression), limit of detection (LOD), limit of quantification (LOQ), accuracy and precision were also evaluated. The actual amount of PGMs found in the water samples were calculated using the obtained regression equation ( $y = mx + c$ ). The results obtained with the SPCE/BiF sensor were further compared to that obtained using ICP-OES analysis. The results obtained are discussed in the following paragraphs.

##### **6.4.1 PGMs analysis in freshwater samples**

Initially, the analysis of the real samples was performed in a 10 ml voltammetric cell vial containing 1 ml of water sample and 9 ml of ammonium buffer (pH = 9.2) solution, with  $1 \times 10^{-5}$  DMG and using the developed AdDPSV procedure. The amount of water sample was determined through the standard addition method using standard solutions containing appropriate concentrations of Pd(II), Pt(II) and Rh(III).

For the validation of this method for quantitative determination of the PGMs, calibration curves were obtained from the results obtained and the corresponding equations for this dependence are given below.

For Pd(II) analysis, the regression equation obtained is given below:

$$I_p (\mu A) = 0.342x + 0.204 \quad (R^2 = 0.993; n = 5; Pd(II)) \quad (\text{Eqn. 6.4})$$

Using the same approach, the calibration curve for Pt(II) analysis was obtained equation is as follows:

$$I_p (\mu A) = 2.542x + 0.120 \quad (R^2 = 0.986, n = 6; Pt(II)) \quad (\text{Eqn. 6.5})$$

The results for Rh(III) analysis is given by the following equation:

$$I_p (\mu A) = 28.96x + 0.051 \quad (R^2 = 0.983, n = 7; Rh(III)) \quad (\text{Eqn. 6.6})$$

In the next paragraph the results obtained for the analysis of freshwater samples collected from sampling sites closely situated to PGM mining activities, are discussed. The sampling sites were ER2 (on the ElandsRiver) and HX1, HX2 (on the HexRiver) in the vicinity of Rustenburg, North-WestProvince. The determination of PGMs in environmental samples was performed with an adapted procedure from Locatelli (2006).

**Table 6.4 Results for concentrations of PGMs in freshwater samples obtained using AdDPSV analysis with the SPCE/BiF and GCE/BiF sensors, compared with results from ICP-AES spectrophotometric analysis.**

Sample	SPCE/BiF			GCE/BiF			ICP-AES		
	Pd ( $\mu\text{g.L}^{-1}$ )	Pt ( $\mu\text{g.L}^{-1}$ )	Rh ( $\mu\text{g.L}^{-1}$ )	Pd ( $\mu\text{g.L}^{-1}$ )	Pt ( $\mu\text{g.L}^{-1}$ )	Rh ( $\mu\text{g.L}^{-1}$ )	Pd ( $\mu\text{g.L}^{-1}$ )	Pt ( $\mu\text{g.L}^{-1}$ )	Rh ( $\mu\text{g.L}^{-1}$ )
ER2	5.17± 0.41	0.71± 0.32	0.07± 0.38	0.44 ± 0.025	0.19 ± 0.014	0.29 ± 0.019	7.4 ± 0.32	8.5 ± 0.19	5.8 ± 0.23
HX1	3.73 ± 0.41	0.45 ± 0.11	0.04 ± 0.14	0.41 ± 0.031	0.08 ± 0.012	0.27 ± 0.035	7.2 ± 0.14	9.3 ± 0.17	6.7± 0.22
HX2	2.56 ± 0.18	0.41 ± 0.17	0.04 ± 0.19	0.43 ± 0.018	0.14 ± 0.011	0.37 ± 0.038	5.8 ± 0.28	20.08 ± 0.15	6.4 ± 0.18

Results in Table 6.4 have indicated that the SPCE/BiF sensor was more sensitive than the GCE/BiF sensor (Van der Horst, 2011) and ICP-AES spectrometer in the determination of the Pd(II), Pt(II) and Rh(III) concentrations in the freshwater samples. This was observed for all three samples of ER2, HX1 and HX2 analysed. Comparison of the AdDPSV results further indicates that the SPCE/BiF sensor was more sensitive than the GCE/BiF sensor in the PGMs determination. This was a promising result for future optimisation of a portable potentiostat and stripping analysis set-up for sample analysis and possible on-site applications.

#### 6.4.2 PGMs analysis in sediment samples

Next, the stripping voltammetric method optimised in this study was applied to the determination of PGMs in environmental sediments samples. There are only a few studies in which the determination of PGMs in soil and sediment samples has been conducted. The sequential extraction method for evaluating different fractions in sediments samples for its metal content have been applied in this study (Li *et al.*, 2010; Morera *et al.*, 2001). This was further done to determine in which fraction of the sediment extraction process, the highest yield of PGMs with minimum matrix effect, can be determined. For quantitative determination of the PGMs, calibration curves were obtained from the results obtained and the corresponding equations for this dependence are given below

For Pd(II) analysis, the regression equation obtained is given below:

$$I_p (\mu\text{A}) = 223.1 x + 0.587 \quad (R^2 = 0.976; n = 4; \text{Pd(II)}) \quad (\text{Eqn. 6.7})$$

Using the same approach, the calibration curve for Pt(II) analysis was obtained equation is as follows:

$$I_p (\mu\text{A}) = 287.6 x + 0.012 \quad (R^2 = 0.968, n = 6; \text{Pt(II)}) \quad (\text{Eqn. 6.8})$$

The results for Rh(III) analysis is given by the following equation:

$$I_p (\mu A) = 204 x + 0.794 \quad (R^2 = 0.9857, n = 6; \text{Rh(III)}) \quad (\text{Eqn. 6.9})$$

The results obtained are displayed in Table 19. The sampling sites were CR1 (on the Crocodile River) near Rustenburg, North-West Province, while sites ZX1 (on the Olifants River) and ZX2 (on the Motse River) were in the vicinity of Burgersfort, Limpopo Province.

**Table 6.5** Results for concentrations of PGMs in sediment fractions obtained using AdDPSV analysis with the SPCE/BiF and GCE/BiF sensors, compared with results from ICP-AES spectrophotometric analysis.

	SPCE/BiF			GCE/BiF <sup>#</sup>			ICP-AES		
	Carbonate-bound	Fe-Mn oxides bound	Organic bound	Carbonate-bound	Fe-Mn oxides bound	Organic bound	Carbonate-bound	Fe-Mn oxides bound	Organic bound
Sample	Pd (µg.L)	Pt (µg.L)	Rh (µg.L <sup>-1</sup> )	Pd (µg.L <sup>-1</sup> )	Pt (µg.L <sup>-1</sup> )	Rh (µg.L <sup>-1</sup> )	Pd (µg.L <sup>-1</sup> )	Pt (µg.L <sup>-1</sup> )	Rh (µg.L <sup>-1</sup> )
CR 1	0.04 ± 0.41	0.01 ± 0.67	0.07 ± 1.14	0.43 ± 0.007	0.14 ± 0.007	0.37 ± 0.015	4.12 ± 0.23	5.19 ± 0.49	6.37 ± 0.25
ZX1	0.02 ± 0.14	0.03 ± 0.60	0.01 ± 0.11	0.44 ± 0.011	0.19 ± 0.012	0.29 ± 0.016	4.47 ± 0.21	3.59 ± 0.28	4.57 ± 0.28
ZX2	0.03 ± 1.62	0.01 ± 0.005	0.05 ± 0.74	0.41 ± 0.016	0.08 ± 0.006	0.27 ± 0.010	11.08 ± 0.42	5.82 ± 0.35	3.29 ± 0.43

# Van der Horst (2011)

Analysis of the results in Table 6.5 again indicated that the SPCE/BiF sensor was more sensitive than the GCE/BiF sensor and ICP-AES spectrometer in the determination of the Pd(II), Pt(II) and Rh(III) concentrations in the sediment fractions. Similar to the freshwater results obtained, comparison of the AdDPSV results further indicates that the SPCE/BiF sensor was more sensitive than the GCE/BiF sensor in the PGMs determination. It was further observed that the sediment fractions that pose matrix interferences for the different chemicals used during the extraction procedure, had no limiting effect on the PGM determination, as was the case for the analysis done by Van der Horst (2011).

## 6.5. Comparison of calculated results for different sensor platforms

Thompson (1998) reported that the detection limit caused problems for analytical chemists because they are difficult to interpret and the arbitrary dichotomising of the concentration domain, provides misleading viewpoints of the behaviour of analytical systems. However, with stripping analysis the main aim has always been the construction of a better optimised system to obtain an improved detection limit. The limit of detection was evaluated as the minimum detectable concentration, which is the lowest concentration of analyte that can be distinguished at a stated level of probability, from a sample not containing the analyte or any one of the analyte (PGMs standards) solutions at the lowest working concentration. This concentration value was calculated using of the formula ( $LOD = \frac{3 \times SD}{m}$ ) (Somerset *et al.*, 2009). In this study 10 blanks were used to calculate standard deviation. Limit of quantification (LOQ) were calculated using the formula,  $LOQ = \frac{10 \times SD}{m}$ .

Table 6.6 shows the comparison of the LOD, LOQ values and the %RSD obtained for both the SPCE/BiF and GCE/BiF sensors.

**Table 6.6** Results obtained for the analytical parameters of applying the SPCE/BiF and GCE/BiF sensors in the AdDPSV analysis of Pd(II), Pt(II) and Rh(III) in ammonia buffer (pH = 9.2) solution as the supporting electrolyte.

PGMs	SPCE/BiF				GCE/BiF			
	R <sup>2</sup>	LOD (µg.L <sup>-1</sup> )	LOQ (µg.L <sup>-1</sup> )	RSD (%)	R <sup>2</sup>	LOD (µg.L <sup>-1</sup> )	LOQ (µg.L <sup>-1</sup> )	RSD (%)
Pd	0.994	0.008	0.029	8.95	0.961	0.12	1.07	7.06
Pt	0.981	0.006	0.018	5.16	0.983	0.04	0.26	6.68
Rh	0.987	0.005	0.016	7.36	0.979	0.23	0.03	6.18

By comparing the responses and results of the two sensors applied in AdDPSV analysis, the results indicate that a lower detection limit was obtained for the SPCE/BiF sensor, compared to the GCE/BiF sensor in terms of sensitivity.

The results obtained has further indicated that the use of the adsorptive differential pulse techniques offer a more sensitive technique for the single determination of PGMs, when compared to traditional ICP - AES spectrometry. The deposition time for the stripping analysis used was 150 s, adding to the better results obtained in a shorter analysis times.

## 6.6. Summary

Interesting recent progress in the development and application of a bismuth modified screen-printed carbon electrode (SPCE/BiF) has been presented in this work. The adsorptive stripping voltammetric method was coupled with the use of a screen-printed carbon electrode (SPCE) in order to improve the sensitivity and selectivity, because of the advantages the SPCE offers with its high mass transport and the enhancement of signal-to-noise ratio. In this study it was evident that parameters such as deposition potential ( $E_d$ ) and the deposition time ( $t_d$ ) were adequately optimised, before the electro-analytical determination of the PGM analytes were performed, improving the quality of the results obtained. The determination of PGMs was made by forming Pd(HDMG)<sub>2</sub>, Pt(HDMG)<sub>2</sub> and Rh(HDMG)<sub>3</sub> complexes which are adsorbed on the SPCE/ BiF sensor surface. The developed method was further successfully applied in the determination of PGMs in freshwater and sediment extraction samples. This was followed by comparing the results obtained with the GCE/BiF sensor, to that obtained by the SPCE/BiF sensor. It was observed that the SPCE/BiF sensor gave an advantage in terms of sensitivity and detection limit. However, the ICP-AES spectrometry analysis was able to separate and analyse all three PGMs simultaneously compared, while the simultaneous stripping voltammetric determination of PGM mixtures needs further optimisation. The LOD values obtained with the SPCE/BiF sensor was 0.008  $\mu\text{g.L}^{-1}$  for Pd(II), 0.006  $\mu\text{g.L}^{-1}$  ppb for Pt(II) and 0.005  $\mu\text{g.L}^{-1}$  for Rh(III). In the case of the GCE/BiF sensor a detection limit of 0.12, 0.04 and 0.23 was found for Pd, Pt and Rh respectively.

It can also be concluded that the proposed AdDPSV method can also be able to determine this metals in the presence of interferences at certain concentrations. This method was found to be sensitive, accurate, precise, fast, and provides an alternative low-cost method for the determination of PGMs (e.g. Pd, Pt, and Rh) in freshwater and sediment samples. This method has a great potential as an alternative method for the future of environmental analysis.

## Chapter 7

### Conclusion and Recommendations

---

#### 7.1. Conclusion

The future is promising for finding the inexpensive, portable and robust analytical techniques for monitoring of environmental pollutants. The major aims and objectives of this thesis have been met with regards to the development of analytical techniques for heavy metals and precious metals determination. In this work the improved development of sensors and effects of heavy metals on human health were described, probably sources of these pollutants were enumerated. The future importance of stripping voltammetry will most likely be found in trace metal monitoring and metal speciation studies.

An introductory chapter was provided to highlight the cause of these pollutants and environment in which sensor technology can be used. The literature review is the supplement for the following chapters: Chapters 3 to 6. All the chapters comprise research using modified electrodes for metal ion determination.

In Chapter 4, majority of work was on the research performed using polymerisation and the copolymerisation of polyaniline (PANI) and 2,2'-polydithiodianiline (PANI-PDTDA) on a GCE surface and in 0.1 M HCl (PANI) and various concentrations of H<sub>2</sub>SO<sub>4</sub> (1, 2.5 and 5 M) solution (PANI-co-PDTDA). The films were characterised by cyclic voltammetry (CV), FTIR and UV-Vis spectroscopy. No supporting electrolyte was necessary for the formation of the PANI and PANI-co-PDTDA films. This ensured that the polymer was only doped by the HCl and H<sub>2</sub>SO<sub>4</sub> solutions. The surface concentration, diffusion coefficient and the thickness of the film were also investigated in this study and reported.

In Chapter 5 a method for investigating inhibition of HRP as enzyme by heavy metals was interrogated, but the work has shown the detection of hydrogen peroxide and heavy metals in the range of the latest literature. The Pt/PANI/HRP and Pt/PANI-co-PDTDA/HRP biosensors were successfully designed and constructed for the investigation of inhibition by heavy metals.



This chapter has further seen the novel construction of the Pt/PANI-co-PDTDA/HRP biosensor for metal inhibition studies. The interaction of horseradish peroxidase and hydrogen peroxide produced dissolved oxygen, which is anticipated to be altered by the binding of heavy metals. The Michaelis-Menten constants were also calculated in this study using Lineweaver-Burk method. The use of differential pulse voltammetry (DPV) detection allowed for the coupling of the biosensor with a portable detection system (PalmSens®). The reported biosensor showed percentage relative standard deviation (% RSD) of 14% and 4.3% for the Pt/PANI/HRP and Pt/PANI-co-PDTDA/HRP biosensors, respectively.

In Chapter 6 an analytical procedure was developed, using differential pulse cathodic stripping voltammetry (DPCSV) technique as an analytical tool for determining trace amounts of PGMs (Pd(II), Pt(II) and Rh(III)) pollutants in the presence of DMG as a complexing agent in water and sediments samples using a SPCE/BiF sensor. This has been successfully applied for the first time in South Africa for the determination of palladium, platinum and rhodium. The performance of the SPCE/BiF sensor was found to be superior than the GC/BiFE that was constructed in our laboratory, with a detection limit of 10 times less although we have experience a slowly increase in voltammetric responses for higher metal concentrations. Probably the sensor has almost reached the saturation of Bi nucleation sites. Analytical parameters (linearity, LOD, LOQ, and repeatability) related to PGMs detection for bismuth-coated SPCE have been given. The sensor response in terms of stability was also investigated. The transduction of the signal was obtained using a portable potentiostat (PalmSens®). Screen-printed electrodes were selected for the project development due to low cost and easy manufacture. Good reproducibility of measurements (RSD = 5 to 8.5%) was obtained. The lower limit of detection of  $5 \times 10^{-3}$  to  $8 \times 10^{-3} \mu\text{g.L}^{-1}$  has proven the suitability of the sensor for environmental applications.

## 7.2. Recommendations for future work

The construction of the biosensors has shown desirable results and the modified bismuth screen-printed carbon electrode has shown interesting results for PGMs determination. More optimisation work needs to be done in order to realise this possibility in practice. The options for further study includes: (i) the effects of temperature and the operational and storage stability in the biosensors; (ii) evaluation of the aforementioned parameters for biosensors constructed on a glassy carbon and screen-printed carbon electrodes. Future work could also include some of the unresolved work encountered in chapter 6. In that case the study should solve the problem for the simultaneous determination of PGMs, using the sensor format applied in this study or a modified sensor. The possible solution could be reached by doing more optimisation of the parameters for stripping voltammetric determination of PGMs.



## 8.1 References

- Abraham, D., Bharathi, A., Subramanyam, S.V. (1996). Highly conducting polymer blend films of polyaniline and nylon 6 by cosolvation in an organic acid. *Journal of Polymer*, 37: 5295–5299.
- Adams, R.N. (1968). *Electrochemistry at Solid Electrodes*, Marcel Dekker, New York, USA.
- Agency for Toxic Substances and Disease Registry (ATSDR). (1994). Toxicological Profile for Dinitrophenols, *Department of Health and Human Services, Public Health Service* Atlanta, GA, USA,
- Agency for Toxic Substances and Disease Registry (ATSDR). (2008). Toxicological Profile for Dinitrophenols, *Department of Health and Human Services, Public Health Service*, , Atlanta, GA, USA.
- Alghamdi, A.H. (2010). Applications of stripping voltammetric techniques in food analysis. *Arabian Journal of Chemistry*, 3: 1-7.
- Amsari, R. and Keivani, M.B. (2006). Polyaniline Conducting Electroactive Polymers: Thermal and Environmental Stability Studies. *E-Journal of Chemistry*, 3(4): 202-217.
- Andreescu, S., Sadik, O.A. (2004). Trends & challenges in biochemical sensors for clinical and environmental monitoring. *Pure Applied Chemistry*, 76: 861-78.
- Anne Andrew Research Group, *Response and Excitation form of Cronoamperometry* <http://www.serotonin.ucla.edu/> accessed on 4 June 2012.
- Artyukhin, A., Bakajin, O., Stroeve, P. and Noy, A. (2004). Layer-by-Layer Electrostatic Self-Assembly of Polyelectrolyte Nanoshells on Individual Carbon Nanotube Template. *Langmuir*, 20(4): 1442-1448.
- Banks, G.E and Compton, R.G. (2006). New electrodes for old from carbon nanotubes to edge plane pyrolytic graphite. *Analyst*, 131: 15–21.
- Barbante, C., Veysseyre, A., Ferrari, C., Van de Velde, K., Morel, C., Capodaglio, G., Cescon, P., Scarponi, G., Boutron, C. (2001). Greenland snow evidence of large scale atmospheric contamination for platinum, palladium, and rhodium. *Environmental Science Technologies*; 35: 835-839.
- Bard, A.J. and Faulkner, L.R. (2001). *Electrochemical Methods: Fundamentals and Applications*, 2<sup>nd</sup> edition, *John Wiley & Sons, Inc.*, New York, USA.
- Barefoot, R. (1997). Determination of platinum at trace levels in environmental and biological materials. *Environmental Science and Technologies*, 31: 309–313.

Barek, J.; Fogg, A.G.; Muck, A.; Zima, J. (2001). Polarography and voltammetry at mercury electrodes, *Critical Reviews in Analytical Chemistry*, 31: 291-310.

Bartlett, P.N. and Cooper, J.M. (1993). A review of the immobilized enzymes in electropolymerised films. *Journal of Electroanalytical Chemistry*, 362(1-2): 1–12.

BASi Instruments, 2701 Kent Ave., West Lafayette, IN 47906, USA. [www.basinc.com](http://www.basinc.com) accessed 30 August 2012.

Bobrowski, A., Gawlicki, M., Kapturski, P., Mirceski, V., Spasovski, F., Zarebski, J. (2009). The silver amalgam film electrode in adsorptive stripping voltammetric determination of palladium(II) as its dimethyldioxime complex. *Electroanalysis*, 21(1): 36–40.

Bonting, S.L. (1992). Chemical sensors for space applications. *Advanced Space Biology Medical*, 2: 263-93.

Borgmann, S., Schulte, A., Neugebauer, S. and Schuhmann, W. (2011). Amperometric Biosensors. *Advances in Electrochemical Science and Engineering* WILEY-VCH Verlag GmbH and Co. KGaA, Weinheim

Bradl, H. (2005). Heavy Metals in the Environment: Origin. Interaction and Remediation. *Elsevier/Academic Press*, London

Brainina, K., Neyman, E. (1993). Electro-analytical Stripping Methods, *John Wiley & Sons*, New York.

Braun, F.; Eng, L.; Loppacher, S.; Trogisch, S.; Voit, B.(2002). Novel Diazosulfonate – terpolymers for the preparation of structured functionalized surfaces – synthesis and Characterization. *Macromolecules. Chemistry. Physics*, 203: 1781-1789.

Britto, P.J.; Santhanam, K.S.V. and Ajayan, P.M. (1996). Carbon nanotube electrode for oxidation of dopamine. *Bioelectrochemistry Bioenergy*, 41(1),: 121-125.

Buerk, D. (1993). Biosensors, Theory and Applications, Technomic Publishing, Lancaster.

Buffle, J., Horvai, G. (2000). In Situ Monitoring of Aquatic Systems: Chemical Analysis and Speciation General Concepts. *John Wiley & Sons Ltd*, Chichester.

Buffle, J., Tercier-Waeber, M.-L. (2005). Voltammetric environmental tracemetal analysis and speciation: from laboratory to in situ measurements. *Trends in Analytical Chemistry*, 24(3): 172-192

Burda, L., Chen, X., Narayanan, R., El-Sayed, M.A. (2005). Chemistry and properties of nanocrystals of different shapes. *American Chemical Society, Chemistry revised*, 105(4): 1025- 1102.

- Calvo, E.J., and Danilowicz, C. (1997). Amperometric enzyme electrode. *Journal Brazillian Chemical Society*, 8(6): 563–574.
- Cai, Y., Luo, Q., Sun, M. and Corke, H. (2004). Antioxidant activity and phenolic compounds of 112 traditional Chinese medicinal plants associated with anticancer. *Life Science*, 74: 2157-2184
- Caroli, S., Bocca, B., Petrucci, F., Alimonti, A. (2000). In: Winter Conference on Plasma Spectrochemistry. *Book of Abstracts 345*. Fort Lauderdale, Florida.
- Carr, G.M. and Neary, J.P. (2008). Water Quality for Ecosystem and Human Health, 2nd Edition, *United Nations Environment Programme Global Environment Monitoring System*. [http://www.gemswater.org/publications/pdfs/water\\_quality\\_human\\_health](http://www.gemswater.org/publications/pdfs/water_quality_human_health), accessed on 14 July 211.
- Castelvetto, V., Manariri, A., De Vita, C., Ciardelli, F. (2002). Synthesis and surface properties of microphase separated or nanostructured coating based on hybrid and fluorinated acrylic copolymer. *Micromolecular Symposium*, 187: 165-176.
- Cetinus, S.A., Oztop, H.N. and Sarayd In, D. (2007). Enzyme and Microbial Technology *Elsevier*, 41: 447.
- Chao, C.M., Wang, G.P., WU, K.H., Chang, I.T.C. (2005). Synthesis and Characterization of Polyaniline–Polyamidoamine Dendrimer Blends. *Journal of Polymer Science, B, Polymer Physics*, 44: 1–8.
- Chen, J. H.; Li, W. Z.; Huang, Z. P.; Wang, D. Z.; Yang, S. X.; Wen, J. G.; Ren, Z. F. (2000). Proceedings of the 197th Meeting of the Electrochemical Society; *Electrochemical Society*, Pennington, NJ.
- Chen, Q., Huang, J., Yin, H., Chen, K., & Osa, T. (2006). The applications of affinity biosensors: IAsys biosensor and quartz crystal microbalance to the study on interaction between *Paeoniae radix*801 and endothelin-1. *Sensors and Actuators. B*, 115(1): 116-122.
- Clark, L.C. and Lyons, C. (1967).“Electrode systems for continuous monitoring in cardiovascular surgery.”*Annals of the New York Academy of Sciences*, 102: 29–45.
- Cordon, F., Ramirez, S.A., Gordillo, G.J. (2002). Adsorption and electrochemical reduction of Co(II)-dimethylglyoxime on mercury. *Journal of Electroanalytical Chemistry*, 534: 131-141.
- Cuenya, B.R., Hyeon, B S., Jaramillo, T.F., Mcfarland, E.W. (2003). Size and support depended electronic and catalytic properties of Au<sup>0</sup>/ Au<sup>3+</sup>, Nanoparticles synthesis from block copolymer micelles. *Journal of American Chemical Society*, 125: 12928-12934.

Cui, G.; Yoo, J.; Lee, J.; Yoo, J.; Uhm, J.; Cha, G.; Nam, H. (2001). Effect of pretreatment on the surface and electrochemical properties of screen-printed carbon paste electrodes. *The Analyst*, 126(8): 1399–1403.

Cui, Y., Wei, Q., Park, H., Lieber, C.M. (2001). Nanowire Nanosensors for Highly Sensitive and Selective Detection of Biological and Chemical Species. *Science*, 293: 1289-1292.

Cyclic voltammetry, [http://en.wikipedia.org/wiki/Cyclic\\_voltammetry](http://en.wikipedia.org/wiki/Cyclic_voltammetry), accessed on the 18 March 2012.

Cyclic voltammetry <http://www.bowdoin.edu/chemistry/instrumentation/cyclic-voltammetry/index.shtml>, accessed on the 20 October 2012.

Daniel, R.T., Klara, T., Richard, A.D., George, S.W. (1999). Electrochemical biosensors: recommendation definitions and classification, IUPAC. *Pure Applied Chemistry*, 71: 2333-48.

Darko, H.F. (2004). Accumulation of Metals in Marine Food Webs [Thesis: Master of Science in Ecological Marine Management]. University of Antwerp, Belgium.

Davidson, C., Shaffer, H.B., Jennings, M.R. (2002). Spatial tests of the pesticides drift habitat destruction, 110 – B, and Climate – change hypothesis for California amphibian declines, *Conservation Biology*, 161: 1588–1601.

De Jong, W.H and Borm, P.J.A. (2008). Drug delivery and nanoparticles: Applications and hazards, *International Journal of Nanomedicine*, 3(2): 133 – 149.

De la Torre., J.R., Walker, C.B, Ingalls, A.E, KönnekE, M and Stahl, D.A. (2008). Cultivation of a thermophilic ammonia oxidizing archaeon synthesizing crenarchaeol. *Environmental Microbiology*, 10(1): 810–818.

Deng, C., Li, M., XiE, Q., Liu, M., Tan, Y., Xu, X., Yao., S. (2006). New glucose biosensor based on a poly(*o*-phenylendiamine)/glucoseoxidase-glutaraldehyde/Prussian blue/Au electrode with QCM monitoring of various electrode-surface modifications. *Analytica Chimica Acta*, 557: 85–94.

Dennison, M.J., Turner, P.F. (1995). Biosensors for environmental monitoring. *Biotechnology, Advance*, 13: 1-12.

Deo, R.P., Wang, J., Block, I., Mulchandani, A., Joshi, K.A., Trojanowicz, M., Scholz, F., Chen, W. & Lin, Y. (2005). Determination of organophosphate pesticides at a carbon nanotube/ organophosphorus hydrolase electrochemical biosensor. *Analytica Chimica Acta*, 530: 185–189.

Diab, N., Oni, J., Schuhmann, W (2005) .Electrochemical nitric oxide sensor preparation: A comparison of two electrochemical methods of electrode surface modification. *Bioelectrochemistry* 66: 105–110.



Dosontos, Jr. D.R., Alvarez- Puebla, R. A., Olievera, Jr.O.N., Ovocar, F. (2005). Controlling the size and shape of gold nanoparticle in fulvic acid and colloidal solutions and their optical characterization using SERS. *Journal Material Chemistry*, 15: 3045- 3045.

Dropsen Technologies, Spain (2012).www.dropsen.com, Accessed on 1. August 2012.

Duncan, R. (2003). The dawning era of polymer therapeutics. *Nature Reviews Drug Discovery*, 2(5): 347-360

Dunford, H. B. (1999). Heme Peroxidases. New York: Wiley-VCH.

Eggins, B.R. (2002). Chemical Sensors and Biosensors Analytical Techniques in the Sciences, 2<sup>nd</sup> Edition, John Wiley & Sons.

Essumang, D.K. (2008). Bioaccumulation of platinum group metals in dolphins, *Stenella sp.* caught off Ghana. *African Journal of Aquatic Science*, 33(3): 255–259.

Essumang, D.K., Dodoo, D.K., Adokoh, C.K., Sam, A., and Doe, N.G. (2008). Bioaccumulation of platinum group metals (PGMs) on some fish species (*Oreochromis niloticus*, *Penaeus laspisculcates*, *Scylla serrate*, *Galaxias brevipinnis* and Mollusc) in the Pra Estuary of Ghana. *Toxicological. Environmental. Chemistry*, 3(90): 625–638.

Essumang, D.K. (2010). First Determination of the Levels of Platinum Group Metals in *Manta birostris* (Manta Ray) caught along the Ghanaian Coastline. *Bulletin of Environmental Contamination and Toxicology*, 84: 720–725.

Farrell-Poe, K. (2000). Water Quality & Monitoring “A river is the report card for its watershed.” - Alan Levere, Connecticut Department of Environmental Protection.

Ferrari, M. (2005). Cancer nanotechnology: Opportunities and Challenges. *Nature Reviews Cancer*, 5: 161–71

Fourier transforms infrared spectroscopy (FTIR), (www.macmillan.org.uk, 2010).

Freire, R.S., Pessoa, C.A., Mello, L.D. and Kubota, L.T.J. (2003). Direct Electron Transfer: An Approach for Electrochemical Biosensors with Higher Selectivity and Sensitivity *Brazilian Chemistry Society*, 14(2): 230-243.

Fusalba, F., Gouérec, P., Villers, D., Bélanger, D. (2001). Electrochemical Characterization of Polyaniline in Nonaqueous Electrolyte and Its Evaluation as Electrode Material for Electrochemical Supercapacitors. *Journal of Electrochemical Society*, 148(1):A1-A6.

Gagnon, Z., Newkirk, C., Hicks, S. (2006) Impacts of platinum group metals on the environment: a toxicological genotoxic and analytical chemistry study. *Environmental Science Health*, 41: 397 – 414.



Gaikwad, P.D., Shirale, D.J., Gade, V.K., Savale, P.K., Kharat, H.J., Kakde, K.P. and Shirsat, M.D. (2006). Immobilisation of GOD on electrochemically synthesised PANI film by cross-linking via glutaraldehyde for determination of glucose. *International Journal of Electrochemical Science*, 1: 425-434.

Gerard, M., Chaubey, A., Malhotra, B.D. (2002). Application of conducting polymers biosensors. *Biosensor and Bioelectronic*, 17: 345-359.

Gomez, B., Palacios, M.A., Gomez, M., Sanchez, J.L., Morrison, G., Rauch, S., MCleod, C., Ma, R., Caroli, S., Alimonti, A., Petrucci, F., Bocca, B., Schramel, P., Zischka, M., Petterson, C. and Wass, U. (2002). Levels and risk assessment for humans and ecosystems of platinum-group elements in the airborne particles and road dust of some European cities. *Science of the Total Environment*, 299: 1–19.

Gomez-Caballero, A.; Unceta, N.; Goicolea, M.A. & Barrio R. J. (2008). Evaluation of the selective detection of 4,6 dinitro-o-cresol by a molecularly imprinting polymer based microsensor electrosynthesized in a semiorganic medium. *Sensors and Actuators*, B, 130(7): 713-722.

González, J.G., Renedo, M., Lomillo, O.D., Martínez, J.A. (2004). Determination of gallium by adsorptive stripping voltammetry. *Talanta*, 62: 457–462.

Gorton, L., Lindgren, A., Larsson, T., Munteanu, F., Ruzgas, D.T. and Gazaryan, I. (1999). “Direct electron transfer between heme-containing enzymes and electrodes as basis for third generation biosensors.” *Analytica Chimica Acta*, 400(1–3): 91–108.

Gosser, D.K. Jr. (1994). Cyclic Voltammetry Reaction Mechanisms, *VCH Publishers*, New York.

Grieshaber, D., MacKenzie, R., Janos V and Reimhult, E. (2008). Electrochemical Biosensors - Sensor Principles and Architectures, *Sensors*, 8(3): 1400-1458

Grieves, K., Maluaney, P., Grieser, F. (2000). Synthesis and electronic properties of semiconductor nanoparticles / quantum dots, *Current Opinion in Colloidal and Interface Science*, 5: 168- 172.

Gu, B. (2011). Functionalized Gold Surface- Enhanced Raman Scattering Substrate for Rapid and Ultra-Sensitive Detection of Anionic Species in the Environment. *U.S. Patent*, 7: 989-211.

Guascito, M R., Filippo, E., Malitesta, C., Manno, D., Serra, A., Turco, A. (2008). A new amperometric nanostructured sensor for the analytical determination of hydrogen peroxide, *Biosensors and Bioelectronics*, 24(4): 1063-9.

Gupta, N., Sharma, S., Mir, I.A. and Kumar, D. (2006) “Advances in sensors based on conducting polymers”. *Journal of Scientific and Industrial Research*, 65(7): 549–557.

Gyoung-Ja, L., Hi Min, L., Young, R U., Min, K.L., Chang-Kyu, R (2008) Square-wave voltammetric determination of thallium using surface modified thick-film graphite electrode with Bi nanopowder, *Electrochemistry Communications*, 10: 1920–1923.

Haberska, K., Ruzgas, T. (2009). Polymer multilayer film formation studied by in situ ellipsometry and electrochemistry. *Bioelectrochemistry*, 76: 153–161.

Hanrahan, G.; Patil, D.G. & Wang, J. (2004). Electrochemical sensors for environmental monitoring: design, development and applications. *Journal Environmental Monitoring*, 6(8): 657 - 664.

Hayes, T.B., Collins, A., Lee, M., Mendoza, M., Noriega, N., Stuart, A.A., Vonk, A. (2002). Hermaphroditic, demasculinized forgs after doses, *Proceedings of the National Academy of Sciences*, USA, 99: 5476–6480.

Hocevar ,S.B., Švancara, I ., Ogorevc ,B., and Vytřas, K. (2007). Antimony Film Electrode for Electrochemical Stripping Analysis. *Analytical Chemistry*, 79(22): 8639–8643.

Holister, P. (2002). Nanotech - the tiny revolution. CMP Cientifica: [http://www.cientifica.com/html/Whitepapers/wpfiles/nanotech\\_accessed 20 June 2012](http://www.cientifica.com/html/Whitepapers/wpfiles/nanotech_accessed_20_June_2012),

Honeychurch, K.C., Hart, J.P., Pritchard, P.R. (2003). Development of an electrochemical assay for 2,6-dinitrotoluene, based on a screen-printed carbon electrode, and its potential application in bioanalysis. *Occupational and Public Health, Biosens Bioelectron*, 19(4): 305-12.

Honeychurch, K.C. (2012). Screen-printed Electrochemical Sensors and Biosensors for Monitoring Metal Pollutants. *International sciences Journal*, 2(1): 1-51.

Horáček, J., Skládal, P. (2000). Effect of organic solvents on immunoassays of environmental pollutants studied using a piezoelectric biosensor. *Analytica Chimica Acta*, 412: 37–45.

Huang, X and Ren, J. (2006). Chemiluminescence detection for capillary electrophoresis And microchip capillary electrophoresis. *Trends Analytical Chemistry*, 25: 155–166.

Huerta-Vilca, D., Moraes, S.R and Motheo, A.J. (2003). Preparation and Evaluation of powder synthesis on microstructured aluminium. *Sao Carlos, Brazil, Journal of Applied Electrochemistry*, 33: 355-360.

Hutton, E.A., Ogorevc, B., Hocevar, S.B., Weldon, F., Smyth, M.R., Wang, J. (2001). "An introduction to bismuth film electrode for use in cathodic electrochemical detection". *Electrochemistry Communications*, 3: 707-711

Hutton, E. A., Ogorevc, B., Hočevár, S.B., Weldon, F., Smyth, M. R. Wang, J. (2003). "An introduction to bismuth film electrode for use in cathodic electrochemical detection". *Electrochemistry Communications*.: 707-711.

Iijima, S. (1991). Helical microtubules of graphitic carbon. *Nature*, 354: 56-58.

Iijima, S.; Ichihashi, T. (1993). "Single-Shell Carbon Nanotubes of 1-nm Diameter". *Nature*, 363: 603-605.

International Occupational Safety & Health centre (IOSHC), (1999). <http://www.ilo.org/safework/cis/lang--en/index.htm>.

Introduction to Enzymes and Catalysis, Biochemistry 3521, Fordham University, [http://dwb4.unl.edu/Chem/CHEM869P/CHEM869PLinks/www.fordham.edu/Biochem\\_3521/lect10/lect10.html](http://dwb4.unl.edu/Chem/CHEM869P/CHEM869PLinks/www.fordham.edu/Biochem_3521/lect10/lect10.html).

Iwuoha, E.I., De Villaverde, D.S., Garcia, N.P., Smyth, M.R. & Pingarron, J.M. (1997b). Reactivities of organic phase biosensors 2. The amperometric behaviour of horseradish peroxidase immobilised on a platinum electrode modified with an electrosynthetic polyaniline film. *Biosensors & Bioelectronics*, 12(8): 749-761.

Iwuoha, E.I. and Smyth, M.R., (2003). Reactivities of organic phase biosensors: 6. Square-wave and differential pulse studies of genetically engineered cytochrome P450cam (CYP1O1) bioelectrodes in selected. *Biosensors & Bioelectronics*, 18: 237-244.

Iwuoha, E.I., Williams- Dottin, A. R., Hall, A. L., Morrin, O., Mathebe, A. G., Smyth, M.R. and Killard, A. (2004). Electrochemistry and application of novel monosubstituted squarate electron- transfer mediator in glucose oxidase- doped poly(phenol) sensor. *Pure Applied Chemistry*. 76: 789-799.

Janata, E. (1992). Instrumentation of kinetic spectroscopy-10. A modular data acquisition system for laser flash photolysis and pulse radiolysis experiments. *Radiation Physics and Chemistry*, 40: 437-443.

Jose-Yacaman, M., Miki-Yoshida, M., Rendon, L. & Santiesteban, J. G. (1993). Catalytic growth of carbon microtubules with fullerene structure, *Applied Physics Letters*, 62: 202-204.

Kadara, R.O. and Tohill, I.E. ((2005). Resolving the copper interference effect on the stripping chronopotentiometric response of lead(II) obtained at bismuth film screen-printed electrode. *Talanta*, 66: 1089-1093

Kalcher, K., Wang, J., Kauffmann, J.M., Svancara, I., Vytras, K., Neuhold, C., Yang, Z. (1995). Sensors based on carbon paste in electrochemical analysis. *Electroanalysis*, 7: 5-22.

Kalcher, K., Švancara, I., Metelka, R., Vytras, K., Walcarius, A. (2006). Heterogeneous electrochemical carbon sensors. *Encyclopedia of Sensors*, 4: 283-429.

Khaled, E., Hassan, H.N.A., Habib, I.H.I and Metelka, R. (2010). Chitosan Modified Screen-Printed Carbon Electrode for Sensitive Analysis of Heavy Metals. *International Journal Of Electrochemical Science*, 5: 158-167.

- Khaled, B., Asma, H., Jos van Pelt., and Abdelfatteh, E. (2012). Toxicity assessment of dreamfish *Sarpa salpa* from the Gulf of Gabes (Tunisia, Eastern Mediterranean Sea). *Journal of Food, Agriculture & Environment*, 10 (2): 1308-1313.
- Katz, E. & Willner, I. (2004). Biomolecule-functionalized carbon nanotubes: applications in nanobioelectronics. *European Journal of Chemical Physics and Physical Chemistry*, 5(8): 1084-1104.
- Kemula, W., Kublik, Z. (1958). Electroanalysis: Theory and application in aqueous and non aqueous media. *Analytica Chimica Acta*, 18: 104-111.
- Kissinger, P. and Ridgway, T. (1996). Small-amplitude controlled-potential techniques," in Laboratory Techniques in Electroanalytical Chemistry, *Marcel Dekker*, New York.
- Kissinger, P., Heineman, W.R. (2006). Laboratory Techniques in Electroanalytical Chemistry, 2<sup>nd</sup> Edition, *CRC Press*, U.S.A.
- Lafleur, J.P., Jensen, T.G. and Kutter, J.P. (2011). Gold Nanoparticle-Based Microfluidic Sensor for Mercury Detection. 15<sup>th</sup> *International Conference on Miniaturized Systems for Chemistry and Life*.
- Landis, W G., and Yu, M. (2003). Introduction to Environmental Toxicology: Impacts of Chemicals upon Ecological Systems, *CRC Press, Lewis Publishers*, Boca Raton, FL.
- Li, G., Liao, J.M., Hu, G.Q., Ma, N.Z., Wu, P.J. (2005). Study of carbon nanotubes modified biosensors for monitoring total cholesterol in blood. *Biosensors Bioelectronics*, 20: 2140–2144.
- Li, N. F., Lei, T., Ouyang, C., He, Y. H., Liu, Y. (2009). An amperometric enzyme based on in situ electrosynthesised core- shell nanoparticle. *Synthetic Metals*, 159: 1608- 1611.
- Li, L., Xu, Z., Wu, J. and Tian, G. 2010. Bioaccumulation of heavy metals in the earthworm *Eisenia fetida* in relation to bioavailable metal concentrations in pig manure. *Bioresource Technology*, 101: 3430-3436
- Liang, Z., Zhang, J., Wang, L., Song, S., Fan, C., Li, G. A. (2007). A centrifugation method for preparation of gold nanoparticle and its application in biodetection. *International Journal Molecular Science*, 8(6): 526-532.
- Liu, S.Q., & Ju, H.X. (2002). Renewable reagentless hydrogen peroxide sensor based on direct electron transfer of horseradish peroxidase immobilized on colloidal gold-modified electrode. *Analytical Biochemistry*, 307: 110–116.
- Liu, H., Zhang, Y., Arato, D., Li, R., Mérel, B., Sun, X. (2008). Aligned multi-walled carbon nanotubes on different substrates by floating catalyst chemical vapor deposition: Critical effects of buffer layer. *Surface and Coatings Technology*, 202: 4114.

- Liz-Marzan, L.M. (2004). Nanomaterial: Formation of Colour. *Materials Today*, 7(2): 26-71.
- Locatelli, C. (2006). Simultaneous square wave stripping voltammetric determination of platinum group metals (PGMs) and lead at trace and ultra trace concentration level, application to surface water. *Analytica Chimica Acta*, 557: 70-77.
- Lu, J., Hočevár, S.B. and Farias, P.A.M. (2000). Bismuth-Coated Carbon electrodes for anodic stripping voltammetry. *Analytical Chemistry*, 72: 3218-3222.
- Luo, X., Xu, J., Wang, J., and Chen, H. (2005). Electrochemically deposited of nanocomposite of chitosan and carbon nanotube for biosensor application. *Chemistry Communications*, 2169 – 2171.
- Lyu, S.C., Zhang, Y and Lee, C.J. (2003). Low-Temperature Growth of ZnO Nanowire Array by a Simple Physical Vapor-Deposition Method. *Chemistry of Materials*, 15:3294-3299
- MacDiarmid, A.G. and Epstein, A.J. (1991). "Synthetic metals": A novel role for organic polymers. *Macromolecular Symposium*, 51: 11-28
- Malhotra, B.D. and Chaubey, A. (2003). Biosensors for clinical diagnostics industry. *Sensors and Actuators, B*, 91: 117–127.
- Mathebe, N. G., Morrin, A., & Iwuoha, E. I. (2004). Electrochemistry and scanning electron microscopy of polyaniline/peroxidase-based biosensor, *Talanta*, 64: 115 - 120.
- McCreery, R.L. (2008). "Advanced Carbon Electrode Materials for Molecular Electrochemistry". *Chemical Reviews*, 108: 2646-2687.
- Mehrvar, M.C., Scharer, J.M., Moo-Young, M., Bis, M.C., Luong, J.H. (2000). Fiber-optic biosensors-trends and advances, *Analytical Science*, 16: 677.
- Mehta, A. (2012). Ultraviolet- visible (UV-Vis) spectroscopy derivation of Berr Lambert law. *Analytical Chemistry*.
- Mello, L. D., Sotomayor, M. D. P. T., Kubota, L. T. (2003). HRP- based amperometric biosensor for the polyphenols determination in vegetable extract. *Sensors and Actuators, B*, 96: 636- 645.
- Michira, I., Akinyeye, R., Somerset, V., Klink, M. J., Sekota, M., Al-Ahmed, A. (2007). Synthesis, characterisation of novel polyaniline nanomaterials and application in amperometric biosensors. *Macromolecules*, 255: 57-69.
- Miscoria, S.A., Baerere, G.D. (2005). Enzymatic biosensor based on carbon paste electrode modified with gold nanoparticle and polyphenol oxidase. *Electroanalysis*, 17: 1778-1582.



- Mohadesi<sup>1</sup>, A., Teimoori<sup>1</sup>, E., Taher, M.A., Beitollah, H. (2011). Adsorptive Stripping Voltammetric Determination of Cobalt (II) on the Carbon Paste Electrode. *International Journal. Electrochemistry Science*, 6: 301 – 308.
- Moldovan, M., Rauch, S., Gomez, M., Palacios, M.A. and Morrison, G.M. (2001). Bioaccumulation of palladium, platinum and rhodium from urban particulates and sediments by the freshwater isopod *Asellus aquaticus*. *Water Resources*, 35(17): 4175–4183.
- Moldovan, M., Palacios, M.A., Gómez, M.M., Morrison, G., Rauch, S., McLeod, C., Ma, R., Caroli, S., Alimonti, A., Petrucci, F., Bocca, B., Schramel, P., Zischka, M., Pettersson, C., Wass, U., Luna, M., Saenz, J.C., Santamaría, J. (2002). Environmental risk of particulate and soluble platinum group elements released from gasoline and diesel engine catalytic converters. *Science of the Total Environment*, 296: 199-208.
- Monk, D.J and Walt D.R. (2004). Optical fiber-based biosensors. *Analytical Bioanalytical Chemistry*, 379: 931–945.
- Monthieux, M., Kuznetsov, V.L. (2006). Who should be given credit for the discovery of carbon nanotubes? *Carbon*, 44: 1621–3.
- Morera, M.T., Echeverria, J.C., Mazkieran, C. and Garrido, J.J. (2001). Isotherms and sequential extraction procedures for evaluating sorption and distribution of heavy metals in soils. *Environmental Pollution*, 113: 135-144.
- Morrin, A., Moutloali, R.M., Killard, A.J., Smyth, M.R., Darkwa, J. & Iwuoha, E.I. (2004). Electrocatalytic sensor devices: (I) cyclopentadienylnickel(II) thiolato Schiff base monolayer self-assembled on gold. *Talanta*, 64: 30–38.
- Morrin, A., Ngamna, O., O'Malley, E., Kent, N., Moulton, S.E., Wallace, G.G., Smyth, M.R., Killard, A.J. (2008). The fabrication and characterization of inkjet-printed polyaniline nanoparticle films. *Electrochimica Acta*, 53: 5092–5099.
- Mozaffarian, D. and Rimm, E.B. (2006). Fish intake, contaminants, and human health: evaluating the risks and the benefits. *Journal of the American Medical Association*. 296(15): 1885–1899.
- Murphy, L. (2006). "Current Opinion in Chemical Biology. " *Biosensors and bioelectrochemistry*. 10(2): 177–184.
- Nguyen, D. M., Mayer, T. M.; Hubbard, S. F.; Singer, K. D.; Mann, J. A.; Lando, J. B. (1997). Polar Polymeric Langmuir-Blodgett-Films for Optical Applications. *Macromolecules*, 30: 6150.
- Njagi, J. & Andreescu, S. (2007). Stable enzyme biosensors based on chemically synthesized Au-polypyrrole nanocomposites. *Biosensors & Bioelectronics*, 23(2): 168-175.

Nomngongo, P.N., Ngila, J.C., Nyamori, V.O., Songa, E.A. & Iwuoha, E.I. (2011). Determination of Selected Heavy Metals Using Amperometric Horseradish Peroxidase (HRP), Inhibition Biosensor. *Analytical Letters*, 44: 2031-2046.

Oberholster, P.J. and Ashton P.J (2008). An Overview of the Current Status of Water Quality and Eutrophication in South African Rivers and Reservoirs. *State of the Nation Report Parliamentary Grant Deliverable*.

Odom, T.W.; Huang, J.-L.; Kim, P. & Lieber, C.M. (1998). Atomic structure and electronic properties of single-walled carbon nanotubes. *Nature*, 391(6662): 62-64.

Osman, M.A.; Srivastava, D. (2001). Nanotechnology, *IOP Science Journal*, 12: 21-24.

Ouch, H., Hendricc, C., Hubenthal, F. Trager. (2005). Lase growth of gold nanoparticle : Shaping and optical characterisation. *Applied Physics*, B, 81: 663-668.

Palacios, M.A, Go´mez, M, Moldovan, M, Gomez, B. (2000). Assessment of environmental contamination risk by Pt, Rh and Pd from automobile catalyst. *Micromolecular Chemistry Journal*, 67: 105–113.

Palaniappan, S., Saravanan, C., Amarnatha, C. A. (2004). Preparation of benzyl acetate using polyaniline salts as catalysts—Part II. *Polymer Advanced Technologies*, 15: 118–121.

Panda, B. R., Chattapadhyay, A. (2007). Synthesis of gold nanoparticles at all pH by H<sub>2</sub>O<sub>2</sub> reduction of HAuCl<sub>4</sub>. *Journal of Nanotechnology*, 7: 708- 711.

Pandey, P.C., Upadhyay, S., Shukla, N.K., Sharma, S. (2003). Studies on the electrochemical performance of glucose biosensor based on ferrocene. *Biosensors and Bioelectronics*, 18: 1257-1268.

Petrovic, Z.S., Javni, I., Waddon, A., Nhegy, G.R.B. (2000). Structure and Properties of Polyurethane–Silica Nanocomposites. *Journal of Applied Polymer Science*, 76: 133–151.

Petrucci, F., Bocca, B., Alimonti, A., Caroli, S. (2000). Determination of Pd, Pt and Rh in airborne particulate and road dust by high-resolution ICP-MS: a preliminary investigation of the emission from automotive catalysts in the urban area of Rome. *Journal Analytical Atomic Spectrometry*; 15: 525-528.

Potolsky, F., Zheng, G.F. and Lieber, C.M. (2006). Nanowire sensors for medicine and the life sciences”. *Nanomedicine*, 1: 51-65.

Pulse Voltammetric Technique

[http://www.basinc.com/mans/EC\\_epsilon/Techniques/Pulse/pulse.html](http://www.basinc.com/mans/EC_epsilon/Techniques/Pulse/pulse.html) accessed 2 July 2012

Pyun, S and Choi, Y-M. (1997). Electrochemical lithium interaction into and deintercalation from porous LiCoO<sub>2</sub> electrode by using potentiostatic current transiewnt technique. *Journal of Power Sources*, 68: 524-529



Rauch, S. and Morrison, G.M. (2008). Environmental relevance of the platinum-group elements. *Elements*, 4(4): 259–263.

Ravindra, K., Bences, L. and Van Grieken, R. (2004). Platinum group elements in the environment and their health risk. *Science of the Total Environment*, 318: 1–43.

Revenge, C., Brunner, J., Henninger, N., Kassem, K. and Payne, R. (2000). Pilot Analysis of Global Ecosystems: Freshwater Systems. World Resources Institute: Washington, D.C. accessed at <http://www.wri.org/wr> 2000.

Rodriguez, H.H., Vargas, G., Cortes, D.A. (2006). Electrophoretic deposition of wallstonite on the 316L stainless steel from different dispersing media. *Journal of Ceramics International*, 34(5): 1303–1307.

Rodriguez-Mozaz, S., Lopez de Alda, M.J., Barceló, D. (2006). Biosensors as useful tools for environmental analysis and monitoring, *Analytical and Bioanalytical Chemistry* 386: 1025–1041.

Rosner, G, Merget, R. (2000). Evaluation of the health risk of platinum emissions from automotive emission control catalyts. Anthropogenic platinum-group element emissions: Their impact on man and environment. *Springer-Verlag*, 267–281.

Rubianes, M.D and Rivas, G.A. (2003). Carbon nanotubes paste electrode. *Electrochemistry Communications*. 5: 689–694.

Runge, S.W., Hill, B.J.F. and Moran, W.M. (2006). Life Sciences, *Education*, 5: 348.

Salingue, N. Lingenfelter, D. Prunici, P. and Hess, P. (2009). Surface reactions of (sub)monolayers of small organic species on oxidized silicon, *Proceedings of SPIE*, 7364.

Saini, R.K.; Chiang, I.W.; Peng, H., Smalley, R.E., Billups, W.E., Hauge, R.H. & Margrave, J. L. (2003). Covalent sidewall functionalization of single wall carbon nanotubes. *Journal of the American Chemical Society*, 125(12): 3617-3621.

Salimi, A., Miranzadeh, L., Hallaj, R. (2008). Amperometric and voltammetric detection of hydrazine using glassy carbon electrodes modified with carbon nanotubes and catechol derivatives. *Talanta*, 75: 147–156.

Shamspur, T. (2012). Solid phase extraction of trace amounts of palladium ions using multiwalled carbon nanotube modified by n,n'-bis (2-hydroxybenzylidene)-2,2'-(aminophenylthio) ethane prior to determination by flame atomic absorption spectrometry. *Bulletin Chemical Society Ethiopia*, 26(1): 19-26.

Sharma, M., Kaushik, D., Singh, R.R., Pandey, R.K. (2006). Study of electropolymerised polyaniline films using cyclic voltammetry, atomic force microscopy and optical spectroscopy. *Journal of Mater Science: Mater Electron*, 17: 537-541.

Single-Beam UV-Vis Spectrophotometer

<http://www.files.chem.vt.edu/chem-ed/spec/uv-vis/singlebeam.html> accessed 11 August 202

Somerset, V.S., Klink, M.J., Sekota, M.M.C., Baker, P.G.L. and Iwuoha, E.I. (2006). Polyaniline-Mercaptobenzothiazole Biosensor for Organophosphate and Carbamate Pesticides. *Analytical Letters*, 39: 1683-1698.

Somerset, V.S., Klink, M.J., Baker, P.G.L. and Iwuoha, E.I. (2007). Acetylcholinesterase-polyaniline biosensor investigation of organophosphate pesticides in selected organic solvents. *Journal of Environmental Science and Health, B*, 42: 297.

Somerset, V., Leaner, J., Mason, R., Iwuoha, E. and Morrin, A. (2009) Development and application of a poly(2,2'-dithiodianiline) (PDTDA)-coated screen-printed carbon electrode in inorganic mercury determination. *Electrochimica Acta*, 30: 31-37.

Somerset, V., Leaner, J., Mason, R., Iwuoha, E. and Morrin, A. (2009) Development and application of a poly(2,2'-dithiodianiline) (PDTDA)-coated screen-printed carbon electrode in inorganic mercury determination. *Electrochimica Acta*, 55: 4240-4246.

Somerset, V., Iwuoha, E., Hernandez, L. (2009). Stripping Voltammetric Measurement of Trace Metal Ions at Screen-printed Carbon Paste Electrodes. *Procedia Chemistry*, 1: 1279-1282.

Somerset, V. (2010). Development of an analytical sensor for the identification, quantitation and detection of heavy metal pollution with precious metal refinery wastewaters. *Research proposal to the WRC for funding*. NRE, CSIR, Pretoria, South Africa.

Somerset, V. (2010) Fundamentals of Electroanalysis and Electroanalytical Chemistry. *Natural Resources & Environment*, CSIR, Stellenbosch, South Africa.

Somerset, V., Leaner, J., Mason, R., Iwuoha, E. and Morrin, A. (2010). Determination of inorganic mercury using a polyaniline and polyaniline-methylene blue coated screen-printed carbon electrode. *International Journal of Environmental Analytical Chemistry*, 90(9): 671-685.

Somerset, V., Van der Horst, C., Silwana, B. and Iwuoha, E. (2011). Synthesis and Evaluation of New Electrochemical Materials. *CSIR-NRE Internal Report*, CSIR, Stellenbosch, Report No. CSIR/NRE/WR/IR/2011/0020/B.

Sugunan, A., Thanachayanont, C., Dutta, J., Hilborn, J.G. (2005). Heavy-metal ion sensors using chitosan-capped gold nanoparticles. *Science and Technology of Advanced Materials*, 6: 335-340.

Sures, B., Zimmermann, S., Messerschmidt, J., von Bohlen, A., Thielen, F., and Baska, F. (2005). The intestinal parasite *Pomphorhynchus laevis* as a sensitive accumulation indicator for the platinum group metals Pt, Pd, and Rh. *Environment Research*, 98: 83-88.

Švancara, I. (2001). Carbon paste electrodes in modern electroanalysis (A Review). *CRAC – Critical Reviews of Analytical Chemistry*, 31: 311-345.

Svancara, I., Vytras, K., Kalcher, K., Walcarius, A., Wang, J. (2009). Carbon paste electrodes in facts, numbers, and notes: A Review on the occasion of the 50-years jubilee of carbon paste in electrochemistry and electroanalysis. *Electroanalysis*, 21: 7-28.

Svobodová, E.1., Baldrianová, L.1., Hočevar, S.B.; Švancara, I.1. (2012). Electrochemical Stripping Analysis of Selected Heavy Metals at Antimony Trioxide-Modified Carbon Paste Electrode. *International Journal of Electrochemical Science*, 7197–210.

Tang, Y., Allen, B.L., Kauffman, D.R., Star, A. (2009). “Electrocatalytic activity of nitrogen-doped carbon nanotube cups.” *Journal of American Chemical Society*, 131: 13200–13201.

Tang, J.L., Wang, B.Q., Wu, Z.Y., Han, X.J., Dong, S.J., & Wang, E.K. (2003). Lipid membrane immobilized horseradish peroxidase biosensor for amperometric determination of hydrogen peroxide. *Biosensor Bioelectronic*. 18: 867-872.

Taub, F.B. (2004), Fish 430 lectures (Biological Impacts of Pollutants on Aquatic Organisms), University of Washington College of Ocean and Fishery Sciences, Seattle, WA.

Tesarova, E., Baldrianova, L., Hocevar, S. B., Svancara, I., Vytras, K., Ogorevc, B. (2009). Anodic stripping voltammetric measurement of trace heavy metals at antimony film carbon paste electrode. *Electrochimica Acta*, 54: 1506-1510.

Thess, A.; Lee, R.; Nikolaev, P.; Dai, H.; Petit, P.; Robert, J.; Xu, C.; Lee, Y. H.; Kim, S. G.; Rinzler, A. G.; Colbert, D. T.; Scuseria, G. E.; Tomanek, D.; Fischer, J. E.; Smalley, R. E. (1996). Crystalline Ropes of Metallic Carbon Nanotubes. *Science*, 273(5274): 483-7.

Thevenot, D.R., Durst, A., Wilson, G.S. (1999). Electrochemical Biosensors: recommended definitions and classification. *Pure Applied Chemistry*. 71: 2333-2348.

The Royal Society and the Royal Academy of Engineering (2004). Nanotechnology and Nanoscience.

Thompson, M. (1998). Perspective Do we really need detection limits? *Analyst*, 123: 405–407.

Trchová, M., Šeděnková, I. (2005). In-situ polymerized polyaniline films 6. FTIR spectroscopic study of aniline polymerisation. *Synthetic Metals Journal*, 154: 1–3.

Trojanowicz, M. and Kaniewska, M. (2009). Electrochemical Chiral Sensors and Biosensors. *Electroanalysis*, 21: 229-238.

Turner, A.P.F. (2005). Biosensors and Bioelectronics homepage.  
[http://www.elsevier.com/wps/find/journaldescription.cws\\_home/405913/description#description](http://www.elsevier.com/wps/find/journaldescription.cws_home/405913/description#description)

Twist, J. (2004). Myths and realities of nano futures.

<http://news.bbc.co.uk/1/hi/sci/tech/3920685.stm> accessed 2012, May 22]

Uosaki, K., Sato, Y., Kita, H. (1991). Electrochemical Characteristics of a Gold Electrode Modified with a Self -Assembled Monolayer of Ferrocenylalkanethiols. *Langmuir*, 7: 1510-1514.

Uslu, B. and Ozkan, S.A. (2007). Solid Electrodes in Electroanalytical Chemistry: Present Applications and Prospects for High Throughput Screening of Drug Compounds. *Combinatorial Chemistry & High Throughput Screening Journal*, 10: 495-513.

Valentini, F.; Amine, A.; Orlanducci, S.; Terranova, M.L. & Palleschi, G. (2003). Carbon Nanotube Purification: Preparation and Characterization of Carbon Nanotube Paste Electrodes. *Analytical Chemistry*, 75(20) 5413-5421.

Van der Horst, C. (2011) Stripping voltammetric characterization of palladium, platinum, and rhodium in environmental samples using dimethylglyoxime (HDMG)<sub>2</sub> complexes at carbon modified carbon electrodes surfaces. Unpublished MSc Thesis, University of the Western Cape, South Africa.

Veitch, N.C. (2004). Horseradish peroxidase: a modern view of a classic enzyme. *Phytochemistry*, 65: 249–259.

Vickers, P.E., Watts, J.F., Christian, P., Mohamed, M.C. (2000). The surface chemistry and acid-base properties of a pan-based carbon fiber. *Carbon*, 38: 675-689.

Vidal, J.C., Garcia-Ruiz, E. & Castillo, J.R. (2003). Recent Advances in Electropolymerized Conducting Polymers in Amperometric Biosensors. *Microchimica Acta*, 143(2-3): 93-111..

Vivekanandan, J., Ponnusamy, V., Mahudswaran, A. and Vijayanand, P.S. (2011). Synthesis, characterization and conductivity study of polyaniline prepared by chemical oxidative and electrochemical methods. *Archives of Applied Science Research*, 3(6):147-153.

Vytras, K., Švancara, I. and Metelka, R. (2009). Carbon paste electrodes in electroanalytical chemistry. *Journal of Serbian Chemical Society*, 74 (10) 1021–1033

Wang, J. (1985). Stripping Analysis: Principles, Instrumentation, and Applications, *VCH Publishers, Inc.*, Deerfield Beach, Florida, USA.

Wang, J., Tian, B., Nascimento, V.B., and Angnes, L. (1998). Performance of screen-printed carbon electrodes fabricated from different carbon inks. *Electrochemistry*, 43(23): 3459–3465.

Wang, J. (1994). *Analytical electrochemistry*. VCH Publishers, New York.

Wang, J.C. (2000). Analytical Electrochemistry. *John Wiley & Sons*, Chichester.

- Wang, B., Zhang, J., Cheng, G., Dong, S. (2000). Amperometric enzyme electrode for the determination of hydrogen peroxide based on sol-gel/hydrogel composite film. *Analytica Chimica Acta*, 407: 111-118.
- Wang, J., Hocevar, S. B., Deo, R. P., Ogorevc B. (2001). Carbon-fiber microsensor for in vivo monitoring of trace zinc (II) based on electrochemical stripping analysis. *Electrochemistry Communications*, 3: 352-356.
- Wang, J. (2005). Nanomaterial- based electrochemical biosensors. *Analyst*, 130: 421-426.
- Wang, J. (2006). Analytical Electrochemistry, 3<sup>rd</sup> edition, Wiley-VCH, Hoboken
- Wang, S., Tan, Y., Zhao, D., Liu, G. (2008). Amperometric tyrosinase biosensor based on Fe<sub>3</sub>O<sub>4</sub> nanoparticles chitosan nanocomposite. *Biosensors and Bioelectronics*, 23: 1781–1787.
- Wang, P., Li, S. and Kan, J. (2009). “A hydrogen peroxide biosensor based on polyaniline/FTO”. *Sensors and Actuators ,B*, 137(2): 662–668.
- Wei, C., Morrison, G.M. (1994). Platinum in road dusts and urban river sediments. *Science Total Environmental*, 146/147: 169-174.
- Wei, J.H., Shi, J., Guan, J.G. and Yuan, R.Z. (2004). Synthesis and electrorheological effect of PAn-BaTiO<sub>3</sub> nanocomposite. *Journal of Mater Science*, 39: 3457-346
- Widera, J., Grochala, W., Jackowska, B.K. (1997). Electrooxidation of *o*-methoxyaniline as studied by electrochemical and SERS methods. *Synthetic Metals*, 89: 29-37.
- Willner, I., Baro, R. and Willner, B. (2006). Growing metal nanoparticles by enzymes. *Advanced Materials*, 18 (9): 1109-1120.
- Wood, S., Jones, R. and Geldart, A. (2003). The Social and Economic Challenges of Nanotechnology, Swindon, UK:
- World Health Organization (WHO) (1991). Environmental Health Criteria Platinum, International Programme on Chemical Safety, Geneva World Health Organisation 125.
- World Health Organization (WHO) (2002). Environmental Health Criteria Palladium, International Programme on Chemical Safety, Geneva World Health Organisation 226.
- Wren, C.D., H.R. McCrimmon, and B.R. Loescher (1983). “Examination of Bioaccumulation and Biomagnification of Metals in a Precambrian Shield Lake,” *Water, Air, and Soil Pollution* 19:277-291.
- Wright, D. A. and Welbourn, P. (2002). Environmental Toxicology, Cambridge University Press, Cambridge, U.K.

Yantasee, W.; Deibler, L.A., Fryxell., G.E., Timchalk, C.; Lin, Y. (2005). Screen-printed electrodes modified with functionalized mesoporous silica for voltammetric analysis of toxic metal ions. *Electrochemistry Communications*, 7: 1170–1176.

Yao, H., Li, N., Xu, S., Xu, J- Z., Xu, J-J., Chen, H-Y. (2005) Electrochemical studies of new methylene blue/silicon oxide nanocomposition mediator and its application for stable biosensor of hydrogen peroxide. *Biosensors and Bioelectronics*, 21: 372- 377.

Yu, D. and Liu, F. (2007). Synthesis of Carbon Nanotubes by Rolling up Patterned Graphene Nanoribbons Using Selective Atomic Adsorption. *Nano Letters*, 7(10): 3046-050.

Zanello, P. (2003). *Inorganic Electrochemistry. Theory, Practice and Application*. Cambridge, UK:

Zhang, Y.; Kang T.; Lu L. & Cheng S. (2008). Preparation and characterization of parathion sensor based on molecularly imprinted polymer. *Huanjing Kexue*, 29(4): 1072-1076.

Zhou, M., Guo, J., Guo, L.P., Bai, J. (2008). Electrochemical sensing platform based on the highly ordered mesoporous carbon-fullerene system. *Analytical Chemistry*; 80(12): 4642-50.

Zhuang, J., Zhang, L., Lu, W., Shen, D., Zhu, R., Pan, D. (2011). Determination of Trace Copper in Water Samples by Anodic Stripping Voltammetry at Gold Microelectrode. *International Journal Electrochemical Science*, 6: 4690–4699.